WORKSHOP ON
NEW VIEWS OF THE MOON:
INTEGRATED REMOTELY SENSED, GEOPHYSICAL,
AND SAMPLE DATASETS

Lunar and Planetary Institute, Houston, Texas
September 18–20, 1998

Edited by

B. L. Jolliff and G. Ryder

Sponsored by

Lunar and Planetary Institute
National Aeronautics and Space Administration
through CAPTEM
(Curation and Analysis Planning Team for Extraterrestrial Samples)

Organizers

Ben Bussey	*European Space Agency*
Cass Coombs	*College of Charleston*
B. Ray Hawke	*University of Hawai'i*
Jim Head	*Brown University*
Brad Jolliff	*Washington University*
Paul Lucey	*University of Hawai'i*
Clive Neal	*University of Notre Dame*
Graham Ryder	*Lunar and Planetary Institute*
Mark Wieczorek	*Washington University*

Introduction

It has been more than 25 years since Apollo 17 returned the last of the Apollo lunar samples. Since then, a vast amount of data has been obtained from the study of rocks and soils from the Apollo and Luna sample collections and, more recently, on a set of about a dozen lunar meteorites collected on Earth. Based on direct studies of the samples, many constraints have been established for the age, early differentiation, crust and mantle structure, and subsequent impact modification of the Moon. In addition, geophysical experiments at the surface, as well as remote sensing from orbit and Earth-based telescopic studies, have provided additional datasets about the Moon that constrain the nature of its surface and internal structure.

Some might be tempted to say that we know all there is to know about the Moon and that it is time to move on from this simple satellite to more complex objects. However, the ongoing Lunar Prospector mission and the highly successful Clementine mission have provided important clues to the real geological complexity of the Moon, and have shown us that we still do not yet adequately understand the geologic history of Earth's companion. These missions, like Galileo during its lunar flyby, are providing global information viewed through new kinds of windows, and providing a fresh context for models of lunar origin, evolution, and resources, and perhaps even some grist for new questions and new hypotheses. The probable detection and characterization of water ice at the poles, the extreme concentration of Th and other radioactive elements in the Procellarum-Imbrium-Frigoris resurfaced areas of the nearside of the Moon, and the high-resolution gravity modeling enabled by these missions are examples of the kinds of exciting new results that must be integrated with the extant body of knowledge based on sample studies, *in situ* experiments, and remote-sensing missions to bring about the best possible understanding of the Moon and its history. This workshop was an effort to bring together the diverse disciplines of lunar science to discuss the new results and to integrate what is known based on the many different sets of lunar data.

Logistics and administrative and publications support for the workshop were provided by the Publications and Program Services Department of the LPI. An electronic version of this report, including color versions of some of the figures contained in the abstracts, is available on the LPI Web site at http://cass.jsc.nasa.gov/publications/moon98.pdf.

Contents

Lunar Science Initiative

This workshop is part of an ongoing Initiative, *New Views of the Moon Enabled by Combined Remotely Sensed and Lunar Sample Datasets*, sponsored through the Curation and Analysis Planning Team for Extraterrestrial Materials (CAPTEM), a standing committee of NASA's Cosmochemistry Program, and the Lunar and Planetary Institute (LPI) to foster an environment and specific activities aimed at bringing together diverse disciplines of the lunar-science community to address fundamental problems of lunar origin, evolution, and resources using synthesis and integration of multiple datasets that are available and coming soon. This workshop is the first in a series of workshops and topical sessions envisaged as part of a community-wide effort to capitalize on the wealth of information now available or coming soon from lunar global datasets. What sets the Moon apart and adds value to those datasets is that there *also* exists an extensive set of rock and soil samples of known geologic and geographic context. These samples provide much of the ground truth with which to interpret the remotely sensed data. Given what is known about the Moon from direct study of the surface and its samples, the opportunity *and responsibility* exist now to synthesize and interpret the remotely sensed data in terms of known surface materials, and to use the diverse datasets in an integrated way to address problems of the origin, planetary evolution, and resources of Earth's nearest neighbor.

To those of us who first discussed the Initiative, there were two broad aspects that we thought should be emphasized:

1. The first aspect is to bring together key information about each of the major lunar datasets, e.g., Lunar Orbiter, Apollo samples, Apollo geophysics and remote sensing, Earth-based telescopic, Galileo, Clementine, and Lunar Prospector, to name just a few. The idea was to summarize how these datasets were obtained; what can be learned from them; what their limitations are; how they are archived, accessed, and used; and how aspects of these functions can be improved. This summary ought to include discussion of resolution (e.g., spectral, spatial) and how the scale of observation affects integration with other datasets. Also, we need to understand as much as possible about the materials that are sensed remotely, and for many of the datasets, that means the lunar soil or regolith. How do its properties and those of its components affect remote observations?

2. The second aspect (the payoff) is to use these datasets in an *integrated* and *multidisciplinary* way to address some of the fundamental and long-standing problems of lunar science — or at least to make some good progress toward solving them — and to employ such integrated approaches to lead to new discoveries and new hypotheses.

Scope of the First Workshop: The major themes addressed during this workshop were as follows, including oral and poster presentations:

- ◆ Lunar differentiation: magma ocean, geochronology and isotopes, crustal structure
- ◆ Crustal evolution: basin modifications, impact record, lunar meteorite record
- ◆ Basaltic volcanism: mare stratigraphy, mare basalts, pyroclastic deposits, evolution of basaltic volcanism

- Global resources: results based on Clementine and Lunar Prospector, site characterization, future studies/missions
- Lunar surface characterization: regolith composition, space weathering, surface temperature, atmosphere
- Integrated approaches to studies of the lunar surface and interior
- Clementine and Lunar Prospector global datasets and Lunar Prospector mission update

In addition to these specific topics, we discussed issues related to the processing, use, and archival of specific datasets. We discussed the characteristics of lunar soil that most influence remote spectroscopy, including theoretical and analytical approaches that are converging on a unified understanding of the reflectance properties. Lunar Prospector results were presented and discussed, as well as what can and must be done to develop those (and other) datasets to full potential. Problems and goals that are common to different lunar science disciplines were discussed, as well as how integrated approaches can be used to address them.

Summary of Technical Sessions

INTEGRATED APPROACHES
Chairs: Paul Lucey and Graham Ryder

Carlé Pieters set the tone for the workshop by introducing the dichotomy of scale vs. concept and making the case that remote-sensing approaches differ fundamentally from sample-science approaches because of scale of observation. An example is the different kinds of constraints that can be determined using pyroxene compositions as determined remotely, on a large scale, vs. those determined on the scale of individual mineral grains in a rock. Much of the discussion throughout the workshop focused on how to bridge gaps in both the scale of observations, and in the subsequent approaches to common problems of lunar geoscience. Discussion centered around limitations in different kinds of observations. Pieters described how one could investigate crustal stratigraphy using remote analysis of large impact craters and their central peaks, with Tsiolkovsky as an example. Jim Papike pursued the limitations of compositional information, for example TiO_2, that could be derived from the spectral reflectance data. Dave McKay commented on the need to distinguish the effects of space weathering and soil maturation from real differences in mineralogy. Steve Saunders suggested that our thinking about future work should include what can be achieved using automated *in situ* analyses in addition to remote sensing and sample-collection studies.

Geophysical constraints are key to understanding lunar structure in any detail, especially to resolving the structure of the lunar crust. Mark Wieczorek reviewed current constraints based on Apollo seismic and heat-flow experiments, and Clementine- and Lunar Prospector-derived gravity and topography. Wieczorek described current models of crustal thickness, structure, and variability, and highlighted critical assumptions and areas where additional data are needed. He also presented ideas on how specific models could be tested using global remotely sensed compositional data. These topics were revisited throughout the workshop, as were the nature and potential causes of global lunar asymmetry. In discussion, others echoed the urgent need for a seismic network to take geophysical models to the next level.

CLEMENTINE AND LUNAR PROSPECTOR DATASETS
Chairs:
Paul Lucey and Graham Ryder (Clementine);
David Lawrence and Bill Feldman (Lunar Prospector)

In his overview and update of the Lunar Prospector mission, Alan Binder focused on issues relating to data accuracy, processing, and application to lunar-science problems. Binder described instrumental, environmental, and operational pa-rameters that will affect the data and what the plans are to compensate for or overcome specific problems such as the γ-ray continuum, solar α-particle flux, and damage to the α-particle spectrometer. He summarized key geophysical results of the mission to date, including the significantly improved resolution of the gravity field, the extremely well defined moment of inertia, elucidation of the lunar magnetosphere, and resolution of local fields that are consistent with shock-induced magnetism. Binder discussed expected constraints on the existence and nature of a small lunar core and other results that are anticipated for the extended mission at 25-km orbit. Substantial discussion centered around what will be needed to turn the extant datasets into products that will be useful to the scientific community, and on the anticipated NRA for Lunar Prospector data analysis.

Paul Lucey took on the issue of what have we learned from remote spectral-reflectance data and what information can we reasonably expect to obtain, both from the extant data and future missions. He reviewed datasets that are critical to quantitative compositional and mineralogical applications of the remotely sensed data; these include laboratory spectra obtained under known conditions on well-characterized samples and "ground truth" spectra obtained remotely, but over areas of known surface characteristics. Lucey discussed the problems with and models for sorting out grain size effects, the presence of different kinds and proportions of glasses, mineral proportions, diverse mafic mineralogy, and the effects of optical maturity associated with micrometeorite impacts and the production of submicroscopic Fe metal.

One of the Clementine datasets that has received relatively little fanfare is the long-wave infrared (LWIR) data. Stephanie Lawson reviewed the calibration of this remarkable global dataset, including an assessment of uncertainties in calibration steps and an absolute calibration adjustment using the Apollo 17 *in situ* temperature measurements. She discussed applications of this dataset, specifically in combination with the UV-VIS data. The dominant effects on surface temperatures near the equator are infrared emissivity and albedo, whereas at higher latitudes, large-scale topography predominates. Lawson described potential constraints on surface roughness, thermal inertia, and lunar heat flow that are emerging from analysis of these data.

The discussion following these introductory sessions was vigorous and wide ranging. Bill Feldman provided an interesting example of diversity of scale: The results of the Lunar Prospector neutron spectrometer will provide constraints on H content, and therefore on space weathering on a scale of hundreds of kilometers, a "prospect" that will be of interest to remote spectral reflectance as well as future lunar-base and resource planning. Jim Papike initiated discussion of one of the key issues for lunar science specifically and planetary

science in general: South-Pole Aitken (SPA) Basin is the largest-known basin in the solar system. How deep did it plumb and did it excavate the upper mantle? What are the implications for the thermal evolution of the Moon subsequent to the SPA event? Further discussion of the limitations of available seismic data and the need for new seismic data came from Dave Stewart. Wendell Mendell addressed the issue of how to move from the knowledge gained directly from samples to interpretation of the remotely sensed data in terms of the samples, and the need for all of us to agree on what it is we are trying to describe as we look at different parts of the lunar elephant. David McKay and Carlé Pieters raised the notion that we are asking new questions as well as addressing old ones that could not be answered adequately prior to the acquisition of new datasets. Jim Head brought the discussion to conclusion with a summary of key work that is still needed to advance to the next level: a geophysics network, key sample returns (e.g., SPA), hyperspectral data, and key laboratory experiments and calibrations.

Four additional presentations were made in the afternoon session on Lunar Prospector spectrometer results and data archives. David Lawrence discussed the γ-ray data, touching on issues of background subtraction, spectral deconvolution, nonsymmetric response, solar energetic particle events, and measurement parameters. He presented some of the results that are detailed in Lawrence et al. (1998), and this became a springboard for vigorous discussion. Jim Papike again raised the issue of the nature of SPA basin interior as well as ejecta. Lunar Prospector geochemical results clearly delineate these provinces as unique. Paul Spudis, Larry Haskin, and Mark Wieczorek followed with vigorous discussion of the extreme topographic expression of the basin, the apparent geochemistry and the less-than-expected Th enrichment in the ejecta, and the geophysically anomalous signature of the crust in this region. The suggestion that the SPA event may have been an oblique impact (Schultz, 1997) and the potential effects in terms of the geochemical and geophysical data were debated. Carlé Pieters added that the floor of the basin is for the most part mafic and that spectral data suggest that it is rich in orthopyroxene and lacks significant olivine.

Presentations by Sylvestre Maurice and Rick Elphic on the neutron spectrometer dataset covered aspects of data processing, an overview of H mapping, a preview of the results related to the search for water-ice at the poles, and an unanticipated but very useful and interesting relationship to the Clementine-derived Fe and Ti datasets. Maurice explained how the spectrometer works, what corrections are made, and what processing is required to extract full information, including a measure of surface temperature. Details of the experiment pertaining to ice in permanently shadowed regolith at the poles were left for Feldman's presentation in a later session. Even so, the discussion focused on questions related to the possible forms of H in the soils. Jim Papike raised the question of potential aqueous alteration if indeed ice persists in regolith, which was also

addressed in the poster by Vilas et al. If residence time was long enough and if a transient source of heat such as a large impact were to warm ice-bearing regolith beneath an ejecta blanket, then some aqueous alteration ought to be possible. It was pointed out that at temperatures exceeding 80 K, residence time would be very short, precluding buildup or alteration.

Rick Elphic compared the systematics of fast and thermal neutron detection by the neutron spectrometer to Clementine UV-VIS-derived Fe and Ti data. Because Fe and Ti enhance fast neutron production but absorb thermal neutrons preferentially compared to other major elements, a map of the fast/thermal neutron-flux ratio corresponds to first order to the Clementine-derived Fe and Ti maps, i.e., readily distinguishing mare from nonmare regions. Other effective neutron absorbers include Ca and the trace elements Gd and Sm. The results of the γ-ray spectrometer for Fe can be used to roughly estimate the Ca present, and Th can be used to estimate Gd and Sm. These can then be added to the absorption expected from Fe and Ti based on Clementine-derived Fe and Ti abundances to compute a sum-effective thermal neutron absorption. The end result is a map of residual fast/thermal neutron values that reflects anomalous compositions of surface materials in several regions or discrepant locations where the Clementine-derived Fe and Ti might be significantly in error. One of those regions is the SPA terrane, which rekindled discussion about the nature and significance of the SPA Basin.

Ed Guinness, representing the NASA Planetary Data System (PDS) Geoscience Node, closed out the session on Lunar Prospector results by first giving an overview of the PDS and which nodes are handling each dataset, and then describing the different levels of data according to their processing history. Those datasets that have significant temporal-related variations in parameters are archived as time-ordered series, whereas others are spatially ordered. Guinness detailed the current plans for distribution of level 0 and level 1 data and what those data would look like. The ensuing discussion keyed on the need to communicate to NASA Code S that the scientific community will need data at greater than level-1 processing.

LUNAR SURFACE CHARACTERIZATION, REGOLITH COMPOSITION, SPACE WEATHERING, AND ATMOSPHERE
Chairs: Carlé Pieters and Larry Taylor

Inferences about the igneous and impact evolution of planetary bodies are based upon spectral remote sensing of their surfaces. However, in the case of the Moon and other airless bodies such as asteroids, regolith covers the entire surface and constitutes the interface between bedrock (or any rocks) and the information sensed remotely, with radar studies being an exception (see Campbell et al.). It is imperative to fully understand the nature of the regolith, particularly its finer fraction

termed "soil," in order to appreciate the possible effects of "space weathering" upon the reflectance spectra. This session addressed the regolith in detail, focusing on those aspects that relate to geology and the rocks from which the regolith derives, and on the effects that regolith parameters have on remotely sensed information. The foundation for remote chemical and mineralogical analyses lies in the physics underlying optical absorption and the linking of spectral properties of materials measured in the laboratory to well-understood mineral species and their mixtures. It was evident from the work presented and the discussion during this session that a thorough integration of the material science of lunar rocks and soils with the remote sensing observations is needed. Toward that end, the lunar samples returned by the Apollo missions provide a direct means to evaluate spectral characteristics of the Moon.

Larry Taylor presented the work that he and other consortium members Carlé Pieters, Dave McKay, and Dick Morris are doing to understand the petrographic characteristics of different size fractions of lunar soils and the corresponding spectral characteristics of those same size fractions. This work is providing "ground truth" for further probes of regolith-bearing planetary and asteroidal surfaces. Using electron petrography, Taylor and coworkers are compiling highly precise modal abundances and chemical compositions of mineral and glass components. Pieters and coworkers are providing the spectral characteristics of those same size fractions as well as of the bulk soils so that the bulk spectra can be interpreted in terms of the petrography of the fractions that most influence the bulk spectral properties. Taylor and Pieters have found that it is the finest size fractions of the bulk lunar soil that dominate the observed spectral signatures. Optically, the 20–44-μm, 10–20-μm, and <10-μm size fractions are the most similar to the bulk soil; however, the detailed petrographic and chemical properties of these finer fractions of lunar soils, most relevant for remote spectroscopy, are poorly known. An issue that received some discussion was how (and whether) to push ahead with these kinds of studies on *additional* suites of soils (nonmare, in particular) and on additional soils in general. Paul Lucey pointed out that this is precisely the kind of information that, if we have enough, is most useful for development of algorithms to extract compositional and mineralogical information from spectra. The need to obtain fully quantitative modal and chemical data on the mineral and glass components of lunar soils was emphasized as was the need to carry out such studies as soon as possible on a suite of nonmare soils.

The lunar regolith as sampled at the Apollo and Luna landing sites has been and will continue to be used for ground-truth "calibration" of remotely sensed data (e.g., Blewett et al., 1997). A. Basu addressed some of the complications that can arise from the use of landing-site data for calibration, mainly those relating to geological variability at the sites, differences related to mineralogy of the soils vs. chemical composition, differences related to size fractions, and the size of the particular footprint in question. In a related poster, Riegsecker et al.

presented average modal mineralogy of the Apollo landing site soils by recasting lithic components in terms of their constituent minerals.

Randy Korotev reviewed compositional variations of lunar soils and noted that all soils from the Apollo missions are mixtures of material from three geochemically distinct terranes: feldspathic material of typical highlands, mare material (basalt and volcanic glass), and mafic, KREEP-bearing material from high-Th area in the vicinity of the Imbrium Basin and Oceanus Procellarum. He warned that few samples of Apollo soils exceed 80% material from one type of terrane, thus it is unlikely that areas of hundreds to thousands of square meters observed from orbit will be dominated by a single rock type. All samples of mare soil contain highland material. Compositional variation of the regolith with depth over distances of centimeters is comparable to that observed laterally at the surface over tens to hundreds of meters. On average, maturity of lunar soils, as measured by ferromagnetic resonance (I_S/ FeO) decreases by a factor of two from the surface to half a meter depth.

Patina on lunar rock surfaces and vapor deposits on soil grains results from surface exposure and space weathering, and has profound effects on remote sensing of the lunar surface. Lindsay Keller and coworkers presented results of electron microscopy (amplified in a poster by Wentworth et al.) and microspectrophotometric studies of <25-μm soil grains that demonstrate the presence and overwhelming effects on reflectance spectra of nanophase Fe metal in agglutinitic glass, in irradiated rims tens to hundreds of nanometers thick coating soil particles, and in surface vapor deposits. Keller discussed the relationship between reflectance properties and the size of Fe metal grains and argued for the formation of most metal-rich rims by vapor deposition. Bruce Hapke, approaching the same problem from the theoretical perspective, showed that the absorption efficiency of Fe metal changes relative to the scattering efficiency according to grain size of the metal. Hapke argued that reduction by preferential loss of O during micrometeorite impact readily produces Fe^0. The approach of Keller et al. using high-resolution analytical methods and the theoretical approach that Hapke has pioneered over the years appear to be converging toward a quantitative solution to understanding the cause and optical effects of lunar soil maturity related to submicroscopic Fe metal.

Finally, for those who believe the Moon has no atmosphere, Drew Potter reminded us that the Moon indeed has a Na exosphere, and that we should not ignore it, especially in light of the possibility raised recently for the capture of water ice in "cold traps" at the poles. Potter discussed possible causes of the Na exosphere, including solar photons, physical sputtering, and chemical sputtering. The latter offers some intriguing possibilities if solar-wind H^+ reacts with Na-bearing silicates to produce Na^+ plus H_2O plus Na-depleted silicates. The possibility that variations in spectral properties with latitude might be related to this process was raised.

LUNAR DIFFERENTIATION: MAGMA OCEAN, GEOCHRONOLOGY AND ISOTOPES, NATURE OF THE CRUST
Chairs: Greg Snyder and Graham Ryder

One of the earliest and most significant fruits of Apollo-era research was the recognition that the Moon has a clearly defined crust, composed of materials less dense than the interior. Seismic, gravity-topography, and sample studies all contributed to the identification and definition of this plagioclase-rich exterior. The crust was demonstrated to be asymmetrical, with properties most compatible with it being about 60 km thick in the Procellarum region and thickening to perhaps twice that in the central farside. Its existence is critical to the concept that the Moon underwent large-scale melting early in its history and that a primary differentiation that included plagioclase separation (in the form of ferroan anorthosites) and the production of a global-scale residue rich in incompatible elements (primordial KREEP) occurred. The concept of a global magma ocean developed from these powerful inferences, combined with those about mare basalt source regions. However, with the recognition of other highland igneous rock types not related to the ferroan anorthosites, and the variations of the crust both vertically and horizontally, the magma ocean concept became at best incomplete. Some view it as erroneous. Detailed studies of samples with the full gamut of available techniques including radiogenic isotopes and detailed modeling of the data, as well as continued remote observations of the crust, have been used in numerous attempts to understand the nature and the evolution of the lunar crust, i.e., how did the Moon undergo its essential differentiation, which clearly was not a single step but a prolonged process? The purpose of the session on this differentiation was several-fold: to review the pertinent sample and remote datasets, to outline the current state of understanding for all participants, and to discuss what integrations are possible and useful in completing — or correcting — our concepts.

One complicating factor is recent isotopic data that suggests that ferroan anorthosite sample 62236 crystallized at only 4.29 Ga and has a distinctly positive ϵ_{Nd} of +3 and thus cannot be from a primitive magma ocean. The significance of this remains to be determined; Paul Warren suggested that the sample may not be pristine, or that it may have been modified by metasomatism. Thus, Warren does not see the new finding as necessarily damaging to the lunar magma ocean concept. However, Greg Snyder presented a more ocean-damaging role for these results, especially as the two other anorthosites for which relevant data exist also show at least mildly positive ϵ_{Nd}. Thus the data suggest early and severe depletion of the lunar interior (a very short-lived magma ocean), and a prolonged period of ferroan anorthosite generation for which a magma ocean was not necessarily the controlling factor.

The crust is dominated by anorthosite to a depth of at least 15 km. Stephanie Tompkins used Clementine spectral data to investigate central peaks of larger craters (40–180 km diam-

eter), which have the advantage of exposing fairly *in situ* crust, and have steep enough slopes to prevent the development of mature soils whose spectra are more difficult to interpret than immature soils. She found that of 109 craters, 70% had peaks with at least some anorthosite, although at local and regional scales the crust is diverse. She also found that more mafic material was concentrated in craters interior to large impact basins, suggesting that the deeper crust was more mafic on the whole. This leaves the following question: What processes can lead to an upper crust dominated by anorthosites? The sample collection contains a dearth of mafic highland rocks that would be expected to be complementary to anorthosites.

Most sample workers consider that the more mafic rocks of the lunar highlands were produced in serial magmatism after ferroan anorthosite generation. Both Warren and Snyder reviewed this magmatism in different ways, which must be acknowledged in thermal models of the Moon. Stu McCallum, in an overview of the stratigraphy of the lunar crust from a petrologic viewpoint, described his attempts to determine depths of intrusion from the compositional profiles across pyroxene lamellae and Fe-Mg ordering in pyroxenes. These are dependent on cooling rates, which are in turn dependent to some extent on depth of intrusion. In these studies, no deep crustal anorthosites (>25 km) were identified, and all the magnesian-suite and alkali-suite rocks studied to date yielded very shallow depths (<2 km). He suggested that this is evidence that their parent magmas were generated by mantle rebound after impact erosion followed by diapirism and focusing of magmas into the uppermost and thinnest portions of the crust. A different line of evidence, the composition of basin-scale impact melts as revealed by samples and by remote sensing, suggests that the lower crust is noritic (see also Bussey and Spudis).

KREEP has been a focus of great attention. Paul Warren suggested that the definition of the anomalously high Th region (KREEP) as revealed by Lunar Prospector was further evidence of a magma ocean. He postulated that the Procellarum Basin may have formed prior to complete magma-ocean solidification, allowing the global dregs to migrate laterally into the region. Thus the later impact that formed the SPA Basin, although nearly as large as Procellarum, would have been into a region devoid of this residuum, accounting for the lack of Th in SPA. McCallum presented circumstantial evidence that the primordial KREEP material lies in the middle crust rather than at the crust-mantle boundary where it is typically assumed to have become concentrated. The duration of time over which the "urKREEP" residue remained molten was discussed, but not resolved.

The early differentiation of the Moon necessarily includes the initial formation of the mare basalt sources. Much of the reasoning in this field comes from inferences from detailed sample studies, but Snyder showed how the greater understanding of mare basalt eruption history derived from global remotely sensed data can be used to create models. In particular, the recognition that Ti-rich mare basalts erupted in at least two different timeframes (~3.8 Ga and ~2.5 Ga) is consistent

with a mantle stratigraphy that was disturbed by sinking of dense ilmenite-rich materials. Such a model is consistent with crude depth constraints provided by experimental data on samples.

Many of the details of sample studies, such as radiogenic isotope studies and some trace-element geochemistry, are unlikely to be directly integrated with remote-sensing studies, but the general characteristics of rocks are essential in the first-order interpretations of remote-sensing observations. In return, the contribution of remote sensing to understanding the stratigraphy and variation of the crust constrains possible models of crustal evolution. With continued investigation of global chemistry through Apollo, Clementine, Lunar Prospector, and potential future mission data, combined with new constraints from sample studies, a better understanding of crustal formation will continue to emerge.

CRUSTAL EVOLUTION: BASIN MODIFICATION AND IMPACT RECORD
Chairs: Brad Jolliff and Ben Bussey

The integration of geophysical data (Clementine, Lunar Prospector gravity), remote chemical analysis (Apollo γ-ray, Clementine-derived Fe, Ti), updated crater-ejecta modeling, and sample studies (Apollo) is leading to a new understanding of lunar geophysical, petrologic, and geochemical terranes. Lunar Prospector Doppler tracking data have provided increased resolution of the lunar gravity field, and this improvement has been used by Wieczorek et al. to refine models of crustal structure. The model currently favored by Wieczorek et al. indicates lower crustal structure and mantle uplift beneath the major impact basins that is consistent with scaling upward from the expected behavior of smaller impacts for all but three of the modeled basins: SPA, Imbrium, and Serenitatis. In particular, the characteristics of the latter two suggest a different mechanism of compensation and appear to be consistent with these impacts having struck anomalously hot lower crust. This in turn is consistent with the concentration of Th and other radioactive elements in the Imbrium-Procellarum region of the crust as argued previously by Haskin (1998) based on Apollo Th (γ-ray) and so clearly shown by the Lunar Prospector Th (γ-ray) and neutron-spectrometer data at this workshop (Lawrence et al. and Elphic et al.).

Using an updated model for the distribution of crater ejecta, Haskin showed that the distribution of ejecta related to the Imbrium event is consistent with the nearly Moon-wide distribution of Th that would be expected from the location of the impact in the Th-rich "Procellarum-Imbrium terrane." This model predicts a buildup of Th-rich ejecta at the antipode to Imbrium, which coincides roughly with an area of observed Th enrichment in the northwestern quadrant of the SPA Basin. Haskin pointed out that the Lunar Prospector Th data show the SPA terrane to be in general only slightly enriched in Th and

argued that the concentration in the northwest could be a result of the Imbrium event as opposed to a relict of the SPA event.

An important corollary of the modeling done by Haskin (1998) is that many of the Th-rich impact-melt breccias collected at different Apollo locations might have been produced by the Imbrium event, although this is disputed on the basis of Ar-Ar age dating (e.g., Dalrymple and Ryder, 1993). Rocks sampled at the Apollo 17 site form a crucial test, because they, among all the lunar samples, contain impact-melt breccia (poikilitic group, boulders) thought to be direct products of an associated basin (Serenitatis). Jolliff and Haskin, using a combined study of samples and Clementine UV-VIS-derived compositional information for the eastern Serenitatis highlands, could not rule out a Serenitatis origin for the impact-melt-rich deposits. A combination of Clementine-derived FeO images and Lunar Prospector Th data are more consistent with a Serenitatis origin, which is consistent with the age dating of Dalrymple and Ryder (1996). However, the lack of a widespread distribution of Th-rich ejecta radial to Serenitatis indicates that Th-rich material was excavated only at depth in the Serenitatis target, which lies at the eastern edge of the Imbrium-Procellarum Th-rich terrane. This is probably related to the geophysically anomalous nature of the Serenitatis Basin (Wieczorek et al.).

Investigations of basin ejecta as probes of crustal composition, based mainly on Clementine-derived compositional information and photogeology, confirm the feldspathic nature of ejecta and presumably of the crustal section excavated by basin impacts such as Orientale and Crisium (Bussey and Spudis). Most of the rim deposits of Imbrium are mafic, consistent with either a complete stripping away of all feldspathic crustal components (Bussey and Spudis) or with there having never been a concentration of feldspathic material in the Imbrium target (Haskin et al.). Humorum, which lies along the south-southwestern edge of the Imbrium-Procellarum Th terrane, excavated mainly feldspathic material, but somewhat more mafic than Orientale. Bussey and Spudis argued for an essentially three-layer crust consisting of a mafic lower crust overlain by an anorthositic zone, which is capped by a mixed megaregolith layer a few tens of kilometers thick.

The high-resolution Clementine and Lunar Prospector gravity fields provide further evidence regarding present-day crustal and upper mantle structure beneath the basins (Neumann et al.). Gravity highs beneath the basins require more mass than can be accommodated by mare basalt of reasonable thickness (or no basalt in basins that contain no mare fill) and indicate substantial mantle uplifts that have resisted viscous relaxation (super-isostatic). Gravity moats surround most basins and coincide with topographic highs, reflecting crustal thickening.

The SPA Basin is the largest known impact crater in the solar system and is one of the most important structures on the Moon; however, the source and nature of materials exhumed by this impact event remain controversial. Spudis et al. describe a digital elevation model based on stereo information

from overlapping Clementine images for south-polar regions that were not covered by Clementine laser altimetry. They report prominent topography corresponding to the Liebnitz Mountains and SPA basin-wall slopes and symmetry that are comparable to basin-wall slopes elsewhere around the basin. Increased resolution of the topography of elements of the SPA terrane coupled with gravity and compositional information have the potential to greatly increase knowledge of how this basin formed and how it modified the early crust of the Moon.

The Clementine global-coverage color dataset continues to provide the impetus for new kinds of investigations. Jennifer Grier reported on a survey of craters and an evaluation of the optical maturity of the ejecta of craters as a measure of relative age. Results presented at the workshop showed a promising correlation between the relative ages of craters of similar size, on the basis of optical maturity estimated from Clementine data, and the generally accepted ages of several craters for which there exists independent age information.

Lunar meteorites collected in Antarctica and elsewhere continue to provide a random lunar sample dataset that supplements the Apollo and Luna samples. Paul Warren reviewed the current state of this important sample dataset and how it influenced our understanding of the composition and distribution of rock types in the Moon's crust. Importantly, compared to the feldspathic lunar meteorites, the Apollo 16 megaregolith is rich in Th and other incompatible elements. This site also is richer in FeO than vast regions of the lunar farside that constitute a "feldspathic highlands terrane." Thus the Apollo 16 site should not in general be considered typical of the feldspathic lunar highlands. Another very significant aspect of the lunar meteorite sample set is the abundance of very-low Ti and low Ti basaltic meteorites, and the very old age (4.0 Ga) of two of them.

Mare Basalts, Mare Stratigraphy, Pyroclastic Deposits, Evolution of Basaltic Volcanism
Chairs: Clive Neal and Jim Head

Remote sensing and sample studies came together during this session integrating knowledge using these two general approaches to study mare volcanism. The first talk of the session by Jim Head concluded that mare volcanism lasted for 2 b.y. and perhaps 3 b.y., commencing prior to the end of the heavy bombardment. The general flux peaked during the late Imbrian period. Head and Wilson (1992) proposed that the mare magmas were delivered to the surface via dikes originating at depth. The presentation developed this concept by proposing that low-density lunar crust provided an effective density barrier to rising diapirs, and magma was only erupted after overpressurization propagated the dikes to the surface. The crustal thickness differences between the lunar nearside and farside may then explain the preponderance of mare basalts

on the nearside of the Moon. .

Clive Neal highlighted some of the dichotomies between remotely gathered and sample data for mare basalts: (1) Not all basalt compositions appear to be present in the sample collection; (2) sample data suggests a relationship between TiO_2 content and age, whereas remote sensing does not; and (3) ages deduced from crater size-frequency determinations suggest volcanic activity for up to 3 b.y., whereas sample data suggest a range of only 1.1 b.y. In addition, the pyroclastic glasses cannot be geochemically related to the crystalline basalts, and trace-element data suggest the glasses were derived from either a primitive portion of the Moon or from one containing garnet (i.e., were derived from greater depths).

Lunar Orbiter, Galileo, and Clementine data were used by Harry Hiesinger et al. to examine mare volcanism in the Australe, Tranquillitatis, Humboldtianum, Serenitatis, and Imbrium Basins. Using crater size-frequency distributions, they concluded that the maximum frequency of volcanic activity was older in the eastern basins (3.6–3.8 Ga) than in the western basins (3.3–3.5 Ga). Volcanic activity decreased markedly at the end of the late Imbrium period. Significantly, they also found no correlation between age and TiO_2 content of the basalts, but basalts of the older basins tend to be more Ti-rich than those of the younger basins. Finally, the youngest basalts are exposed at or near areas with the relatively thinnest crust.

Clementine data were used by Jeff Gillis and Paul Spudis to investigate whether the mare deposits analyzed spectrally are inherently low in Fe or have been diluted with highland material. They concluded that the difference in Fe content of remotely sensed deposits and the ground-truth values determined from sample studies is a result of surface contamination. The magnitude of such contamination reflects the depth, size, and age of the mare basalt unit.

Clementine UV-VIS data were used by Lisa Gaddis et al. to examine pyroclastic deposits that were too small to be defined using Earth-based observations from the Atlas Crater, Franklin Crater, Eastern Frigoris highlands, Oppenheimer Crater, Lavoisier Crater, and Orientale Crater. These deposits were estimated to be ~1 Ga in age. It was concluded that the spatial association of these pyroclastic deposits was related to crustal thinning beneath impact sites (~50 km). Such deposits should be found on the margins of the major maria on the lunar nearside and around deep impacts on the far side (e.g., SPA and Moscoviense Basins).

Galileo and Clementine multispectral data were used by B. Ray Hawke et al. to investigate the extent of the ancient (>3.8 Ga) lunar "cryptomaria." Using these data, Hawke demonstrated that cryptomare has been excavated in the northeast nearside, the Balmer region, and the southern central highlands. Significantly, it was shown that these ancient deposits have been covered with a thin higher-albedo material, thus masking their mare affinities, and that there is some correlation between the cryptomaria and gravity anomalies.

The discussion of this session produced a number of general issues that need to be addressed either by better integration of existing datasets or through the acquisition of new data by future missions: (1) Absolute age determinations are required to determine better the time duration of mare volcanism. (2) What is the nature of the relationship, or lack thereof, between pyroclastic glasses and crystalline basalts? (3) The nature of the lunar interior needs to be defined through geophysical experiments. (4) What was the volatile budget of the lunar interior that produced the crystalline mare basalts? (5) What are the exact stratigraphic relationships between different mare basalt compositions and between the crystalline basalts and the volcanic glasses?

These general questions can be addressed by better age determinations through establishing the composition and flux of mare basalts in space and time, robotic landers/explorers, sample return for absolute age determinations, and the establishment of a lunar seismic network. Better integration of existing datasets would be useful in determining which sites to visit in future missions as well as better constraining the nature and extent of "dilution" from highland material of mare deposits around impact craters and the lunar maria. A significant aspect of the discussion related to the paucity of funding for missions that return remotely sensed data to reduce the data to a form that is usable by the broader planetary science community.

GLOBAL RESOURCES, SITE CHARACTERIZATION, FUTURE INVESTIGATIONS AND MISSIONS
Chairs: Carl Allen and Cass Coombs

At some time in the future, humans will return to the Moon, not just for short visits but to establish long-term outposts. As a result of the extremely high cost of transportation from Earth, an extended human presence on the Moon will require the use of local resources. Two high-leverage lunar resources that have been discussed for years are (1) oxygen for propulsion and life support and (2) radiation and thermal shielding. Four of the papers in this session highlighted the utility of new remotely sensed datasets to identify and map these lunar resources. The fifth presented a proposal for remote subsurface mapping using entirely new techniques.

Carl Allen presented a laboratory study of oxygen extraction from lunar soil using H at elevated temperatures. They demonstrated that oxygen yields correlate directly with Fe abundance in the soil and that the yield is highest for deposits of Fe-rich volcanic glass. Clementine and Lunar Prospector provide complementary measurements of Fe in lunar soil and the extent of such glass deposits across the entire lunar surface. These datasets were convolved with the oxygen extraction results to produce the first global map of a future lunar resource.

On the basis of Lunar Prospector neutron spectrometer results, Bill Feldman et al. presented a much different approach to the search for accessible lunar oxygen — the evidence for water ice in permanently shadowed craters. Such deposits were predicted decades ago and tentatively identified by the Clementine bistatic radar experiment, but strong confirmation and quantification of the resource was claimed by the Lunar Prospector team. Feldman presented, in convincing detail, the recently published evidence for excess H, and by implication, ice-bearing regolith deposits, at both lunar poles.

Results of the Clementine bistatic radar experiment, which were interpreted by Nozette et al. as consistent with the presence of water ice mixed with regolith, were reinterpreted (Simpson) to provide no compelling evidence for water ice at the lunar south pole. This result was vigorously disputed by Nozette of the Clementine science team. The discussion illustrated the complexity and uncertainty of the remote search for lunar ice, particularly using radar. However, the recent Lunar Prospector results reinforce the likelihood of excess H in these regions, and their form as deposits of water ice mixed with regolith remains a viable hypothesis. In a poster presentation, Faith Vilas presented evidence (or the lack thereof) for the presence of hydrated minerals that might be expected if impacts into ice-bearing regolith or megaregolith caused burial and heating of ice deposits and consequent alteration of silicate minerals.

Allen Taylor addressed the use of lava tubes for radiation and thermal protection of a lunar outpost. He presented a model of sinuous rilles as unroofed lava tubes and suggested that interruptions visible in some rilles are intact tube segments. Taylor and colleagues are attempting to adapt a computerized feature recognition program (JARTool) to identify such features in Clementine images. They then intend to catalog lava tube segments across the entire Moon. Taylor also presented a novel proposal by Billings and Gottschalk to locate and map subsurface lava tubes using radar. This idea employs a series of small impactors that convert kinetic energy into electromagnetic pulses (described as "radar flashbulbs"). The radar pulses would illuminate subsurface features, including lava tubes, and the signal would be received on Earth by the Very Long Baseline Array. This is certainly not a mature proposal, and strong doubts were raised by meeting attendees as to whether point sources of radar energy could provide data sufficient for three-dimensional mapping.

Several posters were presented that highlighted newly emerging views of the Moon based on recent datasets and image processing techniques. Eric Eliason presented a spectacular, wall-sized display of part of the global high-resolution UV-VIS mosaic of the Moon based on the Clementine UV-VIS dataset. This mosaic, which is the product of an enormous processing effort of the USGS group at Flagstaff, will become the standard product for investigators needing to use the UV-VIS dataset for detailed scientific studies. Harald Hiesinger presented a compilation of previously published datasets transformed to a standard cylindrical map projection, allowing

direct comparison of diverse datasets. This effort, on behalf of the DLR-Institute of Planetary Exploration, resulted in a CD-ROM that will be very useful to anyone interested in comparing the results of different remotely sensed datasets. Cass Coombs presented a Geographic Information System (GIS) database developed specifically for the Apollo 17 landing site. This method of information organization allows the integration of different kinds of data that have some spatial relationship. This system is ideally suited to educational products as well as detailed scientific investigations.

Two poster presentations focused on specific aspects of the upcoming SELENE mission. Shiraishi et al. described the ground-data processing system for the Lunar Imager/Spectrometer and plans for anticipated databases. The mission team has already begun constructing databases that will be used for the interpretation of anticipated remote datasets. Namiki et al. described the gravity, VLBI, and Doppler tracking experiments, which will include the use of a relay subsatellite for direct measurements over the farside. The poster also addressed testing efforts and expectations for the anticipated datasets.

CONCLUDING REMARKS
Brad Jolliff, Cathy Weitz, and Paul Lucey

By the end of the workshop, a number of major questions of lunar science emerged as key. In most cases, these can be addressed fruitfully using integrated approaches and datasets currently in hand. However, in some cases, there was agreement that specific datasets envisioned for the future are needed to take these to the next level of understanding. Thus we conclude by summarizing some of the key questions and looking forward to the kinds of future missions and information that will enable the next generation of insights as well as provide a firmer foundation for future lunar exploration, resource assessment, and lunar base siting.

1. What is the structure (lateral and vertical) of the lunar interior? Seismic data from Apollo are inconclusive about the depth of the megaregolith, the structure of the crust and mantle, and the size of the core. There remains a need to better understand the composition of the lower crust, i.e., is it noritic or gabbroic, and how variable is it Moon-wide? Do Mg-rich plutons intrude an otherwise anorthositic crust? Is there a ferroan mafic layer at depth and a KREEP layer at the base of the crust or in a midcrustal "sandwich horizon?" Answers to these questions can be applied to models of the evolution of the Moon, particularly the lunar magma ocean hypothesis. A mission that obtains seismic data at specific key locations or a network across the lunar surface will drastically improve our knowledge of the Moon's interior structure and its early thermal and magmatic evolution.

2. How are the Moon's structure, magmatism, and volcanism related to its thermal evolution? How long did the magma ocean or "magmasphere" take to cool, and how hot was the lower crust at the time of deep basin impacts? If urKREEP residue was effectively concentrated in specific locations, how long did it remain molten and how did it interact with nearby crust or upper mantle? What caused the melting of magnesian-suite parent magmas and what were the effects of mantle convection or density overturn on the generation of mantle melts, including mare basalts?

3. What is the cause of the Th anomaly on the nearside of the Moon? Lunar Prospector γ-ray data has revealed a high concentration of Th associated with the Procellarum Basin as suggested by the Apollo remotely sensed data. What is the cause of this high concentration? Is this terrane the surface manifestation of a magmatic hotspot? Did KREEP residua migrate from the farside to the nearside? Why is there little Th associated with material in and around the SPA Basin?

4. Did the SPA Basin expose lower crustal rocks? Given the large size of the basin and its great depth, it may have exposed crustal rocks that could be used to understand the composition of the lower crust or possibly even the upper mantle of the Moon in that region. Clementine results show a relatively high concentration of FeO in the basin, but the spectra are inconclusive about the mineralogic composition of the rocks there. The Th concentration is slightly higher in the basin but is much lower than in the Procellarum-Imbrium terrane, suggesting that rock formations with a high proportion of KREEP were not exposed. A mission to determine the composition of the rocks in the SPA Basin would prove whether lower crust is exposed there.

5. What is the origin, timing, and distribution of mare volcanism? Remote sensing data suggest a wide variety of Ti contents for the mare, yet the sample collections (Apollo, Luna, lunar meteorites) are dominated by relatively high- and low- to very-low-Ti basalts. Crater counts reveal some mare surfaces that appear to be relatively young, perhaps as young as 2 Ga. In contrast, regions of cryptomare appear to represent older volcanics (e.g., ≥4 Ga), subsequently buried by impacts that formed the major basins around 3.8–3.9 Ga. Clementine and Galileo spectra for the mare show no strong correlation between age and Ti content, which is important for understanding the evolution of the lunar interior. Samples of very young and very old mare to determine ages and composition are needed to extend our understanding of the volcanic history of the Moon.

6. What is the volatile history of the Moon? The discovery of a high concentration of H at the lunar poles is consistent with the occurrence of water ice, deposited by comets over time and concentrated by cold entrapment. Is the H at the poles in the form of water ice mixed in regolith? What volatiles are likely to be endogenic vs. exogenic? What is the composition and structure of the lunar atmosphere? A mission to the poles to study areas of apparently high H concentration will ultimately be needed to confirm the concentration and form of entrapped H_2O.

REFERENCES

Blewett D. T., Lucey P. G., Hawke B. R., and Jolliff B. L. (1997) Clementine images of the lunar sample-return stations: Refinement of FeO and TiO_2 mapping techniques. *J. Geophys. Res., 102*, 16319–16325.

Dalrymple G. B. and Ryder G. (1993) $^{40}Ar/^{39}Ar$ age spectra of Apollo 15 impact melt rocks by laser step-heating and their bearing on the history of the lunar basin formation. *J. Geophys. Res., 98*, 13085–13095.

Dalrymple G. B. and Ryder G. (1996) Argon-40/argon-39 age spectra of Apollo 17 highlands breccia samples by laser step heating and the age of the Serenitatis basin. *J. Geophys. Res., 101*, 26069–26084.

Haskin L. A. (1998) The Imbrium impact event and the thorium distribution at the lunar highlands surface. *J. Geophys. Res., 103*, 1679–1689.

Head J. W. III and Wilson L. (1992) Lunar mare volcanism: Stratigraphy, eruption conditions, and the evolution of secondary crusts. *Geochim. Cosmochim. Acta, 56*, 2155–2175.

Lawrence D. J., Feldman W. C., Barraclough B. L., Binder A. B., Elphic R. C., Maurice S., and Thomsen D. R. (1998) Global elemental maps of the Moon: The Lunar Prospector gamma-ray spectrometer. *Science, 281*, 1484–1489.

Schultz P. H. (1997) Forming the South-Pole Aitken Basin: The extreme games (abstract). In *Lunar and Planetary Science XXVIII*, pp. 1259–1260. LPI, Houston.

Workshop Program

Friday, September 18, 1998

7:30–8:30 a.m.   *REGISTRATION*

INTRODUCTORY REMARKS

8:30 a.m.   Brad Jolliff and Graham Ryder
Lunar Initiative, Workshop Purpose, Rules

INTEGRATED APPROACHES TO STUDIES OF THE LUNAR SURFACE AND INTERIOR
Chairs: Paul Lucey and Graham Ryder

8:45 a.m.   Pieters C. M.*
Constraints on Our View of the Moon I: Convergence of Scale and Context

9:15 a.m.   Wieczorek M. A.*   Phillips R. J.
Integrating Geophysics with Remotely Sensed Data and the Apollo Samples

9:30 a.m.   Binder A.*
Prospector Update

10:00 a.m.   Discussion
Integration: Common Problems of Lunar Geoscience

10:30 a.m.   *BREAK*

CLEMENTINE AND PROSPECTOR DATASETS
Chairs: Paul Lucey and Graham Ryder

10:45 a.m.   Lucey P. G.*
*Quantitative Mineralogic and Elemental Abundance from Spectroscopy of the Moon:
Status, Prospects, Limits, and a Plea*

11:15 a.m.   Lawson S. L.*   Jakosky B. M.   Park H.-S.   Mellon M. T.
The Clementine Long-Wave Infrared Dataset: Brightness Temperatures of the Lunar Surface

11:30 a.m.   Discussion
Spectroscopy of the Lunar Surface/Clementine-specific Issues

12:00 noon   *LUNCH BREAK*

Chairs: William Feldman and David Lawrence

1:30 pm.   Lawrence D. J.*   Feldman W. C.   Binder A. B.   Maurice S.   Barraclough B. L.   Elphic R. C.
Early Results from the Lunar Prospector Gamma-Ray Spectrometer

1:45 p.m.   Maurice S.*   Feldman W. C.   Barraclough B. L.   Elphic R. C.   Lawrence D. J.   Binder A. B.
The Lunar Prospector Neutron Spectrometer Dataset

2:00 p.m.   Elphic R. C.*   Maurice S.   Lawrence D. J.   Feldman W. C.   Barraclough B. L.
Binder A. B.   Lucey P. G.
*Lunar Prospector Neutron Measurements Compared to Clementine Iron and
Titanium Abundances*

2:15 p.m.   Guinness E. A.*   Binder A. B.
Lunar Prospector Data Archives

2:30 p.m.   Discussion
Lunar Prospector Datasets, Present and Future

3:00 p.m.   *BREAK*

LUNAR SURFACE CHARACTERIZATION, REGOLITH
COMPOSITION, SPACE WEATHERING, AND ATMOSPHERE
Chairs: Carle Pieters and Lawrence Taylor

3:15 p.m.	Taylor L. A.* Pieters C. McKay D. S. *Reflectance Spectroscopy and Lunar Sample Science: Finally a Marriage After Far Too Long an Engagement*
3:30 p.m.	Basu A.* Riegsecker S. E. *Reliability of Calculating Average Soil Composition of Apollo Landing Sites*
3:45 p.m.	Korotev R. L.* *Compositional Variation in Lunar Regolith Samples: Lateral*
4:00 p.m.	Keller L. P.* Wentworth S. J. McKay D. S. *Surface-Correlated Nanophase Iron Metal in Lunar Soils: Petrography and Space Weathering Effects*
4:15 p.m.	Pieters C. M.* *Constraints on Our View of the Moon II: Space Weathering*
4:30 p.m.	Potter D. *The Lunar Atmosphere*
4:45 p.m.	Hapke B. W.* *The Vapor Deposition Model of Space Weathering: A Strawman Paradigm for the Moon*
5:00 p.m.	Discussion
5:30–7:30 p.m.	*POSTER SESSION, DEMONSTRATIONS, AND RECEPTION*

POSTER SESSION PRESENTATIONS

Bussey D. B. J. Spudis P. D.
Lunar Impact Basins, Probes into the Lunar Crust

Coombs C. R. Meisburger J. L. Nettles J. W.
Another Look at Taurus Littrow: An Interactive Geographic Information System Database

Eliason E. McEwen A. Robinson M. Lucey P. Duxbury T. Malaret E. Pieters C. Becker T.
Isbell C. Lee E.
Multispectral Mapping of the Moon by Clementine

Hiesinger H.
The Lunar Source Disk: Old Lunar Datasets on a New CD-ROM

Namiki N. Hanada H. Kawano N. Heki K. Iwata T. Ogawa M. Takano T. RSAT/VRAD Mission Groups
Measurements of the Lunar Gravity Field Using a Relay Subsatellite

Neumann G. A. Lemoine F. G. Smith D. E. Zuber M. T.
Lunar Basins: New Evidence from Gravity for Impact-formed Mascons

Riegsecker S. E. Tieman A. K. Basu A.
Average Mineral Composition of Apollo Landing Site Soils

Shiraishi A. Haruyama J. Otake H. Ohtake M. Hirata N.
Conceptual Design of the Ground Data Processing System for the Lunar Imager/Spectrometer Onboard the SELENE Mission

Spudis P. D. Cook T. Robinson M. Bussey B. Fessler B.
Topography of the South Polar Region from Clementine Stereo Imaging

Vilas F. Jensen E. A. Domingue D. L. McFadden L. A. Coombs C. R. Mendell W.
Evidence of Phyllosilicates near the Lunar South Pole

Wentworth S. J. Keller L. P. McKay D. S.
Effects of Space Weathering on Lunar Rocks: Scanning Electron Microscope Petrography

Saturday, September 19, 1998

LUNAR DIFFERENTIATION: MAGMA OCEAN, GEOCHRONOLOGY AND ISOTOPES, CRUST
Chairs: Greg Snyder and Graham Ryder

8:30 a.m.   Warren P. H.*   Kallemeyn G. W.
Pristine Rocks, Remote Sensing, and the Lunar Magmasphere Hypothesis

8:45 a.m.   Snyder G. A.*   Taylor L. A.
Geochronologic and Isotopic Constraints on Thermal and Mechanical Models of Lunar Evolution

9:00 a.m.   McCallum I. S.*
The Stratigraphy and Evolution of the Lunar Crust

9:15 a.m.   Tompkins S.*
Composition and Structure of the Lunar Crust

9:30 a.m.   Discussion

10:00 a.m.   *BREAK*

CRUSTAL EVOLUTION: BASIN MODIFICATION AND IMPACT RECORD
Chairs: Brad Jolliff and Ben Bussey

10:15 a.m.   Wieczorek M. A.*   Haskin L. A.   Korotev R. L.   Jolliff B. L.   Phillips R. J.
The Imbrium and Serenitatis Basins: Impacts in an Anomalous Lunar Province

10:30 a.m.   Haskin L. A.*   Jolliff B. L.
On Estimating Provenances of Lunar Highland Materials

10:45 a.m.   Jolliff B. L.*   Haskin L. A.
Integrated Studies of Impact-Basin Ejecta as Probes of the Lunar Crust: Imbrium and Serenitatis

11:00 a.m.   Grier J. A.*   McEwen A.   Strom R.
Use of a Geographic Information System Database of Bright Lunar Craters in Determining Crater Chronologies

11:15 a.m.   Warren P. H.*
A Brief Review of the Scientific Importance of Lunar Meteorites

11:30 a.m.   Discussion

12:00 noon   *LUNCH BREAK*

BASALTIC VOLCANISM: MARE STRATIGRAPHY, MARE BASALTS, PYROCLASTIC DEPOSITS, EVOLUTION OF BASALTIC VOLCANISM
Chairs: James Head and Clive Neal

1:30 p.m.   Head J. W. III*
Lunar Mare Basalt Volcanism: Stratigraphy, Flux, and Implications for Petrogenetic Evolution

2:00 p.m.   Neal C. R.*
Mare Basalts as Mantle Probes: Dichotomies Between Remotely Gathered and Sample Data?

2:30 p.m.   Discussion
Reconciling (Integrating) Remote Sensing and Sample Studies

3:00 p.m.   *BREAK*

3:15 pm.   Hiesinger H.*   Jaumann R.   Neukum G.   Head J. W. III
Investigation of Lunar Mare Basalts: An Integrated Approach

3:30 p.m.	Gillis J. J.* Spudis P. D. *Differences Observed in Iron Content Between Crater Ejecta and Surrounding Mare Basalt Surfaces: Implications for Sample Remote Sensing Integration*
3:45 p.m.	Gaddis L. R.* Rosanova C. Hawke B. R. Coombs C. Robinson M. Sable J. *Integrated Multispectral and Geophysical Datasets: A Global View of Lunar Pyroclastic Deposits*
4:00 p.m.	Hawke B. R.* Giguere T. A. Lucey P. G. Peterson C. A. Taylor G. J. Spudis P. D. *Multidisciplinary Studies of Ancient Mare Basalt Deposits*
4:15 p.m.	Discussion I *Lunar Basalts and Pycroclastic Deposits*
4:45 p.m.	Discussion II *Wrap-up of Crust, Mantle, and Thermal Evolution — How to Integrate Diverse Approaches and Where to Go from Here*

Sunday, September 20, 1998

GLOBAL RESOURCES, SITE CHARACTERIZATIONS, FUTURE INVESTIGATIONS AND MISSIONS
Chairs: Carl Allen and Cassandra Coombs

8:30 a.m.	Allen C. C.* Weitz C. M. McKay D. S. *Prospecting for Lunar Oxygen with Gamma-Ray Spectrometry and Multispectral Imaging*
8:45 a.m.	Feldman W. C.* Maurice S. Lawrence D. J. Barraclough B. L. Elphic R. C. Binder A. B. *Deposits of Hydrogen on the Moon*
9:00 a.m.	Simpson R. A.* *Radar Search for Water Ice at the Lunar Poles*
9:15 a.m.	Taylor A. G.* Gibbs A. *Automated Search for Lunar Lava Tubes in the Clementine Dataset*
9:30 a.m.	Billings T. L.* Godshalk E. *Probing Lunar Lavatube Caves by Radar Illumination*
9:45 a.m.	Discussion
10:00 a.m.	*BREAK*
10:30 a.m.	Discussion/Wrap-up *Future Directions for the Lunar Initiative; Options for Publication of Workshop-related Papers; Theme Sessions; 30th LPSC; Flagstaff Workshop; "Capstone Publication"; and Issues of "Data Advocacy" and Future Integrated Efforts*
12:00 noon	*ADJOURN*

ABSTRACTS CONTRIBUTED FOR PRINT ONLY

Korotev R. L.
Compositional Variation in Lunar Regolith Samples: Vertical

Korotev R. L.
On the History and Origin of LKFM

Korotev R. L. Morris R. V.
On the Maturity of Lunar Regolith

Abstracts

5/-9/

PROSPECTING FOR LUNAR OXYGEN WITH GAMMA-RAY SPECTROMETRY AND MULTISPECTRAL IMAGING.

C. C. Allen[1], C. M. Weitz[2], and D. S. McKay[3], [1]Lockheed Martin, Houston TX 77258, USA (carlton.c.allen1@jsc.nasa.gov), [2]Jet Propulsion Laboratory, Pasadena CA 91109, USA, [3]NASA Johnson Space Center, Houston TX 77058, USA.

Oxygen is a potentially abundant lunar resource that could be used for life support and spacecraft propulsion. The recent identification by Prospector of ice at the lunar poles has renewed interest in the use of *in situ* O production to supply a future base. Siting a lunar base at any significant distance from the poles, however, would require costly transport of O or its extraction from the local regolith.

More than 20 different processes have been proposed for regolith O extraction [1]. Among the simplest and best studied of these processes is the reduction of oxides in lunar minerals and glass using H gas. Oxides, predominantly those containing FeO, are first reduced; O is then liberated to form water. The water is then electrolyzed to yield O, and the H is recycled to the reactor.

Experiments: Allen et al. [2] reported the results of O extraction experiments on 16 lunar soils and three samples of glassy and crystalline volcanic beads. Each sample was reacted in flowing H for 3 hr at 1050°C.

Total O yield correlated strongly to each sample's initial Fe^{2+} abundance (Fig. 1). A linear-least squares fit of O yield vs. Fe^{2+} for 16 lunar soils yielded a regression line with a slope of 0.19, an intercept of 0.55 wt% O, and an r^2 value of 0.87. Oxygen yield did not significantly correlate with the abundance of any element except Fe.

Apollo 17 volcanic glass sample 74220, composed predominantly of orange glass beads with an average diameter of 40 μm, contains 17.8 wt% Fe^{2+}. Reduction of this sample yielded 4.3 wt% O, well above the regression line defined by the experiments on 16 lunar soils (Fig. 1). Sample 74001, taken >25 cm beneath 74220, is dominated by black crystalline beads, the isochemical equivalent of orange glasses. Reduction of 74001 yielded 4.7 wt% O, the highest value for any of the samples.

Remote Sensing — Iron Abundance: These results show that, if the H reduction method is employed, O yield from a lunar soil can be predicted based solely on its Fe abundance. Therefore, it is possible to assess the potential for O production at any location on the Moon for which the soil's Fe concentration is known.

Gamma-Ray Spectrometry: Iron was one of several elements measured from orbit during the Apollo 15 and 16 missions, using γ-ray spectrometry [3]. These data cover approximately 20% of the lunar surface, with spatial resolutions of ~100 km.

An improved γ-ray spectrometer on Prospector is currently mapping the abundances of Fe, as well as Th, K, U, O, Si, Al, Ca, Mg, and Ti, across almost the entire lunar surface. The resolution element at Prospector's current altitude is 150 × 150 km [4]. Approximately one year of orbital operation will be required to obtain statistically meaningful abundances for all elements.

Multispectral Imaging: A technique for Fe assessment based on orbital multispectral imaging has also been developed [5]. This method correlates Fe abundance to a parameter derived from reflectance values at 750 and 900 nm. The authors use data from the Clementine spacecraft to map Fe abundances across nearly the entire lunar surface. These data can support identification of Fe-rich regions as small as a few hundred meters across at any location on the Moon.

Data Correlation: Clark and McFadden [6] attempted to correlate Clementine multispectral Fe determinations with data from the Apollo γ-ray spectrometer. Within the limited areas of the lunar surface covered by both datasets, they found good agreement for most of the nearside but significant deviations at some farside locations. Publication of the entire Prospector dataset will allow such comparison across nearly the entire Moon. Iron abundances determined by γ-ray spectroscopy can be used to calibrate and refine the multispectral determinations. These data, with high spatial resolution, can then be used with increased confidence to locate small areas of particularly high Fe abundance.

Remote Sensing — Volcanic Bead Deposits: Lunar dark mantle deposits (DMDs), composed of glassy and crystalline volcanic beads, have been studied using telescopic and Apollo orbital photography [7]. Recent Clementine multispectral imagery has been employed to determine the precise extent, crystallinity, and thickness of several DMDs [8,9].

The volcanic beads in each DMD vary in the amount of crystallinity, with dark patches at the Sinus Aestuum site having the highest concentration of crystallized beads and the Aristarchus Plateau DMD dominated by glasses [9]. All the other DMDs fall between these two extremes because they represent intermediate mixtures between the glasses and crystallized beads, and have also undergone more mixing with the surrounding soils.

The DMDs are recognized by their low albedo, and their crystallinity is judged by analogy to the Apollo 17 orange and black glasses. However, these are not the only types of volcanic glass beads recognized on the Moon. Delano [10] identified 25 compositionally distinct types of glass beads in lunar soils. Thin section colors range from green and yellow to orange and red to black, depending on TiO_2 content and crystallinity.
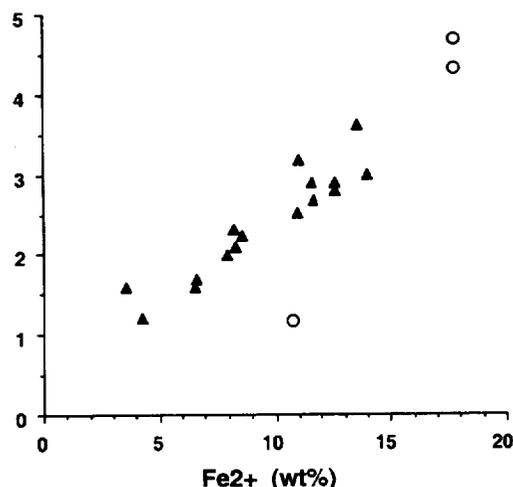

Fig. 1. Correlation of total O yield with initial Fe^{2+} abundance for 16 reduced lunar soils (triangles) and three reduced volcanic bead samples (circles).

No deposits of light-toned volcanic glass, analogous to the DMDs, have been recognized on the lunar surface, and the source vents for most of the 25 glass types are unknown. The combination of TiO_2 concentration data from γ-ray spectrometry, combined with multi-spectral imaging, holds the promise of identifying lunar "light mantle deposits" and locating their eruptive sources.

Volcanic bead deposits represent large volumes of unconsolidated, submillimeter material. Iron-rich beads have been shown to produce more O than other lunar soils when reacted with H. Thus, the deposits could be excellent locations for future lunar bases, both in terms of their scientific potential and their feasibility for maintaining a human presence on the Moon. A recent study by Coombs et al. [11] recommended two sites on the Aristarchus plateau for a future lunar outpost, based on a combination of resource extraction potential and geologic interest.

References: [1] Taylor L. A. and Carrier W. D. III (1992) in *Engineering, Construction and Operations in Space III*, pp. 752–762, Am. Soc. of Civ. Eng. [2] Allen C. C. et al. (1996) *JGR, 101*, 26085–26095. [3] Davis P. A. Jr. (1980) *JGR, 85*, 3209–3224. [4] Feldman W. C. et al. (1996) *LPS XXVII*, 355–356. [5] Lucey P. G. et al. (1995) *Science, 268*, 1150–1153. [6] Clark P. E. and McFadden L. A. (1996) *LPS XXVII*, 227–228. [7] Gaddis L. R. et al. (1985) *Icarus, 61*, 461–489. [8] McEwen M. et al. (1994) *Science, 266*, 1959–1962. [9] Weitz C. M. et al. (1998) *JGR*, submitted. [10] Delano J. (1986) *Proc. LPSC 16th*, in *JGR, 91*, D201–D213. [11] Coombs C. R. et al. (1998) in *Space 98*, pp. 608–615, Am. Soc. of Civ. Eng.

$\mathcal{S} \,\circ\, - \, \mathcal{P}\!/$

RELIABILITY OF CALCULATING AVERAGE SOIL COMPOSITION OF APOLLO LANDING SITES. A. Basu and S. Riegsecker, Department of Geological Sciences, Indiana University, Bloomington IN 47405, USA (basu@indiana.edu).

Lunar soil, i.e., the fine fraction of the lunar regolith, is the ground truth available for calibrating remotely sensed properties of virtually atmosphere-free planetary bodies. Such properties include albedo, IR-VIS-UV spectra, and secondary XRF, which are used to characterize the chemical and mineralogical compositions of planetary crusts [1]. The quality of calibration, however, is dependent on the degree to which the ground truth is represented in the remotely sensed properties. The footprints and spatial resolution of orbital and Earth-based observations are much larger than the sampling areas at the landing sites. Yet an average composition of soils at each landing site is our best approximation for testing calibration.

Previously, we have compiled chemical compositions of lunar soils and estimated the best average composition (CC) for each landing site (Table 7.15 in [2]). We have now compiled and estimated the best average mineralogical composition (MC) of soils (90–150-μm fraction) at each Apollo landing site [3]. In this paper, we examine how these two estimates (Tables 1 and 2) compare and how representative they may be. For the purpose of comparison, we have calculated the normative mineralogy of each site (from Table 1) and recast them on a quartz-apatite-pyrite-free basis, i.e., in terms of feldspar, pyroxene, olivine, and ilmenite + chromite (Table 3).

The modal composition is calculated on a glass-regolith breccia-agglutinate-free basis (GRA-free) on the assumption that they represent the mineralogy of the soils. The chemical composition, however, is that of the bulk. Thus, unless the chemical composition of mineral

and rock fragments (MRF) is identical to that of the GRA fraction of the soils, there would be a difference between CC and MC. Regolith breccias and agglutinates consist of mineral and rock fragments cemented together, the populations of which are not likely to be much different from those in the soils. Chemical analyses of agglutinate separates, however, show a distinct shift from the average composition of the soils to its finer sized-fractions [4]. This shift is small, and the composition of agglutinitic glass may be statistically indistinguishable from the composition of the bulk soil [5]. The composition of glass, on the other hand, is very different from bulk soil compositions. Common but specialized glass types (green, orange, black, and colorless) show a wide variation in their chemical compositions. Modal abundance of glass fragments of most lunar soils, however, is less than 5%. Therefore, unless a soil is made up mostly of glass (e.g., 74220), the composition of a soil should not be significantly different from the composition of its MRF.

Yet, normative and modal compositions are different (Table 4). Several factors may be responsible for the observed deviation. First, it is possible that the modal composition of the 90–150-μm fraction of lunar soils does not represent the bulk, the composition of which is more similar to that of a feldspar-rich finer fraction. Second, the assumption that the composition of GRA of a soil is not significantly different from that of its MRF is not valid despite the reasons given above. Third, modal proportions of mare and highland rocks (Table 3 in [3]) may be based on insufficient and non-representative data, which may have compromised the modal estimate (Table 2). Finally, CIPW norm calculation is not appropriate for deriving standardized mineralogy from lunar soil compositions.

The geographic distribution of soil samples from the landing sites was based on sampling ease, perceived variations in soil types, and location with respect to surface morphology and albedo to maximize representation of diversity. Thus, there is an inherent sampling bias against obtaining an average composition of a site from soil samples. Moreover, lunar soils rarely mimic the composition of lunar rocks (p. 345 in [2]).

We therefore conclude that (1) the average composition of Apollo landing sites is still poorly known, and (2) the task of inferring bedrock composition of a pixel of the Moon from remotely sensed properties is complicated. The latter requires filtering many layers of modification of bedrock material imposed by lunar surface processes and accepting the best averages of the time (Tables 1 and 2).

TABLE 1.   Average chemical composition of lunar soils at Apollo landing sites.

	A 11	A 12	A 14	A 15	A 16	A 17
SiO_2	42.2	46.3	48.1	46.8	45.0	43.2
TiO_2	7.8	3.0	1.7	1.4	0.54	4.2
Al_2O_3	13.6	12.9	17.4	14.6	27.3	17.1
Cr_2O_3	0.3	0.34	0.23	0.36	0.33	0.33
FeO	15.3	15.1	10.4	14.3	5.1	12.2
MnO	0.2	0.22	0.14	0.19	0.3	0.17
MgO	7.8	9.3	9.4	11.5	5.7	10.4
CaO	11.9	10.7	10.7	10.8	15.7	11.8
Na_2O	0.47	0.54	0.70	0.39	0.46	0.40
K_2O	0.16	0.31	0.55	0.21	0.17	0.13
P_2O_5	0.05	0.40	0.51	0.18	0.11	0.12
S	0.12			0.06	0.07	0.09
Total	99.9	99.1	99.8	100.8	100.8	100.1

TABLE 2. Average mineralogic composition of
lunar soils at Apollo landing sites.

	Feld	Oliv	Pyrx	Opq
A 11	26.7	3.2	53.7	16.3
A 12	23.0	8.7	63.4	4.9
A 14	49.7	1.8	47.0	1.5
A 15	37.9	8.4	52.2	1.5
A 16	69.0	2.6	28.2	0.1
A 17	35.5	5.5	56.3	2.7

TABLE 3. Normative composition of lunar soils
at Apollo landing sites.

	Feld	Oliv	Pyrx	Opq
A 11	39.6	0.0	44.8	15.6
A 12	53.8	0.0	39.8	6.4
A 14	52.9	0.0	43.5	3.6
A 15	41.9	10.1	44.7	3.3
A 16	76.4	7.8	14.1	1.6
A 17	48.7	11.2	31.5	8.6

TABLE 4. Percent deviation (modal – normative).

	Feld	Oliv	Pyrx	Opaq
A 11	–48	100	17	5
A 12	–134	100	37	–31
A 14	–6	100	7	–141
A 15	–10	–20	14	–114
A 16	–11	–197	50	–1074
A 17	–37	–103	44	–222

References: [1] Lucey et al. (1995) *Science, 268,* 1150–1153. [2] Heiken et al. (1991) *Lunar Sourcebook,* Cambridge Univ., 736 pp. [3] Riegsecker et al., this volume. [4] Papike et al. (1982) *Rev. Geophys. Space Phys., 20,* 761–826. [5] Hu and Taylor (1978) *View from Mare Crisium,* 291–302.

PROBING LUNAR LAVA-TUBE CAVES BY RADAR IL-LUMINATION.

T. Billings and E. Godshalk, Oregon L5 Society, P.O. Box 42467, Portland OR 97242-0467, USA (itsd1@teleport.com; edg@mixim.com).

A Radar Flashbulb on the Moon: Lava-tube caves under the lunar surface may be very useful as lunar base sites. They have left surface indicators that can be found in computerized searches of the Clementine data. Such a search is being put together by the Lunar Base Research Team (LBRT) of the Oregon L-5 Society, Portland's local chapter of the National Space Society.

Lava-tube sites that are located will need to undergo further investigation before committment to a lunar base can be made. Ground-penetrating radar images of actual voids at particular sites would seem to be the next step, if images can be obtained cheaply. This paper describes what LBRT believes is the cheapest combination of technologies that can obtain such images of lava-tube voids on the Moon.

As early as the Apollo Lunar Sounder Experiment, radar has penetrated the Moon to substantial depths. Only soundings were possible, given the combination of penetrating wavelengths (1–20 m) and the aperture of any antenna that could be carried by the Apollo Service Module. Now, operation of the Very Long Baseline Array (VLBA) by NRAO provides an aperture that, even from the Earth, could provide a resolution of 25–50 m at the lunar surface with wavelengths of 0.5–1 m. The *Lunar Sourcebook* notes that much of the lunar surface is rather transparent to radio waves, because of its low conductivity and lack of water. Lava-tube surface indicators have been found in Apollo photos for caves up to 1100 m across. But where is the radar energy reflecting off the walls of these lava-tube voids to come from?

The fourth power range coefficient in the denominator of the Radar Equation makes this extremely costly if the rf source is on Earth. Likewise, transport of a powerful rf source to lunar orbit is beyond any present budgetary reality. However, if we are investigating only the immediate areas around sites found by the Clementine data search, then a very localized rf source, of appropriate power and wavelength, becomes useful. Such a localized source would give a signal/noise ratio governed by a second power range coefficient in the Radar Equation. This factor, combined with the resolution of the VLBA, may make a low-cost mission possible.

We propose that unconventional rf sources could be placed close to some lava-tube sites located by lunar surface indicators for far less than an orbiting rf source. A free-falling object launched from Earth would posess much kinetic energy at the lunar surface. Converting a large portion of that kinetic energy to rf energy is possible with a two-part probe shaped like two extended concentric metal cylinders that slide past each other as the forward cylinder's end strikes the lunar surface. By allowing a strong magnetic field to brake the rearward cylinder's motion, very large electrical currents can be generated in the second cylinder. These large currents would have to be conditioned and turned into appropriate wavelength rf energy, then radiated into the local lunar surface very rapidly.

Other conversion schemes are possible, including those using changes in electrical fields or the compression of an rf standing wave of the desired frequency inside a resonant superconducting cavity. We believe that the magnetic field system can be demonstrated first.

At a 2.35 km/s impact speed, the probe would have <1/1000 of a second to "flash" the lunar surface with rf energy before the transmitter and power conditioners at the back of the probe smash into the surface themseves. If it can "flash" successfully, then the rf energy can penetrate the dry lunar surface, reflecting off large discontinuities within the lunar material, including the voids of lava-tube caves in the local area.

That rf signal would bounce back to Earth and be picked up by the receivers of the VLBA. Processing of the received signal should allow us to discern which local sites do in fact have lava-tube caverns and characterisics such as overburden, width, depth, and length. Characteristics such as ice within the lava tubes might be determined by sophisticated analysis. Lava-tube ice caves are common in the Pacific Northwest.

The mass of the probe will be determined by the energy requirements for penetration at a given wavelength and for reception at the VLBA, as well as the total efficiency of conversion from kinetic energy to rf energy. Each probe's "flash" may be able to illuminate strata for as much as a few kilometers around the probe impact site. This may allow several voids to be confirmed, or even newly found,

from one probe. The observation time for the VLBA will be short enough to not intrude much on the normal VLBA observation schedule. This should allow small enough "flashbulb" probes to be sent along with other lunar missions on a "mass-budget available" basis.

If a special lunar mission is set aside for these probes, timing of individual impacts might be made provisional by selecting a figure-8 trajectory passing close to both Earth and the Moon that would return the spacecraft "bus" to a release window once each month. Kicking the next small probe out at a slightly different time, with a slightly different push during that window, could change the impact point on the Moon and allow a wide range of sites on the Moon to be sampled by these probes. If there is sufficient excess capability available on a commercial launch, a small package with its own booster might "piggyback" to GTO. From there the ΔV requirements for lunar impact are much reduced. Multiple launch opportunities might be available over some years for a continuing program of exploration with this basic flight concept.

When sites ouside the Moon's nearside features are to be investigated, a phase II sensor array might be made available using arrays of small "nanosats" in a free-flying radar interferometer. If an array is to serve many seperate "flashbulb" illuminations of the Moon, Mercury, or even Mars, then an array of long-term satellites would be appropriate. If a "single-shot" opportunity is being taken at one target on the Moon, or on a near-Earth asteroid, then very small devices making up an array may be viable. In each case, the smaller range to the target will allow greater resolution for the same wavelength, as well as new opportunities.

$5\mathcal{Y} - 9/$

LUNAR IMPACT BASINS: PROBES INTO THE LUNAR CRUST. D. B. J. Bussey[1] and P. D. Spudis[2], [1]European Space Agency/ESTEC, Code SCI-SO, Postbox 299, 2200 AG Noordwijk, The Netherlands (bbussey@estec.esa.nl), [2]Lunar and Planetary Institute, 3600 Bay Area Boulevard, Houston TX 77058, USA.

Impact basins excavate large regions of the lunar crust, bringing rocks from great depths up to the surface for examination. Clementine's UVVIS camera mapped the Moon globally in five different wavelengths (415, 750, 900, 950, and 1000 nm). We have used the full resolution data (250 m/pixel) to undertake a systematic study of the Moon's impact basins. Analysis of the ejecta blankets of basins on both the lunar nearside and farside has allowed us to map the compositionally distinct units associated with the basins. We have constructed both multispectral images and quantitative Fe and Ti maps. Thus, we can use basins as probes into the lunar crust and build up a 3-D reconstruction of the crust. The basins covered so far are Orientale, Humboldtianum, Humorum, Nectaris, Crisium, and parts of the Imbrium Basin.

The 900-km-diameter Orientale Basin was chosen for study as it is the youngest, best-preserved large basin on the Moon. Our research has shown that the basin ejecta units are largely homogeneous and feldspathic in composition with the Montes Rook Formation being slightly more mafic than both the Maunder and Hevelius Formations. The presence of outcrops of pure anorthosite, associated with the scarps of the Inner Rook mountain ring, has been confirmed, and the amount of anorthosite present is far more than previously suspected. These appear as dark blue regions in the multispectral image and as places with very low (<2 wt%) FeO concentrations in the Fe map.

Humorum is a Nectarian-aged multiring basin located on the western nearside. The Clementine data show that the highlands around Humorum Basin are feldspathic, but somewhat more mafic than the deposits of other basins (compare with Orientale). The western basin deposits appear to be slightly more feldspathic than those to the east. As seen in most of the other basins studied, peaks along the inner mare bounding ring of Humorum have extremely low FeO contents and appear dark blue in the multispectral image. These zones correspond to areas for which previously obtained telescopic spectral data had indicated no mafic absorption and had been interpreted to be deposits of pure anorthosite. Most of the outcrops seen are located on the 425-km-diameter ring of Humorum, suggesting, as at Orientale and Crisium, that this is an inner ring. This would make the 800-km-diameter ring the true topographic ring for the basin, something that had previously been in doubt. The mare deposits of central Humorum show FeO contents between 16 and 20 wt%. Some small craters within Mare Humorum appear to have excavated material with lower FeO content. It therefore may be possible to use these craters to put constraints on the thickness of the flows that make up Mare Humorum.

Work has begun on analyzing the Imbrium Basin, starting with the Apennine region in the southeastern part of Imbrium. Imbrium, the largest well-preserved basin on the Moon, has three main ejecta units. The Apenninus and Fra Mauro Formations occur in the southeast and northwest portions of the basin, while the main ejecta blanket in the northeast and southwest is represented by the Alpes Formation. The Apenninus material has Fe of 8–12 wt% and appears to be basaltic highland material, the numbers being consistent with LKFM composition that has previously been proposed as the dominant Imbrium ejecta type. The Alpes Formation at the northern end of the Apennine Mountains also appears to have similar Fe content, although with possibly a lower Ti value. There are a number of feldspathic deposits associated with the Apennine back slope. Clearly the dominant feldspathic area is associated with the crater Conon. Its ejecta is in the 2–6 wt% FeO range, indicating that it is in the noritic anothosite, norite category. The thickness of Imbrium ejecta in this region is probably about 3 km. Therefore it is likely that Conon punched through the ejecta deposit and we are looking at pre-Imbrium material. In fact, feldspathic outcrops are associated with massifs all along the rim crest as well as a number of small craters that have probably punched through the Imbrium ejecta blanket. However, there are still areas on the backslope that have FeO in the <8 wt% range that can't be associated with Conon, possibly indicating that some of the Imbrium ejecta is more feldspathic. Our results show the Apennine bench formation to be similar in composition to the Apollo 15 KREEP basalts with FeO in the 8–12 wt% range (12–14 wt% locally). One thing worthy of note is the lack of anorthositic outcrops in this region. In all previous basins studied, we see anorthosite associated with inner rings. This may indicate that crustal composition with depth is different here, or that Imbrium excavated the entire crustal column.

Analysis of the composition of basin ejecta deposits has allowed us to build up a three-dimensional picture of the lunar crust. Our findings to date support the idea of a three-layer crust. A mixed zone (megaregolith) a few tens of kilometers thick lies above a region of pure anorthosite, representing the primordial crust (this layer is not contiguous over the whole Moon, e.g., it appears to be absent at Imbrium, which may have excavated the entire crustal column), overlying a more mafic basaltic layer.

References: [1] Nozette S. et al. (1994) *Science, 266,* 1835. [2] Bussey D. B. J. and Spudis P. D. (1997) *GRL, 24,* 445–448. [3] Bussey D. B. J. and Spudis P. D. (1996) *Fall AGU Eos Suppl.,* F448–F449. [4] Bussey D. B. J. et al. (1997) *LPS XXVIII.* [5] Bussey D. B. J. et al. (1997) *Meteoritics & Planet. Sci., 32,* A25. [6] Spudis P. D. et al. (1997) *LPS XXVIII.* [7] Bussey D. B. J. et al. (1998) *LPS XXIX.*

INTEGRATING RADAR, MULTISPECTRAL, AND LANDING SITE DATA FOR ANALYSIS OF THE LUNAR SURFACE.

B. A. Campbell[1], D. B. Campbell[2], T. W. Thompson[3], and B. R. Hawke[4], [1]Smithsonian Institution, MRC 315, Washington DC 20560, USA (campbell@ceps.nasm.edu), [2]Cornell University, Ithaca NY, USA, [3]Jet Propulsion Laboratory, Pasadena CA, USA, [4]University of Hawai'i, Honolulu HI, USA.

Introduction: Radar maps of the Moon have been produced since the late 1960s, and have been used by a number of authors to study the surface roughness, subsurface rock abundance, and dielectric properties of the lunar surface [e.g., 1–3]. These studies focused on a range of topics, including the depth and rock population of the regolith, crater ejecta blankets, pyroclastic mantling layers, and cryptomare deposits. Limited radar sounding data from the Apollo missions identified layering in some regions of the maria [4]. As radar datasets have improved in resolution and calibration, it has become more possible to make quantitative comparisons between the backscatter properties of the Moon, other remote-sensing observations, and the ground truth provided by Surveyor photos and Apollo traverses. This presentation will focus on the results of recent studies of the lunar regolith that make use of these diverse sources of information, and discuss research directions that will be possible with radar data to be collected in the near future.

Regolith Properties: The lunar regolith is a mixture of fine soils and rocks formed by repeated impacts from the original "bedrock" of the maria and highlands. In the maria, this basal layer is clearly basalt flow surfaces, while in the highlands the presence of deep ejecta layers from the formation of giant basins implies a jumbled megaregolith of large crustal blocks. In neither case is the rock population with depth and the transition from regolith to substrate well understood. The depth of the regolith is inferred to be shallower on younger mare surfaces, with a greater abundance of surface rocks derived from impacts that penetrate the thin soil veneer. Radar observations can provide a tool for sounding the regolith to depths of several meters or more, and in conjunction with other datasets may permit mapping of regolith chemical properties and rock abundance (i.e., relative age).

Recent comparison of 70-cm wavelength radar data with multispectral estimates of Fe and Ti abundance shows that the microwave loss tangent of the fine soil is likely most dependent upon the Ti present as ilmenite, with no apparent control by the abundance of Fe in pyroxenes or other minerals [5]. The 70-cm data were also found to vary with the estimated age of the mare surface and the thermal eclipse brightness, both of which are linked to the surface rock abundance. The backscatter echoes were compared to those predicted by a simple Mie scattering model for the rock populations seen at various Surveyor landing sites, which showed that single scattering by buried rocks is a reasonable mechanism for producing the observed return. There are also anomalous radar signatures for parts
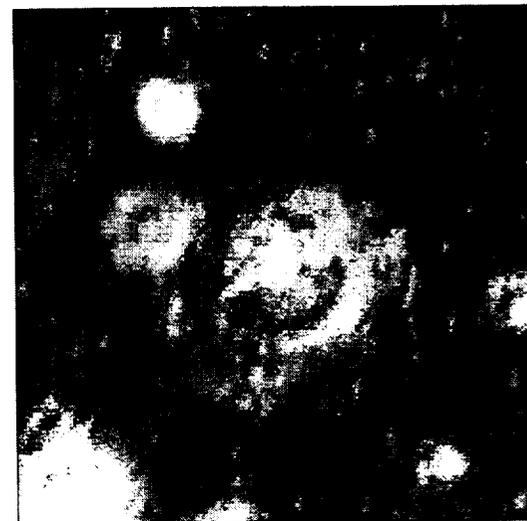
Fig. 1. Clementine visible-wavelength view of Petavius Crater (top), and 70-cm radar image of the same area. Note the halo of low radar return surrounding the crater rim.

of the terrae, including the Montes Jura [3] and a decline in 70-cm echo from west to east in the southern highlands. These changes in radar properties may be linked to compositional shifts in the highland regolith or to differences in the volumetric rock population with changing distance from the youngest large basins.

Future Arecibo high-resolution mapping at 70-cm wavelength, planned for late 1998, will permit these various analyses to be refined. Combining 70-cm and 12-cm radar data with multispectral estimates of Ti abundance and ground-truth rock counts may permit separation of the rock abundance and loss tangent effects, leading to robust estimates of mare age. We are also planning a study of possible terrestrial analog terrains, such as lithic fragments in volcanic ash layers, using the P-band AIRSAR data and possibly ground-penetrating radar. Analysis of the polarization properties and changes in the highland regolith will be used to infer possible compositional changes or variations in rock population due to large basin ejecta.

Crater Floors and Ejecta Blankets: The distribution of fine and coarse ejecta around a crater is linked to the properties of the original target and the age of the impact. Over time, the rough texture of the crater floor is reduced by regolith formation, and larger rocks in the ejecta blanket are broken down by much smaller impacts. These characteristics have been the topic of previous radar studies [e.g., 6].

We have observed a number of low radar-return halos about large craters in the highlands, which imply a layer of material either of higher loss tangent or lower rock abundance than the typical regolith. Figure 1 shows an example for the crater Petavius. Current work focuses on characterizing the variations in composition with distance from the crater rim with multispectral data, as these results will narrow the range of possible origins for the dark halos. We also plan to study the floor texture of large craters with new 70-cm data, and to compare the differences in roughness to the estimated age of these impacts as a guide to regolith formation on rugged impact melt deposits (e.g., Tycho).

Pyroclastic Deposits: Local and regional pyroclastic mantling layers have been studied using combined remote sensing datasets by a number of authors. These fine-grained deposits of glassy beads, likely formed during volcanic fire fountaining, are typically very smooth-surfaced and have high microwave loss tangents [7]. The result is a low backscattered signal even at short (3.8 cm) wavelengths. These layers have been suggested as readily accessible lunar resources, so it is important to map their depth and areal extent. Radar data at 70-cm wavelength have been used to estimate the depth of the Aristarchus Plateau materials, and higher-resolution data should permit the extension of such studies to more localized pyroclastics [8]. We also plan to test the depth-mapping technique with AIRSAR 68-cm data in areas of cinder cover on terrestrial volcanos.

References: [1] Zisk S. H. et al. (1974) *Moon, 10,* 17–50. [2] Thompson T. W. et al. (1970) *Radio Science, 5,* 253–262. [3] Thompson T. W. (1978) *Icarus, 36,* 174–188. [4] Sharpton V. L. and Head J. W. (1982) *JGR, 87,* 10983–10998. [5] Campbell B. A. et al. (1997) *JGR, 102,* 19307–19320. [6] Thompson T. W. et al. (1979) *Moon Planets, 21,* 319–342. [7] Gaddis L. R. et al. (1985) *Icarus, 61,* 461–489. [8] Campbell B. A. et al. (1992) *LPI Tech. Rpt. 92-06,* 16–17.

ANOTHER LOOK AT TAURUS LITTROW: AN INTERACTIVE GEOGRAPHIC INFORMATION SYSTEM DATABASE.   C. R. Coombs, J. L. Meisburger, and J. W. Nettles, College of Charleston, 66 George Street, Charleston SC 29464, USA.

Introduction: A variety of data has been amassed for the Apollo 17 landing site, including topography, sample locations, and imagery. These data were compiled into a Geographic Information System (GIS) to analyze their interrelationships more easily. The database will allow the evaluation of the resource potential of the Taurus Littrow region pyroclastic deposits. The database also serves as a catalog for the returned lunar samples. This catalog includes rock type, size, and location. While this project specifically targets the Taurus Littrow region, it is applicable to other regions as well.

What is a GIS? A GIS is a computer system capable of capturing, storing, analyzing, and displaying geographically referenced information in two or more dimensions (Fig. 1). A GIS package acts as both a data collator and spatial analyzing system, allowing one to

easily query the entire set of spatially-registered data (e.g., local topography, sample sites, Apollo EVA "roadmaps," and photography at various resolutions and spectral ranges). Each type of data is stored as a separate, "transparent" layer, allowing a wide variety of spatial analyses. This greatly enhances our ability to identify and further investigate underlying relationships and trends that would otherwise be difficult to recognize. Once completed, one can answer a number of questions: How do the size and location(s) of the source vent(s) compare to the size of the deposit? How does the composition/spectra vary within a deposit? How does one deposit compare to another? Often, when all available data are included in a GIS, relationships that were never before envisioned become apparent. The potential of a GIS is only limited by the data available and one's imagination. Several computer programs were used to create and compile these GIS packages, including ArcView and ENVI.

Lunar Pyroclastic Deposits: Explosive volcanic, or pyroclastic, materials are unique phases in the lunar soils and are important as they hold clues to the history of lunar volcanism. Pyroclastic glasses, among the most primitive of lunar rocks, originate from depths as great as 400 km [1]. Earth-based telescopic studies have provided most of our information concerning lunar pyroclastic deposits. Based on their unique spectral signatures, two major classes and five subclasses of these deposits have been identified. Regional deposits are more numerous, extensive, thicker, and widely distributed than previously thought, suggesting that they may exhibit distinct compositional variations and that they would provide ideal resource materials for a lunar base [e.g., 2–5]. Returned sample studies and the recently collected Galileo and Clementine data corroborate these findings [e.g., 6–7].

Example — Taurus-Littrow/Apollo 17: Located in the southeastern portion of Mare Serenitatis, the Taurus-Littrow dark mantle deposit covers more than 4000 km² and varies in thickness from 10 to 30 m. This deposit is uniformly fine grained and friable, offering a feedstock that reacts rapidly and can be used with little or no processing. Laboratory analyses of Fe-rich samples represented by the orange glasses collected at this site yielded the highest percentage of O of any lunar sample, supporting its potential as an excellent resource material [e.g., 8–9]. Such a pyroclastic deposit could be a prime candidate for a future lunar O plant, particularly with the high FeO abundance.
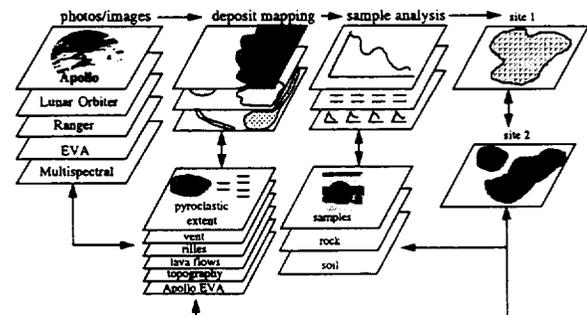

Fig. 1. A schematic of a Geographic Information System (GIS) for a lunar pyroclastic deposit. Transparent data layers are user defined and may be combined in a variety of ways to provide the best assessment and visualization possibilities for a particular query.
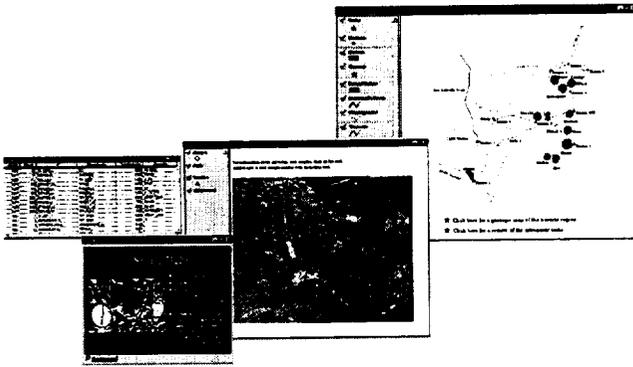
Fig. 2. An example of the Taurus-Littrow GIS. The user can select a site and search for information on samples collected, data acquired, sample location, size, and more.

Lunar Pyroclastic Geographic Information System: To better determine the potential of this resource deposit, a GIS was generated to facilitate data analysis and comparison. Data layers in this GIS package include Apollo 17 surface photographs, panoramic views, and the more recent topographic, geologic, and EVA maps (Fig. 2). Also included were returned sample laboratory analyses and images. Although still in its infancy, the Lunar Pyroclastic GIS has permitted better visualization of the relationship(s) between deposit extent, sample locations, and compositional variation. When completed, the Lunar Pyroclastic GIS will permit comparisons between the different pyroclastic deposits and expedite their evaluation as a potential resource.

Future Work: The current Taurus-Littrow GIS will be expanded to include publication information, sample analysis results. This information will also be available on the Internet.

References: [1] Delano J. D. (1986) *Proc.LPSC 16th*, in *JGR*, *91*, D201–D213. [2] Coombs C. R. (1995) *NASA JSC SP-95*. [3] Coombs C. R. and Hawke B. R. (1995) *LPS XXVII*, 277–278. [4] Coombs C. R. (1988) Ph.D. dissertation, Univ. Hawai'i. [5] Hawke et al. (1989) *Proc. LPS 20th*, 249–258. [6] Greeley et al. (1993) *JGR*. [7] McEwen et al. (1994) *Science, 266*, 1858–1862. [8] Allen et al. (1995) *JGR, 99*, 23173–23195. [9] Allen and McKay (1995) *AIAA Paper 95-2792*.

EXPLORATION OF THE MOON WITH REMOTE SENSING, GROUND-PENETRATING RADAR, AND THE REGOLITH-EVOLVED GAS ANALYZER (REGA). B. L. Cooper[1], J. H. Hoffman[2], C. C. Allen[3], and D. S. McKay[4], [1]Oceaneering Space Systems, 16665 Space Center Boulevard, Houston TX 77058, USA (bcooper@oss.oceaneering.com), [2]Center for Space Studies, University of Texas at Dallas, P.O. Box 830688, Richardson TX 75083-0688, USA (jhoffman@utdallas.edu), [3]Lockheed Martin, Houston TX 77058, USA (carlton.c.allen1@jsc.nasa.gov), [4]NASA Johnson Space Center, Houston TX 77058, USA (mckay@snmail.jsc.nasa.gov).

Introduction: There are two important reasons to explore the Moon. First, we would like to know more about the Moon itself —

its history, its geology, its chemistry, and its diversity. Second, we would like to apply this knowledge to a useful purpose, namely finding and using lunar resources.

As a result of the recent Clementine and Lunar Prospector missions, we now have global data on the regional surface mineralogy of the Moon, and we have good reason to believe that water exists in the lunar polar regions. However, there is still very little information about the subsurface. If we wish to go to the lunar polar regions to extract water, or if we wish to go anywhere else on the Moon and extract (or learn) anything at all, we need information in three dimensions — an understanding of what lies below the surface, both shallow and deep.

The terrestrial mining industry provides an example of the logical steps that lead to an understanding of where resources are located and their economic significance. Surface maps are examined to determine likely locations for detailed study. Geochemical soil sample surveys, using broad or narrow grid patterns, are then used to gather additional data. Next, a detailed surface map is developed for a selected area, along with an interpretation of the subsurface structure that would give rise to the observed features. After that, further sampling and geophysical exploration are used to validate and refine the original interpretation, as well as to make further exploration/ mining decisions. Integrating remotely sensed, geophysical, and sample datasets gives the maximum likelihood of a correct interpretation of the subsurface geology and surface morphology.

Apollo-era geophysical and automated sampling experiments sought to look beyond the upper few microns of the lunar surface. These experiments, including ground-penetrating radar and spectrometry, proved the usefulness of these methods for determining the best sites for lunar bases and lunar mining operations.

Ground Penetrating Radar (GPR): A unique experiment was conducted during the Apollo 17 mission, in which radar data were collected from an orbital platform [1]. The results, although difficult to interpret at the time, nevertheless show that radar is an ideal geophysical method on the Moon. More recent interpretations of the data suggest the presence of layering in Maria Serenitatis and Crisium [2], plutonic intrusions below floor-fractured craters, and the existence of layering in the megaregolith of the highlands [3]. The radar data have also been used to support the hypothesis of the graben origin of the Procellarum Basin [4].

Depending on the wavelength of radar that is used, various depths of the subsurface can be explored. The highest frequencies allow detailed exploration of the shallow subsurface, while lower frequencies give less detailed, but deeper, information. For lunar base construction, one might wish to explore the upper 10–20 m of the regolith for areas that are free of boulders. Areas such as Sulpicius Gallus are thought to contain substantial amounts of loosely consolidated glass that are relatively free of boulders [5]. If these properties are verified by ground-penetrating radar (GPR), then the Sulpicius Gallus formation would be ideal for excavation for shielding of habitats, as well as for extraction of useful resources [6]. Moreover, other regions are known from the Clementine data to be likely candidates for pyroclastic deposits similar to Sulpicius Gallus. Low-orbiting spacecraft, equipped with radar sounding equipment, could rapidly characterize these regions and select the best candidates for follow-up robotic-rover exploration.

Another important use of GPR will be to search for and evaluate lava tubes. A global survey from low altitude of the shallow (<100 m) subsurface would provide definitive information on the existence
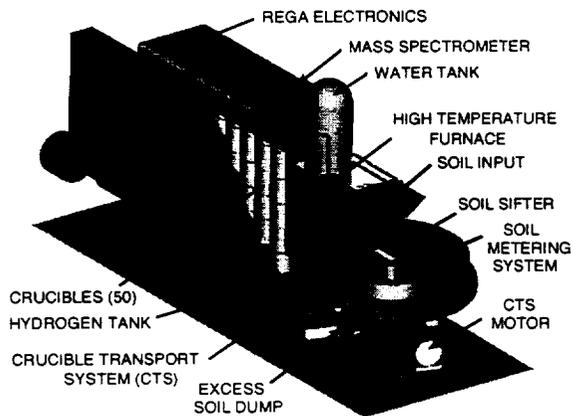
Fig. 1.   REGA instrument preliminary design (enclosures removed).

and location of these interesting and potentially useful structures. However, space weathering, including meteorite bombardment, may have weakened the roof section of a lava tube to such an extent that it would be dangerous to enter or occupy it. The upper 5–10 m of any lava roof has probably been eroded by micrometeorite impact into a fine-grained lunar soil [7]. Cracks associated with this regolith are probably 3–5× deeper than the surface weathering [8] — in other words, 15–50 m. After a lava tube has been located by low-orbit GPR, rover-mounted, high-resolution units can be used to determine the structural integrity of the roof section.

Mass Spectrometers and the Regolith-Evolved Gas Analyzer (REGA):   A mass spectrometer was placed on the surface during the Apollo 17 mission. It provided data on the distributions of many types of rarefied gases, including ^{40}Ar and ^4He [9]. A similar instrument, in combination with a furnace, is currently being developed as protoflight hardware. The Regolith Evolved Gas Analyzer (REGA) [10], is a high-temperature furnace and mass spectrometer instrument for measuring and determining the reactivity and mineralogical composition of soil samples. This instrument, mounted on a rover, would perform the equivalent of a soil sample survey, with the benefit of being able to analyze the samples *in situ* rather than collecting and returning them to a laboratory.

REGA, as shown in Fig. 1, is capable of conducting a number of direct soil measurements, which are unique to this instrument, that will complement ground-penetrating radar data and lead to new insights and discoveries about the lunar surface and subsurface. Soil experimental measurements include:

◆ Evolved gas thermal analysis (e.g., CO_2, SO_2, and H_2O) of heated lunar soil samples from ambient temperature to 900°C

◆ Reactivity of soil samples exposed to water or H

◆ Identification of liberated chemicals, e.g., O, S, Cl, and Fl

The primary components include a flight-tested mass spectrometer, a high-temperature furnace, a microcontroller, and a soil sampling system.

A drill or other device mounted on the rover would be used to collect samples from a few centimeters below the surface, which would provide valuable information about the differences between surface and near-surface soil properties. From these data, it would be possible to model the soil properties at greater depths.

Conclusion: The combination of geophysical and sampling experiments described above will provide useful information in

several areas of interest to lunar geologists and future lunar inhabitants. Exploration of the lunar subsurface, in combination with a soil sample survey using the REGA instrument on a robotic rover, will improve our ability to define and quantify lunar resources.

References: [1] Phillips et al. (1973) *Apollo 17 Preliminary Science Report*, NASA SP-330, pp. 22.1–22.26. [2] Sharpton V. L. and Head J. W. III (1982) *JGR, 87*, 10983–10998. [3] Cooper B. L. and Carter J. L. (1993) *LPS XXIV.* [4] Cooper B. L. et al. (1994) *JGR, 99*, 3799–3812. [5] Hawke B. R. et al. (1994) *Proc. LPSC 20th*, 249–258. [6] Cooper B. L. (1994) in *Space 94: Engineering, Construction and Operations in Space*, pp. 889–896, American Society of Civil Engineers, New York. [7] Hörz F. (1985) *Lunar Bases and Space Activities of the 21st Century*, 405–412. [8] Pohl et al. (1977) in *Impact and Explosion Cratering*, 343–404, Pergamon, New York. [9] Hoffman J. H. et al. (1973) *Apollo 17 Preliminary Science Report*, NASA SP-330, 17-1. [10] McKay D. S. and Allen C. C. (1996) in *Engineering, Construction, and Operations in Space V*, pp. 673–679, American Society of Civil Engineers, New York.

MULTISPECTRAL MAPPING OF THE MOON BY CLE-MENTINE.   E. Eliason[1], A. McEwen[2], M. Robinson[3], P. Lucey[4], T. Duxbury[5], E. Malaret[6], C. Pieters[7], T. Becker[1], C. Isbell[1], and E. Lee[1], [1]U.S. Geological Survey, 2255 North Gemini Drive, Flagstaff AZ 96001, USA, [2]University of Arizona, 1629 East University Boulevard, Tucson AZ 85721-0092, USA, [3]Department of Geological Sciences, Northwestern University, 1847 Sheridan Road, Locy Hall 309, Evanston IL 60208-2150, USA, [4]Hawai'i Institute of Geophysics and Planetology, University of Hawai'i, 2525 Correa Road, Honolulu HI 96822, USA, [5]Mail Stop 301-429, Jet Propulsion Laboratory, 4800 Oak Grove Drive, Pasadena CA 91109, USA, [6]ACT, 112 Elden Street, Suite K, Herndon VA 22070, USA, [7]Department of Geological Sciences, Brown University, Box 1846, Providence RI 02912, USA.

Introduction: One of the chief scientific objectives of the Clementine mission at the Moon was to acquire global multispectral mapping [1,2]. A global digital map of the Moon in 11 spectral bandpasses and at a scale of 100 m/pixel is being produced at the U.S. Geological Survey in Flagstaff, Arizona. Near-global coverage was acquired with the UVVIS camera (central wavelengths of 415, 750, 900, 950, and 1000 nm) and the NIR camera (1102, 1248, 1499, 1996, 2620, and 2792 nm). We expect to complete processing of the UVVIS mosaics before the fall of 1998, and to complete the NIR mosaics a year later. The purpose of this poster is to provide an update on the processing and to show examples of the products or perhaps even a wall-sized display of color products from the UVVIS mosaics.

Geometry: Global mosaics at 750 nm were completed in 1996 and written to a set of 15 CD-ROMs. We estimate that the map achieved better than 0.5 km absolute positional accuracy everywhere on the Moon except for the highly oblique gap fills (~1% of the surface). The basemap is partitioned into 14 geographic zones with each zone filling a CD. Twelve zones, each 30° wide in longitude and ranging from 70°S to 70°N, make up the mid-latitude regions (CD volumes 2–13). The two polar zones cover 360° of longitude from 70° latitude to the pole (CD volumes 1 and 14). The geographic zones are further divided into "tiles." Each tile covers ~7° of latitude with longitude coverage of ~6° at the equatorial regions to larger longitude coverage at higher latitudes. The 966 tiles are stored as image

files of ~2100 pixels on a side. A 15th volume contains reduced-resolution planetwide coverage at 0.5, 2.5, and 12.5 km/pixel. "Backplane" data files for emission, incidence, and phase angle values are also present on volume 15. A software tool called MapMaker is available to extract mosaics of any desired area and scale from the tiles. For more information on obtaining the Clementine Basemap Mosaic and the MapMaker software, contact the Planetary Data System Imaging Node (http://www-pdsimage.jpl.nasa.gov/PDS).

The multispectral mosaics will be geometrically registered to the black-and-white mosaic basemap, except for a small area near the south pole where improved geometric information is available from radar images. The quad layout will also follow that used for the base map.

The registration from bandpass to bandpass is critically important for mapping compositional variations from the subtle differences in reflectivity with wavelength. Misregistration of <1 pixel can cause significant "misregistration noise." We use a program called "subpreg" (part of the ISIS software) to register the images to a precision of 0.2 pixels, and have been very satisfied with the results. For information on obtaining and using the ISIS software, see http://wwwflag.wr.usgs.gov/USGSFlag/Data/data.html.

We recently completed a new geometry model for the NIR camera. For accurate bandpass-to-bandpass registration it was necessary to derive focal lengths, distortions, and spacecraft alignment angles for each filter. The basic approach was to use a handful of overlapping UVVIS images whose alignment and geometric properties are well characterized to produce a control network. This network is then used like a star catalog to solve for the NIR alignment, focal lengths, and geometric distortions.

Radiometric Calibration: Radiometric calibration steps for the UVVIS data (3) have been well tested and validated. We recently determined that some minor calibration problems such as the occasional presence of a "kink" in the spectra near 950 nm was due to our method of merging the long- and short-exposure UVVIS images. The method has been changed to eliminate the problem. From comparison to telescopic standard sites, we believe that the goal of 1% photometry has been achieved.

Radiometric calibration for the NIR camera is described by Lucey et al. [4]. These data have suffered from two serious problems. First, the preflight calibration gain and offset states exhibit residuals of up to 10%. Second, the camera suffered from a drifting additive offset that differs throughout an orbit and from orbit-to-orbit due to fluctuations in temperature of the sensor. The recent work of Lucey et al. has shown that the dataset can be calibrated to levels of about 5% precision, useful for many scientific studies.

Phase Function Normalization: The Clementine images were acquired at phase angles varying from 0° to ~90°; the brightness of the lunar surface varies by about a factor of 4 over this range. Without photometric normalization, the Clementine mosaics would vary dramatically in brightness from equator to poles. Furthermore, the mosaic in equatorial regions requires interleaving of images from month 1 and 2 of Clementine, and phase angles differ by as much as 30°. The Moon is ~2.6x brighter at phase zero than at phase 30, so the uncorrected mosaic would have a pronounced striping. There are also obvious bright spots on each image that includes the zero phase point. Furthermore, there are brightness variations with illumination and emission angle (primarily affecting the oblique images). The phase-angle variations vary with wavelength, so the Moon's color would be highly nonuniform if no phase-angle corrections were applied. There are also differences in phase behavior as a function of terrain type, especially mare vs. highland vs. immature soils. We chose to derive and apply a global average phase function [3,5], which best fits the photometric behavior of mature highland soils. We are also producing a full-resolution map of phase angle, to enable reversal or updating of the phase-angle correction. For example, a researcher interested primarily in mature mare spectral reflectances could use the phase angle backplane to first remove the global average phase function and then apply a function more appropriate to the mature mare soils. The phase angle map also enables empirical fits for improved cosmetics (seamless mosaics).

Database Management for Image Processing: The multispectral mapping effort requires processing of more than 600,000 images, and the procedures needed to ensure that the best images are used grew quite complex. As a result we reorganized the entire effort such that decisions regarding all aspects of processing and order of mosaicking were derived from key image parameters stored in a searchable database. Use of the database during the current production of the UVVIS tiles has greatly increased the speed and accuracy of the processing.

References: [1] Nozette S. et al. (1994) *Science, 266,* 1835. [2] McEwen A. and Robinson M. (1997) *Adv. Space Res., 19,* 1523. [3] McEwen A. et al. (1998) *LPS XXIX.* [4] Lucey P. et al. (1998) *LPS XXIX.* [5] McEwen A. (1996) *LPS XXVII,* 841.

59-91

LUNAR PROSPECTOR NEUTRON MEASUREMENTS COMPARED TO CLEMENTINE IRON AND TITANIUM ABUNDANCES.

R. C. Elphic[1], S. Maurice[2], D. J. Lawrence[1], W. C. Feldman[1], B. L. Barraclough[1], A. B. Binder[3], and P. G. Lucey[4], [1]Mail Stop D466, Space and Atmospheric Sciences, Los Alamos National Laboratory, Los Alamos NM 87545, USA, [2]Observatoire Midi-Pyrénées, 31400 Toulouse, France, [3]Lunar Research Institute, 1180 Sunrise Drive, Gilroy CA 95020, USA, [4]Hawai'i Institute of Geophysics and Planetology, University of Hawai'i, Manoa HI, USA.

Introduction: Knowledge of the distribution of Fe and Ti within the principal lunar terranes can help us understand the bulk composition of the Moon. Materials on the surface that carry information about the interior include (1) the maria, with varying Fe and Ti concentrations, (2) deep impact basins that may have exposed material from the lower crust and upper mantle, and (3) regions rich in KREEP basalts. Consequently, data that provide a global and/or high-spatial resolution assessment of lunar Fe and Ti are especially valuable in studies of lunar geochemistry.

The Clementine spectral reflectance (CSR) data have been used to derive maps of FeO and TiO_2 [1–4]. Because CSR spatial resolution approaches 100 m, such maps are potentially invaluable in lunar studies. The CSR technique depends on mineralogy, and while it has been constrained by returned lunar sample geochemistry, the question remains whether the results are accurate far from the Apollo and Luna landing sites. In this paper we discuss some of the results of a comparison of the Lunar Prospector neutron spectrometer (LPNS) observations and the CSR Fe and Ti maps reported in [5].

Approach: The LPNS footprint on the lunar surface is estimated to be about 350 km FWHM from 100-km orbit for fast neutrons (~500 keV–8 MeV), and about 700 km FWHM from 100 km for thermal neutrons (0–0.3 eV). To compare with CSR data,
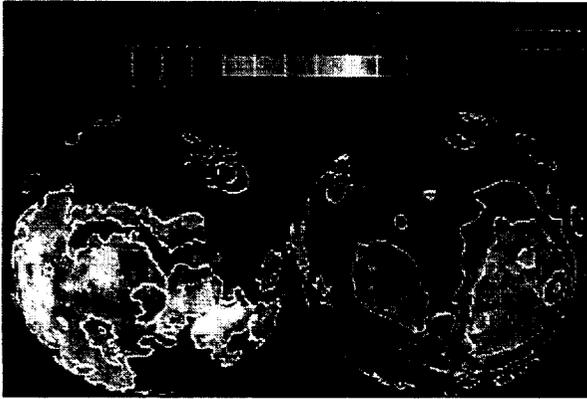
Fig. 1. Clementine spectral reflectance determination of the wt% of Fe. These data are mapped at 2° resolution. The scale ranges from ~1 to 19%.
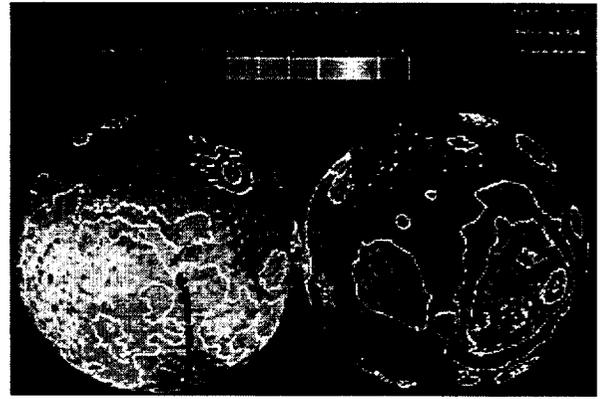
Fig. 2. LP neutron spectrometer map of fast neutron fluxes. The scale ranges from about 300 to 400 counts per 32 s. There are clear highs over the maria and the South Pole-Aitken Basin.

at 0.25° resolution, we convolve the CSR data with the LPNS footprints.

We compare the resulting CSR Fe and Ti maps with both the fast and thermal neutron observations, as each reflects different aspects of lunar surface composition. Fast neutrons are derived from the primary interaction of galactic cosmic rays (GCR) with the nuclei in the regolith — more fast neutrons are produced in regolith rich in the massive nuclei, Fe and Ti [6]. Thermal neutron fluxes are sensitive to a combination of fast neutron production, moderation, and absorption by nuclei. Both Fe and Ti have large cross sections for thermal neutron absorption, so regions rich in these elements have a dearth of thermal neutrons.

When a GCR bombards a nucleus, the resulting fragments are largely individual nuclear particles. Consequently, nuclei with an abundance of neutrons produce relatively more fast neutrons. Iron-56 and ^{48}Ti have 23 and 22 protons and 30 and 26 neutrons, respectively, while lower mass nuclei have roughly equal numbers of protons and neutrons. Thus, Fe- and Ti-rich regions like the maria will produce relatively more fast neutrons than the highlands [7].

The CSR-LP thermal neutron comparison is a bit more complex. First, while Fe and Ti can be the major absorbing species, the effects of other elements must be included. To do this, we account for the anti-correlation between CaO and FeO [8] (Ca can be a very significant absorber in the highlands), and lump together the effects of other elements to create a macroscopic absorption coefficient for thermal neutrons, Σ_{eff}. This then can be compared with the ratio of the LPNS thermal neutron count rate to the fast neutron count rate. The latter ratio corresponds to the number of thermal neutrons absorbed per fast neutron created.

Results: Figure 1 shows the CSR Fe data mapped on both the nearside and farside. As expected, highs are found in western Oceanus Procellarum and within Mare Tranquilitatis. This can be compared with the LPNS results discussed below.

LP fast neutrons and CSR Fe/Ti. Figure 2 shows the LP fast neutron flux [9] mapped in the same way. There is a very clear correlation between LP fast neutron flux and CSR Fe and Ti content. The global correlation coefficient between wt% Fe + Ti and the LP fast neutron flux is 0.811. In a more restricted latitude range, ±60°, the correlation improves to 0.887. For a region including nearside maria and farside highlands (40°–180°E longitude, ±60° latitude),

the correlation coefficient is 0.930. It appears that the fast neutron flux correlates with the CSR Fe and Ti determinations at the ~90% level.

LP thermal neutrons and CSR Fe/Ti. The CSR-derived macroscopic absorption cross section Σ_{eff} correlates with the fast-to-thermal neutron flux ratio: r = 0.849. By restricting the latitude range to ±60°, as described above, the correlation improves to 0.903. A still more limited region covering eastern maria and farside highlands but not including KREEP-rich terrains, 20°–180°E longitude and ±30° latitude, yields a correlation coefficient of 0.978. Thus our calculations of Σ_{eff} based on CSR Fe and Ti abundances agrees with the results of the ratio of fast-to-thermal count rates in regions where contributions from KREEP are minor.

The highlands immediately surrounding Mare Imbrium have the poorest correlation between the LP neutron flux ratio and Σ_{eff}. Here, our estimates of Σ_{eff} fail to include the contributions of rare earth elements such as Gd and Sm, which have anomalously large cross sections for thermal neutron absorption. While Gd and Sm abundances are very low even in KREEP materials, the effect of their cross sections can be comparable to that of Fe in the maria. Consequently, it is possible to map the incompatible elements using these absorptions as proxies, once the Fe and Ti effects are removed using the CSR data. Indeed, the residuals in the LPNS flux ratio correlate very highly with the LP γ-ray spectrometer (GRS) Th variations [10].

Conclusions: The LPNS is a very useful tool for checking the CSR Fe and Ti abundance maps. Using the fast neutron data there appears to be very good agreement, at the ~90% correlation level, between the two totally independent datasets. With further work on the data, it may be possible to improve this correlation further. In particular, fast neutron results may help further constrain the CSR Fe and Ti abundances far from sample return sites.

The most obvious and dramatic effect in the thermal neutrons is a deep low over the maria and a lesser one over the South Pole-Aitken Basin. This is due to the absorption of thermal neutrons by Fe and Ti. A careful analysis of the fast-to-thermal neutron flux ratio and a calculated macroscopic absorption coefficient based on CSR data yields a good correlation between these two independent parameters, at least for regions without significant KREEP contributions. Around the ramparts of the Imbrium basin, however, the correlation is poorer because of additional thermal neutron absorption brought about by

the rare earth elements Gd and Sm.

Thus, the LPNS can also track KREEP as well as Fe and Ti through the rare earth element proxies Gd and Sm, once the LPNS data have been corrected by the CSR Fe and Ti abundances.

References: [1] Lucey P. G. et al. (1995) *Science, 268,* 1150. [2] Lucey P. G. et al. (1996) *LPS XXVII,* 781. [3] Blewett D. T. et al. (1997) *JGR, 102,* 16319. [4] Lucey P. G. et al. (1998) *JGR, 103,* 3679. [5] Elphic R. C. et al. (1998) *Science,* submitted. [6] Drake D. M. et al. (1988) *JGR, 93,* 6353. [7] Reedy R. C. et al. (1998) *Meteoritics & Planet. Sci., 33,* A127. [8] Haskin L. A. and Warren P. H. (1991) *Lunar Sourcebook* (Heiken et al., eds.), p. 357, Fig. 8.3. [9] Barraclough B. L. et al. (1998) *Science,* submitted. [10] Lawrence D. J. et al. (1998) *Science,* submitted.

5/3 - 9/

DEPOSITS OF HYDROGEN ON THE MOON. W. C.

Feldman[1], S. Maurice[2], D. J. Lawrence[1], B. L. Barraclough[1], R. C. Elphic[1], and A. B. Binder[3], [1]Mail Stop D-466, Los Alamos National Laboratory, Los Alamos NM 87545, USA, [2]Observatoire Midi-Pyrénées, 31400 Toulouse, France, [3]Lunar Research Institute, 1180 Sunrise Drive, Gilroy CA 95020, USA.

Although several theories have been proposed to explain the origin of the Moon, the present consensus favors birth initiated by a giant impact of the proto-Earth by a Mars-sized planetoid. If correct, the Moon was born depleted in volatiles, including H. Hydrogen embedded in regolith grains has been found in returned samples. This observation has been explained in terms of solar wind implantation, thereby providing one of several indicators of soil maturity. It has also long been speculated that H has been delivered to the Moon in the form of water ice by comets and asteroids [1,2]. If the amount delivered in any one impact is sufficiently small so that a thick atmosphere does not form, then a sizable fraction (~20%) will migrate to both poles through an exospheric transport process (e.g., [3] and references therein). In this case, if water molecules encounter spots that are sufficiently cold (primarily within permanently shaded craters near both poles), they will plate the surface where they can remain stably trapped for eons if the rate of loss due to a variety of processes does not overwhelm the rate of deposition. However, many comets are sufficiently large that a collisionally thick atmosphere should form [4]. The migration of water molecules for these events has not been modeled, so the efficiency of deposition and the structure of the resultant deposits are not known.

Many searches for deposits of water ice near both lunar poles have been conducted using radar backscatter data. To date, no such deposits have been found (see, e.g., [5] and references therein). A recent analysis of epithermal neutron data measured using the Lunar Prospector neutron spectrometer [6] has provided a positive identification of enhanced deposits of H near both poles. Although a likely interpretation of these deposits is in terms of water-ice trapped within permanently shaded craters, other interpretations that of the migration of solar wind H cannot be ruled out at this time. A preliminary analysis of fast neutron data, also measured using the Lunar Prospector neutron spectrometer, provides only an upper limit to the signature expected for surface deposits of H near the poles. A consistent interpretation of all three datasets (epithermal neutrons, radar backscatter, and fast neutrons) is possible if water ice does indeed reside in permanently shaded craters near both poles, but is buried beneath a few tens of centimeters of dry regolith. Of course low, spatially distributed concentrations of surface deposits of H near both poles cannot presently be ruled out.

We will discuss the neutron measurements and their interpretation, including an opportunity to remap the epithermal fluxes at higher spatial resolution when Lunar Prospector will have its orbital altitude lowered to 25 ± 10 km in Jan. 1999. We will also discuss advances that can be made by correlating the Lunar Prospector data with information returned using other techniques to define the total area contained within permanently shaded craters near both poles. Another investigation that would benefit from correlations among multiple datasets (to include IR spectral reflectance imaging and analyses of returned regolith samples) is the mapping of mature soils.

References: [1] Watson K. et al. (1961) *JGR, 66,* 3033. [2] Arnold J. R. (1979) *JGR, 84,* 5659. [3] Butler B. J. (1997) *JGR, 102,* 19283. [4] Vondrak R. R. (1974) *Nature, 248,* 657. [5] Harmon J. K. (1997) *Adv. Space Res., 19,* 1487. [6] Feldman W. C. et al. (1998) *Science,* submitted.

Ç / - ://

INTEGRATED MULTISPECTRAL AND GEOPHYSICAL DATASETS: A GLOBAL VIEW OF LUNAR PYROCLAS-TIC DEPOSITS.

L. Gaddis[1], C. Rosanova[1], B. R. Hawke[2], C. Coombs[3], M. Robinson[4], and J. Sable[5], [1]Branch of Astrogeology, U.S. Geological Survey, 2255 North Gemini Drive, Flagstaff AZ 86001, USA (lgaddis@flagmail.wr.usgs.gov), [2]Planetary Geosciences Division, School of Ocean and Earth Sciences and Technology, 2525 Correa Road, University of Hawai'i, Honolulu HI 96822, USA, [3]Department of Geology, College of Charleston, Charleston SC 29424, USA, [4]Department of Geological Sciences, Northwestern University, 1847 Sheridan Road, Evanston IL 60208, USA, [5]Amherst College, Amherst MA, USA.

Introduction: We are integrating multispectral Clementine UVVIS data [1] with crustal thickness data [e.g., 2] to examine the composition and distribution of lunar pyroclastic deposits. Examples are the large deposits of Apollo 17/Taurus Littrow and Aristarchus [e.g., 3,4] and the small deposits (or endogenic "dark-halo" craters) located along fractures in the floors of Alphonsus [e.g., 5,6], Atlas [7], and Schrodinger [8] Craters. Our early efforts focus on the small pyroclastic deposits because of their relative youth (~1 Ga in some cases), their broad global distribution, and the fact that their small sizes may have inhibitied early Earth-based (~500-m spectral spot size at best) spectral analyses. We are now studying a variety of small deposits, including those of the Atlas Crater, Franklin Crater, Eastern Frigoris highlands, Oppenheimer Crater, Lavoisier Crater, and Orientale Crater regions. Our goals are to (1) understand the full extent of interdeposit compositional variations among small lunar pyroclastic deposits; (2) evaluate the possible effects of soil maturation and lateral mixing on the "true" compositions of these deposits; (3) determine the prevalence and nature of intradeposit compositional variations; (4) identify and characterize the juvenile components of these deposits; and (5) understand the implications of these results for studying lunar eruption mechanisms.

Previous Work: More than 90 lunar pyroclastic deposits have been recognized [e.g., 9]. Lunar pyroclastic deposits have been split into "regional" and "localized" deposits on the basis of size, morphology, and occurrence. Regional deposits can be up to several thousand square kilometers in size, while localized or small pyroclas-

tic deposits are typically 200–500 km² in size [3]. Regional deposits are thought to have been emplaced as products of continuous or Strombolian-style eruptions, with a wide dispersion of well-sorted pyroclasts [e.g., 10]. Analyses of Apollo samples and Earth-based spectral reflectance studies have identified a significant component of Fe^{2+}-bearing volcanic glass beads in many of the regional pyroclastic deposits [e.g., 3].

Intermittent or Vulcanian-style eruptions are likely to have produced the small pyroclastic deposits, with explosive removal of a plug of lava within a conduit and forming an endogenic vent [10,11]. The small pyroclastic deposits have been further subdivided into three compositional classes on the basis of their "1.0-μm" or mafic absorption bands in Earth-based spectra [e.g., 11]. Group 1 mafic bands are centered near 0.94 μm; spectra resemble those of typical highlands and are indicative of the presence of feldspar-bearing mafic assemblages dominated by opx. Group 1 deposits appear to be mixtures of highland-rich country rock and glass-rich juvenile material with small amounts of basaltic caprock material. Examples of Group 1 deposits are found on the floors of Atlas Crater (45°N, 45°E), Franklin Crater (29°N, 48°E), and near Grimaldi Crater (1°S, 64°W). Group 2 mafic bands are centered near 0.96 μm; Group 2 spectra are similar to those of mature mare deposits, and they are dominated by cpx. Small pyroclastic deposits in Group 2 appear to consist largely of basaltic material. Examples are located east of Aristoteles Crater (50°N, 21°E, and 28°E). Group 3 mafic bands are broad and centered near 1.0 μm; Group 3 deposits are dominated by olivine and opx; the olivine is almost certainly associated with juvenile material, and the opx is likely to have been wall rock [11]. Examples of Group 3 small pyroclastic deposits are those of J. Herschel Crater (62°N, 42°W), Alphonsus Crater (13°S, 4°W), and south of Cruger Crater (17.5°S, 67°W).

Compositional Analyses: We used the USGS ISIS software to create and examine Clementine UVVIS multispectral mosaics (~100 m/pixel) of areas representative of the three major compositional classes of small lunar pyroclastic deposits. Compositional analyses of these deposits are based on color-ratio comparisons for each area. The ratios examined are the 450-nm/750-nm or UV/VIS ratio, suggestive of relative Ti content, and the 950-nm/750-nm ratio, a measure of the 1.0-μm band strength and suggestive of relative mafic content (low = strong or deep 1.0-μm band; high = weak or shallow band). Although the systematics have not been resolved for application to lunar pyroclastic deposits, these ratio values can also be interpreted in terms of relative soil maturity: A mature soil is red and has a relatively shallow 1.0-μm band, while a more immature soil is blue, with a deeper 1.0-μm band.

Figure 1 shows color ratio values extracted from each of the three classes (11 sites, including Orientale, Oppenheimer, Nernst, Lavoisier, and Compton), with spectra obtained in the vicinity of the probable vent area. All the deposits shown have approximately shallow mafic band depths (all >1), and they are relatively blue (UV/VIS ratios >0.54, comparable to many lunar highland deposits). Regarding interdeposit compositional variations, we see three major clusters. The larger cluster (upper right) has a wider range of mafic band depths and UV/VIS values, the mafic bands are shallower (ratio values are higher) than those of the smaller clusters in the center and lower left, and the UV/VIS values are generally higher (bluer). The larger cluster includes several different small pyroclastic units, including those of Atlas/south and Franklin — these are the Group 1 deposits (similar to highlands) — and they are joined by the Orientale
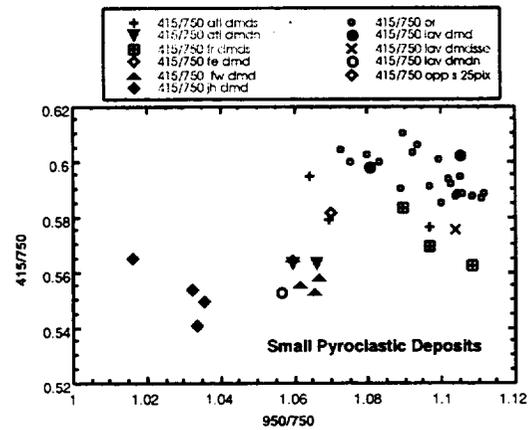
Fig. 1. Clementine UVVIS data: Color ratio data for three types of small pyroclastic deposits on the Moon.

deposits and our "new" deposits at Oppenheimer and Lavoisier. The central cluster has deposits such as Atlas/north, E Frigoris W and E, and the deposit in the crater floor located northeast of Lavoisier — these can be classified as Group 2 deposits (similar to mare deposits). The smaller cluster to the lower left includes only the Group 3 (J. Herschel Crater) deposit.

Several interesting aspects of these data must be noted. First, we have corroborated the Earth-based spectral classification scheme: We generally see three distinct spectral classes. The mafic band depths show the expected trend of increasing mafic band depth from Group 1 > Group 2 > Group 3 deposits. Although mixed spectral signatures cannot be ruled out, it appears that the coarser spatial resolution of the Earth-based spectral data has successfully characterized the small pyroclastic deposits. Second, we have classified the Orientale spectra as a small pyroclastic deposit belonging to Group 1 — this deposit has been described and modeled as Strombolian by Weitz et al. [12]. The unusual annular structure is suggestive of a Vulcanian eruption mechanism, but the large size of the Orientale pyroclastic deposit is compatible with a Strombolian style of eruption. In our observations, the Orientale pyroclastic deposit is bluer than most Group 1 small pyroclastics, but has shallow mafic bands similar to those of the Group 1/Franklin Crater deposits. Finally, the Group 3 spots of J. Herschel form an entire small cluster; with the deepest mafic bands and the reddest of the small pyroclastic deposits, these deposits are so far the most unequivocal representatives of juvenile mafic materials observed among the small pyroclastic deposits.

Distribution and Occurrence: Small pyroclastic deposits are widely distributed across the lunar nearside, and with the Clementine global dataset we now realize that farside and polar regions of the Moon also serve as host to several small pyroclastic deposits. Most small pyroclastic deposits are observed as relatively isolated deposits in highlands near the margins of major mare deposits on the nearside. However, two clusters of small pyroclastic deposits are observed along the northwestern margin of Oceanus Procellarum and near Mare Nubium. Also, several small deposits are found in the floors of floor-fractured craters, where they are associated with endogenic craters on fractures [13]. Many of the floor-fractured craters are Imbrian or pre-Imbrian (>3.2 Ga), although a pyroclastic deposit

near Taruntius Crater appears to be relatively young (~1 Ga) [14]. Of >80 floor-fractured craters mapped by Wilhelms (Plate 5 in [15]), ~15 have pyroclastic deposits, suggesting that these features may have provided an enhanced environment for explosive volcanic eruption.

The spatial association of volcanic eruption sites and impact craters and basins on the Moon is believed to be related to crustal thinning beneath impact sites. Small pyroclastic deposits are observed in regions with crustal thicknesses ranging from 30 to 80 km [2], with the majority near 50 km. On the nearside, these crustal thicknesses are typical of the margins of the major maria; on the farside, thinner crust is observed in the South Pole/Aitken Basin and the Moscoviense Basin, sites where pyroclastic deposits are observed. We are currently evaluating these data to investigate implications for modes of eruptions of lunar pyroclastic deposits.

References: [1] Clementine Basemap Mosaic, 15 volumes, prepared by USGS for NASA, available via the Planetary Data System Imaging Node. [2] Zuber et al. (1994) *Science, 266,* 1839–1843. [3] Gaddis et al. (1985) *Icarus, 61,* 461–488. [4] McEwen et al. (1994) *Science, 266,* 1858–1861. [5] Robinson et al. (1996) *LPS XXVII,* 1087–1088. [6] Head and Wilson (1979) *Proc. LPSC 10th,* 2861–2897. [7] Hawke et al. (1989) *Proc. LPSC 19th,* 255–268. [8] Shoemaker et al. (1994) *Science, 266,* 1851–1854. [9] Gaddis et al. (1997) *LPS XXVII,* 389–390; Gaddis et al. (1998) *LPS XXIX;* Rosanova et al. (1998) *LPS XXIX.* [10] Head and Wilson (1992) *GCA, 56,* 2155–2175. [11] Coombs and Hawke (1992) *Proc. LPS, Vol. 22,* 303–312. [12] Weitz et al. (1997) *LPS XXVIII,* 1533. [13] Schultz (1976) *Moon,* 241; Wichman and Schultz (1995) *JGR, 100,* 21201. [14] Spudis (1989) *NASA TM 4210,* 406–407. [15] Wilhelms (1987) *USGS Prof. Paper 1348.*

5/2 · 9 /

DIFFERENCES OBSERVED IN IRON CONTENT BETWEEN CRATER EJECTA AND SURROUNDING MARE BASALT SURFACES: IMPLICATIONS FOR SAMPLE REMOTE SENSING INTEGRATION.

J. J. Gillis[1,2] and P. D. Spudis[1], [1]Lunar and Planetary Institute, Houston TX 77058, USA, [2]Previously at Rice University, Houston TX, USA; now at Washington University, St. Louis MO 63130, USA (gillis@levee.wustl.edu).

Introduction: Remote sensing techniques [e.g., 1,2] are utilized to extend sample data to regional and global scales. Equally important is knowledge of rock types not represented in the current sample collection [3]. Before either of these questions can be addressed, one question must first be answered: How does remote analysis of a planet's surface relate to the uncompromised composition of bedrock? The paucity of exposed rocks on the lunar surface means that remote chemical and mineralogical analysis (e.g., Clementine [4]) records direct information about the soils. In this work we examine ways to evaluate how and if the composition of the surface material is representative of the bedrock material below.

Methods: Processing of Clementine images was performed using ISIS software developed by the USGS, in Flagstaff [5]. Images were converted to absolute reflectance using photometric equations [6]. Maps displaying the distribution of Fe were constructed using Clementine 750- and 950-nm images [7]. The technique for calculating Fe abundance is shown [8] to have eliminated the effects of surface brightness and albedo, thus yielding accurate Fe concentrations for the Apollo and Luna landing sites.

TABLE 1.   A comparison of Fe concentration between mare surfaces and crater ejecta; crater ejecta tend to have higher FeO content relative to the mare surface they are superposed on.

Location of Mare Unit	Surface FeO wt%	Ejecta FeO wt%
Mare Orientale	6–12	12–16
Lacus Veris	8–10	12–14
Mare Marginis	10–14	14≥16
Mare Smythii	12–14	8–10
Mare Australe	8–12	12–16

Discussion: Maps of Fe abundance for farside mare surfaces show low concentrations of Fe (8–14 wt% FeO) when compared to soil samples from the Apollo landing sites (11–16 wt% FeO). Are farside basalts inherently lower in Fe, or are they more highly contaminated by impact mixing between highland and mare lithologies?

To answer this question we have looked at the composition of small crater ejecta within the maria. Craters serve as bore holes penetrating the surface of the mare unit to expose fresh, less-contaminated mare material. Maps of Fe concentration show that mature mare surfaces and ejecta from craters superposed on the uppermost regolith layer have different FeO percentages (Table 1). Crater ejecta are found with lower and higher concentrations of Fe relative to the surrounding mare surface.

Craters in Figs. 1b and 2b exhibit concentric rings of increasing Fe toward their center. This is an indication that the subsurface is more mafic than the surface composition. Craters have excavated fresh basaltic material that is less contaminated with highland material than the surrounding mare surface. Mare basalt units with low Fe content surfaces are associated with areally small deposits, which are prevalent on the farside, and where craters proximal to mare units have deposited highland material over the basalt (e.g., Maunder and Mare Orientale).

In the second case, the Fe content for crater ejecta is lower than the surrounding mare material (Table 1, Mare Smythii). The low-Fe ejecta is produced when craters are large enough to excavate highland material from beneath the mare unit. This scenario allows an estimate of mare basalt thickness [9]. The thickness of the mare unit is calculated by bracketing the diameter at which craters have excavated low-Fe highland material and diameter at which they have not. The thickness of the basalt is calculated using the relation of crater diameter to depth of excavation [10]. This technique of calculating mare deposit thickness, when combined with previous techniques [11,12], will improve the resolution at which mare units are mapped.

Conclusions: It is important to observe not just the surface composition of the mare unit but also the ejecta from fresh craters. The assessed surface composition represents hybridized rock types that are the product of impact mixing processes. Higher Fe composition for crater ejecta relative to the exposed mare surface signifies contamination with highland material. The difference in Fe abundance relates to the amount of surface contamination. Such contamination must be corrected before attempting to understand lunar basalt compositions. This reflects the depth, size, and age of the mare basalt unit. Craters that have low-Fe concentrations may be used to calculate the thickness of the mare unit.

References: [1] Alder et al. (1973) *Proc. LSC 4th,* 2783–2791. [2] McCord T. B. et al. (1976) *Icarus, 29,* 1–34. [3] Pieters C. (1978) *Proc. LPSC 9th,* 2825–2849. [4] Nozette and the Clementine Sci-

ence Team (1994) *Science, 266*, 1835–1839. [5] Gaddis L. (1996) *GSA Abstr. with Progr., 28(7)*, A386. [6] McEwen A. S. (1996) *LPS XXVII*, 841–842. [7] Lucey P. G. et al. (1995) *Science, 268*, 1150–1153. [8] Blewett D. T. et al. (1997) *JGR, 102*, 16319–16325. [9] Gillis J. J. et al. (1997) *LPS XXVIII*, 419–420. [10] Croft S. K. (1980) *Proc. LPSC 11th*, 2347–2378. [11] Eggleton R. E. et al.

(1974) *LS V*, 200–202. [12] De Hon R. A. and Waskom J. D. (1976) *Proc. LSC 7th*, 2729–2746.
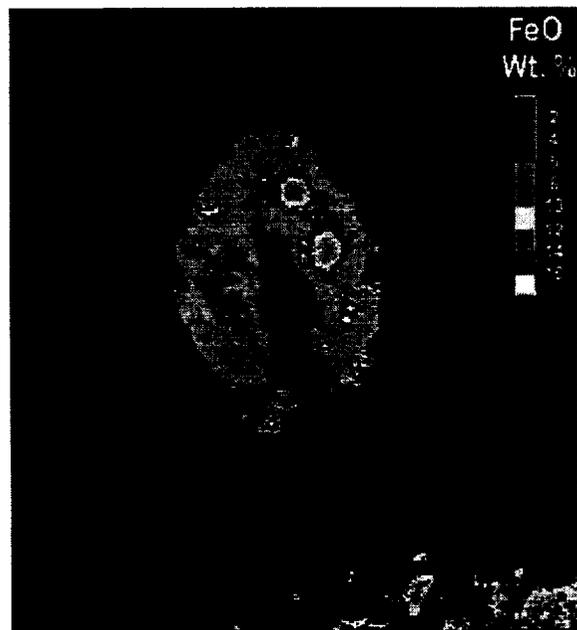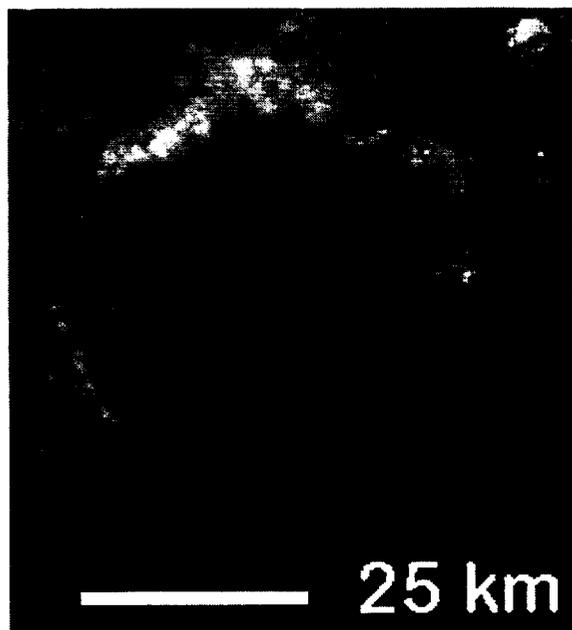
Fig. 1. (a) Clementine 750-nm image of the mare-filled crater Buys-Ballot (175°E, 21°N). It is located near the center of the Freundlich-Sharonov Basin. (b) Iron map of mare basalt within Buys-Ballot. The two high-Fe spots in the upper right of the mare deposit are craters that have exposed subsurface mafic material.
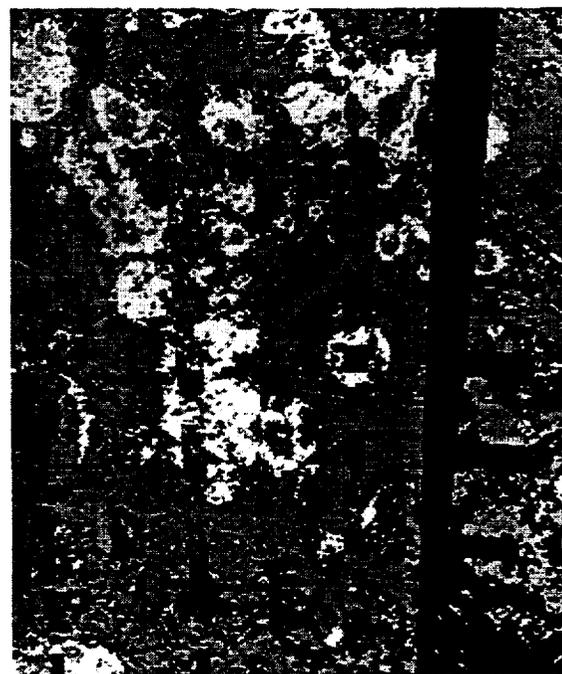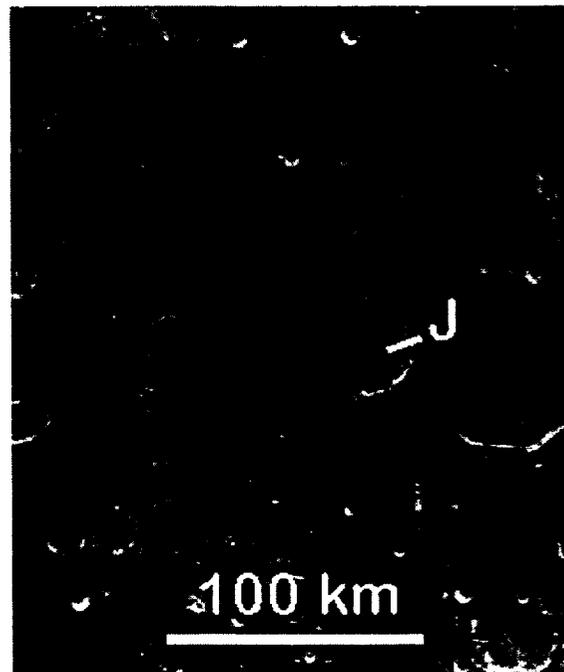
Fig. 2. (a) Clementine 750-nm albedo image of the mare-filled Jenner (J) crater and surrounding mare deposits. Jenner is located in central Mare Australe. (b) Iron concentrations for mare basalt units surrounding the crater Jenner. The surface of the basalt units is low in FeO (scale same as Fig. 1b), while crater ejecta on the surface of the basalt units have consistently higher FeO contents.

Sp - 91

USE OF A GEOGRAPHIC INFORMATION SYSTEM DATABASE OF BRIGHT LUNAR CRATERS IN DETERMINING CRATER CHRONOLOGIES.

J. A. Grier[1], A. McEwen[1], R. Strom[1], and P. Lucey[2], [1]Lunar and Planetary Laboratory, University of Arizona, 1629 North Cherry Boulevard, Tucson AZ 85721, USA (jgrier@lpl.arizona.edu), [2]University of Hawai'i, Honolulu HI 96822, USA.

To determine the flux of impactors onto the lunar and the terrestrial surface in recent (~600 Ma) time, believable, absolute ages for a vast number of bright-rayed craters on the lunar surface are needed [1]. Ideally, absolute ages can be determined by obtaining samples from each crater, radiometrially dating them, and then extrapolating an impactor flux. Realistically, it is clear that only a small number of the larger lunar craters can and will be radiometrically dated. The smaller craters are also of interest, since they will reflect the bulk of any very recent impactor population. Thus, large numbers of dates cannot be generated solely by this method.

On the other hand, a large number of relative ages can conceiveably be generated by examination of lunar spacecraft spectral data with near global coverage. The Clementine color dataset provides global lunar coverage and appropriate spatial resolution to undertake such a survey. The Optical Maturity Parameter (OMAT) developed by Lucey and colleagues [2,3] appears to be a possible tool for assisting in the determination of the relative ages of bright-rayed craters, but the limitations and applicability of this tool for such a survey need to be determined.

An extensive survey of bright-rayed craters down to small sizes (1 km or less) will be conducted using the Clementine color data. A relative crater chronology will be generated using several tools, including superpositioning of rays, OMAT images, current age estimates for craters, current estimates for the rates of soil maturization, etc. The radiometric ages from known craters included in the survey will allow this relative chronology to be constrained absolutely and a crater flux to be generated. Such an endeavor, if sucessfully carried out, would have far-reaching significance in understanding recent/ future cratering on the Earth and Moon, and in the interpretation of cratered surfaces and crater chronologies.

Toward this end, initially, we conducted a survey of bright lunar craters in the 750-nm UVVIS in order to take a preliminary look at the size-frequency distribution of bright craters down to very small sizes, and to explore possible biases such as phase angle and background terrain [4]. Size-frequency distributions generated for the mare and highlands were quite different at smaller sizes. Differences in the size-freqency distributions due to phase angle became statistially significant at latitudes greater than ~40°. We then considered the use of the the specific 750–950 OMAT ratio developed by Lucey et al. as a possible tool for dealing with these and other issues.

We have examined test OMAT images with the purpose of discovering limitations and appropriate uses for the OMAT, and attempting to create a technique using OMAT images to conduct large-scale survey of bright-rayed lunar craters and generate a relative age chronology. Consistent with recent work [2], we see that OMAT images allow the very brightest, youngest craters to stand out. In several cases, it is easier to discern the existence and extent of bright rays/halos of craters in the OMAT images than the UVVIS. Also, we see that the OMAT images assist in normalizing the mare/ highlands differences. Differences in the mare and highlands are clearly important in generating a self-consistent database, since mare/

highlands boundaries played a critical role in changing the apparent size-frequency distribution of craters in the 750-nm filter alone. However, differences in the physical properties of mare and highland soils and slopes also need to be examined.

Craters with a wide range of apparent ages are characterized by a bright torus just inside the tip of the crater rim. Even craters that are morphologically quite degraded can possess this feature, which seems indicative of downslope movement in the interior of the crater wall. Measuring the OMAT of a crater is problematic since the value is different on the center, rim, and ejecta of the crater, albeit systematically [2]. Measurements of the insides of craters show that the interiors are apparently less mature than the ejecta. Lucey et al. believe this may be due to the presence of competent impact melt-inhibiting maturization [2], but downslope movement and other factors may be critical [4]. Examining a larger number of very small craters may shed some light on this, as smaller craters will not have floors lined with competent impact melt, and will not be surrounded by melt halos.

A phase-angle correction is clearly of great importance if the higher lunar latitudes are to be included in the survey. Phase-angle biases will be dealt with using phase-angle backplanes to map rayed-crater frequencies as a function of phase angle to show (and correct for) the bias in detecting bright rays at high phase. Additionally, work is now under way [5] to better normalize the average lunar color and albedo as a function of phase angle. This correction, while not improving detection of rays and halos at high phase angles, will remove seams in the OMAT images. Finally, separation of brightness variations due to albedo (intrinsic brightness of surface materials) from brightness variations due to topographic shading (most prominent at higher phase) [5] could result in much better OMAT images at high latitudes.

The apparent age of a crater, based on crater size-frequency distributions [4] and OMAT images [2], is dependent on the size of the crater. The ejecta of the crater Tycho appears to be less mature than that of South Ray Crater, although South Ray is a younger crater [2] (Tycho is about 100× the size of South Ray). It may be that craters of a certain size can be given apparent relative ages to one another, and an independent means of correlating these size-dependent chronologies can be generated on the basis of maturization rates. Note that simple bowl-shaped craters of similar size have similar shapes; therefore, the slope-dependent maturization processes will be similar from crater to crater within this morphology. It will therefore be meaningful to use OMAT values for crater interiors as a measure of relative age for craters in a particular size bin (such as 2–3 km).

The GIS database we are generating, which includes size, morphologic parameters, ray/halo descriptions, OMAT values, etc., will help us constrain and quantifiy the complications and biases inherent in interpreting the lunar cratering record with the Clementine mosaics. This correlated with actual sample data should generate new insight concerning rayed/haloed craters and move toward a better understanding of the recent crater chronology on the lunar surface.

References: [1] McEwen A. et al. (1996) *JGR*. [2] Lucey P. et al. (1998) *JGR*, in press. [3] Lucey P. et al. (1998) *LPS XXIX*, Abstract #1356. [4] Grier J. et al. (1998) *LPS XXIX*, Abstract #1905. [5] Eliason et al., this volume.

Sp 9/

LUNAR PROSPECTOR DATA ARCHIVES.

E. A. Guinness[1] and A. B. Binder[2], [1]Department of Earth and Planetary Sciences,

McDonnell Center for the Space Sciences, Washington University, St. Louis MO 63130, USA (guinness@wunder.wustl.edu), [2]Lunar Research Institute, 1180 Sunrise Drive, Gilroy CA 95020, USA.

Introduction: The Lunar Prospector (LP) is operating in a 100-km circular polar orbit around the Moon. The LP project's one-year primary mission began in January 1998. A six-month extended mission in a lower orbit is also possible. LP has five science instruments, housed on three booms: a γ-ray spectrometer, a neutron spectrometer, an α-particle spectrometer, a magnetometer, and an electron reflectometer. In addition, a gravity experiment uses Doppler tracking data to derive gravity measurements. The major science objectives of LP are to determine the Moon's surface abundance of selected elements, to map the gravity and magnetic fields, to search for surface ice deposits, and to determine the locations of gas release events [1]. The Geosciences Node of the NASA's Planetary Data System (PDS) is providing a lead role in working with the Lunar Prospector project to produce and distribute a series of archives of LP data. The Geosciences Node is developing a Web-based system to provide services for searching and browsing through the LP data archives, and for distributing the data electronically or on CDs. This system will also provide links to other relevant lunar datasets, such as Clementine image mosaics and telescopic and laboratory spectral reflectance data.

Standard Data Products: The currently planned standard data products for Lunar Prospector will consist of two levels of data reduction known as Level 0 and Level 1 products. Processing for Level 0 products is minimal; it consists mainly of organizing the raw telemetry by time and selecting the best available downlink transmission based on signal-to-noise ratios. A primary Level 0 data product is the merged telemetry files, which contain engineering data and data from the five science instruments. The merged telemetry files will be archived on CD-WO volumes with each volume containing data for a calendar month. These volumes will also contain spacecraft ephemeris and attitude files and command files sent to the spacecraft. Level 0 data products from the gravity experiment consist of raw Doppler tracking data and are archived on CD-WO volumes separate from the science instrument volumes.

The type of processing done to generate Level 1 data products primarily consists of organizing the data by instrument, position, and time and correcting for some instrument and background effects. The currently planned Level 1 data products are as follows: Complete γ-ray and neutron spectra will be aggregated into 5° × 5° bins. Maps with a resolution of 5° will be produced for the 1.46-MeV (K), 2.6-MeV (Th), and γ-ray peaks and for the thermal and epithermal neutron abundances. These maps will be in units of counts but with instrument effects removed. Level 1 data products from the α-particle spectrometer will be time-series files of α-particle events and 5° maps of Rn and Po abundance in units of counts. The magnetometer and electron reflectometer Level 1 data products will be time-series files. Level 1 gravity products will consist of spherical harmonic coefficients and a set of gravity maps including the vertical gravity field and anomaly maps. All Level 1 products will be generated in two versions. The first version will integrate data collected during the first six months of the primary mission, and the second version will integrate all data from the primary mission. The first version of Level 1 products are scheduled to be released in the fall of 1998, and the second version of the products will be released in the spring of 1999.

Web-based Data Access and Retrieval: As the Lunar Prospector standard data product archives are produced and released, the PDS Geosciences Node will make the datasets available over the Internet. The Geosciences Node will host Web-based search and retrieval capabilities similar to those developed for Clementine, Magellan, and Viking datasets. Data can be selected primarily based on instrument, position, and time. The selected subsets of data can be downloaded electronically or distributed on custom CD-WO volumes. To provide an imaging context to the LP data, the retrieval system will be integrated with Clementine image mosaics, where custom mosaics are generated showing areas covered by LP data. Access will also be provided to a series of telescopic and laboratory spectral reflectance datasets produced by the spectroscopy subnode (at Brown University and University of Hawai'i) of the Geosciences Node. In addition, starting in the fall of 1998, the Geosciences Node plans to host a series of workshops on higher-level (relative to Level 1 standard products previously defined) data reduction of spectrometer datasets.

References: [1] Binder A. B. et al.. (1998) *Eos Trans. AGU, 79,* 97108.

$\mathring{\mathfrak{I}} - \mathcal{G}/$

THE VAPOR DEPOSITION MODEL OF SPACE WEATHERING: A STRAWMAN PARADIGM FOR THE MOON. B. Hapke, Department of Geology and Planetary Science, University of Pittsburgh, Pittsburgh PA 15260, USA.

Understanding space weathering on the lunar surface is essential to solving a number of major problems, including correctly interpreting lunar remote-sensing observations, understanding physical and chemical processes in the lunar regolith, and extrapolating to other bodies, especially Mercury, the asteroids, and the parent bodies of the ordinary chondrites. Hence, it is of great importance to correctly identify the process or processes that dominate lunar space weathering. The vapor deposition model [1–11] postulates that lunar space weathering occurs as a result of the production of submicrscopic metallic iron (SMFe, also called superparamagnetic iron and nanophase iron) particles in the regolith by the intrinsic differentiation that accompanies the deposition of silicate vapor produced by both solar wind sputtering and micrometeorite impacts. This is the only process that has been demonstrated repeatedly by laboratory experiments to be capable of selectively producing SMFe. Hence, at present, it must be regarded as the leading contender for the correct model of lunar space weathering. This paper reviews the features of the vapor deposition model.

The basic mechanism of the model relies on the fact that the porous microrelief of the lunar regolith allows most of the vapor produced by sputtering and impacts to be retained in the soil, rather than escaping from the Moon. As the individual vapor atoms impact the soil grain surfaces, they are first weakly bound by physical adsorption processes, and so have a finite probability of desorbing and escaping. Since the O is the most volatile, it escapes preferentially. The remaining atoms become chemically bound and form amorphous coatings on lunar soil grains. Because Fe is the most easily reduced of the major cations in the soil, the O deficiency manifests itself in the form of interstitial Fe° in the glass deposits. Subsequent heating by impacts allows the Fe° atoms to congregate together by solid-state diffusion to form SMFe grains. The impacts dislodge some of the coatings, which form an additional component of the soil, and also shock-weld the mineral grains, impact-vitrified glass, and vapor-deposited glass into agglutinates. Glass generated

by impact vitrification probably plays a negligible role in lunar optical properties.

The model specifically predicts the following observed characteristics of the regolith: (1) production of SMFe that exhibits the characteristic g = 2.1 ESR resonance; (2) correlation of amount of SMFe with maturity; (3) decreased albedo; (4) reddened spectra; (5) obscuration of mineral absorption bands; (6) amorphous SMFe-bearing coatings on soil particles that are chemically different from their host grains; (7) dark glass component containing SMFe; (8) dark patina on the surfaces, especially the undersides, of rocks and boulders protruding above the lunar surface.

If the model is correct, it implies that the presence of SMFe is prima facie evidence of material deposited from a vapor phase. The laboratory vapor deposits contain ~10% by mass of SMFe. Since the regolith is ~0.5% SMFe, this implies that several percent of the lunar soil consists of a component has been processed by evaporation and redeposition.

It must be emphasized that the SMFe is produced by a physical process, selective desorption, and does not require a chemically reducing agent, such as a H atmosphere or interstitial H. Hence, it will also occur on Mercury, in spite of the fact that most of the time the solar wind does not reach the surface there. In fact, more vapor will be generated by impacts on Mercury than on the Moon because of the higher meteorite velocities, so that the fraction of vapor deposited material is higher. The reduction process may have gone nearly to completion there, and converted most of the ferrous iron in the regolith silicates to SMFe, thus accounting for the lack of the 1-μm band in the spectrum. If so, fresh craters should still exhibit the band, a prediction that can be tested by a Mercury orbiter.

The process is probably of only minor importance in the asteroid belt for the following reasons: (1) The solar wind flux is lower by an order of magnitude. (2) Generation of vapors by impact is greatly reduced because of the lower velocities. (3) The soil turnover rate is higher because of the larger meteorite flux so that the proportion of fresh material exposed at the surface is much larger than on the Moon. Hence, the parent bodies of the ordinary chondrites cannot be hidden by a lunar type of space weathering.

References: [1] Hapke B. (1965) *Ann. N.Y. Acad. Sci., 123*, 711. [2] Hapke B. (1966) in *The Nature of the Lunar Surface* (W. Hess et al., eds.), p. 141, Johns Hopkins, Baltimore. [3] Hapke B. (1968) *Science, 159*, 76. [4] Hapke B. et al. (1970) *Proc. Apollo 11 LSC*, 2199. [5] Hapke B. (1973) *The Moon, 7*, 342. [6] Cassidy W. and Hapke B. (1975) *Icarus, 25*, 371. [7] Hapke B. et al. (1975) *The Moon, 13*, 339. [8] Hapke B. and Wells E. (1976) *Science, 195*, 977. [9] Hapke B. and Cassidy W. (1978) *GRL, 5*, 297. [10] Paruso D. et al. (1978) *Proc. LPSC 9th*, 1711. [11] Hapke B. (1986) *Icarus, 66*, 270.

$5/6-9/$

ON ESTIMATING PROVENANCES OF LUNAR HIGHLAND MATERIALS.
L. A. Haskin and B. L. Jolliff, Department of Earth and Planetary Sciences and McDonnell Center for the Space Sciences, Washington University, St. Louis MO 63130, USA.

Introduction: That even relatively small impacts can spread material across the face of the Moon is evident from the rays of Tycho. Tycho ejecta triggered the landslide that produced the light mantle deposit at Apollo 17 and perhaps excavated the Central Valley craters there [e.g., 1]. Basin-sized impacts appear to follow the same scaling laws as smaller impacts, as indicated by the satisfac-

tion of a geophysical model [2]. These giant impacts rearranged huge amounts of premare material, complicating the determination of provenance of materials collected from the highlands. We have developed a model to estimate the probability that material at a particular location might derive from a given basin or large crater [3,4].

This model is based on crater scaling laws [e.g., 5] and effects of secondary cratering [e.g., 6]. Because it accounts for the volume of primary ejecta from the basin-forming transient craters and the excavating and mixing effects of these ejecta with the substrate onto which they fall, it gives much thicker deposits than the early work of [7]. Our modeling [4] takes into account the distribution of sizes of primary ejecta fragments (PriFrags) to obtain the probability at a
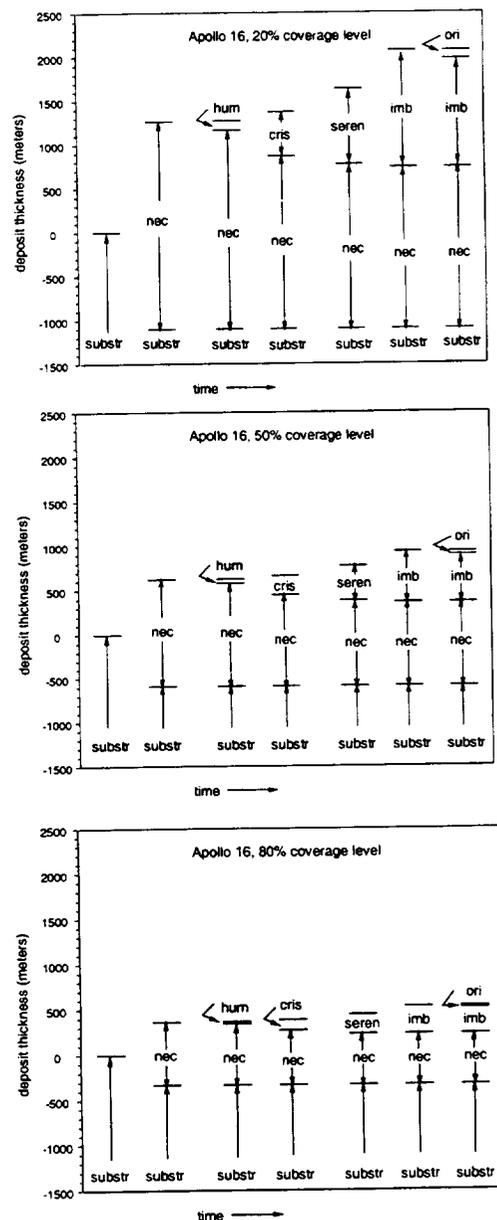
Fig. 1.
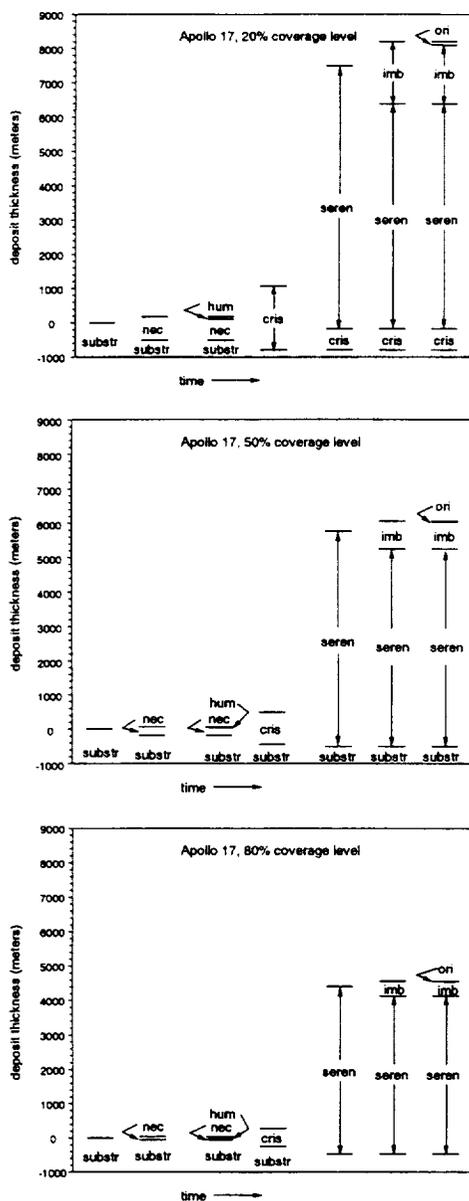
Fig. 2.

given site for a deposit of a particular thickness and with a particular fraction of PriFrags. Put another way, the model estimates the fraction of a 100 × 100 km square of interest (SOI) excavated to a particular depth, with deposits of a particular thickness, and containing a particular fraction of PriFrags. This model estimates only average distributions of these parameters within the SOI and does not indicate which location within an actual SOI would have these properties. Average distributions are useful; similarly scaled SOIs around Copernicus have on average ±50% crater counts at seven transient crater radii from the crater center [3,4].

The model was used to estimate average thicknesses of Imbrium ejecta deposits and the fraction of Imbrium PriFrags in those deposits Moonwide [8]. Those estimates, coupled with a rough average Th concentration for Imbrium PriFrags, predicted average Th concentrations as a function of distance from Imbrium, assuming the high

Th concentrations in the Imbrium-Procellarum region [e.g., 9] represented a unique trace-element-rich geochemical province. The spatial pattern of Th concentrations observed by the Apollo γ-ray experiments agreed qualitatively with the model results. The Lunar Prospector mission finds no other such trace-element-rich provinces, better defines the outline of the proposed province, shows the expected correlation between Th and K concentrations, and generally confirms the pattern of highland Th concentrations as a function of distance from Imbrium, including the modest rise in Th concentration in the vicinity of South Pole Aitken, where Imbrium PriFrags would have converged opposite the Imbrium Basin [10]. Excavation of Th-bearing material by the impact that produced the South Pole-Aitken Basin must also be considered; we await the higher-spatial-resolution data from the Prospector extended mission.

The point is, a basin distributes enormous quantities of ejecta and disturbs the surface to a considerable depth over distances of many transient crater radii from the point of impact. Shown below are "pseudostratigraphies" of basin deposits to illustrate the complexity of deposit stratigraphy and to indicate rough probabilities of encountering material from a particular basin. Transient crater radii from [11] are used except for Serenitatis, for which 250 km was used, providing more self-consistent constraints than in [3]. In Fig. 1, pseudostratigraphies are given for three "coverage levels": 20%, 50%, and 80%. This means that 20% of the average site is covered by deposits of the thickness shown or thicker. Alternatively, it means that a given location has a 20% chance of being on a deposit of that thickness or greater. The progression of stratigraphies from left to right in Fig. 1 shows the thickness of the fresh deposit at the site produced by each basin-forming event.

The "pseudo" part of the stratigraphy is this: Figure 1 shows a 20% Imbrium deposit overlying a 20% Serenitatis deposit, etc., whereas, in fact, an 11% Imbrium deposit may overlie a 62% or 83% Serenitatis deposit. These thicknesses can nevertheless be used to gain a qualitative sense of the probable contributions of various basins and variability in deposit thickness at a site. Thus, for example, according to Fig. 1, at the Apollo 16 site the Serenitatis-derived deposit always consumes the Crisium-derived deposit. If at a given location the Crisium-derived deposit was relatively thick (~20% coverage level) but the Serenitatis-derived deposit was relatively thin (>~80% coverage level), part of the Crisium-derived deposit would survive at least until the Imbrium event occurred. The Imbrium-derived deposit would likely consume it, however.

The model also gives proportions of regolith components deriving from the prebasin substrate and each basin source. At the Apollo 16 site, the calculated provenances of the materials in the Imbrium deposit are 20% local (substrate), 25% Nectaris, <1% Humorum, 6% Crisium, 20% Serenitatis, and 30% Imbrium. At the Apollo 17 site, they are 5% local (substrate), 1% Nectaris, <1% Humorum, 4% Crisium, 55% Serenitatis, and 35% Imbrium. These proportions are not sensitive functions of the coverage level. The model results are merely one constraint on provenance; preexisting topography and general photogeologic evidence must also be considered.

References: [1] Arvidson et al. (1976) *Proc. LSC 7th*, 2817–2832. [2] Wieczorek et al., this volume. [3] Haskin et al. (1995) *LPS XXVI*, 557–558. [4] Moss et al. (1998) *Meteoritics & Planet. Sci.*, submitted. [5] Housen et al. (1983) *JGR, 88*, 2485–2489. [6] Oberbeck (1975) *Rev. Geophys. Space Phys., 13*, 337–362.

[7] McGetchin et al. (1973) *EPSC, 20,* 226–236. [8] Haskin (1998) *JGR, 103,* 1679–1689. [9] Metzger et al. (1974) *Proc. LSC 5th,* 1067–1078. [10] Binder A. and Feldman W., personal communication. [11] M. Wieczorek, personal communication.

S77-91

MULTIDISCIPLINARY STUDIES OF ANCIENT MARE BASALT DEPOSITS.

B. R. Hawke[1], T. A. Giguere[1], P. G. Lucey[1], C. A. Peterson[1], G. J. Taylor[1], and P. D. Spudis[2], [1]Hawai'i Institute of Geophysics and Planetology, University of Hawai'i, Honolulu HI 96822, USA, [2]Lunar and Planetary Institute, Houston TX 77058, USA.

Introduction: Cryptomaria are ancient (>3.8 Ga) mare basalt deposits that are hidden or obscured by superposed higher albedo material [1–3]. As such, they represent a record of the earliest mare volcanism and may be a significant volumetric contribution to the lunar crust. Interdisciplinary studies have resulted in major advances in our understanding of ancient lunar volcanism. Since the aim of this workshop is to promote integrated approaches to key problems of lunar science using multiple datasets, it seems appropriate to review the investigations that produced major advances in our understanding of ancient mare volcanism. The purposes of this report are to examine the way that multiple datasets were used to investigate ancient lunar volcanism and to present the most recent results of our studies of cryptomare using Galileo and Clementine multispectral imagery.

Previous Sample, Remote-Sensing, and Geologic Investigations: In the immediate post-Apollo era, the traditional view was that the onset of mare volcanism occurred at ~3.9 Ga [4]. Ryder and Taylor [5] first presented arguments that mare-type volcanism was initiated far earlier than 3.9 Ga, and cited evidence provided by rare mare-type basaltic lithic and mineral fragments in highland breccias. Hawke and Head [6] concluded that high-alumina mare basalts were emplaced in the Fra Mauro region prior to the Imbrium impact event. A wide variety of lunar sample data was analyzed by Ryder and Spudis [7], and they concluded that ancient mare volcanism started well before the terminal lunar bombardment. Subsequently, Taylor et al. [8] presented data for basaltic clasts in the Apollo 14 breccia 14305 that demonstrated that non-KREEP, mare-type volcanism commenced at least as early as 4.2 Ga in the Fra Mauro region and possibly across much of the lunar surface.

Mare basalt deposits emplaced well before the end of the terminal bombardment would have been thoroughly reworked and mixed with highland material [5,7,9]. While little morphologic evidence of these very early basalts would remain, their presence in highland deposits could be expected to exert an influence on the remotely sensed surface compositions of the regions in which they were emplaced. Later mare basalts, extruded near the end of the terminal bombardment, were less thoroughly disrupted and may have been only thinly buried by layers of highlands debris. Hartmann and Wood [10] pointed out that many highland plains exhibit a lower albedo than the heavily cratered portions of the uplands. They hypothesized that ancient lavas flooded those areas before the end of the ancient intense bombardment and that subsequent cratering events were sufficient to cover these regions with a relatively thin veneer of highland-rich debris. If so, mare material may have been excavated from beneath lighter surface units by dark-haloed impact craters.

Schultz and Spudis [11,12] have published the results of a major study concerning the identification, origin, and distribution of dark-haloed impact craters that had exposed mare basalts from beneath higher albedo surface units. They suggested that basaltic volcanism may have predated the last major impact basins, that early farside volcanism may have been widespread, and that at least some lunar light plains may be early volcanic deposits that were subsequently buried by of impact ejecta of varying thicknesses.

The Apollo orbital geochemistry datasets have been successfully used to investigate ancient mare basalt deposits. Analyses of the orbital geochemistry data have shown that some lunar regions have unusual abundances of certain elements relative to surrounding or adjacent areas, or have a surface chemistry unlike that which would be anticipated from the examination of local geologic relationships. Investigation of the formation of the geochemical anomalies can provide important clues to understanding volcanic processes operative during the early phases of lunar evolution. Schultz and Spudis [11] correlated high-Mg/Si intensity ratios with dark-haloed impact craters in the Langemak region. The existence of dark-haloed impact craters with associated high FeO, TiO_2, and Mg/Si values strongly suggests the presence of a buried ancient basalt layer in this region. Hawke and Spudis [9] and Hawke et al. [13] demonstrated that the lunar geochemical anomalies on the eastern limb and farside of the Moon (e.g., Balmer Basin, northeast of Mare Smythii, Langemak region, north of Taruntius) are commonly associated with light plains units that exhibit dark-haloed impact craters. Later, improved Apollo X-ray data were utilized to investigate cryptomare composition and distribution in the Undarum-Spumans and Smythii Basin regions [2,14,15].

Hawke and Bell [16,17] presented results of spectral studies of dark-haloed impact craters in various portions of the lunar nearside. Both multispectral images and near-infrared reflectance spectra obtained with Earth-based telescopes were utilized. Since the spectral properties of lunar soils and rocks had been investigated extensively in the laboratory, it was possible to use Earth-based spectra to determine the composition of small areas on the surface of the Moon [18,19]. Analysis of near-infrared spectra clearly demonstrated that dark-haloed impact craters on the Moon have excavated mare basalt from beneath highland-rich surface material. Hawke and Bell [16,17] suggested that a large but discontinuous mare similar to Mare Australe existed in the Schiller-Schickard region before the Orientale impact event and was covered with a layer of highland debris as a consequence of the formation of Orientale Basin.

Mustard et al. [20] and Head et al. [3] used spectral mixture analysis of Galileo SSI data to investigate the interaction between Orientale primary ejecta and prebasin mare in the Schiller-Schickard cryptomare region. It was determined that major amounts of local mare material were incorporated into the Orientale ejecta deposit by secondary cratering in the Schiller-Schickard region. Blewett and coworkers [21] used Earth-based near-infrared spectra and multispectral imagery to provide additional support for the local-mixing hypothesis. Antonenko and coworkers [2] are currently using Clementine images and other remote-sensing data to investigate the Schiller-Schickard cryptomare. Both Earth-based and spacecraft spectral data have recently been utilized to study cryptomaria northwest of Mare Humorum and near Mare Crisium [e.g., 22,23].

Current Results: We are currently using Clementine UVVIS and Galileo SSI images to conduct detailed investigations of selected lunar cryptomaria. The techniques described by Lucey et al. [24,25] and Blewett et al. [25] were applied to calibrated Galileo SSI images

to produce FeO and TiO_2 abundance maps for the lunar nearside. These maps have a spatial resolution of 1–2 km and were the primary datasets used in this study. Global Clementine FeO and TiO_2 maps with a variety of resolutions (1–35 km) were also used to investigate selected cryptomaria [24–26].

Northeast nearside (NEN) region. Dark-haloed impact craters occur on the extensive light plains deposits on the northeastern portion of the lunar nearside. Hence, ancient mare volcanism may have occurred in at least some parts of the NEN region. Gartner D is a small crater (diameter = 8 km) with a partial dark halo that excavates material from beneath the surface of a light plains unit in the interior of Gartner Crater. Two near-infrared spectra obtained for Gartner D exhibit characteristics that clearly indicate that mare basalt was exposed by this impact event [27]. The Galileo Fe map shows enhanced FeO values associated with Gartner D and other nearby impact craters.

A light plains unit was mapped in the area south of Hercules and Atlas Craters by Grolier [28]. The spectrum for a dark-haloed crater south of Hercules indicates that mare basalt was excavated from beneath the highland-rich ejecta blanket emplaced by the Hercules impact event [27]. Other impact craters in the vicinity excavated FeO-rich mare material from beneath the surface of the light plains unit. It appears that this light plains unit was produced by the contamination of a mare deposit with highland-rich ejecta from Hercules and Atlas Craters [29].

Balmer region. In general, the Balmer cryptomare exhibits elevated FeO and TiO_2 values relative to the surrounding highlands. Some small, circular areas exhibit FeO values of 14–16% and correlate directly with dark-haloed impact craters. Many of these dark-haloed craters also exhibit elevated TiO_2 values [29]. It has been proposed that this region was the site of ancient mare volcanism and that the basaltic units were later covered by a thin, higher-albedo surface layer enriched in highland debris contributed by surrounding large impact craters [13,14]. The existence of dark-haloed impact craters that exhibit elevated FeO and TiO_2 values supports this proposal.

Southern central highlands. Most of the southern portion of the lunar central highlands exhibit FeO values that range between 5 and 9 wt%. However, a small area with anomalously high FeO values has been identified near Maurolycus Crater. The highest FeO values (13–15 wt%) are centered on the dark-rayed crater Buch B (diameter = 6 km), which is located on the rim and wall of Buch C. Lesser FeO enhancements are associated with the dark-rayed crater Maurolycus A (diameter = 15 km) and Barocius M (diameter = 17 km), which may also excavate dark material. However, it should be noted that none of these craters is located on a light plains deposit. We suggest that mafic intrusions were excavated from depth by the dark-rayed craters [29].

References: [1] Head J. W. and Wilson L. (1992) *GCA, 56,* 2144–2175. [2] Antonenko I. et al. (1995) *Earth, Moon, Planets, 56,* 141–172. [3] Head J. W. et al. (1993) *JGR, 98,* 17149–17181. [4] Taylor S. R. (1975) *Lunar Science: A Post-Apollo View.* [5] Ryder G. and Taylor G. J. (1976) *Proc. LSC 7th,* 1741–1755. [6] Hawke B. R. and Head J. W. (1978) *Proc. LPSC 9th,* 3285–3309. [7] Ryder G. and Spudis P. D. (1980) *Proc. Conf. Lunar Highlands Crust,* 353–375. [8] Taylor L. A. et al. (1983) *LPS XIV,* 777–778. [9] Hawke B. R. and Spudis P. D. (1980) *Proc. Conf. Lunar Highlands Crust,* 467–481. [10] Hartmann W. K. and Wood C. A. (1971) *Moon, 3,* 3–78. [11] Schultz P. H. and Spudis P. D. (1979) *Proc. LPSC 10th,*

2899–2918. [12] Schultz P. H. and Spudis P. D. (1983) *Nature, 302,* 233–236. [13] Hawke B. R. et al. (1985) *Earth, Moon, Planets, 32,* 257–273. [14] Clark P. E. and Hawke B. R. (1987) *Earth, Moon, Planets, 38,* 97–112. [15] Clark P. E. and Hawke B. R. (1991) *Earth, Moon, Planets, 53,* 93–107. [16] Hawke B. R. and Bell J. F. (1981) *Proc. LPS 12B,* 665–678. [17] Bell J. F. and Hawke B. R. (1984) *JGR, 89,* 6899–6910. [18] McCord T. B. and Adams J. B. (1973) *Moon, 7,* 453–474. [19] McCord T. B. et al. (1981) *JGR, 86,* 10833–10892. [20] Mustard J. F. et al. (1992) *LPS XXIII,* 957–958. [21] Blewett D. T. et al. (1995) *JGR, 100,* 16959–16977. [22] Hawke B. R. et al. (1995) *GRL, 20,* 419–422. [23] Blewett D. T. et al. (1995) *GRL, 22,* 3059–3062. [24] Lucey P. G. et al. (1995) *Science, 268,* 1150–1153. [25] Lucey P. G. et al. (1998) *JGR, 103,* 3679–3699. [26] Blewett D. T. et al. (1997) *JGR, 102,* 16319–16325. [27] Hawke B. R. et al. (1993) *LPS XXIV,* 617–618. [28] Grolier M. J. (1974) *U.S. Geol. Survey Map I-841.* [29] Giguere T. A. et al. (1998) *LPS XXIX,* Abstract #1782.

$\mathcal{S}/\mathcal{B} - \mathcal{G}/$

LUNAR MARE BASALT VOLCANISM: STRATI-GRAPHY, FLUX, AND IMPLICATIONS FOR PETROGE-NETIC EVOLUTION. J. W. Head III, Department of Geological Sciences, Brown University, Providence RI 02912, USA (James_Head_III@brown.edu).

Introduction: Lunar mare basalt deposits are an example of a vertically accreting secondary crust (derived from partial melting of planetary mantles) superposed on a platform of primary crust (derived from accretional and related heating) [1]. The small total area covered by mare deposits (~17% of the surface) [2] and the small volume (~1 × 10⁷ km³) [2] are such that the stratigraphy, fluxes, and modes of emplacement can be documented and studied, particularly with the availability of Clementine multispectral imaging [3], complementary Apollo and Luna sample collections [e.g., 4–6], and Lunar Prospector data. These data can then be used to test models for the origin, ascent, and eruption of basaltic magmas, and to document the early stages of secondary crustal formation and evolution. The topic of this contribution is a synthesis of the emerging new stratigraphy, estimates of flux, an analysis of outstanding problems, and emerging constraints on petrogenetic models for generation and emplacement of secondary crustal magmas.

Stratigraphy, Duration and Flux: Photogeologic, remote-sensing, and returned sample studies [7,8] show that mare volcanism had begun prior to the end of heavy bombardment (period of cryptomare formation [9–12]), in Early Imbrian and pre-Nectarian times, and possibly continued until the Copernican Period, a total duration approaching 3 b.y. Recent analyses have shown that there were widespread mare regions during the cryptomare period [9–12] comparable in area to presently exposed maria such as Serenitatis [15–17].

For later deposits, detailed analyses revealing the range of volumes typical of individual eruptions [13] and Clementine data are revealing the compositional affinities and volumes of units in individual basins and regions [14–17]. The source of heat required for melting and depth of origin is a major outstanding question in the petrogenesis of mare basalts [6,18] and the onset of mare-type volcanism is key to understanding some types of models [19] for the origin of mare basalt source regions. Increasing detection of cryptomaria has clearly demonstrated that mare volcanism began

and was areally extensive [9–12,15–17,20] prior to the formation of Orientale, the last of the large impact basins, ca 3.8 Ga [7]. Presently unresolved is the actual age of onset and areal and volumetric significance of this early mare-type volcanism. New information on the diversity and distribution of mare basalts as a function of time are beginning to accumulate from the analysis of Clementine data. Initial Apollo models emphasized the high-Ti nature of Apollo 11 basalts and the low-Ti nature of Apollo 12 basalts, leading to the hypothesis that melting of the mare basalt source region began at the ilmenite-rich residuum and deepened with time into the mantle [18]. Remote-sensing data from unsampled western maria [21], however, showed that young high-Ti basalts were widespread and largely of Eratosthenian age [7,21]. These and subsequent analyses [e.g., 15–17,22] have shown that each of the mare basins is characterized by a diversity of mare basalt volcanic fill. Utilizing these data and our own analyses, we are producing a stratigraphic synthesis of mare basalts in individual basins and regions; this synthesis is beginning to show that temporal compositional heterogeneity is at least as important as sequential heterogeneity.

These analyses also provide information on the flux. Abundant geologic evidence shows that the vast majority of observed volcanic deposits (>90%, ~9.3 × 10⁶ km³) were emplaced in the Late Imbrian Period, spanning 600 m.y. from ca 3.8 to 3.2 Ga [7,9,23]; new crater-count data confirm this and place diverse stratigraphically dated mare deposits in this period [e.g., 17]. Preliminary analyses suggest that a wide range of basaltic compositions was emplaced in virtually all the nearside mare basins, with earliest and intermediate deposits dominated by (but not confined to, e.g., see [15–17]) high-Ti basalts; later deposits of this period are dominantly low in Ti and represent the major late fill of nearside basins (e.g., Crisium, Serenitatis, Imbrium, and Procellarum). The emerging picture is that the maximum period of production, ascent, and emplacement of mare basalts was between 3.8 and 3.2 Ga; magmas produced during this period were diverse in space and time, but dominated by an early phase of high-Ti basalts.

Following this, <5% of the total volume of mare basalts was emplaced during the Eratosthenian Period (spanning ~2.1 b.y.); a few of the latest flows may extend into the Copernican Period [8]. Predominantly high-Ti basalts were emplaced largely on the central and western nearside (Imbrium and Procellarum [21]). The low overall volume and low average effusion rate of the latest deposits is partly due to global cooling and the increasingly compressional state of stress in the lithosphere [24], both factors minimizing production of basaltic magmas and their ascent to the surface. A key conclusion is that the heat source for melting of parental material was operating for possibly as long as an additional 2 b.y., and that it produced high-Ti basalts extruding over a limited portion of the lunar surface.

In summary, mare deposits testify to the production and extrusion of mare basalts for a period of at least 2 b.y. and perhaps as long as 3 b.y.; surface volcanism, however, has not been volumetrically significant on the Moon since about the late Archean on Earth. Mare volcanic flux was not constant, but peaked during the Late Imbrian Period; average global volcanic output rate during this peak period was ~10⁻² km³/yr, comparable to the present local output rates for individual volcanos on Earth such as Kilauea, Hawai'i. Some single eruptions associated with sinuous rilles may have lasted about a year and emplaced 10³ km³ of lava. The flux was variable in space and time during this period, and the patterns revealed by the stratigraphy show evidence for regional concentrations of sources and compositional affinities; these patterns are the basic data for defining the

configuration, size, and density of mantle source regions throughout the period of mare basalt emplacement. Evidence for emplacement style suggesting that magmas are commonly delivered to the surface in large quantity through dikes originating from depth [e.g., 9] include areally extensive lava flows [25], sinuous rilles attributable to thermal erosion [26], lack of large shield volcanos [27], and evidence for the emplacement of large dikes in the vicinity of the surface [28]. The low density of the lunar highland crust provides a density barrier to the buoyant ascent of mantle melts [29] and ascending diapirs are likely to stall at a neutral buoyancy zone there, before reservoir overpressurization propagates dikes toward the surface [9]. In summary, these data provide an emerging picture of the nature, flux, and mode of emplacement of lunar mare deposits.

Testing Models of Petrogenesis and Modes of Emplacement: These emerging data on mare heterogeneity in time and space can be used to test models for the petrogenesis and mode of emplacement of mare basalts. As an example, in one model [19], the dense ilmenite-rich (with high concentrations of incompatible radioactive elements) and underlying Fe-rich cumulates forming at the base of a stratified lunar differentiate are negatively buoyant and sink to the center of the Moon. Subsequent radioactive heating causes mantle melting and diapiric rise of magmas. The low-density highland crust acts as a density barrier to the buoyant ascent of mare basalt magmas, likely causing them to stall and overpressurize, sending magma-filled dikes to the lunar surface. This density-barrier factor may be responsible for much of the areal difference in distribution of mare basalt deposits, most notably in the nearside-farside asymmetry [9]. The emerging details of the stratigraphic record, and increasing ability to read through the primary crustal density filter, permit us to begin to constrain aspects of this model and examine others. The ongoing studies and emerging syntheses of lunar mare stratigraphy are being combined with other parallel analyses of lunar samples and remote-sensing data that will help to characterize secondary crustal evolution [1] on the Moon. These data will provide a significant baseline for the study of secondary crustal formation and evolution on other planetary bodies.

References: [1] Taylor S. (1989) *Tectonophysics, 161,* 147. [2] Head J. (1975) in *Origins of Mare Basalts,* p. 66, LPI. [3] McEwen A. et al. (1994) *Science, 266,* 1858. [4] Nyquist L. and Shih C. (1992) *GCA, 56,* 2213. [5] Neal C. and Taylor L. (1992) *GCA, 56,* 2177; Shearer C. and Papike J. (1994) *GCA, 57,* 4785. [6] Delano J. (1986) *Proc. LPSC 16th,* in *JGR, 91,* D201. [7] Wilhelms D. (1987) *USGS Prof. Paper 1348,* 302 pp. [8] Head J. (1976) *Rev. Geophys. Space Phys., 14,* 265; Basaltic Volcanism Study Project (1981) *Basaltic Volcanism on the Terrestrial Planets,* Pergamon, 1286 pp.; Schultz P. and Spudis P. (1983) *Nature, 302,* 233. [9] Head J. and Wilson L. (1992) *GCA, 56,* 2155. [10] Head J. et al. (1993) *JGR, 98,* 17149. [11] Greeley R. et al. (1993) *JGR, 98,* 17183. [12] Hawke B. et al. (1993) *GRL, 20,* 419; Antonenko I. et al. (1995) *Earth, Moon, Planets, 69,* 141; Mustard J. and Head J. (1996) *JGR, 101,* 18913. [13] Yingst A. and Head J. (1996) *LPS XXVII,* 1477; *LPS XXVII,* 1479. [14] Yingst A. and Head J. (1997) *LPS XXVIII,* 1609. [15] Staid et al. (1996) *JGR, 101,* 23213. [16] Hiesinger H. et al. (1996) *LPS XXVII,* 545; *LPS XXVII,* 547. [17] Hiesinger H. et al. (1997) *LPS XXVIII,* 571. [18] Taylor S. R. (1982) *Planetary Science: A Lunar Perspective,* LPI. [19] Hess P. and Parmentier E. (1995) *EPSL, 134,* 501. [20] Bell J. and Hawke B. (1984) *JGR, 89,* 6899; Hawke B. et al. (1991) *GRL, 18,* 2141. [21] Pieters C. (1978) *Proc. LPSC 9th,* 2825; Whitford-Stark J. and Head J. (1980) *JGR, 85,* 6579.

[22] Johnson J. et al. (1991) *JGR, 96*, 18861. [23] Hartmann W. et al. (1981) in *Basaltic Volcanism on the Terrestrial Planets*, p. 1049, Pergamon. [24] Solomon S. and Head J. (1980) *Rev. Geophys. Space Phys., 18*, 107. [25] Schaber G. (1973) *Proc. LSC 4th*, 73. [26] Hulme G. (1973) *MG, 4*, 107; Carr M. (1973) *Icarus, 22*, 1. [27] Head J. and Wilson L. (1991) *GRL, 18*, 2121. [28] Head J. and Wilson L. (1993) *Planet. Space Sci., 41*, 719. [29] Solomon S. (1975) *Proc. LSC 6th*, 1021.

Sp.-71

THE LUNAR SOURCE DISK: OLD LUNAR DATASETS ON A NEW CD-ROM. H. Hiesinger, Institute of Planetary Exploration, Deutsches Zentrum für Luft-und Raumfahrt, Berlin, Germany, and Department of Geological Sciences, Brown University, Providence RI 02912, USA (Harald.Hiesinger@dlr.de).

I present here a compilation of previously published datasets on CD-ROM. This Lunar Source Disk is intended to be a first step in the improvement/expansion of the Lunar Consortium Disk [1], in order to create an "image-cube"-like data pool that can be easily accessed and might be useful for a variety of future lunar investigations. All datasets were transformed to a standard map projection that allows direct comparison of different types of information on a pixel-by-pixel basis.

Introduction and Challenges: Lunar observations have a long history and have been important to mankind for centuries, notably since the work of Plutarch and Galileo. As a consequence of centuries of lunar investigations, knowledge of the characteristics and properties of the Moon has accumulated over time. However, a side effect of this accumulation is that it has become more and more complicated for scientists to review all the datasets obtained through different techniques, to interpret them properly, to recognize their weaknesses and strengths in detail, and to combine them synoptically in geologic interpretations. Such synoptic geologic interpretations are crucial for the study of planetary bodies through remote-sensing data in order to avoid misinterpretation. In addition, many of the modern datasets, derived from Earth-based telescopes as well as from spacecraft missions, are acquired at different geometric and radiometric conditions. These differences make it challenging to compare or combine datasets directly or to extract information from different datasets on a pixel-by-pixel basis. Also, as there is no convention for the presentation of lunar datasets, different authors choose different map projections, depending on the location of the investigated areas and their personal interests. Insufficient or incomplete information on the map parameters used by different authors further complicates the reprojection of these datasets to a standard geometry. The goal of our efforts was to transfer previously published lunar datasets to a selected standard geometry in order to create an "image-cube"-like data pool for further interpretation. The starting point was a number of datasets on a CD-ROM published by the Lunar Consortium [1]. The task of creating an uniform data pool was further complicated by some missing or wrong references and keys on the Lunar Consortium CD as well as erroneous reproduction of some datasets in the literature (e.g., [2] vs. [3]).

Data Format: All datasets on the Lunar Source Disk are available in a simple cylindrical map projection. I chose this type of projection as the standard because numerous lunar datasets are restricted to ±30° lattitude. The storage of all important map parameters in a VICAR label guarantees easy reprojection of the maps for special scientific questions. The spatial resolution of our maps at the

equator is 1.2 km/pixel or 25.269 pixel/°. Assuming a spherical lunar radius of 1737.4 km, we obtained a map size of 9091 × 4545 pixels. This map size can still be displayed on most PCs or Macs, without the need for a sophisticated high-end computer. Additionally, for easy location of data points relative to morphologic features, all datasets were superimposed on a USGS shaded relief map. This is one advantage of the new Lunar Source Disk over the Lunar Consortium Disk [1], since it allows the interpretation of different types of information relative to the lunar topography. For easy and convenient access independent from the computer platform, all datasets with or without the USGS shaded relief map were stored as PICT images on the CD.

Available Datasets: At present the following datasets are available on CD (see also Fig. 1):

Data from the Clementine Laser Altimeter (LIDAR). This dataset was published by Zuber et al. [4] and provides global information on free-air gravity, Bouguer anomalies, topography, and crustal thickness.

Data from Earth-based observations performed at the Mauna Kea Observatory in 1989. This dataset consists of 12 mosaics in the spectral range between 402 nm and 991 nm. The dataset covers the entire lunar nearside.

Data from the Galileo EM-1 encounter. The dataset consists of SSI mosaics in six filters (409 nm, 562 nm, 660 nm, 756 nm, 889 nm, and 993 nm) published by McEwen et al. [5]. The mosaics cover the western farside of the Moon.

Data from the Galileo EM-2 encounter. This dataset covers the northern nearside and is based on the SSI LUNMOS-05 sequence.

Data from the Apollo γ-ray experiment. This dataset contains information on the abundances of Fe, Ti, and Th as published by Davis [6] and Metzger [7]. The image coverage is restricted to the flight paths of the Apollo 15 and 16 Command Modules.

Data from the Apollo X-ray experiment. This dataset allows the estimation of the Mg/Si and Al/Si ratios as published by Clark and Hawke [8]. The image coverage is restricted to the flight paths of the Apollo 15 and 16 command modules.

Data from the Apollo Laser Altimeter. I normalized this dataset to the Clementine altimeter data; therefore it must be treated with caution because of possible inaccurancies in absolute and relative heights. The image coverage is restricted to the flight paths of the Apollo 15 and 16 command modules.

Multispectral classification of lunar nearside mare basalts. Earth-based multispectral observations were used to classify lunar mare basalts according to spectral characteristics [9]. The dataset covers all mare basalts on the lunar nearside.

Albedo map of Pohn and Wildney [10]. This map is constructed from Earth-based albedo observations of the Moon and classifies the lunar surface into 20 albedo classes from 0.069 to 0.239. The dataset covers the entire lunar nearside.

Albedo map for differential photometric corrections according to the classes (bright, average, dark) of Helfenstein and Veverka [11]. Based on the albedo map of Pohn and Wildney [10] I subdivided the lunar surface into bright areas (A_N 0.13–0.16), average areas (A_N 0.10–0.12), and dark areas (A_N 0.06–0.09). This subdivision corresponds to the albedo classes of Helfenstein and Veverka [11] so their parameters for a differential photometric correction can be applied directly.

Surface age data. This map was published by Boyce [12] and Boyce and Johnson [13] and is based on crater degradation/density investigation. Data cover large areas of the lunar nearside.
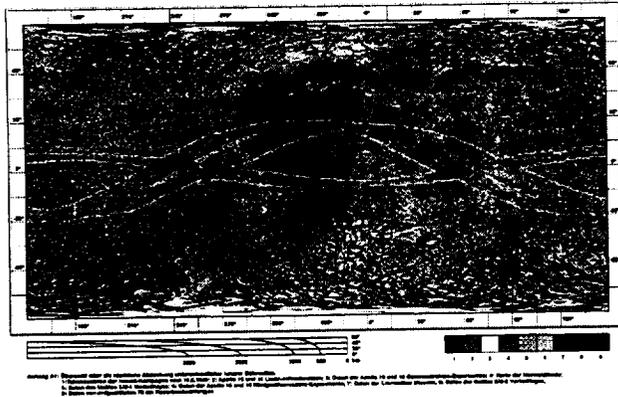
Fig. 1. Simple cylindrical map of the Moon showing the spatial coverage of datasets available on the Lunar Source Disk. Data from (1) multispectral Earth-based observations performed at Mauna Kea Observatory; (2) Apollo 15 and 16 Laser Altimeter; (3) Apollo 15 and 16 γ-ray experiment; (4) map of the normal albedo; (5) Galileo EM-1; (6) Apollo 15 and 16 X-ray experiment; (7) Clementine mission; (8) Galileo EM-2; (9) Earth-based radar.

Polarized/depolarized radar maps. This dataset was published by Thompson [14] and covers the entire lunar nearside.

References: [1] The Lunar Consortium. [2] Basaltic Volcanism Study Project (1981) *Basaltic Volcanism on the Terrestrial Planets,* Pergamon, 1286 pp. [3] Heiken et al., eds. (1991) *Lunar Sourcebook,* Cambridge Univ., 736 pp. [4] Zuber et al. (1994) *Science, 266.* [5] McEwen et al. (1993) *JGR, 98.* [6] Davis (1980) *JGR, 85.* [7] Metzger (1977) *Proc. LSC 8th.* [8] Clark and Hawke (1981) *Proc. LPS 12B.* [9] Pieters (1978) *Proc. LPSC 9th.* [10] Pohn and Wildney (1970) *USGS Prof. Paper 599-E.* [11] Helfenstein and Veverka (1987) *Icarus, 72.* [12] Boyce (1976) *Proc. LSC 7th.* [13] Boyce and Johnson (1978) *Proc. LPSC 9th.* [14] Thompson (1987) *The Moon, 10.*

5 : 3 - 9 /

INVESTIGATION OF LUNAR MARE BASALTS: AN INTEGRATED APPROACH. H. Hiesinger[1,2], R. Jaumann[2], G. Neukum[2], and J.W.Head III[1], [1]Department of Geological Sciences, Brown University, Providence RI 02906, USA, [2]Institute of Planetary Exploration, Deutsches Zentrum für Luft-und Raumfahrt, Berlin, Germany (Harald.Hiesinger@dlr.de).

Introduction: From previous studies we know that 17% of the lunar surface is covered by mare basalts, most of them exposed in the large impact basins of the lunar nearside [1]. From these investigations we also know that lunar mare basalts exhibit a broad variety of ages as well as geochemical compositions [2]. Here we present ages that are based on crater size-frequency distributions for spectrally defined lunar nearside mare basalts that are exposed in the Australe, Tranquillitatis, Humboldtianum, Serenitatis, and Imbrium Basins. We also present geochemical data for the Ti concentrations of mare basalts in Mare Tranquillitatis, Mare Humorum, Mare Serenitatis, and Mare Imbrium. From the lunar sample collection it is known that Ti-poor basalts are generally younger than Ti-rich basalts [3]. On the other hand, we learned from remote-sensing data that there are also young basalts with high TiO_2 concentrations. Therefore, in this study, we investigate the relationship between ages and TiO_2 concentrations, and we also stress the question of whether there is a correlation between these two parameters and what kind of correlation it is. Additionally, we discuss the influence of topography and crustal thickness on basalt eruptions on the lunar surface.

Approach and Description of the Database: In this study we combine and make use of different types of remote-sensing datasets: ages derived from Lunar Orbiter images, geochemical data derived from multispectral Earth-based data and Galileo images, and crustal thickness and topography derived from Clementine data. A combination of spectral, geochemical, and radiometric work on returned lunar samples in the laboratory forms the basis for our compositional investigation of the lunar surface with remote-sensing techniques. In 1992 the Galileo spacecraft passed the Earth-Moon system on its way to the jovian system. During this second flyby (EM-2), the northern central parts of the lunar nearside hemisphere were imaged at a spatial resolution of 1.5 km/pixel. From this dataset we calculated several ratios and displayed them simultanously as a color ratio composite in order to enhance subtle spectral differences of the lunar mare basalts. On this color ratio composite we mapped units with homogeneous spectral characteristics and transferred the unit boundaries to Lunar Orbiter IV images. The boundaries were also compared closely to the Lunar Orbiter images and adjusted to fit morphological and/or albedo features. This yielded spectrally and morphologically homogeneous areas for which we performed crater counts to determine their surface ages. The spatial resolution of the Lunar Orbiter IV images is ~100 m/pixel.

To obtain the Ti concentrations of each of these units we again made use of the Galileo dataset and Earth-based telescopic data. The images were corrected for radiometric and photometric effects, projected onto a map, mosaicked, and normalized to MS2, a spectral calibration area in Mare Serenitatis. The UV/VIS ratio is an appropriate method for deriving Ti concentrations of unsampled mature mare regions from multispectral remote-sensing data [4]. We used this empirical relationship to determine the mean TiO_2 concentrations of our units. To do so, we made use of the classification by [5], which allows us to distinguish four different classes of TiO_2 concentrations. Low-Ti basalts exhibit TiO_2 contents of <2 wt%, medium-Ti basalts show less than 4 wt%, medium-to-high-Ti basalts are characterized by 3–7 wt% Ti, and high-Ti basalts contain <6 wt% Ti. As this classification allows variations in Ti content of up to several weight percent ages, it was necessary to define the Ti concentration more precisely in order to calculate the mean TiO_2 content of each unit. Therefore we used the mean value of each class (1, 2, 5, and 9 wt%) to calculate the mean Ti concentration in each unit.

Crustal thickness and topography were globally measured and interpreted by the Clementine laser altimeter. Zuber et al. [5] published maps of these two parameters and we reprojected these maps to compare with our data. As a result, we obtained a data pool that consists of the age and mean TiO_2 content, as well as the crustal thickness and topography for 98 different units in four basins.

Conclusions: We combined high-resolution Lunar Orbiter images with several types of multispectral Galileo data, applied different techniques, and made use of an empirical relationship that was originally detected in returned lunar samples. We also made use of Clementine laser altimeter data to investigate the influence of topography and crustal thickness on lunar basalt eruptions. Even if our study is only a first step in combining different lunar datasets in a synoptic geologic interpretation, we believe that ongoing efforts to create an "image-cube"-like lunar data pool will greatly expand our knowledge of the Moon.
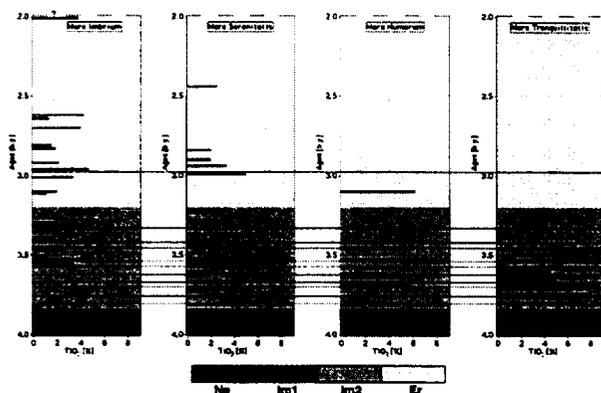
Fig. 1. Ages and Ti content in the investigated mare regions. Each bar represents a single basalt unit. Basins are aligned by age (oldest basin on the righthand side, youngest basin on the lefthand side). Ne = Nectarian, Im1 = Early Imbrian, Im2 = Late Imbrian, Er = Eratosthenian.

So far our results indicate that lunar volcanism was active in these areas for at least 2 b.y (4.0–2.0 Ga). We also see that volcanism lasted longer in the western (younger) basins than in the eastern (older) basins. In the eastern basins the maximum frequency of the basalt eruptions is 3.6–3.8 b.y., and in the western basins it is 3.3–3.5 b.y. At the end of the late Imbrian Period the volcanic activity decreased drastically and we see only a small number of Eratosthenian eruptions. Basalts of Copernican age have not been identified in the investigated basins. From our data we conclude that with decreasing basin age the maxima of the measured ages shift to younger ages and the width of the age distribution broadens significantly. All investigated dark mantle deposits exhibit similar ages of 3.6–3.8 Ga and the oldest basalts observed in each basin are determined to have formed within 100 m.y. after the basin-forming impact.

However, the most important result of our investigation is that we found no correlation between the age and the corresponding TiO_2 content in any of the investigated basins. In each single basin, the TiO_2 concentrations seem to vary independently from the ages of the units. Both Ti-rich and Ti-poor basalts can erupt at the same time at different locations in the basin. However, our data suggest that there is a trend that shows the basalts of the older basins to be more Ti rich than the basalts of the younger basins. It is also obvious that with decreasing basin age, the variety of ages and compositions increases. From the stratigraphic columns (Fig. 1) we learn that the basalts that exhibit the relatively highest Ti contents often appear simultanuously in all investigated basins. From the narrow distribution of the ages in Mare Tranquillitatis and Mare Humorum, we conclude that these basins may have been filled in relatively short periods of time and therefore show very similar geochemical composition. For the other two basins, differentiation processes in the magma reservoirs or the lunar mantle during the longer active volcanic period may have led to the different compositions.

Concerning the influence of topography and crustal thickness, we found that the youngest basalts are often exposed in or near areas with the relatively thinnest crust. Crustal thickness seems to be a key factor for the eruption of basalts. We see that volcanism is active for longer periods of time in regions with a thinner crust, and that the maximum crustal thickness for a lunar basalt eruption is ~50–60 km.

Future Work: One of the most interesting questions in inves-

tigating the thermal and geochemical evolution of the Moon as well as the stratigraphic relation of basalt eruptions of different compositions concerns the amount of mare basalts that were errupted over time. To answer this question, precise estimates of the volumes of distinct lava flows are required. These estimates may be obtained by stereo processing of digitized high-resolution images of the Apollo metric camera in order to derive the flow height. Given the areal extension of a previously spectrally defined flow, which can be easily measured, this will allow high-precision calculations of single flow volumes. Therefore we seek to digitize high-resolution Apollo images to perform these height estimates and to include the obtained basalt volumes into our interpretation.

References: [1] Head (1975) *Origins of Mare Basalts.* [2] Wilhelms (1987) *USGS Prof. Paper 1348.* [3] Tera and Wasserburg (1975) *LSC VI.* [4] Charette et al. (1974) *JGR, 79.* [5] Pieters (1993) *Topics in Remote Sensing, 4,* Cambridge Univ.

INTEGRATED STUDIES OF IMPACT-BASIN EJECTA AS PROBES OF THE LUNAR CRUST: IMBRIUM AND SERENITATIS.

B. L. Jolliff and L. A. Haskin, Department of Earth and Planetary Sciences and the McDonnell Center for the Space Sciences, Washington University, St. Louis MO 63130, USA (blj@levee.wustl.edu).

Introduction: The large, late, basin impacts on the Earth side of the Moon fundamentally reshaped the structure of the crust, its surface morphology, and the composition of the megaregolith and surface soils. The latest (except for Orientale on the western limb) and largest was the Imbrium impact, which produced massive ejecta deposits over much of the Procellarum region and beyond [1], and ejected material that mixed with surface regolith nearly Moonwide [2]. The basins serve as natural probes into the lunar crust; therefore, understanding the nature and composition of ejecta produced by them provides information about the crust at depth [e.g., 3]. Gravity data allow modeling of the structure of the crust beneath the basins, and from such models one can infer depths of excavation and the nature of crustal response following impact [4].

Highland Materials at and near the Rim of the Imbrium Basin: Highland deposits at the Apollo 14 and 15 landing sites contain Imbrium ejecta. Apollo 14 sampled the Fra Mauro Formation, which proved to be rich in impact-melt breccia. These rocks are relatively mafic (9–10 wt% FeO) and rich in incompatible trace elements (ITE) [5]. Although some of them have been reworked locally, they are generally thought to represent material ejected by Imbrium from the lower crust. The Apollo 15 landing site, at the topographic rim of the Imbrium basin, contains a variety of ITE-rich impact-melt rocks [6] as well as volcanic KREEP basalt. Although age relationships among the impactites are complex [7], it is clear that these rocks have a deep crustal source, similar to, if not the same as, the Apollo 14 ITE-rich melt breccias. Based on Clementine UV/VIS data, the Apennine Front and other highlands along the rim of the Imbrium Basin have high FeO concentrations (8–12 wt% [8,9]) relative to most highland soils, indicating the predominance of impact-melt breccias in the Imbrium proximal ejecta.

Highland Materials at the Rim of the Serenitatis Basin: Impact-melt breccias from the Apollo 17 site are also relatively mafic (8–10 wt% FeO) and have KREEP-like enrichment of incompatible elements. If they were formed by the Serenitatis impact, then their

source region is similar to the region excavated by Imbrium. This is important, especially if, as suggested by [2], Imbrium struck and excavated a geochemically anomalous ("Th-rich") region of the crust.

The Apollo 17 landing site lies at the southeastern edge of the Serenitatis Basin near its topographic rim. Highland massifs in the area have been interpreted as the upper part of thick ejecta deposited by the Serenitatis impact [10,11]. The Imbrium Basin is younger than the Serenitatis Basin, however, and much of the highlands east of Serenitatis show evidence of later deposition of ejecta from the Imbrium event [12]. At the Apollo 17 site, the Sculptured Hills, which typify extensive hilly deposits in the region and resemble the Alpes Formation around Imbrium [13], postdate the massifs. It is unclear, however, whether these deposits are a late phase of Serenitatis ejecta, or whether they might instead be Imbrium-induced deposits [12].

From the fact that the blocky massif structures in the Taurus-Littrow region are consistent with an origin related to the Serenitatis event [10–13], and from the lack of recognizable Imbrium structures in the region, it has been inferred that the Apollo 17 site may lie within a window that was relatively unaffected by Imbrium ejecta [1]. However, geochemical similarities between the melt breccias at this landing site and the Apollo 14, 15, and 16 sites, supported by recent modeling of the distribution of basin ejecta (physical distribution and mixing and orbital geochemistry), led [14] to reexamine the possibility that these rocks might have been formed in the Imbrium event.

To further test this possibility, we are investigating the distribution around the Serenitatis Basin of mafic impact melt of the kind found at the Apollo 17 site. By comparing FeO concentrations derived from Clementine multispectral data for the landing site, where soil compositions and lithology are known, to Clementine data for the massifs and other surrounding highland units, we find the highland units, including "sculptured hills material" as well as parts of the massifs, to be relatively rich in FeO. Given the highland rock types at the landing site, we interpret this to mean that regolith developed on the highland units contains a high proportion of mafic impact-melt breccia. The Apollo 17 melt breccias have FeO concentrations of about 8–10 wt%, whereas other highland lithologies at the landing site contain on average only 5–7 wt% [15]. Areas of lower FeO concentrations (<8 wt%) appear to be exposed mainly on steep slopes where mass wasting has caused mixing or where small impacts have punched through the impact-melt-rich upper layer. This stratigraphy is consistent with what would be expected if impact melt flowed over the top of the topographic rim of the Serenitatis basin prior to compensation uplift, the formation of grabens, and the onset of inter-massif mass wasting. However, this stratigraphy might also have been produced by blanketing of the region by Imbrium ejecta, with subsequent exposure of the underlying, more feldspathic highland material (Serenitatis ejecta?) mainly where steep slopes gave rise to extensive mass wasting.

The distribution of FeO and TiO_2 in highland deposits north of the Apollo 17 site to crater Le Monnier and up to 200 km east of the basin provides evidence of the origin and emplacement of impact-melt deposits there. Regions of knobby terrain similar to the Sculptured Hills have concentrations of FeO and TiO_2 similar to those of the Sculptured Hills and to areas at high elevations on the massifs, suggesting enrichment in mafic impact melt [16]. If Imbrium ejecta, consisting mainly of impact melt of ~10 wt% FeO, mixed with feldspathic substrate, the resulting surface deposits should have

significantly less than 10% FeO. In this region, concentrations of FeO decrease from >10 to <8 wt% with distance from the Serenitatis rim along a band that is concentric to Serenitatis, consistent with a decrease in the proportion of mafic impact melt and a Serenitatis origin for most of the melt-breccia deposits.

Distribution of Thorium and Relationship to the Imbrium Basin: Incompatible trace elements such as Th are concentrated in mafic impact-melt breccias and volcanic KREEP basalts. The approximate proportions and Th concentrations of mafic melt breccias in Apollo landing-site soils are known, and Haskin [2] showed that Th concentrations as determined by the Apollo 15 and 16 orbital γ-ray experiments were roughly consistent with the proportions of melt breccias found as rock fragments in the sampled soils. Furthermore, the concentrations of Th along the orbital ground tracks fall off with radial distance away from the Imbrium basin and are consistent with the amount of impact debris that should, on average, occur mixed in with the local regolith at different distances. On the other hand, there are no similarly elevated Th concentrations in eastern-Serenitatis ejecta.

These observations provide the basis for the "re-hypothesis" that all mafic impact-melt breccias sampled by the Apollo missions may derive from the Imbrium basin-forming event. That all of these rocks have geochemically very similar ITE signatures is consistent with this hypothesis and may not necessarily require the existence of a global layer of KREEP source rock that could be tapped by any basin-forming impact large enough to excavate the deep crust. Subtle compositional differences between mafic melt-breccia groups, which have been taken by some to imply different impacts, may be a consequence of a single, large, basin impact into a heterogeneous target, which could produce impact melt of different composition along different ejecta trajectories, or from incorporation and digestion of local material at the point of secondary impact. Similarly, differences in siderophile-element signatures between different groups of melt breccias may be due mainly to variable mixing of metal from the Imbrium bolide with metal already present in some of the target materials [17]. Continued analytical work and evaluation of results of Ar-Ar radiometric dating of lunar impact-melt breccias [e.g., 18] may yet provide the critical constraint on this hypothesis.

If the Apollo 17 impact-melt breccias *are* Serenitatis ejecta, then the Serenitatis impactor sampled a crustal section at the eastern edge of the high-Th "geochemical province" similar at depth to that beneath Imbrium. Gamma-ray data from Lunar Prospector show clearly the high Th concentration in the Procellarum-Imbrium region and the Imbrium-radial nature of Th-rich ejecta. The Th-rich area is slightly larger than the extrapolation of [2] based on Apollo γ-ray data, roughly coincident with the resurfaced area bounded by Procellarum, Frigoris, and Cognitum, and extends to the western part of the Serenitatis basin.

The distribution of Th at the lunar surface, coupled with an understanding of the origins of the geologic formations and structures, provides a critical test of how much of the present-day surface distribution of material was influenced by the Imbrium event. If, among the large lunar basins, only Imbrium (and possibly Serenitatis) excavated ITE-rich impact melt, then it seems likely that the ITE-rich residue of early lunar differentiation was concentrated beneath the "Th oval" region. The implications of this hypothesis for crustal asymmetry on a global scale and for the thermal evolution of the Moon are enormous. If, as suggested by [2], the Imbrium impact struck a geochemically anomalous region where Th and other heat-

producing elements were concentrated, then the crust in that region would have been anomalously hot and an area of active plutonism (and volcanism). It may have produced an unusually high proportion of ejected melt [19] and an anomalous crustal response [4] to basin impacts. Models for global differentiation of the Moon such as the magma-ocean hypothesis would have to be modified to account for the asymmetric or localized distribution of residual melt (i.e., beneath the Procellarum-Imbrium Th-rich terrane).

Acknowledgments: Funding for this work is through NASA grants NAGW-4906, NAG5-4172, and NAG5-6784.

References: [1] Wilhelms (1987) *USGS Prof. Paper*, 1348. [2] Haskin (1998) *JGR, 103*, 1679. [3] Ryder and Wood (1977) *Proc. LSC 8th*, 655. [4] Wieczorek et al., this volume. [5] Taylor et al. (1993) *Lunar Sourcebook*, Ch. 6. [6] Ryder and Spudis (1987) *Proc. LPSC 17th*, in *JGR, 92*, E432. [7] Dalrymple and Ryder (1993) *JGR, 98*, 13085. [8] Bussey et al. (1998) *LPS XXIX*, Abstract #1352. [9] Blewett et al. (1998) *LPS XXIX*, Abstract #1339. [10] Head (1974) *Moon, 9*, 355. [11] Reed and Wolfe (1975) *Proc. LSC 6th*, 2443. [12] Spudis (1993) *The Geology of Multi-Ring Impact Basins: The Moon and Other Planets*. [13] Wolfe et al. (1981) *USGS Prof. Paper*, 1080. [14] Haskin et al. (1998) *Meteoritics & Planet. Sci.*, in press. [15] Jolliff et al. (1996) *Meteoritics & Planet. Sci., 31*, 116. [16] Jolliff (1998) *LPS XXIX*, Abstract #1850. [17] Korotev et al. (1998) *LPS XXIX*, Abstract #1231. [18] Dalrymple and Ryder (1996) *JGR, 101*, 26069. [19] Warren (1996) *LPS XXVII*, 1379.

⊃ɔɔ - ᧞ /

SURFACE-CORRELATED NANOPHASE IRON METAL IN LUNAR SOILS: PETROGRAPHY AND SPACE WEATHERING EFFECTS.

L. P. Keller[1], S. J. Wentworth[2], and D. S. McKay[3], [1]MVA Inc., 5500 Oakbrook Parkway, Suite 200, Norcross GA 30093, USA (lkeller@mvainc.com), [2]Mail Code C23, Lockheed Martin, Houston TX 77058, USA, [3]Mail Code SN, NASA Johnson Space Center, Houston TX 77058, USA.

Introduction: Space weathering is a term used to include all of the processes that act on material exposed at the surface of a planetary or small body. In the case of the Moon, it includes a variety of processes that formed the lunar regolith, caused the maturation of lunar soils, and formed patina on rock surfaces. The processes include micrometeorite impact and reworking, implantation of solar wind and flare particles, radiation damage and chemical effects from solar particles and cosmic rays, interactions with the lunar atmosphere, and sputtering erosion and deposition. Space weathering effects collectively result in a reddened continuum slope, lowered albedo, and attenuated absorption features in reflectance spectra of lunar soils as compared to finely comminuted rocks from the same Apollo sites [1,2]. Understanding these effects is critical in order to fully integrate the lunar sample collection with remotely sensed data from recent robotic missions (e.g., Lunar Prospector, Clementine, Galileo). Our objective is to determine the origin of space weathering effects in lunar soils through combined electron microscopy and microspectrophotometry techniques applied to individual soil particles from <20 µm size fractions (dry-sieved) of mature lunar soils. It has been demonstrated [3] that it is the finest size fraction (<25 µm) of lunar soils that dominates the optical properties of the bulk soils.

Methods: Lunar soil grains are extracted from <20 µm sieve fractions and placed on a highly polished Be disk. Multiple reflectance spectra from each grain are collected using a Zeiss MPM400 microscope photometer. Spectra are obtained over the wavelength range of 380–850 nm using oblique illumination. Following the reflectance measurements, the bulk compositions and morphologies of the particles are obtained by SEM-EDX techniques. Selected particles are embedded in low-viscosity epoxy; thin sections are obtained using ultramicrotomy and analyzed in a transmission electron microscope equipped with a thin-window EDX spectrometer. Using these techniques, we have shown that it is the distribution (volume- or surface-correlated) and the size of the nanophase Fe metal in lunar soils that are the two main factors that determine the optical properties of individual lunar soil grains [4]. The approach here is unique in that we are not making bulk measurements on mixtures (e.g., sieve fractions) of soils, but are measuring the optical properties and petrographic characteristics on a grain-by-grain basis.

Results and Discussion: We have identified three components in the finest size fraction of lunar soils that have major effects on optical properties: (1) agglutinitic glass fragments, (2) mineral grains with accretionary coatings, and (3) radiation processed grains. We describe these components in detail below.

Fragments of agglutinitic glass are a common component of the <20-µm size fraction of lunar soils. The fragments are typically very dark (nearly black in reflected light), although the albedos are variable because of differences in surface roughness. The reflectance spectra from these particles show reddened slopes over much of the visible spectrum (a slope of ~32% reflectance/1000 nm, between 500 and 800 nm). TEM/EDX analysis of thin sections shows that the fragments are compositionally similar to the bulk soil, and are dominated by glass with abundant submicroscopic Fe metal grains distributed throughout their volume. In the optically "black" particles, the nanophase metal grains are typically >10 nm in diameter. Some fragments are distinctly orange in color (with strongly reddened spectra) and in these instances, the nanophase metal is predominantly <5 nm in diameter.

All the soil particles that we have analyzed to date have some accretionary material (e.g., splash glass, vapor deposits, sputter deposits, etc.) on their surfaces, although the amount of material can be highly variable. A common characteristic in the accretionary material is the occurrence of nanophase metal as randomly oriented inclusions or in layers. In the coated particles, the metal grains are concentrated in thin (50–150-nm-thick) rims surrounding mineral grains (mainly plagioclase and augite). The inclusion-rich rims on mineral grains likely result from depositional processes in the lunar regolith, either condensation of impact-generated vapors or sputter deposition [5]. This accretionary material can have profound effects on the optical properties of the soil grains. The reflectance spectra from these grains are characterized by steep red slopes (a slope of ~65% reflectance/1000 nm, between 500 and 800 nm).

Radiation effects can also produce surface-correlated nanophase Fe metal in Fe-bearing minerals such as ilmenite and olivine. For the ilmenites, the spectra tend to be spectrally dark and relatively flat over the visible (a slope of ~10% reflectance/1000 nm, between 500 and 800 nm), although many of the ilmenites show a slight blue-slope at short wavelengths (~400–550 nm) and a slight red-slope at longer wavelengths (>550 nm). TEM analysis of the ilmenites shows that the grains are surrounded by altered rims up to 200 nm thick where Fe has been preferentially removed from the ilmenite surface, nanophase Fe metal grains have been produced, and Ti has been partly reduced to Ti^{3+} [6–8] While these altered rims contain submicroscopic metal grains, they do not have a large effect on the reflec-

tance data. A more dramatic effect is observed in olivine grains. We have observed altered rims on olivine grains where much of the Fe within ~50 nm of the surface has been reduced to nanophase Fe metal surrounded by Mg-silicate glass. Spectra from the "altered" olivine grains are much darker than pristine olivine of similar composition, and the slopes of the spectra are not significantly changed.

Conclusions: These results suggest that fragments of agglutinitic glass and mineral grains with inclusion-rich coatings in the fine size fractions of lunar soils are among the major contributors to the reddened continuum slope and to the lowered albedo in reflectance spectra. The optical effects are controlled by the size of the Fe metal grains and their distribution. Much of the darkening appears to result from the presence of Fe metal grains >10 nm in diameter, whereas the reddening is only prominent in glasses and rims where the average grain size of the nanophase metal is ≤5 nm in diameter.

References: [1] Adams J. B. and McCord T. B. (1970) *GCA, Suppl. 1*, 1937. [2] Adams J. B. and McCord T. B. (1971) *Science, 171*, 567. [3] Fischer E. (1995) Ph.D. thesis, Brown Univ. [4] Keller L. P. et al. (1998) *LPS XXIX*, Abstract #1610. [5] Keller L. P. and McKay D. S. (1997) *GCA, 61*, 2331. [6] Christoffersen R. et al. (1997) *Meteoritics & Planet. Sci., 31*, 835. [7] Bernatowicz T. J. et al., (1994) *LPS XXV*, 105. [8] Keller L. P. et al. (1995) *LPS XXVI*, 729.

5 ⟨ ,‿ ⟩/

COMPOSITIONAL VARIATION IN LUNAR REGOLITH SAMPLES: LATERAL.

R. L. Korotev, Department of Earth and Planetary Sciences, Washington University, St. Louis MO 63130, USA (rlk@levee.wustl.edu).

The composition of samples of lunar regolith collected on the Apollo and Luna missions are highly variable; the lunar meteorites, most of which are breccias of lithified regolith from unknown locations on the Moon, extend the compositional range (Fig. 1). Here I discuss some aspects of regolith composition as inferred from studies of samples that are relevant for interpretation of data obtained remotely.

Database: During the Apollo and Luna missions, regolith samples were obtained with scoops and coring equipment. Apollo scoop samples were taken from near the surface (<10 cm depth) as well as from the bottom of trenches dug as deep as 30 cm. Some nominal "soil" samples are fines derived largely from a single rock (e.g., 12057, 67700, 73130, and 76320) [1].

Most Apollo scoop samples were passed through sieves of 10 mm, 4 mm, 2 mm, and 1 mm mesh size in the curatorial facility at the NASA Johnson Space Center. Most chemical and physical measurements on samples of "lunar soil" have been made only on bulk samples of material that passed through a 1-mm sieve, i.e., the "<1-mm fines." For the Luna samples and some Apollo cores, compositional data are for <0.25-mm fines. With a few important exceptions, material in the 1–2 mm and 2–4 mm grain-size fractions has been largely unstudied.

The number of samples of surface and trench soils ranges from 7 at Apollo 11 to 68 at Apollo 17. Remarkably, a number of samples of Apollo surface and trench soils are not well characterized compositionally. The dataset is poorest for the Apollo 12 samples.

Classes of Lithologic Material: From the compositional perspective, regolith samples are composed mainly of three classes of material, each representing a distinct geologic environment (Fig. 1a):
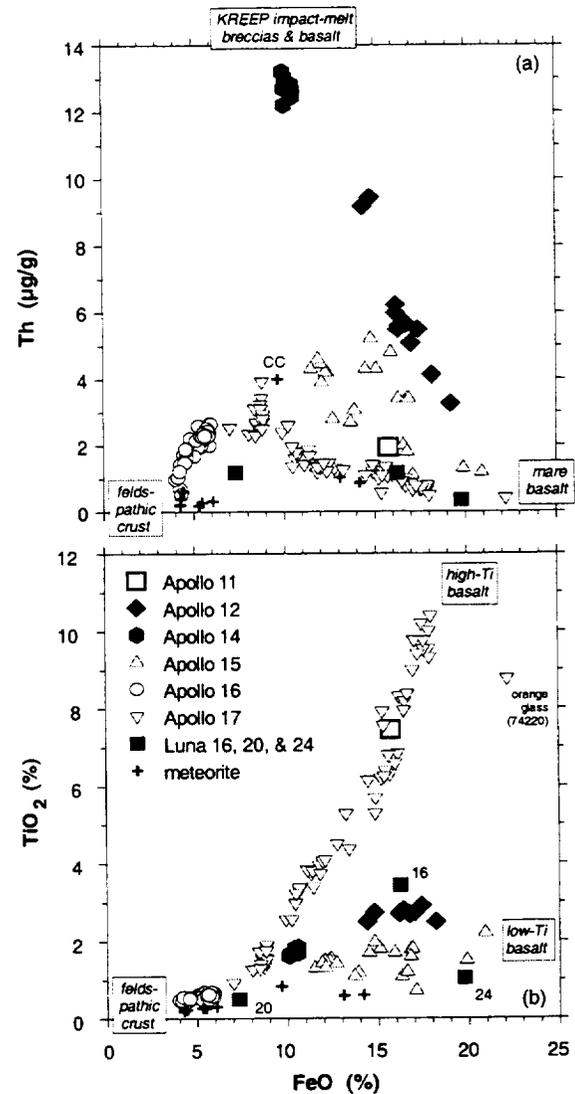
Fig. 1. Concentrations of FeO, TiO_2, and Th in samples of lunar regolith. For the Apollo missions, each point represents the composition of a numbered (e.g., 64221) surface or trench soil (<1 mm). For the Luna missions, a single point for each mission is plotted. "Meteorite" points each represent one of the regolith-breccia lunar meteorites (e.g., MAC 88105).

(1) mare basalt and volcanic glass, (2) mostly feldspathic rocks of the lunar highlands, and (3) mafic, KREEP-bearing impact-melt breccias and KREEP basalt.

Each of these classes of material encompasses a variety of lithologies. For example, there are many compositionally distinct types of mare basalt and volcanic glass; the distinction between soils dominated by low-Ti and high-Ti mare basalts is evident on Fig. 1b.

A few regolith samples consist predominantly (>90%) of a single class of material. For example, some soils from Apollo 15 (Hadley Rille) and 17 (Taurus-Littrow, Central Valley) and from Luna 24 (Mare Crisium) contain mainly mare basalt or volcanic glass. The most feldspathic of the lunar meteorites consist almost entirely of feldspathic highland material with a bulk composition that corre-

sponds to that of noritic anorthosite, although the meteorite regolith breccias are mixtures of a variety of rock types (granulitic and impact-melt breccias, plutonic anorthosite, noritic and troctolitic anorthosite, rare mafic lithologies). It is likely that these meteorites best represent typical feldspathic upper crust distant from the nearside basins [e.g., 2]. Presumably because all the Apollo missions landed near the High-Th Oval Region [3] surrounding the Imbrium Basin, all nonmare Apollo regoliths contain a substantial component of Th-rich, mafic impact-melt breccias (a component often misleadingly designated "LKFM."). The Apollo 14 regolith (Fra Mauro) is derived mainly from such material. The mafic melt breccias are the principal carrier of incompatible elements like Th in Apollo highlands regoliths, although igneous KREEP basalt is probably an important component of the Apollo 15 regolith. With ~10% FeO, the mafic melt breccias are also the principal carrier of Fe in those Apollo regoliths that contain little mare material (e.g., 44% of the Fe at Apollo 16 [4]).

As evident from Fig. 1, however, most regolith samples are mixtures containing two or more classes of material. In part this is an artifact of having deliberately chosen sample locations at major geologic boundaries (Apollo 15 and 17) where mare-highland mixing trends are clearly evident in regolith compositions. However, geologically important mixtures also occur where not necessarily expected. Samples of Apollo 12 (Oceanus Procellarum) regolith reflect binary mixing between low-Ti mare basalt and some type of KREEP component (Fig. 1a,b). The low FeO concentrations of regoliths from Apollo 11 (Mare Tranquillitatis) and Luna 16 (Mare Fecunditatis) (Fig. 1b) compared to mare basalt (~20% FeO) result from the fact that the regoliths consist of only ~75% mare basalt; the rest is highlands material. Some Apollo 15 and 17 soils as well as the Calcalong Creek lunar meteorite (a regolith breccia; CC in Fig. 1b) contain subequal amounts of all three classes of material, and three other meteorite regolith breccias (9–15% FeO, Fig. 1) are mixtures of mare and highland material. On average, the Apollo 16 regolith (Cayley Plains) is largely a mixture of feldspathic highland material similar to that of the feldspathic lunar meteorites (~64%, from chemical mass balance [4]) and Th-rich mafic melt breccias (29%); variation in the proportions of these components about the mean causes the trend of Fig. 1a. The Apollo 16 regolith is atypical of highlands distant from the Imbrium Basin in containing such a high abundance of Th-rich melt breccias. Although not evident in Fig. 1, the Apollo 16 regolith also contains mare-derived (6%) and, like all mature regolith, meteoritic material (1%) [4].

Variations in Composition with Grain Size: Several studies have shown that the lunar regolith varies in composition and mineralogy with grain size. In soil dominated by mare basalt, the finest material (<10 μm or <20 μm grain-size fraction) is consistently more feldspathic and, therefore, richer in Al and poorer in Fe than the coarser fractions [5–7]. Ferrous oxide concentrations in the <10-μm material are typically 70–95% of that in <1-mm material [6]. This effect has been attributed to preferential comminution of plagioclase compared to pyroxene during formation of the regolith by meteorite impact [5–7]. Thus the plagioclase/pyroxene ratio of the finest regolith is probably greater than that of the basalt from which it forms.

Also, in regolith composed of several lithologies, it is unlikely that all of them will have the same grain-size distribution. If the various lithologies have different compositions, then the composition of the regolith will vary with grain size. Older (mature) regolith is generally finer grained than younger (immature) regolith [8]. At

Apollo 16, for example, the mature surface soil has a high proportion (29%) of Th-rich mafic melt breccia. Impacts that punched through this surface layer encountered anorthositic rocks and ejected coarse fragments onto the surface. Thus the ejecta of North Ray Crater is a mixture of (1) mature, fine-grained Fe- and Th-rich material and (2) immature, coarse-grained Fe- and Th-poor material. Consequently, finer grain-size fractions are richer in Fe and Th than coarser fractions [4,6]. At the Apollo 17 South Massif, the 2–4-mm fines are richer in Fe and Th than the <1-mm fines because they contain a greater ratio of mafic melt breccia to feldspathic highland material (~12:1) compared to the <1-mm fines (~1:1), probably because the feldspathic material is more friable [9,10].

Implications for Remote Sensing: Lunar regolith is a mixture of several lithologies that are typically petrogenetically unrelated. Many to most mare surfaces are contaminated with some nonmare material. Although the bulk composition of Apollo 16 soil, for example, corresponds to anorthositic norite, the regolith is, in fact, composed mostly of unrelated noritic (melt breccias) and anorthositic lithologies. Systematic variation in composition across an interface may lead to correlations that extrapolate toward the composition of a rock type, as with the Apollo 17 samples in Fig. 1 [4]. Techniques sensitive to grain size may find literature data on <1-mm fines inadequate for establishing ground truth.

References: [1] Morris R. V. et al. (1983) *Handbook of Lunar Soils*, JSC 19069, NASA Johnson Space Center, Houston, 914 pp. [2] Korotev R. L. et al. (1996) *Meteoritics & Planet. Sci., 31*, 909–924. [3] Haskin L. A. (1998) *JGR, 103*, 1679–1689. [4] Korotev R. L. (1997) *Meteoritics & Planet. Sci., 32*, 447–478. [5] Korotev R. L. (1976) *Proc. LSC 7th*, 695–726. [6] Papike et al. (1981) *Rev. Geophys. Space Physics, 20*, 761–826. [7] Laul J. C. et al. (1987) *GCA, 51*, 661–673. [8] McKay D.S. et al. (1974) *Proc. LSC 5th*, 887–906. [9] Jolliff B. L. et al. (1996) *Meteoritics & Planet. Sci., 31*, 116–145. [10] Korotev R. L. and Kremser D. T. (1992) *Proc. LPS, Vol. 22*, 275–301.

$5.3 / / - ? /$

COMPOSITIONAL VARIATION IN LUNAR REGOLITH SAMPLES: VERTICAL.

R. L. Korotev, Department of Earth and Planetary Sciences, Washington University, St. Louis MO 63130, USA (rlk@levee.wustl.edu).

Some techniques for measuring composition and mineralogy remotely detect only the upper few micrometers to millimeters of material. Is this a serious concern for lunar regolith studies? Here I show the centimeter-scale variation with depth in the composition of lunar regolith based on results of the studies of regolith cores taken on the Apollo missions.

In short, the compositional variation of lunar regolith with depth over tens of centimeters is equivalent to that observed laterally at the surface over kilometers (Figs. 1 and 2). On average, however, the composition of material in the upper half centimeter is probably reasonably representative of the upper half meter or more (the depth of most Apollo cores), particularly for measurements made from orbit that integrate over a large surface area.

The noise in the INAA data is largely a sampling artifact as each point represents only 50–120 mg of soil. Large grains of plagioclase lead to occasional negative spikes. Apollo 16 soil is unusual in
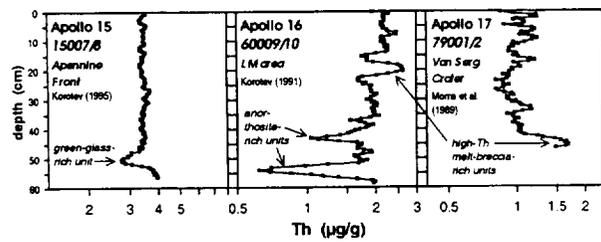
Fig. 1. Variation in Th concentration with depth in three Apollo regolith cores. The logarithmic scale is the same on each of the Th axes and the width of each plot is a factor of 6. The Apollo cores were sampled at 5-mm intervals, leading to high depth resolution. Compositional variation with depth is caused by variation in the relative proportions of the lithologic constituents of the soils (see companion abstract). For example, areas of low Th concentration (Fig. 1) in the 60009/10 core are accompanied by low Fe (Fig. 2) and are caused by an excess of coarse-grained anorthosite [1,2] compared to the soil at the surface.
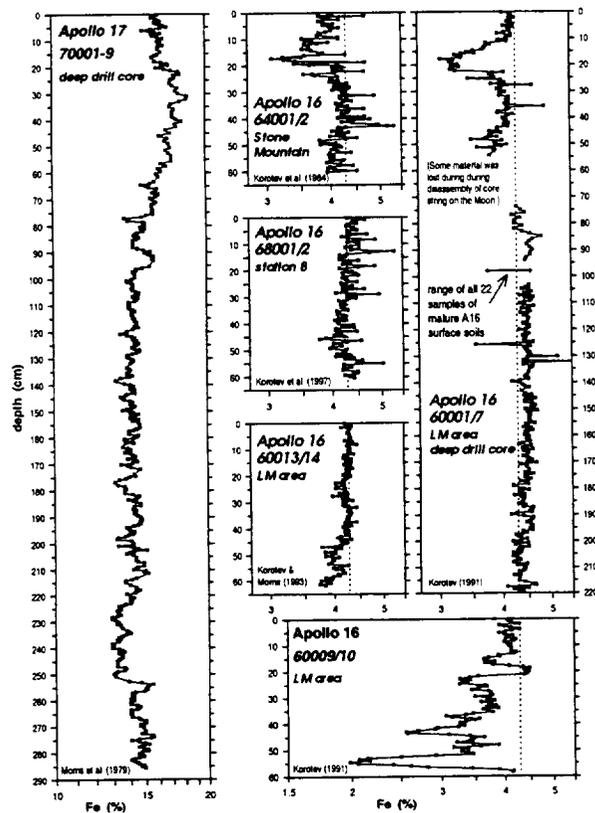
Fig. 2. Variation in total Fe concentration with depth in six Apollo regolith cores. For reference, the vertical dotted line in the Apollo 16 plots represents the average Fe concentration of 22 samples of mature surface soil from the site; the range is shown in the 60001/7 plot. Iron concentrations in the Apollo 17 deep drill core, the deepest of all the Apollo cores, were determined by magnetic techniques [3]; instrumental neutron activation (INAA) was used for the other cores [4–8].

containing large grains of FeNi metal, which leads to many positive spikes in the profiles. About 9% of the Fe in a typical Apollo 16 soil is carried by grains of FeNi metal of meteoritic origin [3]. Consecu-

tive samples with locally high or low Fe (or Th) concentrations represent compositionally distinct units of soil. For example, the Fe enrichment at 43 cm depth in the 64001/2 core is not due to metal but to a narrow layer enriched in mare-derived material.

The three Apollo 16 LM area cores were taken in a triangular array about 50 m on a side, the only such core array taken on the Moon. The regions of low Fe in each core (~18 cm depth in 60001/7, bottom of 60013/14, and 54 cm in 60009/10) are each characterized by fragments of coarse anorthosite and may represent a single depositional event. Various lines of evidence suggest that at 50–100 m depth (Descartes Formation), the Apollo 16 megaregolith is poorer in Fe and that the surface material is largely an ejecta deposit from Imbrium (Cayley Formation).

References: [1] McKay D. S. et al. (1977) *Proc. LSC 8th*, 2929–2952. [2] Korotev R. L. (1991) *Proc. LPS, Vol. 21*, 229–289. [3] Morris R. V. et al. (1979) *Proc. LPSC 10th*, 1141–1157. [4] Korotev R. L. (1995) *LPS XXVI*, 783–784. [5] Korotev R. L. and Morris R. V. (1993) *GCA, 57*, 4813–4826. [6] Korotev R. L. et al. (1984) *Proc. LPSC 15th*, in *JGR, 89*, C143–C160. [7] Korotev R. L. et al. (1997) *GCA, 61*, 2989–3002. [8] Morris R. V. et al. (1989) *Proc. LPSC 19th*, 269–284. [9] Korotev R. L. (1987) *Proc. LPSC 17th*, in *JGR, 92*, E447–E461.

5? 6 - //

ON THE HISTORY AND ORIGIN OF LKFM.

R. L. Korotev, Department of Earth and Planetary Sciences, Washington University, St. Louis MO 63130 (rlk@levee.wustl.edu).

Fra Mauro is the name of a geologic formation surrounding the Imbrium Basin of the Moon as well as the name of the region of the Apollo 14 lunar landing site [1]. The formation was named for a 16th-century Italian geographer and cartographer [e.g., 2].

Etymology and Evolution of LKFM: In its original invocation in 1971 by the Apollo Soil Survey (ASS), Fra Mauro basalt was not a crystalline basalt, but the designation of a "compositional group" of impact glasses found in the Apollo 14 soil that were basaltic in composition [3]. The ASS noted the similarity between the Fra Mauro basalt glass composition and sample 14310, an unbrecciated, crystalline Apollo 14 rock that would now be designated an impact melt rock [4]. In 1972 the term Fra Mauro basalt was first applied to a rock, sample 14310 [5], although in related papers, Fra Mauro basaltic glass was equated with KREEP [6,7].

In 1973 the ASS noted that a wide range of K concentrations occurred among glasses of Fra Mauro basaltic composition in the Apollo 15 regolith [7]. The terms high-K, moderate-K and low-K Fra Mauro first occurred in that context, but always as an adjective. Low-K Fra Mauro glasses were those with 0.12 ± 0.07% K$_2$O (± = standard deviation?), compared with 0.47 ± 0.17% and 1.1 ± 0.4% for moderate and high-K Fra Mauro glasses and 0.6% for Apollo 15 KREEP basalt. An important evolutionary step in the concept of low-K Fra Mauro basalt occurred in 1973 when the composition was first used as a component in a mass-balance (mixing) model for Apollo 16 soils [8,9] and later average highlands crust [10], despite that the term had not yet been applied to an actual rock sample.

The first use of the acronym LKFM occurred in a 1973 paper describing glass compositions in Apollo 16 soil [11]. That paper made a distinction between the LKFM composition and medium-K

(alternately, moderate-K [7] and intermediate-K [12]) and high-K Fra Mauro basaltic glass compositions, which were still equated with KREEP. Again, LKFM was used as an adjective. The practice of using LKFM as a noun was well established by 1977, however [13–17]. At that time, the first reports of detection of Fra Mauro basalt from orbit by remote-sensing techniques occurred, based on Fe [17] and Th [18].

Ryder and Wood made another important advance in the LKFM concept when they reasoned that the LKFM composition was that of the lower crust because rocks of LKFM composition were impact-melt breccias they believed to have formed in very large impacts, those forming the Imbrium and Serenitatis basins [14]. The hypothesis that the average composition of the lower crust is that of LKFM is now largely accepted [19,20], although we question it below.

In their classic paper "In search of LKFM," Reid et al. [13] reviewed the significance of the LKFM composition. They recognized that there was no igneous LKFM, only impact-melt breccias, glasses, and soils. All the rock samples they listed and identified with LKFM were impact-melt breccias from Apollos 15, 16, and 17. Curiously, the average K_2O concentration of the listed rocks is 0.24%, approximately twice that of the original LKFM glasses, and for some of the rocks (60315, 62235, and 77135), K_2O concentrations fall instead in the range of the medium-K Fra Mauro glasses (~0.3%). Reid et al. reviewed the arguments about whether the LKFM composition is that of a mixture or an igneous rock. It was clearly a mixture in that all samples were either glasses or breccias, but the composition is very similar to that of an equilibrium liquid in the silica-anorthite-olivine system [15].

By 1980, LKFM had become synonymous with mafic impact-melt rocks and breccias, although the K_2O concentration of samples used to represent LKFM had continued to "kreep" up to values as high as 0.49% [12,19]. Recently, the LKFM concept has been extended based on results of the Clementine mission: "the Fe abundance of the interior of [the] South Pole Aitken [basin] lies within the LKFM field.... Thus, the lower crust in this part of the Moon is also LKFM in composition" [20]. The implication is that LKFM is Moonwide in occurrence, not a special product or component of the Fra Mauro formation and that LKFM can now be identified without knowledge of the concentration of K or other incompatible elements.

Throw It Out? In this observer's opinion, the term LKFM has outlived its usefulness and should be abandoned because of its ambiguity. It has been used interchangeably to refer to a composition, a chemical component, a rock type, and the lower crust. The composition associated with LKFM has evolved to cover such a wide range (Al/[Fe+Mg], Fe/Mg, K_2O, etc.) that most mafic polymict rocks from the highlands are included. The term is nondescriptive and misleading in the literal sense and, like KREEP, is jargon that justifiably offends nonlunaphiles. Rocks identified as LKFM are usually better designated as impact-melt breccias. As detailed below and elsewhere [21,22], it is likely that all of the Apollo Fra Mauro basalts (i.e., KREEP basalt and Th-rich mafic impact-melt breccias) are related and that those on the low-K end of the range have no special significance. If the Fe-rich material of the interior of the SPA basin is, in fact, impact melt and the concentration of Th is as low as preliminary results of the Lunar Prospector mission imply [23], and if the Th-rich impact-melt breccias of the Apollo missions all derive from an anomalous geochemical province [21,22], then there is little genetic link between the SPA material and those materials that have been historically identified with LKFM.
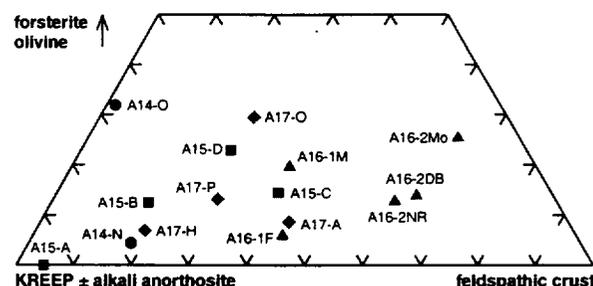
Fig. 1. Preliminary model results. Most of the points represent averages of many samples of recognized compositional groups; some points represent unique samples with anomalously high Mg concentrations: A14-O (the Apollo 14 olivine vitrophyres of [30], A17-O (sample 76055), and A16-2Mo (sample 62295).

Model: In an extension of previous work [24], I can demonstrate that to a good first-order approximation, the composition (31 elements) of all Apollo Th-rich, mafic melt breccias, i.e., the low- and medium-K Fra Mauro basalts and VHA basalts of Apollo 16, can be modeled as a mixture of three major components: (1) a material with a composition very similar to Apollo 15 KREEP basalt, (2) highly magnesian olivine (Fo_{90-95}), and (3) typical feldspathic upper crust. In this model the crustal component is represented by the average composition of the feldspathic lunar meteorites [e.g., 25]. The olivine component is required to account for the wide range of Mg/Fe ratios in the breccias and the high normative (and modal) abundance of high-Mg/Fe olivine in some specific breccias (Fig. 1). In order to account for concentrations of incompatible elements (IEs), the KREEP component of some melt breccias must have IE concentrations up to 2× lower or higher than the average of Apollo 15 KREEP basalt. Some minor components are also required. In order to account for Ti, ilmenite must be included as a distinct component, although its abundance in best-fit solutions remains in the narrow range of −0.6% to 1.1%. A component of alkali anorthosite (or albite) is required to account for variation in Na, Sr, and Eu, and this component varies between −7% and 10%. Two meteoritic components are required to account for siderophile elements: FeNi metal (up to 1.9% in Apollo 16 breccias) which derives from the impactor [22,25], and CI chondrite (up to 0.6% in Apollo 17 poikilitic breccias), which derives from clasts [26].

Interpretation: The abundance of KREEP component in the Fra-Mauro-type impact-melt breccias is so high (mean: 51%, Fig. 1) that such material must have been the dominant material of the target area. This observation plus other lines of evidence now suggest that KREEP (or urKREEP [27]) was not necessarily a material distributed Moonwide in a narrow zone at the base of the crust, but instead was concentrated massively in the Imbrium-Procellarum area prior to the Imbrium impact [21,22,28]. The LKFM melt breccias are precisely the types of products to be expected from an impact into a region dominated by KREEP magma by a bolide large enough to encounter the upper mantle and provide some olivine component to the melt (0 to ~20%, Fig. 1). The wide compositional range of the breccias reflects (1) minor regional variation in the extent of differentiation of the KREEP magma (variable IE abundance and variable alkali anorthosite and ilmenite subcomponents of the KREEP model component) and (2) variable incorporation of material of the mantle and the feldspathic upper crust into breccias formed in different parts

of the basin. Such variation is to be expected from a large impact into a partially molten, heterogeneous target [22]. Much of the feldspathic component occurs as clasts. The virtual absence of lithic clasts of LKFM or KREEP composition in the melt breccias [29] argues that this component was largely at or near the liquidus at the time of the impact(s).

References: [1] Wilhelms D. E. (1987) *The Geologic History of the Moon*, USGS Prof. Paper 1348, 302 pp. [2] Cowan J. (1997) *A Mapmaker's Dream, The Meditations of Fra Mauro, Cartographer to the Court of Venice*, Warner Books, 177 pp. [3] Apollo Soil Survey (1971) *EPSL, 12*, 49–54. [4] Stöffler D. et al. (1980) *Proc. Conf. Lunar Highlands Crust*, 51–70. [5] Ridley W. I. et al. (1972) *Proc. LSC 3rd*, 159–170. [6] Reid A. M. et al. (1972) *Proc. LSC 3rd*, 363–378. [7] Reid A. M. et al. (1972) *Meteoritics, 7*, 395–415. [8] Taylor S. R. et al. (1973) *GCA, 37*, 2665–2683. [9] Schonfeld E. (1974) *Proc. LPS 5th*, 1269–1286. [10] Taylor S. R. and Jakeš P. (1974) *Proc. LSC 5th*, 1287–1305. [11] Ridley W. I. et al. (1973) *Proc. LSC 4th*, 309–321. [12] Vaniman D. T. and Papike J. J. (1980) *Proc. Conf. Lunar Highlands Crust*, 271–337. [13] Reid A. M. et al. (1977) *Proc. LSC 8th*, 2321–2338. [14] Ryder G. and Wood J. A. (1977) *Proc. LSC 8th*, 655–668. [15] McKay G.A. and Weill D.F. (1977) *Proc. LSC 8th*, 2339–2355. [16] Taylor S. R. and Jakeš P. (1977) *Proc. LSC 8th*, 433–446. [17] Charette M. P. et al. (1977) *Proc. LSC 8th*, 1049–1061. [18] Haines E. L. et al. (1978) *Proc. LPSC 9th*, 2985–3011. [19] BVSP (1981) in *Basaltic Volcanism on the Terrestrial Planets*, pp. 268–281. [19] Spudis P. D. and Davis P. A. (1986) *Proc. LPSC 17th*, in *JGR, 91*, E84–E90. [20] Lucey et al. (1995) *Science, 268*, 1150–1153. [21] Wieczorek M. et al., this volume. [22] Haskin L.A. (1998) *Meteoritics & Planet. Sci.* [23] Feldman W. C. et al. (1998) *LPS XXIX*. [24] Korotev R. L. (1997) *LPS XXVIII*, 751–752. [25] Korotev R. L. et al. (1996) *Meteoritics & Planet. Sci., 31*, 909–924. [26] Korotev R. L. et al. (1998) *LPS XXIX*, Abstract #1231. [27] Warren P. H. and Wasson J. T. (1979) *Rev. Geophys. Space Phys., 17*, 73–88. [28] Haskin L. A. (1998) *JGR, 103*, 1679–1689. [29] Ryder G. et al. (1997) *GCA, 61*, 1083–1105. [30] Shervais J.W. et al. (1988) *Proc. LSC 18th*, 45–57.

Ƨƈ ƶ - ƴ/

ON THE MATURITY OF LUNAR REGOLITH.

R. L. Korotev[1] and R. V. Morris[2], [1]Department of Earth and Planetary Sciences, Washington University, St. Louis MO 63130, USA (rlk@levee.wustl.edu), [2]Mail Code SN, NASA Johnson Space Center, Houston TX 77058, USA (richard.v.morris1@jsc.nasa.gov).

Spectral reflectance properties of the lunar regolith change as the regolith "matures" with exposure to the space environment; a regolith composed of fragments from freshly disaggregated rock is lighter, is less red, and has more spectral contrast than the same regolith after it has received lengthy exposed to the solar wind, cosmic charged particles, and micrometeorite impact [e.g., 1–3]. In this work we discuss some aspects of lunar regolith maturity based on the study of Apollo regolith samples that may be important to interpretation of data obtained remotely.

Background: The changes that occur to regolith exposed at the surface are collectively called maturation. These changes include decrease in mean particle size, increase in the concentration of those elements derived largely from the solar wind (H, He, C, N, noble gases) and micrometeorites (Ir, Au), increase in the abundance of
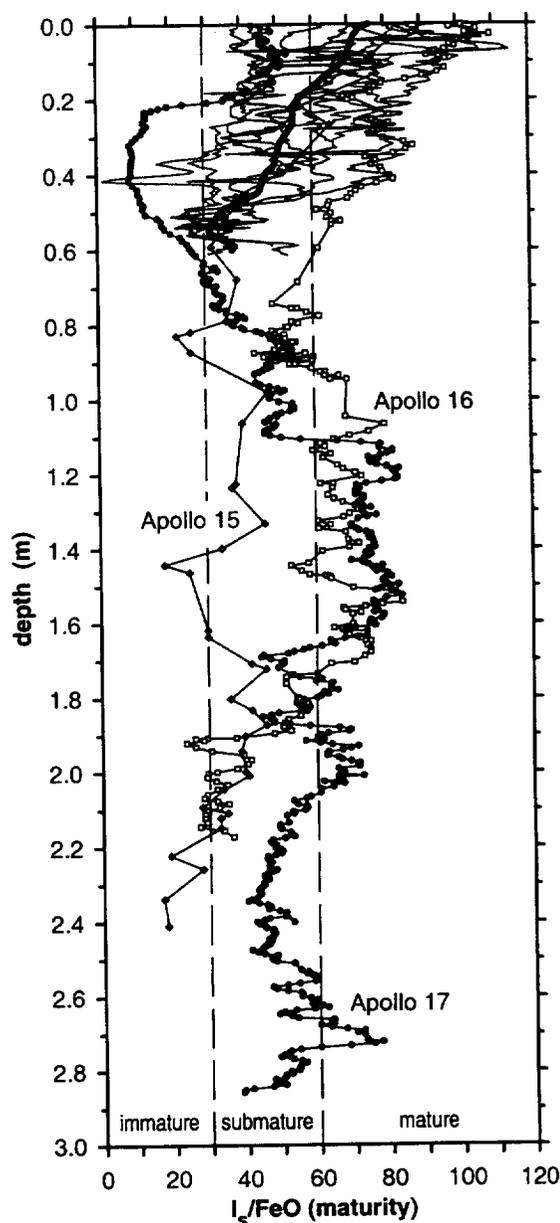
Fig. 1. Variation of the maturity parameter I_s/FeO with depth in 12 lunar regolith cores (14210/11, 15001–6, 15007/8, 15009, 15010/11, 60001–7, 60009/10, 60013/ 14, 68001/2, 70001–9, 76001, 79001/2 [1–11]). The thick line above 60-cm depth is the smoothed average of all 12 cores. The labeled profiles are those of deep drill cores. The boundaries between immature, submature, and mature are those of Morris [12].

nanophase Fe metal grains produced by reduction of lunar Fe by solar wind H, increase in the abundance of agglutinate particles (small glass-bonded soil aggregates produced by micrometeorite impact), and increase in the fraction of particle surfaces with amorphous rims and coatings. (See [4] for a discussion of these topics and many references.)

Most information about the relative maturity of lunar regolith samples, particularly with depth [e.g., 5–15], has been obtained by measuring the relative concentration of nanophase metallic Fe (I_s)

with ferromagnetic resonance (FMR) in <1-mm fines. Division of I_s by the concentration of total Fe, expressed as FeO, gives the maturity index I_s/FeO [e.g., 16]. It is necessary to divide I_s by the FeO concentration in order to obtain a maturity index because the concentration of nanophase metal is proportional to both the amount of surface exposure (i.e., maturity) and the amount of Fe available for reduction in the soil.

Most lunar regolith cores were "double-drive tubes" (e.g., 15010/11) that obtained material down to a depth of 50–60 cm, although a few single-drive tubes were taken (~30 cm, e.g., 76001). One "deep drill core" was taken on each of the Apollo 15, 16, and 17 missions (Fig. 1).

Results from Apollo: Most impact-derived soil (as opposed to volcanic-ash soils) collected at the surface of the Apollo sites is mature (I_s/FeO > 60, e.g., [16] and Fig. 1). However, based on the Apollo cores, the maturity of lunar regolith, as measured by I_s/FeO, decreases by about a factor of 2, on average, over the first half meter. Clearly, I_s/FeO must approach zero at some depth. However, based on the deep drill cores, maturity is not systematically less at 2 m depth than it is at 0.5 m (Fig. 1). If the upper half meter is taken as the average zone of *in situ* reworking, i.e., the region of "gardening" by small meteorites, then about 1 b.y. of such gardening is required to extend the reworking zone to a depth of 0.5 m [17].

Interpretation: Soils of high maturity or very low maturity are the easiest to interpret. In a mature soil, much or most of the material has spent a relatively long time at the surface. Mature surface soil is the expected product in an area that has not been recently influenced by an impact large enough to penetrate the surface layer of mature regolith and deposit and mix ejecta of low maturity at the surface. In a highly immature soil, in contrast, very little of the material has had much exposure at the surface. Among Apollo samples, immature surface soils were only found near fresh craters or on steep slopes. Units of immature soil were found at depth in several cores, however (Fig. 1).

Soils of intermediate maturity are more difficult to interpret. If a fresh deposit of previously unexposed rock fragments is undisturbed by further large impacts, all particles at the surface experience the same degree of exposure and the soil matures uniformly. This is "soil evolution path 1" of [18], where "reworking dominates [large scale] mixing." I_s/FeO will increase with exposure time and during some range of time will pass through the submature zone of Fig. 1. In "soil evolution path 2," on the other hand, "[large-scale] mixing dominates reworking" [18]. If a mature soil of, e.g., I_s/FeO = 90 is mixed with an immature soil of the same composition but with I_s/FeO = 0, the resulting soil will be in the submature range, with I_s/FeO = 45. Thus, it is likely that the spectral reflectance properties will be different for a Path-1 soil and Path-2 soil, even if both have the same composition, mineralogy, and I_s/FeO, because of their different histories.

Effect of Grain Size: Spectral reflectance properties are strongly dependent on grain size [e.g., 19] and most quantities that increase with maturity also increase with decreasing grain size. For example, in the 60009/10 core, the value of I_s/FeO is typically a factor of 2 greater in the <20-µm grain-size fraction than in the 90–150 µm fraction [20,21]. More generally, log-log plots of the relative concentration of nanophase metallic Fe vs. soil-particle diameter are nearly linear [22]. The slopes of those plots vary in a regular way with maturity. For immature soils, the slope approaches –0.8. With increasing maturity, the slope flattens to a value of approximately –0.2

for highly mature soils. The value of approximately –0.8 represents the lower limit of production of nanophase metal as a function of particle diameter by micrometeorites. The value of approximately –0.2 is a steady-state value and reflects a balance between the production of nanophase metal and the changes in particle size accompanying constructional (agglutination) and destructional (comminution) processes. The steady-state extreme represents Path-1 soils. For the Path-2 example given above, the mature component will have smaller average grain size, which leads to the same effect, i.e., the fine material will be more mature than the coarse material. As noted in a companion abstract on regolith composition [23], most measurements of bulk properties of lunar soils, such as I_s/FeO, have been made on <1-mm fines or <0.25-mm fines. Thus the statement, "sample 61121 is immature" applies strictly to the <1-mm grain-size fraction. The bottom line is that studies that compare maturity of Apollo soils as determined by spectral reflectance with tabulated values of I_s/FeO may encounter poor correlations that are related to grain size and mixing effects. An additional complication is that spectra data may be more sensitive to the total concentration of nanophase metal (i.e., I_s) than to maturity [24].

References: [1] Adams J. B. and McCord T. B. (1973) *Proc. LSC 4th*, 163–177. [2] Lucey P. G. et al. (1995) *Science, 268*, 1150–1153. [3] Fischer E. M. and Pieters C. M. (1996) *JGR, 101*, 2225–2234. [4] McKay D. S. et al. (1991) in *Lunar Sourcebook*, pp. 285–356, Cambridge Univ. [5] Bogard D. D. et al. (1980) *Proc. LPSC 11th*, 1511–1529. [6] Bogard D. D. et al. (1982) *Proc. LPSC 13th*, in *JGR, 87*, A221–A231. [7] Gose W. et al. (1977) *Proc. LSC 8th*, 2909–2928. [8] Korotev R. L. et al. (1993) *GCA, 57*, 4813–4826. [9] Morris R. V. et al. (1976) *Proc. LSC 7th*, 1–11. [10] Morris R. V. et al. (1976) *Proc. LSC 7th*, 93–111. [11] Morris R. V. et al. (1978) *Proc. LPS 9th*, 2033–2048. [12] Morris R. V. et al. (1979) *Proc. LPSC 10th*, 1141–1157. [13] Morris R. V. et al. (1989) *Proc. LPSC 19th*, 269–284. [14] Korotev R. L., unpublished data. [15] Morris R. V., unpublished data. [16] Morris R. V. (1978) *Proc. LSC 9th*, 2287–2297. [17] Morris R. V. (1978) *Proc. LSC 9th*, 1801–1811. [18] McKay D. S. et al. (1974) *Proc. LSC 5th*, 887–906. [19] Taylor L. A. et al. (1997) *LPS XXVIII*, 1421–1422. [20] McKay D. S. (1976) *Proc. LSC 7th*, 295–313. [21] McKay D. S. (1977) *Proc. LSC 8th*, 2929–2952. [22] Morris R. V. (1977) *Proc. LSC 8th*, 3719–3747. [23] Korotev R. L., this volume. [24] Lucey P. G. et al., personal communication.

$\mathcal{S}7 - 9/$

EARLY RESULTS FROM THE LUNAR PROSPECTOR GAMMA-RAY SPECTROMETER.

D. J. Lawrence[1], W. C. Feldman[1], A. B. Binder[2], S. Maurice[3], B. L. Barraclough[1], and R. C. Elphic[1], [1]Mail Stop-D466, Los Alamos National Laboratory, Los Alamos NM 87545, USA (djlawrence@lanl.gov), [2]Lunar Research Institute, Gilroy CA 95020, USA, [3]Observatoire Midi-Pyrénées, Toulouse, France.

Introduction: One of the instruments onboard the recently launched Lunar Prospector spacecraft is a Gamma-Ray Spectrometer (GRS) designed to map the surface elemental composition of the Moon. Specifically, the objectives of the GRS are to map abundances of Fe, Ti, U, Th, K, Si, O, Mg, Al, and Ca. The GRS consists of a

bismuth germanate (BGO) crystal placed within a well-shaped bo-rated plastic scintillator anti-coincidence (ACS) shield. Events trig-gering only the BGO are labeled as accepted events; events triggering both the BGO and ACS are labeled as rejected events. BGO spectra for both accepted and rejected events are telemetered to the ground for later analysis. These spectra have integration periods of 32 s and are continuously collected throughout the mission.

Results: As of this writing, we have been collecting GRS data for five months from January 16–June 16, 1998. During this period, 5.1% of the data were lost due to either incomplete DSN coverage [1] or bad sync words and/or check sums in the GRS data frames. Another 7% of the data was not directly usable because of high background counts associated with solar energetic particle events that occurred during the period between April 20–May 10. As a result, through the first five months of the mission, we have a total of 132 days of data, or 343,956 separate 32-s γ-ray spectra. The average number of spectra per 5° × 5° latitude/longitude pixel at the equator is 140 (the GRS footpoint is around 150 × 150 km or 5° × 5° at the equator), which is equivalent to 74 m of integration time. Because LP is in a polar orbit, this integration timescales as 1/cos(latitude), so that the collection times for equivalent areas in the polar regions are substantially larger. For comparison, the combined Apollo 15 and 16 GRS dataset collected over 5x less data (12.6 minutes) per 5° × 5° latitude/longitude pixel at the equator [2] than the first five months of LP GRS data.

Figure 1 shows γ-ray spectra measured using GRS during the first 3 1/2 months in mapping orbit. These spectra were measured for a 20° latitude × 20° longitude region contained within the Mare Imbrium and a similar-sized region in the lunar highlands containing the Joule crater. These spectra were created by subtracting 3x the rejected BGO spectra from the accepted BGO spectra. This is done to reduce background from the 0.511 MeV escape peaks and Compton con-tinuum γ-rays [3].

The spectra in Fig. 1 show clear differences between mare (Imbrium) and highlands (Joule) chemistries. Count rates for Fe (7.6 MeV) and Ti (6.76 MeV) γ-rays are clearly higher for Imbrium than for Joule. The most striking differences between the two re-gions, however, are the count rates for Th (2.6 MeV) and K (1.46 MeV) γ-rays. As reported by Lawrence et al. [4] and Binder et al. [5], when the Th and K counts are plotted in a 5° × 5° grid over the lunar surface, it is observed that both the Th and K abundances are concentrated on the nearside with a maximum concentration near the Apollo 14 landing site at Fra Mauro. Secondary Th and K concentrations are observed in the Mare Ingenii/South Pole Aitken region close to the antipode of Mare Imbrium. These measurements strongly indicate that the Imbrium impact spread much of the Th and K over the lunar surface.

Count-rate maps from the 7.6-MeV Fe γ-rays have also been made. While a full year of data is needed to obtain adequate statistics, the data already show the broad compositional variations associated with the lunar mare and highlands. As expected, relatively high Fe content is seen in the nearside mare and South Pole Aitken Basin and low Fe content is seen in the farside highlands.

References: [1] Binder A. B. (1998) *Science*, submitted. [2] Metzger A. E. (1993) *Remote Geochemical Analysis: Elemental and Mineralogical Composition*, 341–363. [3] Feldman W. C. et al. (1998) *Nuc. Inst. Meth.*, submitted. [4] Lawrence D. J. et al. (1998) *Science*, submitted. [5] Binder A. B. (1998) *Science*, submitted.

THE CLEMENTINE LONG-WAVE INFRARED DATASET: BRIGHTNESS TEMPERATURES OF THE LUNAR SUR-FACE. S. L. Lawson[1], B. M. Jakosky[1], H.-S. Park[2], and M. T. Mellon[1], [1]Laboratory for Atmospheric and Space Physics, University of Colorado, Boulder CO 80309, USA (lawson@argyre.colorado.edu), [2]Lawrence Livermore National Laboratory, Livermore CA 94550, USA.

The scientific payload on the Clementine spacecraft included a Long-Wave Infrared (LWIR) camera with a single passband of width 1.5 μm centered at a wavelength of 8.75 μm. The LWIR camera had a 128 × 128 mercury cadmium telluride focal plane array and used a catadioptric lens. The field of view of the instrument was 1° × 1°. The Clementine orbit deviated ±30° from sun synchronous, and for two lunar months, dayside nadir-looking images were obtained near local noon [1]. The LWIR spatial resolution ranged from 200 m near the poles to 55 m at the equator. Contiguous pole-to-pole imaging strips were obtained with ~10% overlap between adjacent frames. How-ever, significant longitude gaps exist between successive orbital passes. During the systematic mapping phase of the Clementine mission, approximately 220,000 thermal-infrared images of the lu-nar surface were obtained. Observed LWIR radiances can be con-verted to brightness temperatures that provide information on various physical properties of the lunar surface. Topography, albedo, and latitude are dominant factors in determining dayside lunar thermal emission.

We have completed the calibration of the LWIR camera using both preflight and in-flight data. Preflight calibration was performed at Lawrence Livermore National Laboratory in an effort to measure camera characteristics such as radiometric sensitivity, gain and offset scale factors, temporal/spatial noise, and dark-noise dependence on focal-plane array temperatures [2]. The several steps involved in the calibration routine include: converting measured DN values to radi-ance values; identifying and eliminating bad pixels; correcting for pixel response variation across the detector array; determining the zero-flux background of the instrument; comparing LWIR measured radiances of the Apollo 17 landing site to *in situ* temperature mea-surements in order to derive absolute calibration adjustments; and finally, converting measured radiance values to temperatures via the Planck function.
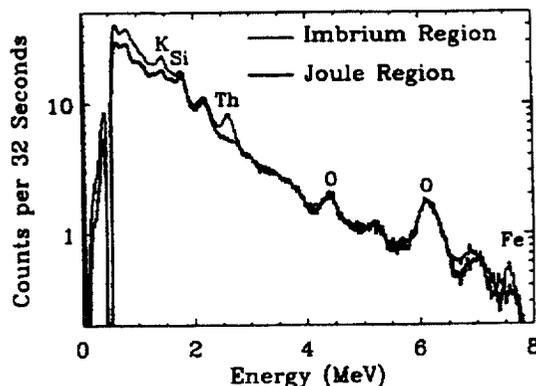
Fig. 1.

The first step in the routine to calibrate the LWIR images involves converting measured DN values (ranging from 0 to 255) to equivalent radiance values through a preflight calibration equation. This equation corrects for the changing gain and offset states used throughout an imaging orbit in order to account for the increase in surface thermal emission near the equator:

$$d = gfact \, (c1 * L * \tau + c2 + V * offset) + c3$$

where

d = digital counts;
$gfact$ = electronic gain factor;
$c1$ = sensitivity coefficient;
L = blackbody radiance;
τ = integration time;
$c2$ = gain-dependent fixed pattern counts;
V = offset scale factor;
$offset$ = global offset;
$c3$ = gain-independent fixed pattern counts.

The next step in the calibration process is to create bad-pixel maps and flat fields. This is accomplished by averaging together, on a pixel-by-pixel basis, hundreds of lunar images from a single orbit. Thus, a lunar mean image and an associated lunar standard deviation image are generated. Bad pixels are identified on these images as pixels that (1) do not vary (low or zero standard deviation); (2) vary randomly (high standard deviation); or, (3) are pegged at high values such that their dynamic range is limited (high mean). Pixels with low means also appear bad on lunar images. As many as 15% of the 16,384 detector array pixels can be characterized as bad. A flat field frame is created by multiplying the lunar mean image and the bad-pixel map, smoothing over the bad pixels, and normalizing the resultant image to unity. Due to the varying response of the instrument and the varying characteristics of the lunar surface, three separate bad-pixel maps and flat fields are required for each orbit.

The primary uncertainty in the calibration routine is the subtraction of a zero-flux radiance. Fortunately, space-looking frames were acquired at the beginning and end of many lunar mapping orbits; we will refer to these frames as prespace and postspace images. We are able to account for the increasing background level through an orbit by fitting a line, on a pixel-by-pixel basis, to the prespace and postspace radiance values as a function of time. Thus, for any given image time in the orbit, a zero-level is subtracted based on the lunar image time between the prespace and postspace image times. If no space images are available for an orbit, then a mean zero-level value from adjacent orbits is used. We considered our 3-s standard deviation for each orbit to be one-half the difference between the average of the prespace images and the average of the postspace images. Therefore, the standard deviation is constant in radiance and varies in equivalent temperature throughout an orbit, being lower near the equator where the surface temperatures are higher. For the entire mission, an average 2-s uncertainty is ±7 K or greater.

Absolute calibration involved comparing the LWIR-derived temperatures at the Apollo 17 landing site to temperatures determined *in situ* from the heat-flow experiment [3]. Keihm and Langseth present a full lunation plot of deduced lunar-surface brightness temperatures for the Apollo 17 site at Taurus Littrow. We were able to replicate their diurnal curve using a simple thermal model of the lunar surface. We then proceeded to use a better estimate of the mean solar constant
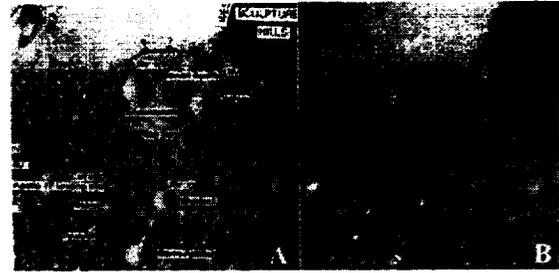
Fig. 1. Apollo 17 landing site (20.2°N, 30.8°W). (a) The photograph is from *Lunar Sourcebook: A User's Guide to the Moon*. The Apollo lunar surface experiments package is located approximately 200 m west of the landing site. Our model-derived temperature for the site on 21 April 1994 is 369 K. (b) The LWIR-derived temperature of 386 K was averaged in a 10 × 10 pixel box on image LLA3286L.289. The pixel scale is 0.059 km and the LWIR image is stretched from 360–400 K.

as well as lunar orbital information to model a temperature for April 21, 1994, the date of the Clementine observations of the landing site. The moon was farther away from the Sun in April 1994 than it was in December 1972; thus, instead of calibrating the LWIR to the Apollo temperatures, we calibrated to our more accurate model temperatures. The difference between our model temperature and our measured temperature was 17 K, which corresponds to a 22% difference in radiance. Therefore, as the final step in the calibration process, we multiply all of the LWIR-derived radiance values by 0.82. Brightness temperatures are calculated using the Planck function assuming a blackbody of unit emissivity. Relative uncertainties are found by comparing adjacent overlapping images in an orbit. These 2-s uncertainties for orbit 289 (containing the Apollo 17 landing site) average to approximately ±5 K, but can be as good as ±3 K.

There are a variety of applications for the LWIR dataset. When combined with the Clementine Ultraviolet-Visible (UVVIS) data, information on topography, infrared emissivity, and albedo can be gleaned. Comparing LWIR and UVVIS images at mid and high latitudes demonstrates that the dominant effect on surface temperatures in these areas is large-scale topography. However, near the equator, infrared emissivity and albedo have a greater effect on surface temperature. By comparing daytime LWIR images with Apollo 17 Infrared Scanning Radiometer nighttime measurements of the same areas, various thermophysical properties of the lunar surface, such as surface roughness and thermal inertia, can be constrained.

LWIR data can also be used independently. Analysis of the brightness temperature as a function of latitude provides information on the general nature of the energy balance of the lunar surface. LWIR images of the same area of the surface from different viewing angles yield information about angular variation of thermal emission properties. Comparing LWIR measured surface temperatures with those temperatures derived from diurnal models and from crater-temperature models can yield information on albedo, rock abundance, and infrared emissivity. We plan to further pursue these applications of the data. The LWIR data reduction algorithm will soon be made available to the scientific community.

References: [1] Nozette S. et al. (1994) *Science, 266*, 1835–1839. [2] Priest R. E. et al. (1995) *SPIE Proceedings in Infrared*

Detectors and Instrumentation for Astronomy, Vol. 2475, 405–416. [3] Keihm S. J. and Langseth M. G. (1973) *Proc. LSC 4th,* 2503–2513.

5๖๙-๙/

QUANTITATIVE MINERALOGIC AND ELEMENTAL ABUNDANCE FROM SPECTROSCOPY OF THE MOON: STATUS, PROSPECTS, LIMITS, AND A PLEA.

P. G. Lucey, Hawai'i Institute of Geophysics and Planetology, 2525 Correa Road, Honolulu HI 96822, USA (lucey@pgd.hawaii.edu).

The methods developed recently for derivation of Fe and Ti from multispectral imaging of the Moon [1–4] are empirical, but were guided in their development by a qualitative model of the lunar surface spectral properties enunciated in Rava and Hapke [5]. Their development also critically depended on a dataset for lunar soils where both reflectance spectra and the elemental abundance methods have known (at least upper) limits on their accuracy and precision by comparing abundance measurements of the soils used to develop and test these techniques. Some of the uncertainty observed in the deviations between measured and predicted element concentrations are likely due to shortcomings in the assumptions in the methods. These include that particle size or size distribution is constant or a smooth function of composition, that Ti is primarily partitioned into ilmenite and that ilmenite, is the sole opaque, or that the ratio of ilmenite to other opaques is constant or a smooth function of TiO_2 content, and that the specific mineral in which ferrous Fe resides is unimportant. In the list above the phrase "smooth function of composition" is often repeated. Because the methods are empirical, that is, they are calibrated against known compositions, certain types of these assumption violations do not give rise to errors. The types are those where important parameters such as grain size are highly correlated with composition. Any parameter that ordinarily might be a profound source of error will be compensated if its variations are primarily correlated with the relevant elemental concentration.

Limitations in accuracy and precision due to mineralogic variations have not been sufficiently explored. The major mafic minerals all possess absorption bands near 1 μm and to first order they have similar strengths at the same concentration of Fe, but this has not been quantified. Any differences in band strengths at constant FeO among the different minerals will give rise to mineralogy-dependent systematic errors [6]. Lucey et al. [1] made preliminary measurements that suggested that this effect is minor, but more work is necessary. Also, mineralogy can affect the distribution of Fe. Do two soils with identical FeO values but greatly different Mg numbers give rise to the same FeO content predicted from spectra? Again, Lucey et al. [1] made preliminary measurements that suggested this effect is minor, but more work in this area is necessary. These dependencies will be presented at the workshop.

Quantitative Mineralogy: To date, information on lunar mineralogy derived from spectroscopy has been almost wholly qualitative or descriptive [e.g., 7]. Spectra are classified on the basis of their similarity to spectra of known minerals, with inferences about rock type being derived from subtle details of the spectrum. Thus a region with a spectrum with a band center close to 0.9 μm is judged to have a mafic assemblage dominated by orthopyroxene and is termed "noritic" after Stoffler et al. [8]. If the bands are relatively weak, but the area seems to be immature based on albedo and geologic setting,

then the interpretation is that the region is likely composed of "noritic anorthosite, or anorthositic norite." By similar reasoning, if the region has a relatively strong band, then it would be termed a "norite." Spectra are sometimes parameterized to aid these qualitative interpretations, but the assignment is subjective and made in the context of common lunar lithologies.

There are promising approaches to achieving true quantitative mineralogy. Two of the most promising are the curve-fitting approach developed by Jessica Sunshine under the rubric "MGM" [9] and nonlinear mixing models.

MGM (modified Gaussian model) is a curve-fitting technique using a highly effective band profile discovered by Sunshine. This Sunshine band profile seems to fit Fe^{2+} features observed in reflectance extremely well, and Sunshine has outlined a semiquantitative set of arguments to lend it theoretical credence. Sunshine and Carle Pieters present data parameterizing olivines as a function of composition in terms of MGM parameters. In principle, one could use this and similar analysis of other minerals, along with the empirically derived constraints, to determine the mineral chemistry and possibly relative abundance of minerals possessing absorption features. The development of MGM has not reached this level of sophistication, but there is no technical obstacle.

The second approach can be called "theory of (almost) everything" models. This is an attempt to model a lunar reflectance spectrum including all the first-order variables present: modal mineralogy, grain size, mineral composition, and maturity. The approach uses measured optical constants of minerals as a function of mineralogy coupled with a nonlinear mixing model and a model of lunar optical maturation to match the unknown reflectance spectra of some lunar soil. Examples of these fits will be shown at the workshop.

Neither of these approaches (nor any other approach) can actually achieve reliable quantitative mineralogy for one simple reason: There exists no data with which to test algorithms. Except for a very small amount of data collected by Carle Pieters and Larry Taylor for mare soils using X-ray imaging [10,11], there are no lunar soils for which spectra exist and for which adequate modal mineralogies exist. "Adequate" means that mineral compositions as well as modal mineralogy must be measured, and categories that lack specific compositional meaning such as "lithic fragments" cannot be used. In the absence of data, how can mineral abundance models be tested? They cannot. Thus, they do not exist. Thus there is no hope that believable quantitative mineralogy algorithms can be developed in their absence. Until test datasets are available, mineralogy as derived from lunar spectroscopy will remain qualitative.

The Plea: Excellent progress was made in deriving elemental abundance from lunar spectra in large part because of the existence of small (~30 samples each) but barely adequate datasets with which to develop and test algorithms. A comparable dataset does not exist for testing models of quantitative mineralogy (or quantitative X-ray or Raman spectroscopy for that matter). I propose that one recommendation of this workshop be that reflectance spectra, modal mineralogy derived from X-ray imaging and major-element chemistry be measured for 100 mare and 100 highland soils within the next three years. Arguments can be made that we should wait to "do it right," as there are numerous unknowns about how precisely to make these measurements. However, at present, any survey would be superior to the near total lack of data, which is the current situation.

Lacking these crucial ground truth data, quantitative mineralogical analysis of Clementine and Selene data is not possible.

References: [1] Lucey P. G. et al. (1995) *Science, 268,* 1150–1153. [2] Blewett D. T. et al. (1997) *JGR, 102,* 16319–16325. [3] Lucey P. G. et al. (1998) *JGR, 103,* 3679–3699. [4] Jolliff (1998) *JGR,* submitted. [5] Rava B. and Hapke B. (1987) *71,* 397–429. [6] Clark P. and Basu (1998) *LPS XXIX.* [7] Pieters C. M. (1986) *Rev Geophys., 24,* 557–578. [8] Stöffler et al. (1980) *Proc. Conf. Lunar Highlands Crust,* 51–70. [9] Sunshine J. M. et al. (1990) *JGR, 95,* 6955–6966. [10] Pieters C. M et al. (1998) *LPS XXIX.* [11] Taylor L. A. et al. (1998) *LPS XXIX.*

530 - 9/

THE LUNAR PROSPECTOR NEUTRON SPECTROMETER DATASET.

S. Maurice[1], W. C. Feldman[2], B. L. Barraclough[2], R. C. Elphic[2], D. J. Lawrence[2], and A. B. Binder[3], [1]Observatoire Midi-Pyrénées, 31400 Toulouse, France (maurice@obs-mip.fr), [2]Los Alamos National Laboratory, Los Alamos NM 87545, USA, [3]Lunar Research Institute, Gilroy CA 95020, USA.

Introduction: Lunar Prospector carries a Neutron Spectrometer (NS) whose purpose is (1) to search for H, perhaps in the form of buried water ice at the lunar poles and/or in the form of solar wind implanted in mature regolith, and (2) to map the surface composition in Ti, Fe, and KREEP. Initial analysis of the data has shown that NS measurements may also (3) provide valuable clues to the sub-surface temperature and, perhaps, surface thermal heat flow. The NS consists of two 5.7-cm diameter by 20-cm long ^{3}He gas proportional counters. One is covered with Cd and so responds only to epithermal neutrons (0.3 eV<E<.5MeV). The other is covered with Sn and so responds to both thermal and epithermal neutrons. The difference in their counting rates provides a measure of the flux of thermal neutrons (E < 0.3 eV).

Results: Since it was powered up (Jan. 8, 1998), the NS has operated flawlessly, returning data of excellent quality. Pulse height spectra over 32 channels in both energy ranges are gathered every 32 s. During this accumulation time, typically 600 neutrons are counted (for a spacecraft altitude of 100 km). Measurements during the cruise phase showed that most, if not all, of these neutrons originate from the Moon. As of late June 1998, 12 full map-cycle coverages of the Moon have been completed.

The presentation will explain how the NS dataset was obtained and processed. Counts integrated over portions of pulse height spectra that are low in background counts will be presented as a function of the surface content in Fe and Ti. In addition to these spectra, we shall detail the data of different origins that support the NS analysis: quantities that are proxies for the rate of cosmic rays, as well as data that give spacecraft location and housekeeping information. The main steps of the data processing (integrity of the 32-s frames, gain drifts, latitude and altitude corrections) will be discussed. We will specify the stages of the analysis that have been completed and the ones that are planned to obtain more elaborate data products. Naturally, early science results on the science objectives mentioned above will be reviewed.

53/- 9/

THE STRATIGRAPHY AND EVOLUTION OF THE LUNAR CRUST.

I. S. McCallum, Department of Geological Sciences, University of Washington, Seattle WA 98195, USA (mccallum@u.washington.edu).

Introduction: Reconstruction of stratigraphic relationships in the ancient lunar crust has proved to be a formidable task. The intense bombardment during the first 700 m.y. of lunar history has severely perturbed the original stratigraphy and destroyed the primary textures of all but a few nonmare rocks. However, a knowledge of the crustal stratigraphy as it existed prior to the cataclysmic bombardment ca 3.9 Ga is essential to test the major models proposed for crustal origin, i.e., crystal fractionation in a global magmasphere [1] or serial magmatism in a large number of smaller bodies [2]. Despite the large difference in scale implicit in these two models, both require an efficient separation of plagioclase and mafic minerals to form the anorthositic crust and the mafic mantle.

Despite the havoc wreaked by the large body impactors, these same impact processes have brought to the lunar surface crystalline samples derived from at least the upper half of the lunar crust, thereby providing an opportunity to reconstruct the stratigraphy in areas sampled by the Apollo missions. As noted by Spudis [3], ejecta from the large multiring basins are dominantly, or even exclusively, of crustal origin. Given the most recent determinations of crustal thicknesses [4], this implies an upper limit to the depth of excavation of ~60 km.

Of all the lunar samples studied, a small set has been recognized as "pristine" [5], and within this pristine group, a small fraction have retained some vestiges of primary features formed during the earliest stages of crystallization or recrystallization prior to 4.0 Ga. We have examined a number of these samples that have retained some record of primary crystallization to deduce thermal histories from an analysis of structural, textural, and compositional features in minerals from these samples. Specifically, by quantitative modeling of (1) the growth rate and development of compositional profiles of exsolution lamellae in pyroxenes and (2) the rate of Fe-Mg ordering in orthopyroxenes, we can constrain the cooling rates of appropriate lunar samples [6]. These cooling rates are used to compute depths of burial at the time of crystallization, which enable us to reconstruct parts of the crustal stratigraphy as it existed during the earliest stages of lunar history.

First-Order Stratigraphy of the Lunar Crust: The distribution of impact melts and breccias in and around multiring basins on the lunar nearside has led to a widely accepted model of crustal stratigraphy in which an upper layer of ferroan anorthosite is underlain by a lower crust layer of more mafic composition [3,7]. However, several features suggest that a simple two-layer model is inadequate. The Moon has a much thicker crust on the farside [4] and, while it is possible that this asymmetry is a primary feature, it is more likely to be the consequence of cataclysmic impacts focused on the nearside that have thinned the crust, redistributed the upper layers, and affected melt migration patterns. The low abundance of anorthosites relative to noritic and KREEP-bearing rocks in the Imbrium and Serenitatis ejecta blankets is consistent with the removal of a large fraction of the anorthositic upper crust from the nearside in earlier (Procellarum?) impact events. If not anorthosite, what comprised the upper crust in the northern part of the nearside hemisphere?

Lower Crust: Basin impact melts, most notably the low-K Fra Mauro (LKFM) glasses and fine-grained breccias associated with the Imbrium and Serenitatis Basins, have compositions corresponding to norite and troctolitic norite. Cratering models suggest that such melts are generated at lower to middle crustal depths (30–60 km) in the largest impacts. The correlation between basin size and FeO content of the ejecta [8] indicates a vertically zoned crust becoming

increasingly mafic with depth. The paucity of unequivocal deep-seated crystalline plutonic rocks is consistent with cratering models that suggest that unmelted fragments in ejecta blankets are derived from the upper part of the crust [3]. It is possible, even likely, that all crystalline samples returned from the Moon have been derived from the uppermost 30 km or so of the crust. This is consistent with our cooling rate studies to date, which indicate depths of formation of <25 km for crystalline samples. If the mafic impact melt breccias represent KREEP-contaminated melts of lower crustal norite, does the norite component represent cumulates formed during the initial crystallization of the magma ocean or cumulates formed during the crystallization of the younger Mg-suite magmas? Our results to date favor the former interpretation since Mg-suite norites and gabbros appear to have formed in a near-surface environment [6].

Upper Crust — Anorthosites: Remote-sensing data support a model of an upper crust predominantly anorthositic (*sensu lato*) in composition. However, anorthositic rocks are not uniformly distributed in the lunar crust and, in fact, are present in low abundance around the Imbrium and Serenitatis basins (A14, A15, and A17 sites). While there is little doubt that anorthosite is the dominant upper crustal lithology on the farside [9], on nearside areas, anorthosite is common only in the central (A16 site) and northern highlands, in a narrow band from the Inner Rook Mountains in the west to the crater Petavius in the east, and as isolated occurrences such as the central peak of Aristarchus [11]. Is the absence of anorthosite in the western half of the Earth-facing hemisphere a primary or secondary feature? The occurrence of remnants of anorthosite in this region suggests that anorthosite was initially present and that it has largely been removed and redistributed by impact erosion prior to the Imbrium and Serenitatis events. Cooling-rate studies on ferroan anorthosites reveal that most are slowly cooled rocks that crystallized and cooled in the upper half of the lunar crust. No samples yet studied are from a depth greater than 25 km [6]. The ages, compositions, depths of crystallization, and global distribution of anorthosites are consistent with their formation as flotation cumulates in a global magma ocean early in lunar history.

Upper Crust — Highland Magnesian and Alkali Suites: Norites and troctolites form a coherent group (highlands magnesian suite, or HMS) on the basis of their ages, mineral compositions, and distinctive trace-element characteristics. Gabbronorites have also been assigned to the HMS, but it is likely that they formed from different parental magmas [11]. Alkali anorthosites, quartz monzodiorites and the rare granites (felsites) are grouped into the highlands alkali suite (HAS). HMS and HAS rocks are common at A14, A15, and A17 and have been reported from A16, but it is not known to what extent they occur in other parts of the lunar crust. Both suites formed from endogenic magmas emplaced during the latter stages of lunar crust formation.

We have determined the cooling rates of a number of HMS and HAS samples [6,12] and have shown that, in every sample studied, the depth of crystallization was within 1–2 km of the lunar surface. Impact-induced mantle rebound coupled with the removal of a significant fraction of the upper crust from the nearside of the Moon early in lunar history may have triggered mantle diapirism and melting and focused the migration of the HMS, HAS, and KREEP magmas to the thinner crustal regions where they crystallized as flows and shallow-level plutons.

KREEP: Lunar differentiation models generally show a layer of urKREEP forming a global sandwich layer at the crust-mantle boundary. The global distribution of KREEP has been questioned by Haskin [15], who points out that KREEP-rich material appears to be restricted to an oval-shaped region on the nearside that occupies only 5% of the lunar surface. Also, placing the primary urKREEP layer at the crust-mantle boundary is a model-dependent conclusion for which there is little hard evidence. In terrestrial-layered intrusions, KREEP-like sandwich horizons are located above, not below, thick sequences of norites, troctolites, and gabbros. There is no obvious reason why the Moon should be different. KREEP is a prominent constituent of the ejecta blankets surrounding the Imbrium Basin, and, to a lesser extent, the Serenitatis basin and it is difficult to see how KREEP could be excavated by impact while the upper mantle was not. It might be argued that LKFM is a mixture of lower crustal plus upper mantle material but, if so, it is difficult to explain why LKFM compositions are multisaturated. The distribution of melt rocks and clasts in Imbrium and Serenitatis ejecta is consistent with a crustal model in which KREEP was concentrated in a middle crustal layer beneath nearside anorthositic cumulates.

Summary and Model. The early lunar crust (near the end of a global differentiation event) was layered with mafic lower layers (norites and troctolites) and anorthositic (*s.l.*) upper layers. Bombardment was intense at this time with the influx of large impactors focused on the Earth-facing side. The impacts effectively stripped off much of the upper anorthositic layer from the nearside and redeposited this material as ejecta blankets elsewhere on the lunar surface. Late-stage differentiates (KREEP) migrated toward the zone of thinned crust and formed a localized sandwich horizon between the mafic cumulates and the anorthositic remnants. Internal melting, possibly triggered by the overturn of the lunar mantle, was initiated toward the end of the magma ocean event. These magmas interacted strongly with crustal rocks and crystallized to form the HMS, HAS, and KREEP suites. They formed surface flows and shallow-level plutons as they resurfaced much of the nearside of the Moon, generating vertical and later heterogeneity. Impact erosion and resurfacing was probably a continuous but declining process until the terminal lunar cataclysm.

References: [1] Warren P. (1985) *Annu. Rev. Earth Planet. Sci., 13,* 201. [2] Longhi J. and Ashwal L. (1985) *JGR, 90,* 571. [3] Spudis P. (1993) *The Geology of Multi-Ring Impact Basins,* Cambridge Univ., 263 pp. [4] Neumann G. et al. (1997) *LPS XXVIII,* 1095. [5] Warren P. (1993) *Am. Mineral., 78,* 360. [6] McCallum I. and O'Brien H. (1996) *Am. Mineral., 81,* 1166. [7] Ryder G. and Wood J. (1977) *Proc. LSC 8th,* 655. [8] Spudis P. et al. (1996) *LPS XXVII,* 1255. [9] Pieters C. et al. (1996) *LPS XXVII,* 1035. [10] Peterson C. et al. (1996) *LPS XXVII,* 1025. [11] James O. and Flohr M. (1983) *Proc. LPSC 13th,* in *JGR, 88,* A603. [12] McCallum I. et al. (1998) *LPS XXIX,* Abstract #1300. [13] Gooley R. et al. (1974) *GCA, 38,* 1329. [14] Dymek R. et al. (1975) *Proc. LSC 6th,* 301. [15] Haskin L. (1997) *LPS XXVIII,* 521.

MEASUREMENTS OF THE LUNAR GRAVITY FIELD USING A RELAY SUBSATELLITE. N. Namiki[1], H. Hanada[2], N. Kawano[2], K. Heki[2], T. Iwata[3], M. Ogawa[3], T. Takano[4], and the RSAT/VRAD Mission Groups, [1]Department of Earth and Planetary Sciences, Kyushu University, 6-10-1 Hakozaki, Higashi-ku, Fukuoka

812-8581, Japan (nori@geo.kyushu-u.ac.jp), [2]National Astronomical Observatory, 2-12 Hoshigaoka, Mizusawa, Iwate 023-0861, Japan, [3]National Space Development Agency of Japan, 2-1-1 Sengen, Tsukuba, Ibaraki 305-8505, Japan, [4]Institute of Space and Astronautical Science, 3-1-1 Yoshino-dai, Sagamihara, Kanagawa 229, Japan.

Introduction: Estimating spherical harmonic coefficients of the lunar gravity field has been a focus in selenodesy since the late 1960s when Doppler tracking data from lunar orbiters were first analyzed [1]. Early analyses [e.g., 1,2] were limited by the low degree and order of the spherical harmonic solutions, mostly due to the slow speed and low memory of the then-available computers. However, rapid development of the computational ability has increased the resolution of the lunar gravity models significantly. Konopliv et al. [3] analyzed Doppler tracking data from lunar orbiters 1–5 and Apollo subsatellites up to degree and order 60 (Lun60d). Further, Lemoine et al. [4] incorporated the tracking data from the Clementine spacecraft launched in 1994, and developed a model complete to degree and order 70 (GLGM-2). These high-resolution gravity models have been used for studies of internal structure and tectonics of the Moon [e.g., 5]. Interestingly, Lun60d and GLGM-2 show significant differences in the spherical harmonic coefficients for degree greater than 20. Because the semimajor axis of Clementine's orbit is nearly twice as large as the radius of the Moon, the contribution of the new tracking data is prevailed in the low-degree field. Methodologically, the differences in the high-degree field arise from the different weighting of the tracking data and gravity model [4], but, in principle, these are caused by a lack of tracking data over the farside. While the current Lunar Prospector mission is expected to improve the spatial resolution over the mid- to high-latitude regions of the nearside significantly, the absence of Doppler tracking data over the farside remains unresolved. To complete the coverage of tracking over the farside, we are developing a satellite-to-satellite (four-way) Doppler tracking experiment in SELENE (the SELenological and ENgineering Explorer) project of Japan.

Outline of the Mission: The SELENE is a joint project by the National Space Development Agency of Japan (NASDA) and the Institute of Space and Astronautical Science (ISAS) [6]. Two spacecraft, a main orbiter and a relay subsatellite, constitute the SELENE. The SELENE is scheduled to be launched in 2003. After the SELENE is injected into an elliptical polar orbit of 100-km periapsis altitude and 2424-km apoapsis altitude, the relay subsatellite is separated from the main orbiter. Then the main orbiter gradually decreases the eccentricity to a circular orbit in which altitude and inclination are 100 km and 95°, respectively. When the mission instruments, including a relay subsatellite transponder for the gravity measurement (RSAT), complete global mapping after a nominal 1-year period, the propulsion module of the main orbiter is deorbited to land on the Moon. A differential VLBI experiment by two radio sources on the relay subsatellite and the propulsion module (VRAD-1 and 2) continues until the relay subsatellite will fall on to the lunar surface approximately two months later [6].

RSAT Mission: RSAT is a communication subsystem on the relay subsatellite [7] for four-way Doppler tracking among the main orbiter, the relay subsatellite, and the Usuda Deep Space Center of ISAS (UDSC) [8], as well as two-way range and Doppler measurements, between the relay subsatellite and UDSC (Fig. 1). At the same time, the Tracking and Communication Stations (TACS) of NASDA conduct conventional two-way ranging and Doppler observations of the main orbiter when the main orbiter is visible from Earth.
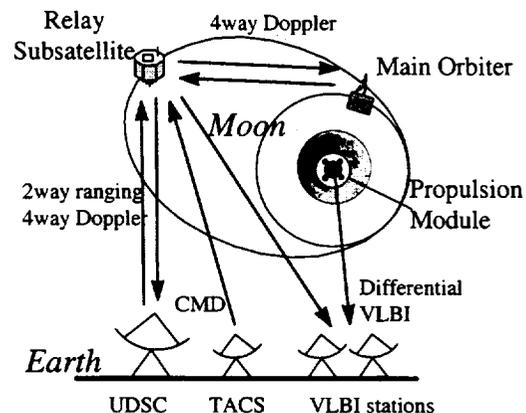
Fig. 1. The concept of RSAT and VRAD missions.

The two-way and four-way Doppler data acquired at UDSC are averaged over an interval from 1 to 60 s. We examined an accuracy of the UDSC system and found that the intrinsic noise level is well below 0.1 mm/s for 60-s integration. An actual noise of the tracking data will, however, be dependent on the signal processing procedures to remove other systematic errors such as ionospheric and tropospheric refraction, spin of the relay subsatellite, and solar radiation pressure. On the other hand, the noise level of the TACS has not been examined yet, but is likely to exceed 2–3 mm/s. Thus an improvement of TACS receiver system before 2003 is required.

The tracking data will be processed and analyzed by both the GEODYN II program of NASA and the NOCS program of NASDA. Since the orbits and gravitational potential are calculated in the domain consisting of Keplerian elements and spherical harmonics, the relevance between the resolution of the gravity field and a data coverage is not straightforward. As a preliminary test, we evaluated the coverage of the four-way Doppler measurements by the density of observational points over the farside relative to the total number of the unknown parameters, i.e., the sum of the number of the gravity field coefficients and the Keplerian elements multiplied by the number of arcs (Fig. 2). Unity of the relative coverage indicates the minimum density for inversion. The nominal observational period of 1 yr and assignment of UDSC for the SELENE project of 6 hr/day on average are assumed. In Fig. 2, the coverage is evaluated at each latitudinal belt of 5° for an initial semimajor axis of the relay subsatellite of 3000, 3200, and 3400 km, respectively. While the changes in the initial semimajor axis result in no significant difference in coverage, it is obvious that the coverage in the northern hemisphere is better than in the southern hemisphere. This is because the apoapsis of the relay subsatellite is on the northern hemisphere, and the link between the main orbiter and the relay subsatellite is therefore easier when the main orbiter is in the north than in the south. Figure 2 shows that the four-way Doppler coverage by RSAT over the farside is sufficient except for the small region around the south pole.

VRAD Mission: Both the relay subsatellite and the propulsion module are equipped with radio sources for the differential VLBI experiment. The VRAD mission starts as soon as the propulsion module is deorbited and lands on the lunar surface. Radio signals from the two sources will be received at the VLBI stations (Fig. 1) and averaged over an interval of 100 s to derive delay and delay rate. Because the semimajor axis of the relay subsatellite is larger than that
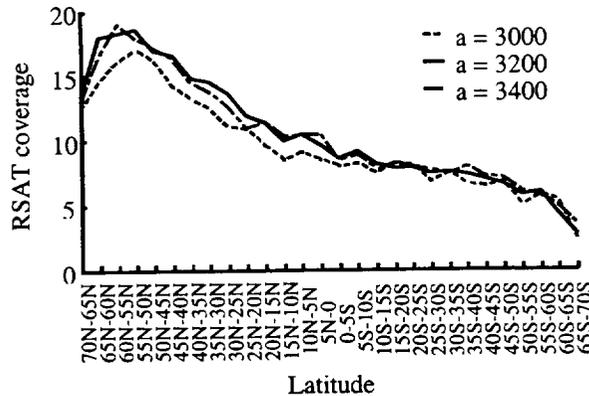
Fig. 2. Relative coverage of the four-way Doppler measurements over the farside by RSAT mission.

Fig. 1.

of the main orbiter, the VRAD experiment is not sensitive to high-degree gravity field of the Moon. Instead, VRAD is about 10× more accurate than conventional Doppler measurements [9]. Besides, VRAD is sensitive to the displacements perpendicular to the line of site (LOS) as well as that along the LOS. Thus, VRAD can improve the precision of the low-degree gravity field significantly and gives an accurate estimate of lunar moment of inertia as measurements from lunar laser ranging experiments [10] are combined.

Summary: The two selenodetic missions in the SELENE project, RAST and VRAD, provide a new dataset of the gravity field of the Moon for the studies of lunar interior and tectonics. The new dataset compensates for the current lack of direct measurements of two-way tracking over the farside, and reveals coefficients of the gravitational potential for low degree and order with precision nearly 10× higher than at present. Further examination of the experimental system on board and on the ground is required.

References: [1] Lorell J. and Sjogren W. L. (1968) *Science, 159,* 625–628. [2] Bills B. G. and Ferrari A. J. (1980) *JGR, 85,* 1013–1025. [3] Konopliv A. S. et al. (1993) *AAS Paper 93-622.* [4] Lemoine F. G. et al. (1997) *JGR, 102,* 16339–16359. [5] Neuman G. A. et al. (1997) *JGR, 101,* 16841–16863. [6] Sasaki S. et al. (1998) *Proc. 21st ISSTS,* 98-i-01. [7] Iwata T. et al. (1998) *Proc. 21st ISSTS,* 98-i-03. [8] Hayashi T. et al. (1994) *Proc. IEEE, 82.* [9] Hanada H. et al. (1994) in *VLBI Technology,* 277–281. [10] Dickey J. O. et al. (1994) *Science, 265,* 482–490.

⌐ ⌐ - ¹/

MARE BASALTS AS MANTLE PROBES: DICHOTOMIES BETWEEN REMOTELY GATHERED AND SAMPLE DATA?

C. R. Neal, Department of Civil Engineering and Geological Sciences, University of Notre Dame, Notre Dame IN 46556, USA (neal.1@nd.edu).

Mare basalts and pyroclastic glasses allow our only petrologic look at the lunar mantle, as *bona fide* mantle xenoliths are not present in the existing lunar sample collection. Knowledge thus gleaned demonstrates that the there was an early "lunar magma ocean" (LMO) [1,2], the cooling of which produced an igneous cumulate mantle forming source regions for mare basalts [3,4]. More sophisticated models demonstrated that late-stage ilmenite-rich cumulates would be denser than early cumulates and sink [5,6], or cause limited [7] to
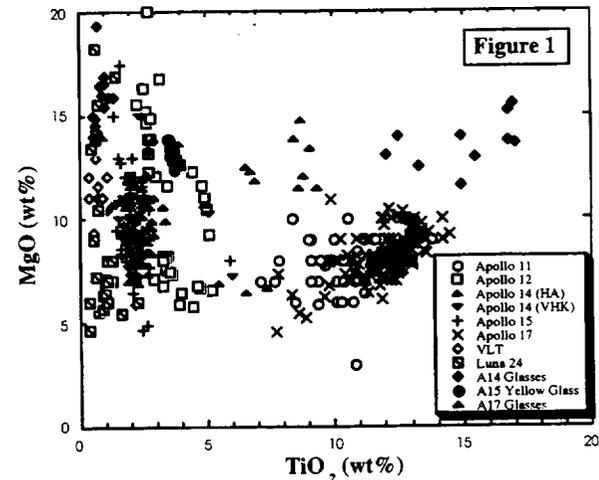
full-scale overturn of the cumulate pile [8–10]. Still under debate is the scale of the LMO: Was this whole Moon melting [10] or only the outer ~400 km [4]? If whole Moon melting is invoked, then differentiation of the Moon into a flotation plagioclase-rich crust, a mafic mineral cumulate mantle, and an Fe-rich core is more easily facilitated. Hess and Parmentier [10] suggested that the lunar core is made up of the dense, ilmenite-rich, late-stage cumulates from the lunar magma ocean because the material that formed the Moon came primarily from already differentiated Earth mantle, so it would not contain enough Fe to form a metallic Fe core. How can mare volcanism be used to constrain such models?

Sample-based Studies: Attempts to link mare basalts with volcanic glasses have not established any unequivocal relationships [11–15]. Compositions of mare basalts are defined primarily on the basis of TiO_2 (<1–15 wt%) [18], with gross divisions into low Ti (<6 wt%) and high Ti (>7.5 wt%) (Fig. 1). Source modeling suggests low-Ti mare basalts were derived from distinct source regions relative to high-Ti variants [7,8,16,17]. Furthermore, individual groups of basalts have been identified at each site and most were derived from distinct source regions [18,19].

The oldest basalts in the sample collection are the low-Ti Apollo 14 (>4 Ga) [20]. However, low-Ti basalts from Apollo 12, and 15, and Luna 16 and 24 sites are younger (3.1–3.5 Ga) than high-Ti basalts from Apollo 11 and 17 sites (3.6–3.9 Ga) [21,22]. The fact that the high-Ti basalts from Apollo 11 and 17 are generally older than the low-Ti basalts from Apollo 12 and 15 and Luna 16 [21] is consistent with the sources of the former containing a greater proportion of incompatible (radioactive) elements, promoting faster melting.

Similar to basalts, volcanic glasses have extreme ranges in TiO_2 (from <1 to >16 wt%) and appear to be undersaturated with respect to ilmenite [23–26]. Twenty-five distinct groups of volcanic glasses have been defined from existing lunar sample collections [27]. Galbreath et al. [28] and Shearer et al. [29] concluded that the primitive members of each of the 25 glass groups were composed of both primitive and evolved cumulate components. If this is the case, then the magmas which formed the volcanic glasses do not represent a single source, but rather a mixture, and any source modeling will yield results consistent with (1) catastrophic/limited overturn of the cumulate pile [7–9]; (2) polybaric melting models [24]; or (3) assimi-

Fig. 2.

Fig. 3.
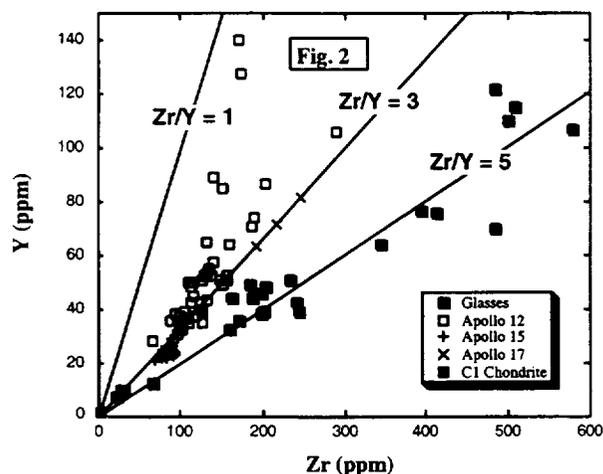
lation models [30–31]. Hess [23] demonstrated that the major-element concentrations of the glasses could not be modeled using a cumulate overturn model and concluded that picritic glasses ranging from 4.6 wt% to 13.5 wt% TiO_2 were derived from depths of 400–500 km leaving an olivine + opx residuum [23].

Experimental studies on volcanic glasses indicate derivation from depths of 400–500 km [23,32,33] possibly below the cumulate mantle formed by LMO crystallization [24,25,27,34]. Conversely, crystalline mare basalts originated at shallower depths than volcanic glasses, within the region of "cumulate" mantle formed by LMO crystallization [23,35]. Geochemical data suggest that the glasses originated from a primitive, possibly garnet-bearing layer, having higher Zr/Y ratios and PGE abundances (Figs. 2 and 3).

Remotely Gathered Data: This identifies compositional variations at both local and regional scales [36–38]. For example, basalts in the eastern hemisphere of the lunar nearside are higher in Fe and Ti relative to those in the west. In addition, remote studies demonstrated that two-thirds of the basalts on the nearside were not represented in the returned samples [37]. On the lunar farside, mare basalts have a similar range in FeO and TiO_2 contents to those of the nearside, but high-Ti basalts were not present [39]. Basalt flows on the farside tend to be thinner and less extensive and pyroclastic glass deposits are rare, a function of the thicker crust in this region [39,40]. However, there are problems in calibrating such data with actual sample compositions [41,42]. This is due to space weathering mechanically mixing different lithologies [43,44]. However, better spatial resolution now allows analysis of small craters that have sampled individual basalt flows or fresh exposures of basalt stratigraphy in crater walls [38,44].

Studies using Clementine and Galileo data have suggested a relationship between pyroclastic glasses (dark mantle deposits) and mare basalts. For example, Hawke et al. [45], Bussey et al. [46], and Blewett et al. [47] reported UVVIS and IR data from the Hadley-Appennine region and suggested the dark mantling deposits (probably pyroclastic in origin) were related.

Photogeologic evidence of the age of mare volcanism (crater counting/degradation) suggests basalts as young as 2.5 Ga or less are present on the Moon [48]. In addition, Hiesinger et al. [49,50] concluded that there was no correlation between TiO_2 content of
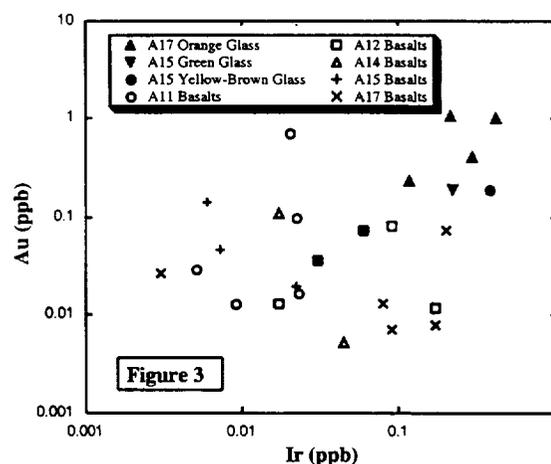
basalts and age. This is contrary to the age determinations on returned samples. Hiesinger et al. [49,50] also concluded that volcanism persisted for a longer period in the western hemisphere and that the younger the volcanism, the greater the compositional variability.

Synopsis: Distinct dichotomies exist between basalt studies using samples and those using remotely gathered data: (1) Not all mare basalt compositions are represented in the sample collection. (2) Sample data suggest a relationship between TiO_2 content of basalts and age, while remotely gathered data do not. (3) Radiometric ages of returned basalts indicate volcanism from 4.2 Ga to 3.1 Ga, while crater counting suggests volcanism lasted until 2.5 Ga. (4) Sample data suggest the pyroclastic glasses and basalts are unrelated, while remotely gathered data (at least in some cases) suggest they are.

It could be concluded that studies on samples from <5% of the lunar surface give a misleading view of the Moon. A thorough integration of remotely gathered basalt data in geochemical modeling is needed. Detailed geophysical studies of the lunar interior would be invaluable in understanding whether there is a primitive layer to the Moon and/or if garnet is present [51]. Integrating such studies with sample data will allow a better understanding of whether the pyroclastic glasses were derived from deeper (garnet-bearing? primitive?) levels in the Moon than basalts and define the nature of the lunar core.

References: [1] Smith et al. (1970) *Proc. Apollo 11 LSC*, 897. [2] Wood et al. (1970) *Proc. Apollo 11 LSC*, 965. [3] Taylor and Jâkes (1974) *Proc. LSC 5th*, 1287. [4] Warren (1985) *Annu. Rev. Earth Planet. Sci.*, *13*, 201. [5] Kesson and Ringwood (1976) *EPSL*, *30*, 155. [6] Ringwood and Kesson (1976) *Proc. LSC 7th*, 1697. [7] Snyder et al. (1992) *GCA*, *56*, 3809. [8] Hughes et al. (1988) *GCA*, *52*, 2379. [9] Spera (1992) *GCA*, *56*, 2253. [10] Hess and Parmentier (1995) *EPSL*, *134*, 501. [11] Longhi (1987) *Proc. LPSC 17th*, in *JGR*, *92*, E349. [12] Delano (1990) *LPI Tech. Rpt. 90-02*, 30. [13] Shearer and Papike (1991) *LPS XXII*. [14] Vaniman and Papike (1977) *Proc. LSC 8th*, 1443. [15] Taylor et al. (1978) *Mare Crisium*, 357. [16] Hughes et al. (1989) *Proc. LPSC 19th*, 175. [17] Snyder et al. (1994) *GCA*, *58*, 4795. [18] Papike et al. (1976) *Rev. Geophys. Space Phys.*, *14*, 475. [19] Neal and Taylor (1992) *GCA*, *56*, 2177. [20] Dasch et al. (1987) *GCA*, *51*, 3241. [21] Nyquist and Shih (1992) *GCA*, *56*, 2213. [22] Dasch et al. (1998) *LPS XXIX*. [23] Green

et al. (1975) *Proc. LSC 6th*, 871. [24] Longhi (1992) *GCA, 56*, 2235. [25] Longhi (1993) *LPS XIV*. [26] Hess (1993) *LPS XIV*. [27] Delano (1986) *Proc LPSC 16th*, in *JGR, 91*, D201. [28] Galbreath et al. (1990) *GCA, 54*, 2565. [29] Shearer et al. (1991) *EPSL, 102*, 134. [30] Hubbard and Minear (1976) *Proc. LSC 7th*, 3421. [31] Wagner and Grove (1993) *LPS XXIV*. [32] Kesson (1975) *Proc. LSC 6th*, 921. [33] Walker et al. (1975) *GCA, 39*, 1219. [34] Shirley and Wasson (1981) *Proc. LPS 12B*, 965. [35] Longhi et al. (1974) *Proc. LSC 5th*, 447. [36] McCord (1969) *JGR, 74*, 4395. [37] Pieters and McCord (1978) *Proc. LSC 7th*, 2677. [38] Staid and Pieters (1998) *LPS XXIX*. [39] Gillis and Spudis (1998) *LPS XXIX*. [40] Solomon (1975) *Proc. LSC 6th*, 1021. [41] Lucey et al. (1998) *LPS XXIX*. [42] Giguere et al. (1998) *LPS XXIX*. [43] Adams (1974) *JGR, 79*, 4829. [44] Jolliff (1998) *LPS XXIX*. [45] Hawke et al. (1979) *Proc. LPSC 10th*, 2295. [46] Bussey et al. (1998) *LPS XXIX*. [47] Blewett et al. (1998) *LPS XXIX*. [48] Boyce and Dial (1973). [49] Hiesinger et al. (1998a) *LPS XXIX*. [50] Hiesinger et al. (1998b) *LPS XXIX*. [51] Beard et al. (1997) *GCA, 62*, 525.

$\mathcal{D}_{\dot{\sigma}} \cdot - \dot{\zeta} \mathcal{V}$

LUNAR BASINS: NEW EVIDENCE FROM GRAVITY FOR IMPACT-FORMED MASCONS.

G. A. Neumann[1], F. G. Lemoine[2], D. E. Smith[2], and M. T. Zuber[1,2], [1]Department of Earth, Atmospheric, and Planetary Sciences, Massachussetts Institute of Technology, Cambridge MA 02139, USA (neumann@tharsis.gsfc.nasa.gov), [2]Laboratory for Terrestrial Physics, NASA Goddard Space Flight Center, Greenbelt MD 20771, USA.

Fig. 1. Line-of-sight (LOS) acceleration profile (top) from historically reduced Apollo 17 satellite tracking over Mare Crisium. Satellite altitude above lunar surface varied from 19 to 50 km, providing the most detailed gravity information available to date over this basin with ~1-mGal precision. Longitude corrected for ~1° orbital error. Lower curves: LOS acceleration simulated along the A17 orbital track from a suite of constrained gravity models. Lunar Prospector tracked at ~100 km altitude provided JGL75D [6], while LGM309a, b, e, and n represent the Goddard Lunar Gravity Model 2 (GLGM2) derived from Clementine and historical tracking at higher altitudes [2]. Letters a, b, e, and n represent solutions with power-law constraints with 1, 2, 4, and 8× that used for GLGM2.

Introduction: The prominent gravity highs (mascons) associated with uncompensated mass anomalies in lunar mare basins are a dramatic expression of the present-day rigidity of the lunar lithosphere. First discovered in Lunar Orbiter tracking data [1], these ~350-mGal gravity highs have been redetermined from the analysis of Clementine and historical tracking [2]. These highs coincide with topographic lows, indicating nonisostatic support. One of the rediscoveries of this analysis is the encirclement of the highs by substantial negative anomalies [1] over topographic highs. Recent gravity fields are providing the increased resolution necessary to determine the causes of this unique mascon signature.

The compensation of the basin anomalies remains controversial. The mascon highs have long been interpreted as the result of mare loading, subsequent to the decay of residual stresses resulting from the impact [e.g., 3]. Substantially more mare fill is required to produce mascon highs than has been inferred on geological grounds [4], and the amount of near-surface mass deficit required to produce a gravity moat exceeds bounds inferred from terrestrial examples [5]. This problem is most acute for the youngest basin, Orientale. Recent gravity fields from Lunar Prospector [6] have suggested mascon highs associated with nonmare basins such as Mendel-Rydberg, or minimally filled basins like Humboldtianum, further calling this explanation into question.

We suggest that the mascon gravity signal is produced by a combination of crustal thickness changes, manifested by central mantle uplift, outward displacement of crust, and downward flexure of the lithosphere under mare loading. The mantle uplift is super-isostatic, maintained by residual stresses resulting from the process of impact cratering and modification. In particular, the process of crater collapse and mantle rebound terminates abruptly, leaving the mantle plug in a non-equilibrium state, surrounded by a ring of thickened crust. Viscous relaxation over geological timescales has erased some, but not all, of the signature of the impact process.

Mantle uplift inferred from gravity modeling is inversely correlated with age [7]. While the oldest basins such as South Pole Aitken are mainly compensated isostatically [8], the younger basins appear to have been in a state of superisostatic loading prior to mare emplacement. If this is true, this places an important constraint on the impact process at basin scales. The idea that rebound of the transient crater via acoustic fluidization [9] may freeze substantial stresses into the lithosphere at the time of impact, and that relaxation is incomplete to this day, may be tested by examining the gravity signatures of major basins on terrestrial bodies. The Moon provides the clearest resolved examples to date, but uncertainty in gravity knowledge remains problematic.

Recent Gravity Data: Figure 1 compares gravity fields from Clementine and historical tracking, the latest Lunar Prospector field JGL75D, and a very low-altitude line-of-sight (LOS) acceleration profile from Apollo 17 over Mare Crisium. The Doppler tracking data from this satellite is not available, but the historically reduced LOS data provide independent checks on global solutions.

The amplitude of the mascon high is most nearly matched by JGL75D, but A17 LOS shows more power in the gravity signal than current models. The mass deficit over the topographic high at 48° longitude is strikingly revealed by the LOS data and JGL75D. Similar negative anomalies are seen in A17 LOS over the edges of Serenitatis and Orientale. The earlier fields [2], of which LGM309a (GLGM2) is the most conservative, do not reproduce its amplitude or location well, regardless of the amount of power-law constraint employed.

We shall present gravity models for these basins that account for flexural downwarp of the Moho, crustal displacement, and residual impact uplift. The models provide a quantitative test of the hypothesis that basins are locally compensated by density contrasts within the crust or at the lunar Moho prior to mare emplacement. Our results indicate that the mass excess required to produce mascon highs and flanking lows is greater than can reasonably be attributed to mare emplacement, suggesting that some of the nonisostatic loading remains from the impact process itself.

References: [1] Muller P. M. and Sjogren W. L. (1968) *Science, 161*, 680–684. [2] Lemoine et al. (1997) *JGR, 102*, 16841–16863. [3] Bratt S. R. et al. (1985) *JGR, 90*, 3049–3064. [4] Williams K. K and Zuber M. T. (1998) *Icarus, 131*, 107–122. [5] Neumann G. A. and Zuber M. T. (1997) *LPS XXVIII*, 1015–1016. [6] Konopliv A. S. et al. (1998) *Eos Trans. AGU Spring Mtg. Suppl.* [7] Neumann G. A. et al. (1996) *JGR, 101*, 16841–16863. [8] Zuber M. T. et al. (1984) *Science, 266*, 1839–1843. [9] Melosh H. J. (1979) *JGR, 84*, 7513–7520.

535- 7/

COMMENTS ON "RADAR SEARCH FOR ICE AT THE LUNAR SOUTH POLE" BY R. SIMPSON AND G. L. TYLER.

S. Nozette[1], C. L. Lichtenberg[2], R. Bonner[2], P. Spudis[3], and M. Robinson[4], [1]Lawrence Livermore National Laboratory, USA, [2]Naval Research Laboratory, USA, [3]Lunar and Planetary Institute, Houston TX, USA, [4]Northwestern University, USA.

This paper is a good start to providing a second analysis of the original Clementine bistatic radar data [1]. However, the paper does not replicate the analysis contained in [1], and omits several key points that call the conclusions of this paper into question. There are also a number of misunderstandings concerning the previous work in [1] that require correction. It appears the author's primary objective is to refute the findings of [1] with an incomplete analysis, not to perform a thorough search for evidence of ice in the data. Specific points are as follows.

Theoretical Background: The Clementine bistatic radar experiment observed the lunar south polar area surface at a highly grazing incidence angle ($\approx 85°$). The scattering elements (ice deposits) cover only a small fraction of the observed area (45,000 km^2). Under these conditions the ice-specific coherent backscatter opposition effect (CBOE) will be muted and broadened [2,3]. Therefore, the key measurement that must be extracted from the data is the phase function of the surface, sampling all the permanently shadowed terrain because, over a broad range of β ($\pm 3°$) the RCP/LCP peak (and RCP and LCP separately) will be much broader than for cases of smaller incidence angle. The analysis by Simpson and Tyler (hereafter referred to as S/T) only locates a few Doppler bins closest to the south pole at the time β goes to 0. Since these few bins only peak up a bit, and are not unique, S/T concludes no enhancement is present. The Clementine team observed the same effect very early in their data reduction and concluded at that time that the analysis needed to be taken to a much greater level of detail. The analysis in [1] used all β values over a range $\pm 10°$, and each and every Doppler bin, at all times in the sample, to derive the RCP/LCP ratio as a phase function for the entire south pole region. It was this function that showed enhancement, not just a few individual Doppler bins. This function is never calculated by S/T. The Clementine team performed geometrical calculations with in-house science mission planning tools and NAIF

software. High-accuracy versions of ephemeris, attitude, and planetary data files were used, including the NASA/Goddard precision orbit determination and precision lunar orbit libration data. The target areas were isolated by Doppler shift, which relates bands of constant frequency to a set of lunar ground locations (the β = 0 track). The analyses to extract radar scattering information from local regions on the surface used range, range-rate, and angular relationships of a ray from the spacecraft to a point on the lunar surface. Similar calculations were performed for the ray from that lunar target point to the DSN receiver site. These two sets of parameters were appropriately combined, and together they represent the echo "reflected-ray" geometry as a function of time and lunar location. A Doppler-broadened echo spectrum results from the differential motions of all points on the surface relative to the spacecraft and receiver. The "direct-ray" geometry was calculated for the ray emanating at the spacecraft and terminating at the DSN receiver site. The direct-ray spectrum, recorded simultaneously with the reflected-ray spectrum, was used as the frequency reference for the south pole orbits. The low altitude of the north pole orbits precluded observing the direct ray. In this case the observed frequency at the RF terminator was used as the frequency reference. For every instant in time, the pattern of iso-dops was mapped onto a lunar grid. Thereafter the analysis was performed by "sorting" the Doppler data according to the parameter of interest (e.g., β, angle of incidence). The proximity to the south pole was not the most important criteria; it is the fraction of permanently shadowed area to total area sampled that was important. This fraction was varied by the analysis in [1], and the maximum RCP/LCP peak response was observed only when this shadowed/total area ratio was maximum. This calculation is not contained in the S/T paper.

An objective analysis should contain the "β function," i.e., RCP/LCP vs. β should be plotted for all pertinent orbits and for several regions of surface. The plot of raw, calibrated, RCP/LCP vs. time for orbit 234 fit with a cubic spline function is required. To further differentiate the possible effects of the shadowed terrain, the Clementine team compared orbit 234 with orbit 235, which contained no shadowed terrain. This comparison was not done by S/T and is central to any conclusions drawn. Additionally, at the suggestion of Simpson in September 1995, the Clementine team performed a global analysis of all four orbits as a function of angle of incidence, as described in [1], to isolate effects of unusual scattering due to high incidence angle. This analysis also yielded an enhancement in RCP/LCP only for orbit 234. This calculation serves as an internal check and must be performed by any credible reanalysis of [1] as originally suggested by Simpson in 1995. The S/T reanalysis is incomplete, and its conclusion should not be considered definitive until all four Clementine orbits are treated in comparable, internally consistent, manner. Until this is done, the conclusions presented by S/T are premature and the statement that "comparable analysis methods were used" requires substantial modification.

Specific Analysis Issues: *Calibration.* Despite the fundamental differences in data analysis with [1], the calibration described by S/T appears equivalent, but not superior, to that used in [1]. Simpson and Tyler stated that the Clementine team did not use frequency flattening in calibration. This is incorrect; it was used. It is also stated that the Moon occupied a majority of the Goldstone beam while centered at the south pole. This was not the case.

Filtering. Simpson and Tyler state that median filtering was used to replicate the application in [1]. Median filtering was used in [1],

but in a different manner than applied by S/T. This single difference is sufficient to account for the failure of S/T to detect the enhancement reported in [1]. Simpson and Tyler applied a high-order (360) median filter to the raw, calibrated, FFT data files, and then calculated RCP/LCP for the $\beta = 0$ condition at the south pole for selected Doppler bins. The Clementine team calculated the power and RCP/LCP ratio for each raw Doppler bin, on a bin-by-bin basis, averaged over the 4-s period, and then summed these over the full range of β, selected for specific regions on the lunar surface. The last step was application of an order 60 median filter to the phase function, creating Fig. 3 in [1]. Because of the high frequencies in the raw data, application of the high-order median filter to the raw polarization channel FFTs prior to calculating an RCP/LCP ratio, as done by S/T, suppresses the RCP/LCP enhancement. As S/T does not sum all the RCP/LCP values over all angles for selected regions (e.g., maximum shadow area), it does not capture sufficient statistical samples to replicate the enhancement reported in [1]. The Clementine team also attempted S/T's approach and found that it incorrectly suppresses the RCP/LCP enhancement.

Detection thresholds. The detection thresholds quoted are in good agreement with the minimum "pure ice" area calculated by Simpson prior to the original Clementine bistatic experiment (1 km^2). Given the *a posteriori* knowledge about the presence of H provided by the Lunar Prospector neutron spectrometer experiment, the paper misinterprets these results and the original Clementine and Arecibo radar results. There is no *a priori* knowledge of the range of purity of ice in the neutron spectrometer footprint, only that it represents a fairly gross mixing average within 0.5 m of the surface over the entire footprint. Given the 1 wt% value quoted by S/T, and the 10,000 km^2 neutron spectrometer footprint, the area surface density of "pure ice" is ~200 km^2 of pure ice equivalent area, assuming ice has 0.5 the density of lunar regolith. The neutron spectrometer cannot determine *a priori* what fraction of this is "pure ice" and how deep it is beyond the 0.5-m limit. Clementine [1] observed a large area (6–15,000 km^2) area of permanent shadow at the lunar south pole. Theory suggests that ice must be confined to the permanently shadowed areas. It is unlikely that ice exists in a single state over the entire region. The deposition process is likely to be random. At cryogenic temperatures ice behaves like rock and becomes a regolith component. It may be a fine regolith component, a continuous strata, a broken-up strata, outcrops, or inclusions, all mixed with varying amounts of regolith. Radar observations of Mercury indicate the ice deposition process creates enough thick pure deposit to produce distinctive CBOE radar signatures [4]. Given the quantities of H detected by Lunar Prospector, it would be unlikely if some relatively pure ice did not exist over the large area observed by Clementine. The Lunar Prospector and Earth-based radar observations of Mercury are sampling larger amounts of permanent shadowed terrain due to better geometry than did the Clementine lunar observations. The Clementine experiment did not sample all the permanently shadowed terrain at the south pole, and due to local topography, it is difficult to estimate just what fraction was observed. The Clementine team calculated the fractional pure ice equivalent area in accordance with the method described in [3], at 0.2–0.3 %, not 0.024% as quoted by S/T. When applied to the entire orbit 234 footprint, this translates to ~85–135 km^2. Since the area contained by b $\pm$ 1°–2° is an order of magnitude less, this represents about 10 km^2. Examination of the Arecibo RCP/LCP images [5,6] and detailed estimates of area and shadow indicate that >80% of anomalous high RCP/LCP area at the south pole is in

permanent shadow. Simpson and Tyler report these findings as negative, as they are not different than a "control area" in Sinus Iridium. Close examination of the Earth-facing wall of Shackleton suggests anomalous scattering behavior, as the radar brightening increases with depth in the crater. This effect was not observed at the control areas or anywhere else on the Moon, and it was suggested this could be due to ice [5]. Detailed analysis of the south pole terrain and lighting conditions indicate that Shackleton contains at least 2.44 km^2 (and very likely an additional 16.25 km^2) of anomalous high RCP/LCP area in permanent shadow. The Clementine bistatic experiment sampled this entire anomalous area at favorable geometry in orbit 234. The Arecibo authors [6] chose to interpret this data (prior to Lunar Prospector) as surface roughness, but the data are consistent with greater than 1 km^2 of relatively pure ice in an area observed by Clementine orbit 234. Given the Lunar Prospector findings, there is no reason these high RCP/LCP areas in Shackleton cannot be ice. Simpson and Tyler are correct that the regolith processes mute the ice signature in monostatic observations. However, ice covered with 10–20 cm of regolith should be detectable [4] by radar. Estimates from the neutron spectrometer are 10–40 cm regolith cover, but this could be greater or less in regions small relative to the instrument footprint [7]. This factor, combined with the grazing incidence angle, makes it difficult to interpret the monostatic observations as ice unique [6]. They are consistent with >1 km^2 area of ice in the permanently shadowed areas in the south polar region, specifically Shackleton. We conclude the Clementine bistatic analysis did show a muted CBOE effect and detect lunar ice, a detection confirmed by the Lunar Prospector neutron spectrometer.

References: [1] Nozette S. et al. (1996) *Science, 274,* 1495. [2] Gorodnichev E. E. et. al. (1990) *Phys. Lett. A, 144,* 48. [3] Mishchenko M. I. (1992) *Earth Moon Planets, 58,* 127. [4] Butler B. J. et al. (1993) *JGR, 98,* 15003. [5] Stacy N. J. S. (1993) Ph.D. thesis, Cornell Univ. [6] Stacy N. J. S. et al. (1997) *Science, 276,* 1527. [7] Feldman W. (1998) personal communication.

S . . . . . /

CONSTRAINTS ON OUR VIEW OF THE MOON I: CONVERGENCE OF SCALE AND CONTEXT.

C. M. Pieters, Geological Sciences, Brown University, Providence RI 02912, USA.

Perhaps the greatest challenge to using remotely acquired compositional information to resolve fundamental planetary science questions is realistically understanding the difference between information gathered with remote detectors and that obtained with sophisticated instruments in the laboratory. Small-scale processes associated with space weathering are discussed in a companion abstract. Outlined here are issues associated with interpreting data from different scales and context.

Differences in Scale: There are several important differences of scale when merging remote compositional analyses with results from Earth-based laboratories.

Spatial scales. Laboratory spatial scales are typically micrometers to centimeters, whereas remote-sensing scales are hundreds of meters to hundreds of kilometers. For example, pyroxene composition measured in the laboratory is very exact and designed to show differentiation and cooling trends — important, but something entirely different from what is possible with remote sensing. Spectros-

copy can characterize pyroxene composition, but it is necessarily a single average value for the bulk.

Accuracy and precision. These terms are almost synonymous in the laboratory, with scales typically being several hundredths of a percent (relative units). With remote-sensing measurements, accuracy is a fuzzy term (involving a mix of physics, detector calibration, and empirical and theoretical predictions and beliefs) that is often difficult for anyone but the most technically involved to really unravel. Precision can at least be mathematically defined as the repeatability of a remote measurement.

Scope and breadth of measurements. Purity of the information, or scope and breadth of measurements, suggests a difference in content scale. Individual elements, isotopes, or minerals are readily separated in the laboratory, whereas remote measurements must almost always deal with mixtures or ambiguity.

These differences must be consciously bridged in order to integrate the strengths of both into a New View of the Moon. To address any significant lunar science issue requiring compositional information, a convergence is needed between what is desired from the geochemist's perspective and what is possible from remote-sensing approaches.

Geochemists who are accustomed to a wealth of high-precision data for well-defined materials are often frustrated by the loose bounds to compositional measurements remote-sensing scientists are able to provide. On the other hand, one of the biggest aggravations or fears of scientists involved in remote sensing is to have the results of their efforts viewed simply as data to be used by others. To make matters worse, the two communities often use the same language to mean different things. Integration of diverse data on all scales is a multi-disciplinary challenge.

The Context: Even though the Moon does not recycle material the way Earth does, few materials currently on the surface are in their original location. Several types of mixing issues must be addressed to use compositional information in the proper context to understand crustal evolution. (All numbers given here are first order estimates.)

Regolith. All relatively smooth lunar surfaces develop several meters of fine-grained regolith that constitute most (90%) of what is seen by remote sensors. The regolith is the great equalizer, a regionally homogeneous product of the *average* composition on a very local scale (~1 km), but with varying amounts of nonlocal components (5–20%) intimately mixed. At finer scales (meters to hundred meters) stochastic processes destroy the statistical uniformity of the regolith. The type and amount of the nonlocal material depends on the specific geologic setting. *Mare regolith* surfaces are dominated by local basalt components. Note, however, that no mare regolith represents any single basalt type as defined by geochemists. *Highland regolith* surfaces are developed on the uppermost megaregolith (latest deposit) of the region (see below).

Immature mare. Not all the 18–20% of the lunar surface covered by maria has a well-developed regolith. Small fresh craters that have not penetrated through the mare deposits expose unweathered basaltic materials that are much more similar to the rock chips familiar to petrologists. Perhaps <2% of the lunar surface seen by remote sensors represent such immature mare materials.

Megaregolith. For our purposes a useful definition of the lunar megaregolith is the column of broken materials, typically 1–3-km thick, that have been excavated and deposited at a given location by large-scale impact events. This generally means the cumulative sequence of basin ejecta and impact melt. Large-scale variations across

the highlands reflect this stratigraphy of basin deposits. The emplacement process itself implies a *mixture of crustal materials*, and highland surface units are defined only to the extent that soils developed on such deposits are distinctive. The megaregolith itself is exposed on the surface by small (<30 km) fresh craters in the highlands or by steep-sided features unable to accumulate a mature regolith. Such surfaces account for perhaps 6% of the area seen by remote sensors.

Submegaregolith. There are only a few types of sites on the Moon where *pristine components* of the original lunar crust might be observed: (1) places where the megaregolith does not exist, such as on uplifted massifs of some circular basins, or (2) places where large craters (>50 km in diameter) have excavated through the megaregolith and uplifted underlying crustal material to the surface (e.g., central peaks of large craters; see abstract by Tompkins). Such surfaces account for perhaps 2% of the area seen by remote sensors. Depending on the early history of such sites, it is evident that naturally some fraction of such features (say, 30%) do not represent primary crustal components, but only earlier massively reworked materials.

To some extent, all the above discussion of scales and content is now self-evident if the matter is given attention. Nevertheless, if we are to seriously move forward with the integration of detailed compositional information derived from lunar samples and diverse but less-constrained information from remote sensing, then recognition of these differences in scale and content must continually permeate all approaches to science issues.

537-91

CONSTRAINTS ON OUR VIEW OF THE MOON II: SPACE WEATHERING.

C. M. Pieters, Department of Geological Sciences, Brown University, Providence RI 02912, USA.

A variety of processes set limits on how closely remote sensing data can be coupled to science issues requiring detailed compositional analyses. Issues related to small-scale regolith processes, and space weathering in particular, are outlined here. Larger-scale issues are discussed in a companion abstract. This outline is presented to provoke discussion and is not assumed to be comprehensive. Numerous authors have built the foundation and provided relevant ideas, including J. Adams, C. Allen, A. Basu, J. F. Bell, R. Binzel, D. Britt, C. Chapman, B. Clark, E. Fischer, M. Gaffey, B. Hapke, T. Hiroi, R. Housley, L. Keller, R. Johnson, P. Lucey, D. Matson, T. McCord, D. McKay, L. Moroz, R. Morris, C. Pieters, Y. Shkuratov, L. Taylor, J. Wasson, and S. Wentworth.

Definition: The most general working definition of space weathering is a family of processes active in the space environment that combine to alter the physical and/or compositional properties of materials. The use of remotely acquired data to infer compositional information about a body requires that we understand how space weathering has changed a surface's appearance. Because multiple processes are involved, there is no single description of space weathering and its effects. Issues include: (1) What are the individual processes active and what do they produce? (2) What aspects of the environment control each process and what is the magnitude of the effect? (3) What is the timescale required for each process to have a measurable effect? (4) How do various processes combine? (5) Which processes are dominant in a specific environment? There is no single answer to these questions. For example, answers are quite different for materials in low Earth orbit, on the Moon, and on the surface of an asteroid.

The Role of the Moon: The return of the first lunar samples brought home the concept of space weathering. The Apollo 11 rocks were recognized as basaltic, but the soils, or regolith as it came to be known, were quite different. The fine-grained soils contained lithic and mineral fragments, glass, and abundant "gunk" — the complex amorphous glass-welded agglutinates. Spectra obtained remotely for the Moon looked like spectra for the soils rather than rocks, and it was quickly recognized that the space environment turned perfectly good rocks into this poorly understood but heavily altered soil. Since lunar soils are currently the only samples available that have experienced space weathering, they provide the principal template with which to test our understanding of the processes at work.

For the Moon, the well-known observable effects of space weathering in the visible and near-infrared spectrums include (1) a darkening or lowering of albedo, (2) a weakening of diagnostic absorption bands, and (3) an increasing reflectance toward longer wavelengths (steepening of the continuum). These effects are seen for all lunar compositions (highland and mare). At longer mid-infrared wavelengths absorption features are substantially weakened and often reshaped. The only lunar materials studied in the laboratory that are free of the optical effects of space weathering are crystalline samples, such as basalts or "pristine" samples (bulk and particulate). All soils exhibit space weathering effects to some degree (some more than others) as do most breccias.

Outlined below is a summary of several of the primary processes that occur in the space environment and secondary processes (a result from one or more primary processes) active on the Moon. The challenge is to understand how the secondary processes are related to the primary processes — in an accurate and quantifiable manner that allows extrapolation in space and time.

Primary Processes of the Space Environment:

♦ Meteorite bombardment (largely micrometeorites)
- comminution
- shock
- melt formation
- vaporization
- contamination (foreign material)

♦ Solar wind and cosmic ray
- implantation
- sputtering

Secondary Processes Active on the Moon:

♦ Nanophase $Fe°$ formation
♦ Amorphous rind or "patina" formation
♦ Recrystallization of melt and amorphous material
♦ Escape (loss) from the surface
♦ Lateral mixing of foreign material
♦ Agglutinate formation (all the above)

Debate and Confusion: Each of the processes listed above has received at least some attention in the decades since return of the lunar samples. Everyone agrees agglutinates are a typical product of lunar space weathering and regolith formation, but beyond that, there is there is very little consensus. There is not yet agreement on such seemingly simple aspects such as the site of principal effects: surface vs. body. The timescale is almost unconstrained. The relative importance of each process seems to be dependent on the investigator. To make matters worse, the literature contains great confusion about key terms such as "glass." Glass has often been used to refer to almost anything complex and messy and therefore amorphous. The term has been used and misused to refer to many products that are clearly

produced, at least in part, by different processes (and exhibit different optical properties): quench glass droplets, impact melt, amorphous rinds, lithified fragments, and agglutinates.

Progress: On the other hand, perhaps we really are on the verge of developing a consistent paradigm. Some ideas have been almost abandoned while evidence for others is getting stronger. For example, the color of quench glass is dependent on composition and is now recognized as *not* being a significant factor controlling the shape of the continuum. On the other hand, the role of pervasive nanophase $Fe°$ is increasing in importance for both continuum slope and albedo. Multiple aspects of agglutinate formation are being addressed separately. When mineralogy is accurately assessed, the strength of individual absorption bands can be directly related to the abundance of Fe-bearing minerals and less a function of masking effects of other absorbing species. Recently, advanced analytical techniques have provided unprecedented new data with which to readdress integrated issues such as surface properties of individual grains and their role in characteristics of bulk soil.

Space weathering isn't really a problem to be solved. Being able to understand how space weathering affects materials in a quantifiable manner, however, is a prerequisite for accurate remote compositional analyses, and we must develop workable answers for all the questions listed under the "Definition" paragraph above.

 ⌐⌐₃ ₃ 9/

AVERAGE MINERAL COMPOSITION OF APOLLO LANDING SITE SOILS. S. Riegsecker, A. Tieman, and A. Basu, Department of Geological Sciences, Indiana University, Bloomington IN 47405, USA (basu@indiana.edu).

The purpose of this paper is to express the average composition of lunar soils at Apollo landing sites in terms of four principal mineral groups, i.e., plagioclase, pyroxene, olivine and opaque (mostly ilmenite). Several studies have shown that lunar soil predominantly consists of lithic fragments of mare and highland rocks, glass fragments, fused soil particles, and the single grains of minerals. To achieve this goal, we have compiled modal data from the literature and recast them in terms of these minerals. The distribution of percentages for the lithic and mineral components of the lunar soil samples (90–150 μm) was compiled from the modal data in the *Handbook of Lunar Soils* [1] and checked against primary sources. We used our own analyses for soils 14141, 15271, 15401, 15431, 67941, and 72161 [2–6]. The population of glass, regolith breccia, and fused soil was neglected on the assumption that they approximately represented the modal distribution of the minerals in the soil. Grains classified as anorthosites, gabbronorite, crystalline breccias, and highland basalt were grouped as "highland rocks"; those classified as mare basalt and KREEP basalt were grouped as "mare rocks."

A few analysts had classified pyroxene and olivine together in one "mafic" category (soils 10084, 12001, 12003, 12037, 12042, 12057, 12060, 14163, and 67461). For these soils, the "mafic" category was distributed into olivine and pyroxene in a 5:95 ratio (assumed from mare basalts) and the modal data normalized to 100%. An example is shown in Table 1 for soils 10084 and 12001. Note that "mafic" (12.5 and 46.7) is redistributed into pyroxene (11.9 and 44.3) and olivine (0.6 and 2.3) respectively.

The principal minerals are also present in mare and highland rock fragments. Modal distribution of these minerals for both lunar rock types [7,8] from each Apollo mission was compiled and averaged

(Table 2). For Apollo 11 highland rocks, no published information on the modal mineral abundance could be found. Modal data from Apollo 17 highland rocks were used as an estimate. Rock fragments in the soils were then redistributed into the monomineralic population of each soil using the appropriate ratios obtained from Table 2. An example of this redistribution process is shown in Table 3 for soils 10084 and 12001. Note how the percentage of each mineral increases as those of rock fragments go to zero (compare Tables 1 and 3).

The final redistributed mineral composition of each soil sample was calculated. Table 4 summarizes the results, as average soil compositions, for each Apollo landing site.

TABLE 1. Redistribution of "mafic" into pyroxene and olivine.

Soil	Plag	Oliv	Pyrx	Opq	Mafic	Mrx	HldRx
10084	5.7	0.6	11.9	3.3	12.5	71.6	6.9
12001	9.9	2.3	44.3	0.5	46.7	32.9	9.9

TABLE 2. Modal distribution of minerals in mare and highland rocks.

	Plag	Pyrx	Oliv	Opq
A11 Mrx	25.1	55.2	2.0	17.7
A11 Hrx	46.3	34.7	17.4	1.62
A12 Mrx	22.0	60.9	8.0	9.18
A12 Hrx	60.0	36.5	1.9	1.51
A14 Mrx	43.0	53.8	0.0	3.2
A14 Hrx	65.3	32.6	0.0	2.11
A15 Mrx	28.8	62.6	4.0	4.57
A15 Hrx	92.5	7.04	0.0	0.5
A16 Mrx	34.9	61.6	3.5	0
A16 Hrx	64.9	30	5.0	0.1
A17 Mrx	30.2	53.3	3.0	13.6
A17 Hrx	46.3	34.7	17.4	1.62

TABLE 3. Redistribution of rock fragments into minerals.

Soil	Plag	Oliv	Pyrx	Opq	Mrx	HldRx
10084	5.7	0.6	11.9	3.3	71.6	6.9
12001	9.9	2.3	44.3	0.5	32.9	9.9

Applying ratios from Table 2 we obtain

Soil	Plag	Oliv	Pyrx	Opq
10084	27	3.2	54	16
12001	23	5.2	68	3.6

TABLE 4. Average mineralogic composition of lunar soil at Apollo landing sites.

	Plag	Oliv	Pyrx	Opq
A 11	26.7	3.2	53.7	16.3
A 12	23.0	8.7	63.4	4.9
A 14	49.7	1.8	47.0	1.5
A 15	37.9	8.4	52.2	1.5
A 16	69.0	2.6	28.2	0.1
A 17	35.5	5.5	56.3	2.7

References: [1] Morris R. V. et al. (1983) *Handbook of Lunar Soils*, JSC 19069, Planetary Materials Branch Publ. 67. [2] McKay D. S. et al. (1972) *Proc. LSC 3rd*, 987. [3] Griffiths S. A. et al. (1981) *Proc LPS 12B*, 475–484. [4] Basu A. et al. (1979) *Proc. LSC 10th*, 1413–1424. [5] Basu A. et al. (1984) *Proc. LPSC 14th*, in *JGR, 89*, B535–B541. [6] Basu A. et al. (1975) *The Moon, 14*, 129–138. [7] Heiken et al. (1991) *Lunar Sourcebook*, Cambridge Univ., 736 pp. [8] Wood J. A. et al. (1971) *Mineralogy and Petrology of the Apollo 12 Lunar Samples*, SAO Spec. Rpt. No. 333.

537 - 91

CONCEPTUAL DESIGN OF THE GROUND-DATA PROCESSING SYSTEM FOR THE LUNAR IMAGER/SPECTROMETER ONBOARD THE SELENE MISSION.

A. Shiraishi, J. Haruyama, H. Otake, M. Ohtake, and N. Hirata, Advanced Mission Research Center, National Space Development Agency of Japan, 2-1-1 Sengen, Tsukuba-shi, Ibaragi-ken, 305-0047, Japan (Shiraishi.Atsushi@nasda.go.jp).

Introduction: The lunar orbiter and lander system SELENE (Selenological and Engineering Explorer) is now in preliminary design phase toward an expected launch day in 2003. Along with the hardware design, we have started the conceptual discussion of a ground-data processing facility with other SELENE members. We are also constructing related databases for the ground-control experiments, such as spectral research on Earth, lunar, and meteoritic minerals. In our poster, we will introduce the current status of the development of the ground-data processing and database system for one of the SELENE mission instruments, LISM, the Lunar Imager/Spectrometer.
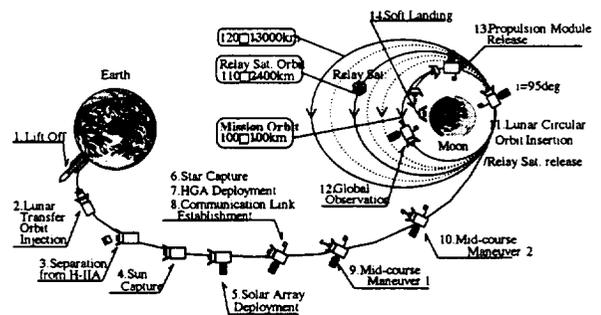
Fig. 1.   Mission outline of SELENE.
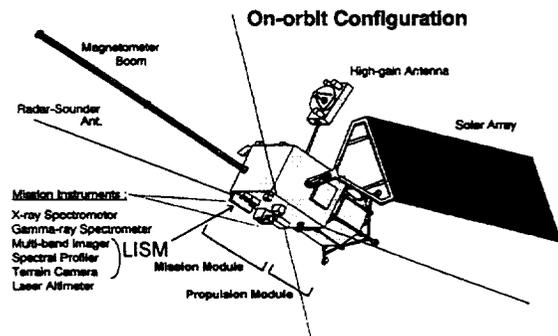
Fig. 2.   SELENE in lunar orbit.

TABLE 1. LISM specifications.

	TC Terrain Camera	MI Multiband Imager	SP Spectral Profiler
Spatial resolution at 100 km altitude	10 m/pixel	VIS 20 m/pixel NIR 62 m/pixel	500 m
Field of view	20° (35km)	11° (19.3 km)	0.29° (500 m)
MTF (@Nyquist)	>0.2 within 10° of FOV	>0.2	N/A
B/H ratio	0.6	N/A	N/A
Band area	0.45–0.7 μm	0.4–1.6 μm	0.5–2.6 μm
Spectroscope	Band-pass filter	Band-pass filter	Grating
Colors	2	9	~300
Band width	250nm	20–50nm	6–8nm
Onboard Calibration	N/A	N/A	Radio-metric and Spectro-metric cal
S/N*	>100	>100	>2600
Radiometric Resolution	10 bit	VIS 10 bit NIR 12 bit	16 bit
Data rate (before compression)	10.8 Mbps	3.9 Mbps	14.9 kbps
Data compression ratio	30 (Lossy)%	80 (Lossless)%	N/A

*Values at the Moon surface reflection rate of 2%, 5%, and 6% respectively, and at 0.7–1.5 μm for SP.

Fig. 3.   LISM ground-data processing flow.

TABLE 2.   LISM ground-data storage volume.

Data Level	TC	MI	SP	Comment
Level 0 (raw)	33 Tbit × (1/3)	13 Tbit × 0.8	220 Gbit	Store/No publication Compressed to 1/3 in TC (lossy) and 0.8 in MI (lossless)
Level 1	33 Tbit × 0.8	13 Tbit × 0.8	220 Gbit	Lossless compression (×0.8) in TC & MI
Level 2a	0	13 Tbit × 0.8	220 Gbit	Lossless compression (× 0.8). Will be public one year after flight mission.
Level 2b	660 Gbit	260 Gbit	—	One week storage only for the LISM PI group
Level 2c	33 Tbit × 0.8	13 Tbit × 0.8	220 Gbit	Lossless compression (× 0.8). Will be public one year after flight mission.
Low res. image for browsing	0.33 Tbit × ~0.8	—	—	Stored & opened for SELENE scientist grp. Will be public after one year
SP measurement line	—	—	407 Gbit	Stored & opened for SELENE scientist grp. Will be public after one year
DEM Geological map	4.6 Tbit	760 Gbit		
Total data volume to be stored	69.32 Tbit (=8.67 Tbyte)	42.62 Tbit (=5.33 Tbyte)	1.29 Tbit (=161 Gbyte)	

SELENE: Figure 1 shows the mission outline of SELENE. The explorer will be launched in 2003 and will execute 13 scientific missions for one year (including the system-certification period of about two months) in a lunar orbit of 100-km altitude with 95° inclination. At the end of the orbital mission, the propulsion module will be separated and descend onto the Moon surface. After soft landing, it will act as a radio-wave source for the 14th mission, VLBI, for two months. Figure 2 shows the in-orbit configuration of SELENE.

LISM: LISM consists of three passive optical sensors for lunar surface observation: TC (Terrain Camera), MI (Multiband Imager), and SP (Spectral Profiler). The major specifications of LISM are shown in Table 1.

Ground-Data Processing: LISM will produce 47 Tbit of the raw spectral and imaging data of lunar surface in the 10-month orbital mission period. The data will be processed through radiometric, geometric, and spectrometric (for SP only) calibration as shown in Fig. 3. The major middle products and final calibrated data will be stored in the data-processing facility and opened to the public just one year after the end of the orbital mission of SELENE. Not only the calibrated data but also some scientific products such as the full surface lunar DEM (Digital Elevation Map) and the geological map may be made public on the same computer server. The total volume of the data that should be stored and/or publicly opened is summarized in Table 2.

We have just started the consideration of the real-time data processing system for LISM. The calculation speed required for this system will be a level of that of high-end workstation network. However, the details of the faculties and/or the workability of the system have not yet been determined.

LISM Data Publication Concept: The PIs and CoIs of LISM will be exclusively authorized to access all the tentative and final version of the data from LISM. The low-resolution browsing maps delivered from TC data are opened to scientists in the SELENE project at first and will be made public, with all other calibrated data

and calibration protocols, one year after the end of the orbital operation period of SELENE.

Fig. 4. (a) Schematic drawing of MIRAI system. (b) Example of MIRAI product. (c) Mineral reflectance database concept.

For the convenience of scientists outside the SELENE project, a bit of the calibrated data will be published in the first quarter of the orbital mission period.

LISM Ground Reference Database: Along with the designing of the ground-data processing facility, we have started data accumulation and database construction of the reference spectroscopic reflection data of minerals of Earth and meteorites for various grain sizes and phase angles. After launch of SELENE mission, this database will work for interpretation of the data from MI and SP to determine the mineralogical composition of the lunar surface. Figure 4a shows the schematic function of our Mineral Reflectance Analysis Instrument (MIRAI), which we are now using for the reference data measurement. In this system, the incidence angle and the emergence angle can be set independently. Figure 4b shows an example of measurement results by MIRAI. Figure 4c shows the concept of the mineral reflectance database.

RADAR SEARCH FOR WATER ICE AT THE LUNAR POLES.   R. A. Simpson, Center for Radar Astronomy, Stanford University, Stanford CA 94305-9515, USA (rsimpson@magellan.stanford.edu).

Introduction: Unusual signatures were discovered in radar backscatter data from Europa, Ganymede, and Callisto 20 years ago [1,2] and have since been widely interpreted as arising from electromagnetic interactions with inhomogeneities in low-loss materials such as water ice [3]. Radar echoes from Mars, Mercury, and Titan also appear to exhibit some of the same features and are consistent with the water ice interpretation [4]. During April 1994, the Clementine spacecraft high-gain antenna was aimed toward the Moon's surface and the resulting 13-cm wavelength radio echoes were received on Earth. Using those data, Nozette et al. [5] have claimed detection of an enhancement in echoes with right circular polarization from regions near the south pole in a near-backscatter geometry and have inferred the presence of water ice. We have reanalyzed the same data and have reached a different conclusion.

Experiment and Original Analysis: Clementine provided a unique experimental opportunity to observe scattering as a function of bistatic angle b — the angle between transmitter and receiver as viewed from the target. Most models of radar scattering by ice [e.g., 3] predict a decrease in amplitude and a change in polarization ratio as b diverges from $0°$. Strength of the variation depends on the purity and quantity of ice. Since $b = 0$ for monostatic experiments, no such dependence can be measured in a monostatic experiment.

Despite its uniqueness, the Clementine experiment was limited in two ways. Its intrinsic sensitivity was several orders of magnitude lower than for comparable monostatic experiments, such as those conducted at Arecibo Observatory. Although no b dependence can be measured from Arecibo, spatial variations might indicate the presence of ice near the pole; but none has been found [6]. Secondly, the use of continuous wave transmissions from Clementine meant that the surface could be resolved only into Doppler strips, rather than the more desirable "pixels" that can be obtained from radar imaging. Each strip represented the combined echo from a large number of individual surface elements probed at a variety of b angles but all having the same Doppler shift. Nozette et al. assigned the minimum b to each strip as a function of time, then accumulated a composite echo as a function of b_{min} by summing over time. The 1-dB enhancement reported is based on echoes obtained when the $b = 0$ point was within $5°$ of the south pole. Nozette et al. found no comparable enhancement on another orbit that missed the south pole by about $5°$, and they found no enhancements in the vicinity of the north pole [5].

New Analysis: By studying the global properties of Clementine echoes at high angles, we found that the lunar surface follows a Lambertian scattering law

$$\sigma_o = K_D \cos\theta_i \cos\theta_s \qquad (1)$$

with $K_D \sim 0.003$ for the opposite (expected) sense of circular polarization and $K_D \sim 0.001$ for the unexpected sense. We also found that there are large deviations from this simple form.

Echoes from the vicinity of the south pole appear to be composed of a general background diffuse level with strong contributions from discrete scattering centers. The discrete units may result from topography; small changes in incidence or scattering angles near $90°$ in equation (1) will have large impacts on s_o. Because Doppler contours

in the polar region are similar to lines of constant latitude, it is possible to estimate the latitude of particularly striking features; no longitudes can be determined, however, because of the strip nature of the bistatic resolution elements.

We sought patterns from individual measurements that would mimic the result published by Nozette et al. [5] but have been unable to find any. Although additional work is planned, our results to date indicate that echo variability is as likely to have caused the reported radar enhancement as water ice.

Conclusions: Early results from Lunar Prospector suggest that H_2O is present in lunar regolith at the poles — with the stronger signature in the north. Very small concentrations of water ice, mixed uniformly through the soil, would be consistent with the measurements. Such slightly frosty soil is in striking contrast to the nearly pure ice that is required to give enhanced backscatter at radar frequencies. The Prospector detection is therefore consistent with either a positive or negative radar result.

A confirmed radar enhancement would indicate significant quantities of nearly pure ice within a few centimeters of the lunar surface, adding considerably to the total volume of H_2O inferred from Prospector alone. Our inability to confirm the Clementine result, in light of Prospector, suggests that extracting resources on the Moon may be just as difficult as on Earth.

References: [1] Campbell D. B. et al. [1978] *Icarus, 34,* 254–267. [2] Goldstein R. M. and Green R. R. [1980] *Science, 207,* 179–180. [3] Hapke B. and Blewett D. [1991] *Nature, 352,* 46–47. [4] Muhleman D. O. et al. [1995] *Annu. Rev. Earth Planet. Sci., 23,* 337–374. [5] Nozette S. et al. [1996] *Science, 274,* 1495–1498. [6] Stacy N. J. S. [1997] *Science, 276,* 1527–1530.

⠂⠂⠔⠶⠤⠼⠇

GEOCHRONOLOGIC AND ISOTOPIC CONSTRAINTS ON THERMAL AND MECHANICAL MODELS OF LUNAR EVOLUTION.

G. A. Snyder and L. A. Taylor, Planetary Geosciences Institute, Department of Geological Sciences, University of Tennessee, Knoxville TN 37996-1410, USA (gasnyder@utk.edu).

Both short-lived and long-lived geochronometers are key to our understanding of the thermal and mechanical evolution of planets and satellites. These isotopic studies not only allow us to set time constraints on various processes (core formation, melting, crystallization, impact), but also allow us to determine the chemical and mineralogic characteristics of plausible sources. Thermal and mechanical models derived from remote spectroscopy and geophysical data must be tempered by such studies. We present three case studies where the ground truth afforded by radiogenic isotopic studies and geochronology have drastically changed (or should change) prevailing models determined from remote sensing and geophysics: (1) ferroan anorthosites (FANs) and the magma ocean hypothesis, (2) highlands plutonic-suite rocks and late KREEP formation from a magma ocean, and (3) high-Ti basalt sources and ilmenite-sinking in the lunar mantle. In addition, we will mention several other outstanding problems in lunar petrology and geochemistry where remote sensing and geophysics could prove useful in cutting the Gordian knot.

Introduction: A plethora of studies (including our own work) can be cited in lunar petrology where remote-sensing, telescopic, and geophysical studies have been practically or literally ignored. However, the same can also be said of the treatment that petrology has endured at the hands of scientists in the remote-sensing and geophysical communities. It is our aim to point out several cases where mutual and amicable feedback has proved fruitful for all communities involved. Remote-sensing and telescopic observations of the Moon allow lunar petrologists and geochemists to "fix" the returned samples within the greater context of lunar stratigraphy and to know whether these samples are representative of local or more global magmatic manifestations. Geophysical models involving mascons, thermal conductivity, heat flow, and density considerations also allow us to evaluate the physical plausibility of our geochemical and petrologic models.

Geochronometers can be split into two groups, those containing short-lived nuclides (^{182}Hf-^{182}W, ^{53}Mn-^{53}Cr, ^{146}Sm-^{142}Nd; $t_{1/2}$ = 9 m.y., 3.7 m.y., and 103 m.y., respectively) and long-lived nuclides (^{147}Sm-^{143}Nd, ^{87}Rb-^{87}Sr, ^{176}Lu-^{176}Hf, ^{187}Re-^{187}Os, ^{232}Th-^{208}Pb, ^{235}U-^{207}Pb, ^{238}U-^{206}Pb, ^{40}Ar-^{39}Ar; $t_{1/2}$ > 10,000 m.y.). Short-lived nuclides are useful for constraining the timing of events early in the solar system, such as core formation (^{182}Hf-^{182}W) or an early silicate differentiation (^{146}Sm-^{142}Nd). Long-lived nuclides are used as tracers of silicate evolution in planets and satellites.

Case Study 1 — Ferroan Anorthosites as Flotation Cumulates from a Magma Ocean: The currently favored model for ferroan anorthosite (FAN) genesis involves the formation and crystallization of a global lunar magma ocean (LMO) to form a cumulate lunar upper mantle, and subsequent flotation of plagioclase in this LMO after some 70–80% total crystallization [e.g., 1–2]. Thus, FANs would represent samples of nascent lunar crust. Although only three FANs have been studied using the Sm-Nd-isotopic system, this system often yields the most reliable ages for old highlands rocks. The three samples yield ages of 4.56 ± 0.07 Ga (67016), 4.44 ± 0.02 Ga (60025), and 4.29 ± 0.03 Ga (62236), respectively [3–5]. This range in FAN ages would then lead to the conclusion that the LMO persisted for at least 300 m.y.! How does this fit with thermal models of a magma ocean as well as recent Hf-W-isotopic studies of the Moon? Not well, it would seem.

All these FAN samples point to an old LILE-depleted (i.e., initial ε_{Nd} is positive: 60025 = +0.9 ± 0.6; 67016 = +0.9 ± 0.2; 62236 = +3.1 ± 0.9) source for FANs. Such an early depletion event is consistent with the signficant positive ^{142}Nd anomaly observed in 62236 [5]. Indeed, if FANs were derived from residual LMO liquids (which are increasingly LILE-enriched with fractionation), then they should yield signatures of this enrichment (i.e., their initial ε_{Nd} values should be negative). Instead, the three FANs indicate a source that is progressively more radiogenic, relative to a chondritic bulk composition, over time. This is suggestive of a source that was LILE-depleted early in lunar evolution. More importantly, the Sm-Nd-isotopic composition of FANs brings into question the LMO flotation model for their evolution.

Case Study 2 — Alkali Suite and Mg-Suite "Plutonic" Rocks and KREEP Formation: After early FAN formation, crustal evolution likely proceeded by intrusion of more evolved plutons into the nascent crust, thought to be represented by alkali suite and Mg-suite rocks. Scarce age information on lunar rocks suggests that magnesian-suite magmatism was initiated at progressively more recent time from the northeast to the southwest on the lunar nearside from 4.45 to 4.25 Ga [6]. A precise Sm-Nd age of 4108 ± 53 Ma (ε_{Nd}(T) of –1.0 ± 0.2) for an alkali anorthosite, 14304,267 [7], in conjunction with U-Pb zircon ages for two other alkali-suite rocks from the Apollo 14 landing site and one from the Apollo 16 landing site

indicate production of alkali-suite rocks also over an extended time period spanning at least 300 m.y. from 4.34 Ga to 4.02 Ga [7]. This long-lived magmatic "event" could be due to melting of the lunar mantle beneath these regions and could have been generated either by latent heat during crystallization of the final, KREEP-rich (and, thus, Th- and U-rich), residual, lunar magma ocean liquid or heating due to radioactive decay of K, Th, and U. The choice of model is highly dependent upon the longevity of the LMO as allowed by thermal modeling. Furthermore, the broad age range for the Mg suite and alkali suite indicates that parental KREEP basalt magmatism was not a unique event, but was an important process possibly repeated several times throughout the first 600–700 m.y. of lunar history. Thermal modeling of the Moon must take this long-lived "event" into account.

Case Study 3 — High-Ti Basalts, Ilmenite Sinking, and Convective Overturn: The study of high-Ti mare basalts is an excellent example where interdisciplinary studies combining telescopic observations, remote-sensing data, geophysics, experimental petrology, radiogenic isotopes, trace- and major-element geochemistry, and mineralogy-petrology have been paramount in gaining a clearer picture of the evolution of the Moon's interior. First, any lunar-mantle melting model must include provisions for two major pulses, separated in time, of high-Ti basaltic volcanism; one pulse very early and dated at between 3.56 to 3.85 Ga [8–10] and another much later at 2.5 ± 0.5 Ga [11]. These magmatic pulses, separated by a large hiatus, are indicated by remote-sensing and telescopic observations of the Moon [11–12].

Mare basalts with elevated Ti content are thought to be the consequence of melting of ilmenite-bearing layers formed late in the crystallization of the lunar magma ocean [2,13]. The lower mantle of the Moon should be relatively primitive, composed of mostly olivine and orthopyroxene and extremely poor in ilmenite. If this is so, one would not expect picritic magmas, which come from the lower mantle, to have high Ti content. How might primitive picritic magmas attain this high-Ti signature?

The high-Ti nature of many picritic magmas (extant as glass beads) must have either been inherited from the source region or introduced after initial melting in the source region. Spera [14] stated that, due to density contrasts in lunar magma ocean cumulates, ilmenite-bearing layers from the uppermost portion of the upper mantle will sink relative to other cumulates in the upper mantle. This was first suggested as an important tenet of mare basalt genesis by Ringwood and Kesson [15]. However, Hess and Parmentier [16] further project that most of the ilmenite will continue sinking until it forms a lunar core. They also consider it likely that some of this ilmenite will mix with the lunar mantle, thus creating fertile high-Ti source regions throughout the mantle. The mean depth of melting of high-Ti picritic magmas is estimated at 400–500 km, near the base of the differentiated lunar upper mantle [17]. However, the depth of incipient melting could be much greater than this, especially if one considers that picritic magmas were formed by polybaric fractional fusion [18]. Therefore, high-Ti picritic magmas could be formed at a variety of depths throughout the lunar lower mantle. In fact, it may be possible to track the descent of some of these sinking blobs of ilmenite-bearing material by looking at the ages and depths of melting of ilmenite-rich basalts and picrites.

The earliest ilmenite-rich basalts are those found at the Apollo 11 and 17 landing sites and indicate melting of shallow sources [10]. Sparse age data from high-Ti picritic magmas (as evidenced by picritic glass beads) from these landing sites seem to give younger ages than the mare basalts, in some cases (i.e., Apollo 17) much younger (possibly up to 200 m.y. younger [19]). These high-Ti picritic melts were probably derived from very deep sources (400 to >500 km [20]). The ilmenite basalts from the Apollo 12 landing site are extruded much later and also come from a very deep source (350–400 km). Thus, extant data suggest that fertile, ilmenite-bearing sources were melted at greater depths over time. This is at least consistent with sinking of the ilmenite-bearing, late LMO, cumulate source over time. An important test of this hypothesis would be the return of samples from the uppermost volcanic units in a broad basin, such as volcanics from the Sharp Formation in Oceanus Procellarum, that are demonstrably younger (2.5 ± 0.5 Ga; [11]), yet high-Ti in nature [21]. One might suspect that these volcanics would be derived from a very deep source and yield picritic and not basaltic magmas.

The effects of large impacts on basin excavation, fracturing, and regolith formation and insulation undoubtedly contributed to the timing and style of melting of the lunar mantle and magma emplacement. In addition, two major controlling factors may prove to be the proportion of trapped, residual, incompatible-element-enriched LMO liquid in the cumulate source and the sinking of fertile, ilmenite-bearing material into the lower mantle.

Other Outstanding Problems: Several outstanding problems remain to be solved, and it appears that satisfactory solutions can only be achieved by a marriage of several disciplines: (1) Are high-Al basalts the oldest known mare type, spanning a range in ages from 4.24 to 3.96 Ga [22–24]? Are they represented by the cryptomare detected in remote-sensing and telescopic observations? Or are they polymict breccias representative of impact mixing in the regolith [25]? (2) Is the postulated LMO a short-lived phenomenon as suggested by some thermal models and recent Hf-W-isotopic studies [26–28]? Or is it a complex long-lived phenomenon as suggested by isotopic studies of FANs? (3) Why do high-Ti mare basalts represent such a large proportion of (a) returned lunar samples and (b) the inferred areal and volume extent of mare magmatism from remote sensing? (4) Are alkali-suite and Mg-suite rocks really representative of shallow highlands "plutonic" rocks as suggested by most lunar petrologists [e.g., 29]? Or are they possibly cumulates from thick impact melt sheets?

Isotopic geochemistry has many radiogenic systems of varying half-lives at its disposal, but if we cannot determine with any degree of certainty what the samples represent (basalt, plutonic rock, or impact melt), the interpretation of ages and sources will be fraught with confusion. In the inimitable words of the late Frank Schairer, "You can measure horseshit to five 9s [i.e., 5 decimal places], but it's still horseshit!" Remote-sensing and experimental studies, in concert with detailed petrology, should allow us an avenue to know more clearly what we are analyzing in the lab, as well as its ultimate importance to lunar evolution.

References: [1] Warren P. H. (1985) *Annu. Rev. Earth Planet. Sci., 13*, 201–240. [2] Snyder G. A. et al. (1992) *GCA, 56*, 3809–3823. [3] Alibert C. et al. (1994) *GCA, 58*, 2921–2926. [4] Carlson R. W. and Lugmair G. W. (1988) *EPSL, 90*, 119–130. [5] Borg L. et al. (1998) *EPSL*, submitted. [6] Snyder G. A. et al. (1995) *JGR, 100*, 9365–9388. [7] Snyder G. A. et al. (1995) *GCA, 59*, 1185–1203. [8] Nyquist and Shih (1992) *GCA, 56*, 2213–2234. [9] Snyder G. A. et al. (1994) *GCA, 58*, 4795–4808. [10] Snyder G. A. et al. (1996) *Meteoritics & Planet. Sci., 31*, 328–334. [11] Pieters C. M. et al. (1980) *JGR, 85*, 3913–3938. [12] Whitford-Stark J. L. and Head

J. W. (1980) *JGR, 85,* 6579–6609. [13] Hughes S. S. et al. (1989) *Proc. LPSC 19th,* 175–188. [14] Spera F. J. (1992) *GCA, 56,* 2253–2265. [15] Ringwood A. E. and Kesson S. E. (1976) *Proc. LSC 7th,* 1697–1722. [16] Hess P. C. and Parmentier E. M. (1995) *EPSL, 134,* 501–514. [17] Hess P. C. (1993) *LPS XXIV,* 649–650. [18] Longhi J. (1992) *Proc. LPS, Vol. 22,* 343–353. [19] Taylor S. R. et al. (1991) in *Lunar Sourcebook,* 183–284. [20] Longhi J. (1992) *GCA, 56,* 2235–2251. [21] Snyder G. A. et al. (1997) *GCA, 61,* 2731–2747. [22] Taylor L. A. et al. (1983) *EPSL, 66,* 33–47. [23] Dasch E. J. (1987) *GCA, 51,* 3241–3254. [24] Warren P. H. et al. (1997) *LPS XXVIII,* 1501–1502. [25] Snyder G. A. and Taylor L. A. (1996) *LPS XXVII,* 1233–1234. [26] Harper C. L. and Jacobsen S. B. (1996) *GCA, 60,* 1131–1153. [27] Lee D-C. and Halliday A. N. (1995) *Nature, 378,* 771–774. [28] Lee D-C. et al. (1997) *Science, 278,* 1098–1103. [29] McCallum I. S. and O'Brien H. E. (1996) *Am. Mineral., 81,* 1166–1175.

Fig. 1.   Stereo DEM overlain on Clementine LA base image. Polar stereographic projection.

$54.2 - 1$

TOPOGRAPHY OF THE SOUTH POLAR REGION FROM CLEMENTINE STEREO IMAGING.

P. D. Spudis[1], A. Cook[2], M. Robinson[3], B. Bussey[4], and B. Fessler[1], [1]Lunar and Planetary Institute, Houston TX 77058, USA (spudis@lpi.jsc.nasa.gov), [2]Center for Earth and Planetary Studies, National Air and Space Museum, Smithsonian Institution, Washington DC 20560, USA, [3]Northwestern University, Evanston IL 60208, USA, [4]ESTEC, European Space Agency, 2200 AG Noordwijk, The Netherlands.

The Clementine spacecraft made the first near-global topographic map (referenced to a mean lunar radius of 1738 km) of the Moon from laser altimetry LA [1]. Because the spacecraft was in an elliptical orbit and the laser ranger could not detect returns when the spacecraft was farther than 600 km from the Moon, we do not possess ranging data for latitudes within 15° of the poles [2]. However, the UVVIS imager on Clementine obtained images from different perspectives in space from which stereo information may be derived and topographic models produced [3]. The poles were especially well covered in stereo and we have used images of the south polar area to infer topographic information in areas not sampled by the laser altimeter. We here describe preliminary results in our construction of a Digital Elevation Model (DEM) of the south polar area of the Moon.

Method: The south polar DEM was created by processing systematically several orbital strips of Clementine UVVIS images [3,4]. Common points between overlapping images were initially chosen manually. These points were used by an automated patch-based correlation stereo matcher, to find all corresponding points on a grid spacing of 3 pixels, in the overlap region between images on each given orbit. The matched image points were fed through a stereo intersection camera model, using nominal camera pointing to produce relative height Digital Terrain Model (DTM) tiles of longitude, latitude, and height. An iterative fitting procedure followed whereby DTM tiles were fitted in elevation to laser altimeter points, and then for the remaining tiles with no underlying altimeter measurement, to previous adjacent fitted tiles. South of 78° latitude, DTM tiles form islands for which the absolute elevation is unknown due to lack of altimeter measurements or connectivity to fixed adjacent tiles. In such cases, these have been fitted to interpolated altimeter measurements, and therefore heights measured in this area are relative to each island DTM. A 1-km pixel size DEM mosaic in polar stereographic projection was produced from the collection of DTM tiles that
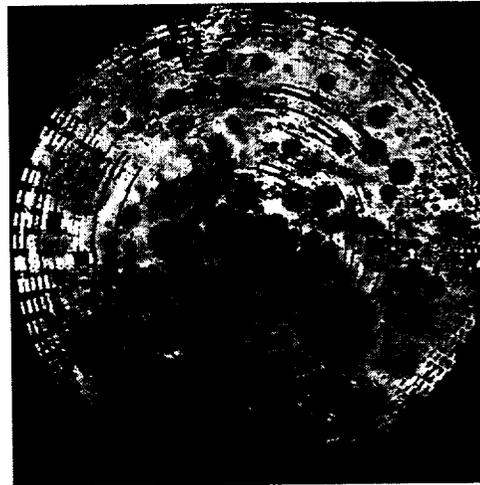
resulted. This DEM was merged with existing Clementine LA data to study the topography of the polar area.

Results: The merged dataset is shown in Fig. 1 and an elevation color-coded version is shown in Fig. 2. Note that the stereo DEM has significantly better resolution (~1 km) than the LA data (~50 km). But equally important, the new DEM extends topographic coverage into the south polar region. We have previously described an area on the rim of the crater Shackleton that appears to be illuminated by sunlight for more than 70% of the lunar day [5]; this means that it must be elevated above the mean lunar radius on the order of +600 m. In the new data, the rim of the Shackleton Crater is 1.0 km ± 0.6 km above the surrounding terrain within 10 km of the crater, and within 30 km of the south pole, the dynamic range of elevation is at least 2.8 km. Within 150 km of the pole on the farside, the dynamic range of elevation is at least 6.5 km, with spot elevations as low as –9.4 km around 87.2°S, 180°. Within 150 km of the pole on the nearside, the dynamic range in elevation is at least 7.9 km. This spot on our merged elevation image (Fig. 2) occurs at an elevation of about 0.5 km, in accordance with the predictions of our illumination study [5].
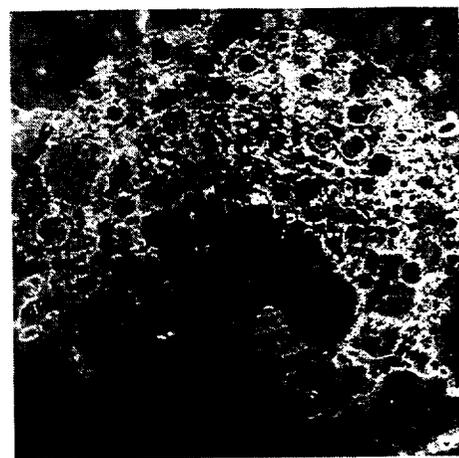

Fig. 2.   Topographic map of the south polar region of the Moon, including both Clementine LA data and the newly derived DEM.

The South Pole-Aitken (SPA) Basin was revealed by Clementine to be the largest known impact crater in the solar system, with a diameter of ~2600 km and a maximum depth of almost 12 km [6]. The new coverage shows prominent topography associated with the SPA Basin occurring near 75°S between 0° and 30°E longitude. These massifs, known from Earth-based telescopic study as the Liebnitz Mountains [e.g., 7], crest between 4 and 5 km elevation. The basin wall extends over the polar region, from ~70°S on the nearside to ~85°S at 180° longitude, a distance of ~800 km. In this span, the elevation drops over 10 km, from ~ + 4 km to about –6 km elevation (Fig. 2). This slope is comparable to and symmetric with basin wall slopes elsewhere around the eastern farside of SPA Basin (e.g., south of Korolev at 12°S, 160°W, the basin rim crest stands at almost + 7 km and slopes down to –5 km, a drop of 12 km over about a 600 km span. Thus, the new topographic data suggest that SPA Basin shows prominent rim crest symmetry, at least over more than 180° of its circumference.

These topographic data are preliminary, and we plan to refine and extend the stereo model to cover as much of the south polar region and the Moon as possible.

Acknowledgments: T. Cook would like to acknowledge University College London for use of the stereo matcher and DLR Berlin where processing was done.

References: [1] Nozette S. et al. (1994) *Science, 266,* 1835–1839. [2] Zuber M. et al. (1994) *Science, 266,* 1835–1841. [3] Oberst J. et al. (1997) *Eos Trans. AGU, 78,* 445 and 450. [4] Day T. et al. (1992) *Int. Archives Photogram. Remote Sens., 29,* 801–808. [5] Bussey D. B. J. et al. (1998) *LPS XXIX,* 1373. [6] Spudis P. D. et al. (1994) *Science, 266,* 1848–1851. [7] Alter D. (1964) *Lunar Atlas,* Dover, New York, Plate 25.

AUTOMATED SEARCH FOR LUNAR LAVA TUBES IN THE CLEMENTINE DATASET.

A. G. Taylor[1] and A. Gibbs[2], [1]Mathematics Department, Pacific University, 2043 College Way, Forest Grove OR 97116, USA (taylor@pacificu.edu), [2]Lewis & Clark College, 0615 Southwest Palatine Hill Road, Portland OR 97219-7899, USA (gibbs@lclark.edu).

Introduction: A significant problem in computer science, which has become increasingly acute recently, is the automatic extraction and cataloging of desired features from large sets of complex images. Solution of this problem could potentially have broad applicability.

As a prototype of this kind of problem, our group has chosen to attempt the automatic retrieval of lava tubes from the Clementine dataset. Lunar lava tubes have long been recognized as desirable locations for the placement of manned lunar bases. Advantages include that (1) little construction is needed; (2) building materials need not be lifted out of Earth's gravity well; (3) the tubes provide natural environmental control; and (4) the tubes provide natural protection from cosmic rays, meteorites, micrometeorites, and impact crater ejecta [1].

Coombs and Hawke [1] identified about 100 probable lava tubes associated with sinuous rilles in the Lunar Orbiter and Apollo photos, primarily in the nearside maria.

The lava tubes that are visible to Earth-based telescopes might be too large to provide good candidates for lunar bases. Such lava tubes of large diameter need a great depth of overlying rock to keep from collapsing. Any intact large tubes would lie inconveniently far underground. Most useful would be lava tubes that are too small to be discerned from Earth.

The Clementine spacecraft, which mapped the entire surface of the Moon to an unprecedented level of detail in 1994, gives us a view of these smaller lava tubes. Over 1.9 million images in the visible, near infrared, and mid-infrared portions of the spectrum were captured.

Our task is to find and catalog the small lava tubes in the Clementine dataset. Of particular interest are small sinuous rilles that contain interruptions, which represent uncollapsed portions of a tube that has partially collapsed. Once cataloged, the candidate base locations can be examined more closely for suitability. Considerations would be proximity to resources, sites of scientific interest, or favorable locations for siting of a railgun satellite launcher.

Clementine Imagery: Clementine captured images of the lunar surface in several spectral bands, spanning the visible, near infrared, and long wavelength infrared. Collapsed lava tubes show up well in the visible part of the spectrum, given that the sun angle is suitable. Of the 1.9 million images taken, 620,000 were high-resolution images in the visible spectral band. Manual examination of even a significant fraction of those images is far too time consuming to be feasible. Some form of automated search is the only practical way to thoroughly analyze such a large number of images in a reasonable time.

Difficulty of Characterization: Lunar rilles are inherently difficult to characterize, making it difficult to teach a computer how to find them. Such geological features do not have a common form or a characteristic diameter or length. Due to differences in topography, some have numerous sharp bends, while others are quite straight. Some appear in clusters, while others seem to be isolated from other rilles.

Lack of Ground Truth: Only 12 human beings have ever set foot on the Moon. Only two of them landed near a rille (Hadley Rille). Since no further human expeditions to the Moon are planned any time soon, it is not possible to verify that features identified as rilles are actually collapsed lava tubes. Any identifications based on currently available datasets cannot be absolutely verified.

Lacking on-site verification, the next best method to obtain accurate identifications is consensus ground truth. It this method, several experts independently evaluate a sample of the total dataset. These identifications are then compared against each other, and the identifications on which most experts agree are considered to be valid.

Acquiring Appropriate Training Examples: To prepare an adaptive learning feature identification tool to find members of a desired class of features, one must train it by showing it examples of ground truth. One must then present it with as representative a set of different examples as possible of the class of features that are sought. In the case of lunar rilles, the consensus ground truth produced by human experts is the best that we can do. The goal is to create an automated system that is comparable to human experts in its ability to identify sinuous rilles caused by ancient lava flows.

An Adaptive Feature Recognition Tool: A similar, but smaller-scale problem was faced by researchers at the California Institute of Technology and the Jet Propulsion Laboratory in searching the Magellan radar dataset for small volcanos on the surface of Venus. An adaptive recognition tool named JARTool was developed for the purpose of automated analysis of large datasets, and the Magellan dataset was used to test the effectiveness of the tool at recognizing

target features, and rejecting features that might resemble the target features but that are not of the class.

The CIT/JPL team, led by M.C. Burl, used JARTool to find volcanos in a set of 30,000 Magellan radar images [2] that contain approximately 1 million small volcanos. Burl's team developed an algorithm that proved to be effective at identifying volcanos, based on a series of training images containing volcanos identified by geologists, that were presented to the JARTool before it was tasked with identifying volcanos in the remaining images.

Applying JARTool to the Clementine Dataset: Our effort has adapted JARTool to identify sinuous rilles in the Clementine images of the lunar surface, particularly those with interruptions or gaps in the rille. We assume that such gaps represent uncollapsed segments of lava tubes. The goal of our project is to produce a catalog of uncollapsed lava tubes on the Moon. Researchers can then search the catalog for a wide variety of research purposes, including finding the best candidates for lunar bases, based on proximity to lunar resources or areas of scientific interest.

References: [1] Coombs C. B. and Hawke B. R. (1988) *Lunar Bases and Space Activities in the 21st Century, II,* PGD #541. [2] Burl M. C. et al. (1996) *Trainable Cataloging for Digital Image Libraries with Applications to Volcano Detection, Computation and Neural Systems Technical Report CNS-TR-96-01.*

⟶⟋⟋⟋

REFLECTANCE SPECTROSCOPY AND LUNAR SAMPLE SCIENCE: FINALLY A MARRIAGE AFTER FAR TOO LONG AN ENGAGEMENT. L. A. Taylor[1], C. Pieters[2], and D. S. McKay[3], [1]Planetary Geosciences Institute, University of Tennessee, Knoxville TN 37996, USA (lataylor@utk.edu), [2]Department of Geological Sciences, Brown University, Providence RI 02912, USA, [3]Planetary Exploration Division, Mail Code SN, NASA Johnson Space Center, Houston TX 77058, USA.

Introduction: Inferences about the igneous and impact evolution of planetary bodies are based upon spectral remote sensing of their surfaces. However, it is not the rocks of a body that are seen by the remote sensing, but rather the regolith, that may contain small pieces of rock but also many other phases as well. Indeed, recent flybys of objects even as small as asteroid Ida have shown that these objects are covered by a regolith. Thus, spectral properties cannot be directly converted into information about the igneous history of the object. It is imperative to fully understand the nature of the regolith, particularly its finer fraction termed "soil," to appreciate the possible effects of "space weathering" on the reflectance spectra. We have initiated a study of our nearest, regolith-bearing body, the Moon, as "ground truth" for further probes of planetary and asteroidal surfaces.

The foundation for remote chemical and mineralogical analyses lies in the physics underlying optical absorption and the linking of spectral properties of materials measured in the laboratory to well-understood mineral species and their mixtures. From this statement, it is obvious that there should be a thorough integration of the material science of lunar rocks and soils with the remote-sensing observations. That is, the lunar samples returned by the Apollo missions provide a direct means for evaluation of spectral characteristics of the Moon. However, this *marriage* of the remote-sensing and lunar sample communities *has suffered from a prolonged uncon-summated betrothal,* nurtured by an obvious complacency by both parties. CAPTEM, in all their inimitable wisdom, has recently focused upon this marriage.

To make more direct and quantitative links between soil chemistry/mineralogy and spectral properties, we have initiated a program to (1) obtain accurate characterization of the petrography of lunar soils (in terms relevant to remote analyses), coupled with (2) measurement of precise reflectance spectra, with testing and use of appropriate analytical tools that identify and characterize individual mineral and glass components.

It is the finest-sized fractions of the bulk lunar soil that dominate the observed spectral signatures [1,2]. Optically, the 20–44-μm, 10–20-μm, and <10-μm sized fractions are the most similar to the bulk soil [3]. However, the detailed petrographic and chemical properties of these finer fractions of lunar soils, most relevant for remote spectroscopy, are poorly known.

Mare Soils: Taylor et al. [4] examined the mineralogy and petrography of the 90–150-μm-sized fraction of nine lunar soils, from all Apollo mare sites, using X-ray digital-imaging analyses. These soils were chosen because they represent different compositions and contrasting maturities, as depicted by I_s/FeO values [5]. These soils are the same ones that are being investigated in our newly initiated program. Prior study of these soils [4] has provided significant insight into the difficulties of distinguishing the various glass types.

The <100 μm portion of each soil was sieved dry, using a Sonic Sifter, into 20–44 μm, 10–20 μm, and <10 μm fractions, and splits were taken for various analyses in our overall investigation. Representative portions of each size fraction were utilized for (1) spectral reflectance; (2) I_s determination; (3) preparation of polished grain mounts; and (4) fused-bead bulk-chemical analysis.

Petrographic Methodology: Standard optical point-counting methods are inadequate for determining modal abundances (area/volume percentages) of particles in the fine (<45 μm) size fractions. This is because the all-important agglutinates are largely broken up into individual mineral and glass grains, thereby losing their identifying characteristics (e.g., vesicles, inclusions). Using an Oxford Instrument Energy Dispersive Spectrometer Unit (EDS) on a Cameca SX-50 electron microprobe at the "real" UT (in Knoxville), we have recently established the software and chemical/shape parameters with which to perform X-ray digital-imaging analyses on grain mounts of lunar soils. We can produce accurate modal analyses of individual mineral and glass components, independent of their associations in the soil particles. Basically, each mineral and glass type is defined by a range of chemistry. For example, impact-produced, agglutinitic glasses have high Ca, Al, and Si (plag component) and elevated Fe (from Ol and Cpx), with Fe high enough to rule out plag, and Al high enough to rule out Ol and Cpx. Ilmenite ($FeTiO_3$) has high Fe and Ti, and low Cr, etc. The details of this technique are given in Taylor et al. [4] and other studies by the group in Tennessee [6–10]. In addition to the recognition of the phases in modal analyses, it is very important that the chemistry of each phase be approximated. In particular, we have been able to distinguish at least three, possibly five, different compositional ranges of pyroxenes.

Sieving Problems: It is well known that the <10-μm-sized fraction of the lunar soils has strange, as-yet-unaccounted-for, spectral properties. This may be due to the Freon wash method of size sieving that was routinely used for most lunar soils. It seems that the Freon wash for the complete range of sieves accumulates in the bottom pan with the <10-μm fraction. The Freon is allowed to

evaporate off, possibly leaving a minute, albeit significant, amount of matter that it has picked up. This is presently being investigated.

This problem with the finest-grain fraction during Freon sieving was the reason for using the dry Sonic Sifter. However, this dry technique releases significant quantities of fine dust and may not give a correct representation of the lunar soil size distribution. For example, when I_s measurements were made on the various size splits, it was determined that some soils did not give a systematic increase in I_s with decreasing grain sizes. The values obtained were compared with earlier values from Freon sieving back in the 1970s and found to be markedly different. It is suspected that the sonic sifting is actually breaking up delicate glass-aggregated agglutinates, thereby creating an "artificial weathering" of the soil. It must be determined which of these two, dry vs. wet, techniques can be made to produce the most reliable, uncontaminated size splits. This is a top priority.

Modal Abundances: Some of our modal analyses on the RSPL soils were discussed at the recent LPSC. As shown in Figs. 1 and 2 in Taylor et al. [11], the most impressive change for the Mare soils with decreasing grain size is for agglutinitic (i.e., impact-produced) glass. In many soils, there is an over 2-fold increase in this glass between the 90–150-μm- and 10–20-μm-sized fractions. It was stated by Labotka et al. [12], Simons et al. [13], and more recently by Fischer [3] that the abundance of agglutinates (by inference, also agglutinitic glass) decreases as grain size decreases. *The results from the present study are the first fully quantitative verification that the abundance of agglutinitic glass increases in lunar soils as grain size decreases.* It is this glass that contains the nanophase, single-domain Fe^0, which is responsible for the general increase in I_s/FeO with decrease in grain size, as reported by Morris [14].

There is a distinct and not unexpected decrease in pyroxene abundances with decreasing grain size. It appears that there is a slight increase in plagioclase with decreasing grain size, supporting the F^3 model [15].

Summary: There is a dire need for fully quantitative modal and chemical data on the mineral and glass components of lunar soils. These should be modeled and integrated into the spectral data in order to improve the chemistry, mineralogy, and petrology of the remote-sensing observations for the Moon, as well as for other airless heavenly bodies.

References: [1] Fischer and Pieters (1994). [2] Pieters et al. (1993) *Remote Geochemical Analysis*, 309. [3] Fischer (1995) Ph.D. thesis, Brown Univ. [4] Taylor (1996) *Icarus, 124*, 5596. [5] Morris (1976) *Proc. LSC 7th*, 315. [6] Taylor et al. (1993) *LPS XXIX*, 1409. [7] Chambers et al. (1994) *Space 94*, ASCE, 878. [8] Chambers et al. (1995) *JGR, 100*, 14391. [9] Higgins et al. (1995) *LPS XXVI*, 601. [10] Higgins et al. (1996) *Meteoritics & Planet. Sci., 31*, 356. [11] Taylor et al. (1998), *LPS XXIX*. [12] Labotka et al. (1980) *Proc. LPSC 11th*, 1285. [13] Simons et al. (1981) *Proc. LPS 12B*, 371. [14] Morris (1977) *Proc. LSC 8th*, 3719. [15] Walker and Papike (1981) *Proc. LSC 7th*, 421.

$\mathcal{S} \mathcal{4} \mathcal{5} \cdot \mathcal{7} \mathcal{1}$

COMPOSITION AND STRUCTURE OF THE LUNAR CRUST.

S. Tompkins, Science Applications International Corporation, 4501 Daly Drive, Suite 400, Chantilly VA 20151, USA (tompkinss@saic.com).

Introduction: A multispectral-based survey of the central peaks of lunar impact craters has suggested intriguing compositional trends
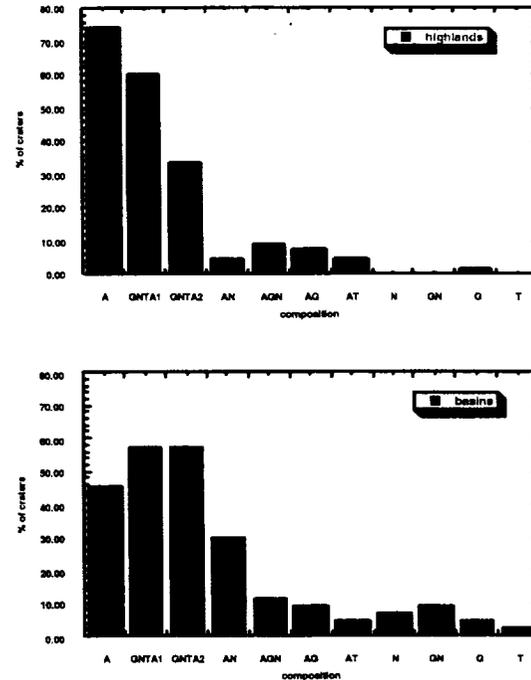

Fig. 1. Distribution of rock types in highland and basin terrains. Rock types described are: A (anorthosite), GNTA1 and GNTA2 (gabbroic-noritic-troctolitic-anorthosite, indicating lithologies whose mafic mineralogy cannot be determined but whose plagioclase abundance is between 80% and 90%), AN (anorthositic norite), AGN (anorthositic gabbronorite), AG (anorthositic gabbro), AT (anorthositic troctolite), N (norite), GN (gabbronorite), G (gabbro), and T (troctolite).

in the lunar crust [1]. More detailed studies are necessary to refine the results of the survey, however, regarding the maturity of central peak surfaces, and the depth of origin of central peak rocks with respect to the original structure of the lunar crust. These studies will rely upon a combination data, including geophysical predictions of crustal thickness, impact cratering predictions, laboratory spectra of lunar samples, and both telescopic and space-based spectral measurements of lunar surface.

Background: The central peaks of 109 impact craters were analyzed in Clementine UVVIS camera multispectral images to assess their mineralogical composition [1]. The craters range in diameter from 40 to 180 km, and are believed to have excavated material in the peaks from 5 to 20+ km depth [2]. Representative five-color spectra from spectrally and spatially distinct areas within the peaks were selected and classified on a relative scale, from which mineralogical abundances were estimated by comparison to laboratory spectra of lunar samples. The mineralogical abundances were translated to rock types based on the sample-derived classification scheme of Stöffler et al. [3]. Illustrated in Fig. 1 are the percentages of surveyed craters that contain each rock type. Note that many craters contain more than one rock type, so that the numbers in the plot sum to >100%.

Tentative conclusions were reached regarding the vertical and lateral structure of the Moon. The survey results suggest a crust that is globally dominated by anorthosite to ~15 km depth. At local and

regional scales, composition is diverse, with multiple rock types appearing within individual craters, or within sets of craters. Mafic rocks are identified across the Moon and are located preferentially in craters interior to major impact basins (see Fig. 1), suggesting that such craters are sampling more mafic material that originally formed deeper in the crust. However, even the most mafic rocks are typically more anorthositic than predicted by the lunar sample collection.

More detailed and robust conclusions are hampered by two key questions. The first concerns the maturity of the central peak surfaces, which can affect mineralogical interpretations by causing overestimation of the abundance of anorthosite relative to mafic materials. The second question relates to the depth of uplift of central peaks rocks from within the lunar crust. Estimates for the depth of central peak origin must consider crustal material that has been stripped or added by basin-scale impacts, and rely upon estimates of crustal thickness as well as models for the uplift of central peaks in impact craters.

Maturity: The optical effects of space weathering have been well documented [e.g., 4]. Maturation of lunar soils alters their spectra such that mineralogical interpretation is difficult, and quantitative mineralogical comparisons nearly impossible. For the central peaks survey, it is assumed that the central peaks of all craters may be compared directly because they are steeply sloped enough to prevent the development of mature soils. While this is reasonable for simple large-scale comparisons, it is not sufficient for detailed comparisons of spectra between peaks of significantly different ages. Older peaks have less topographic relief and are likely to have accumulated enough soil to have some effect upon the measured reflectance spectra. The presence of mature soils can lead to an overprediction of anorthosite abundance. Mitigation of this effect requires a careful comparison between Clementine spectra and telescopic spectra for the same locations on the Moon. With high spectral-resolution telescopic measurements, the effects of space weathering can be mitigated sufficiently to allow better mineralogical estimates. This comparison is currently under way. An alternative approach under consideration is the modification of empirically-based approaches such as developed by Fischer et al. [5,6] and Lucey et al. [7] for use with the central peak measurements.

Depth of Central Peak Origin: The crater diameters of the surveyed craters are correlated [2] to the depth of central peak uplift from beneath the planetary surface. However, the amount of peak uplift is not necessarily related to the depth within the crust at which the central peak rocks may have formed. For example, while a crater may have exhumed rocks from 5 km beneath the preimpact surface, if the crater is itself within an impact basin that has removed large volumes of crust, the central peaks may in fact have originated at depths much greater than 5 km.

For the central peaks survey, the effect of crustal thickness variations was not considered. This limitation affects the interpretation of compositional trends within the crust. Better depth estimates are under way, using the simple relationship

$$depth_0 = depth_x + (H_0 - H_x)$$

where H_0 and H_x respectively are the reference crustal thickness and the actual crustal thickness at any location x on the Moon, and $depth_0$ and $depth_x$ are the depths of central peak origin relative to these crustal thickness estimates. Geophysical model predictions of crustal thickness will be used to estimate H_x.

References: [1] Tompkins S. and Pieters C. M. (1998) *Meteoritics & Planet. Sci.*, submitted. [2] Cintala M. J. and Grieve R. A. F. (1994) in *Large Meteorite Impacts and Planetary Evolution* (B. O. Dressler et al., eds.), GSA Spec. Paper 293. [3] Stöffler D. et al. (1980) in *Proc. Conf. Lunar Highlands Crust* (J. J. Papike and R. B. Merrill, eds.), pp. 51–70, Pergamon, New York. [4] Pieters C. M. et al. (1993) *JGR, 98*, 20817–20824. [5] Fischer E. M. and Pieters C. M. (1994) *Icarus, 111*, 475–488. [6] Fischer E. M. and Pieters C. M. (1996) *JGR, 101*, 2225–2234. [7] Lucey P. G. et al. (1995) *Science, 268*, 1150–1153.

5⁻¼6⁻9/

EVIDENCE FOR PHYLLOSILICATES NEAR THE LUNAR SOUTH POLE.

F. Vilas[1], E. Jensen[2], D. Domingue[3], L. McFadden[4], C. Coombs[5], and W. Mendell[1], [1]NASA Johnson Space Center, Houston TX 77058, USA, [2]Texas A&M University, College Station TX 77843, USA, [3]Applied Physics Laboratory, Johns Hopkins University, Laurel MD 20723, USA, [4]University of Maryland, College Park MD 20742, USA, [5]College of Charleston, Charleston SC 29424, USA.

While theoretically water ice could be stable in permanently shadowed areas near the lunar poles [1], there is conflicting observational evidence for the existence of water ice at either pole. Clementine's bistatic radar returned a weak signal commensurate with water ice in the South Pole Aitken Basin [2]; however, groundbased radar searches have not detected such a signal at either pole [3]. Lunar Prospector measured large amounts of H (attributed to water) at both poles [4]; however, Galileo near-infrared spectral measurements of the north polar region did not detect the prominent 3.0-μm absorption feature due to interlayer and adsorbed water in phyllosilicates [5]. Evidence for the existence of water at the lunar poles is still ambiguous and controversial. We present evidence, based on the analysis of Galileo SSI images, for the presence of phyllosilicates near the lunar south pole.

Using the color image sequence (560 nm, 670 nm, 756 nm, and 889 nm) of Lunmap 14 [6] taken during the Galileo Earth-Moon pass 1, we have identified areas that show evidence for a 0.7-μm absorption feature present in Fe-bearing phyllosilicates. This absorption feature is attributed to an $Fe^{2+} \rightarrow Fe^{3+}$ charge transfer transition in six-fold coordination in oxidized Fe in phyllosilicates. This feature is present in the reflectance spectra of many terrestrial phyllosilicates, carbonaceous chondrite meteorites (CM2), and low-albedo asteroids (C, B, F, G, and P class). We correlate this feature with the permanently shadowed northern rims of complex, degraded craters in the lunar south pole region.

We developed a test that calculates the slopes of the segments formed by straight lines between the photometric values corresponding to adjacent pairs of filters and orders the slopes of these three segments. The ordering indicates the presence of absorption features near 0.7 μm and the 0.9–1.0-μm mafic silicate absorption, while accommodating the presence and magnitude of the lunar spectral slope due to space weathering. Synthetic Galileo color data created from laboratory reflectance spectra of terrestrial rock samples and Apollo lunar soil samples [7,8] were tested in addition to groundbased telescopic spectra of the lunar nearside [9]. Among these datasets, ~7% show an unusual absorption feature indicative of the 0.7-μm feature. Many of the higher-resolution laboratory spectra of lunar

glasses and agglutinates in one specific dataset show a feature centered near 0.6 μm attributed to Ti in ilmenite. This test flags the synthetic Galileo data created from these laboratory spectra. We separate the spectral signatures seen in the Lunmap 14 image photometry from ilmenites by comparing the areas where we see this absorption feature to the global TiO_2 abundance map created from Clementine spectral reflectance data [10], and maps of Ti wt% from Apollo 15 and 16 γ-ray measurements [11]. In the Clementine data, the regions that we examined near the lunar south pole show little to no TiO_2 content. Since the absorption feature we see in the Galileo photometry is in an area of low TiO_2 content, and effectively absent in areas with higher TiO_2 content, we conclude that Ti, in the form of ilmenite, is not the source of the feature in the Galileo data.

The mechanism we propose for the creation of phyllosilicates near the lunar south pole involves the interaction of solar wind H atoms with the FeO in the minerals and glasses of the lunar regolith. Interaction of H_2 with FeO (FeO + H_2 → Fe + H_2O) creates minor amounts of water vapor and small samples of Fe metal. The water vapor formed in this manner at the equator sublimes and is quickly removed by the high surface temperatures (although 5–10% could hop to any permanently shadowed regions). Near the lunar poles, however, the water is trapped in the permanently shadowed regions. Desorption occurs as a function of surface temperature, such that surface temperatures of 100 K can retain water for ~100 yr. At lunar latitudes of 60°–80°, temperatures of 100 K are expected in shaded portions of larger craters [12]. The timescales for aqueous alteration reactions vary, requiring hours to tens of years, depending on temperatures and water-to-rock ratios in the starting materials. Thus, we have water vapor or condensed water resident with anhydrous lunar materials, probably in very small amounts (limiting the fluid-to-rock ratio to 1:1), over a sufficient time interval to effect aqueous alteration of some of the surface material. Continuous bombardment of the lunar surface provides heat pulses strong enough to melt water and produce aqueous alteration at these scales. Subsequent gardening of the material near the equatorward, shaded rims of these larger craters would move some of the aqueously altered material to a visibly illuminated location adjacent to the shadowed complex crater rims.

References: [1] Arnold J. (1979) *JGR, 84,* 5659. [2] Nozette S. et al. (1996) *Science, 274,* 1495. [3] Stacy N. J. S. et al. (1997) *Science, 276,* 1527. [4] Feldman W. C. et al. (1998) *Science, 281,* 1496. [5] Kieffer H. H. (1995) *Bull. AAS, 27,* 1110. [6] Gaddis L. et al. (1995) *JGR, 100,* 26345. [7] Adams J. B. et al., prepared for Planetary Data System. [8] Tompkins S. et al. (1997) *LPS XXVII,* 1441. [9] McCord T. B. et al., prepared for Planetary Data System. [10] Lucey P. G. et al. (1998) *JGR, 103,* 3679. [11] Metzger A. E. and Parker R. E. (1979) *EPSL, 45,* 155. [12] Hodges R. R. (1980) *Proc. LPSC 11th,* 2463.

$\mathcal{J}4\ ^{\prime}/-\mathcal{G}/$

A BRIEF REVIEW OF THE SCIENTIFIC IMPORTANCE OF LUNAR METEORITES. P. H. Warren, Institute of Geophysics, University of California, Los Angeles CA 90095-1567, USA (pwarren@ucla.edu).

The lunar meteorites (lunaites) represent a valuable extension to the Apollo/Luna sampling of the Moon's surface debris. In this abstract, I briefly review the insights that have been gained from studies of these meteorites.

Basic Petrographic Features: (1) Rocks typically come through the violence of launch off a large, almost planet-sized body

with only modest overall shock metamorphism.

(2) An important question is whether in some cases loose regolith may be lithified during the same launch process that begins the trip to Earth. The answer appears to be no, because in several of the regolith breccia lunaites, broken impact spherules are found where they were manifestly sheared apart by fractures that extend through the breccia matrix [1]. The matrix had to be already rigid before the severe shock that sheared the spherule in half.

Moreover, fast ejection of solid debris (as distinguished from jetting of melt) probably requires that acceleration occur instantaneously after maximum compression (i.e., too soon for shock-lithification, which requires solidification of scattered traces of melt), at a stage when a steep pressure gradient is tending to burst material apart.

(3) Regolith breccia is the most common rock type in the upper few meters of the regolith. Sampling by Apollo astronauts apparently shunned this relatively friable, easily recognized, and notoriously unexciting (well-mixed, soil-like) rock type.

The Maturity Issue: Contrary to some early inferences, the present database for noble-gas contents of lunaites indicates that as a population they are not significantly less mature compared to Apollo regolith breccias [2]. Of course, even Apollo regolith breccias tend to be less mature than Apollo surface soils.

Toughness — A Key to Lunaite Survival: Lunaite regolith breccias, as a population, show vastly greater cohesiveness and lower porosity than Apollo breccias [2]. At some stage of the transport process a bias is introduced against weak samples. The most likely discriminator is stress during launch. Screening during/after arrival at Earth appears insignificant, based on the generally far weaker, more porous character of analogous breccias from the HED asteroid.

Cosmic-ray Exposure Evidence: (1) Of ~12 unpaired lunaites studied for CRE thus far, 11 were apparently launched from a depth of 3 m or less, and more than half from 1 m or less [3,4]. This means that even for relatively conservative assumptions about launch crater size, the fertile zone for lunaites is only ~0.001 crater-diameters deep. This strong depth dependence confirms that near-surface shock-wave interference [5], which on the Moon must be strongly enhanced by the density gradient within the upper few meters of the regolith [6], plays a key role in the launch process.

It also implies that lunaite/crater yield is proportional to r^2, not r^3. Further, since the number of craters at any given size is proportional to r^b, where *b* is probably ≥2, we can infer that in general (statistically, long-term) the flux of lunaites is derived from many small craters, rather than dominated by ejecta from a few rare events.

(2) The spectrum of CRE launch ages, 1–10 Ma but mostly <0.1 Ma, is entirely consistent with dynamical models for meteoroid orbital evolution [7,8], especially if launch-pairing is uncommon among the many lunaites with launch ages irresolvably <0.1 Ma.

(3) The Mars/Moon meteorite ratio (~1.0) is still mysterious, but in contrast to lunaites, martian meteorites generally arrive long after being launched from depths of (at least) several meters, i.e., they have been launched in a few, rare, big events. Lunaites from comparably rare/ancient events have mostly arrived too long ago to be collectable.

Trace Elements: (1) Lunaite Th vs. K/Th systematics [9] show that insufficiently rigorous processing of the Apollo orbital γ-ray spectrometry data indicated spuriously high K (and thus K/Th) in many highland areas. This problem was to some extent already appreciated before the lunaites were studied, however [10].

(2) The Apollo 16 regional megaregolith is atypically Th-rich for an Al-rich highland [9]. Six comparably Al-rich lunaite regolith

breccias are only 0.2–0.5× as Th-rich as the Apollo 16 regolith. This observation has important implications for bulk composition of the crust, bulk composition of the Moon, and origin of the Moon.

(3) The Apollo 16 regional megaregolith is atypically rich in Ni [11]. Rather than implying a high and Earthlike Ni content in the bulk composition of the Moon [12], the high Apollo 16 Ni/Ir ratio is merely a local anomaly, possibly derived from a single nearby impact [13].

Mare Basalts: (1) The statistics are still very limited, but among the lunaites (including clasts in highland breccias [e.g., 14]) VLT and near-VLT types are more common than they are among Apollo/Luna mare basalts. Unfortunately, the Clementine TiO_2 mapping technique was not sensitive enough to reliably resolve VLT from LT mare basalt [15].

(2) The 4.0-Ma age [16] of two near-VLT mare basaltic lunaites (A 881757 and Y 793169, a suspected launch pair) dispelled the notion that Ti content is inversely correlated vs. age among mare basalts.

(3) Several of the mare-dominated meteorites, including EET 87521 (and EET 96008, which our new INAA data indicate is probably paired with EET 87521), Y 793274, and QUE 94281, feature exceptionally coarse pyroxene exsolution compared to Apollo/Luna mare basalts [17,18]. The annealing that facilitated exsolution is consistent with burial of cryptomare beneath a thick deposit of hot impact ejecta [17].

Highland Petrology: (1) Studies of mixed mare-highland regolith breccias Y 793274 and QUE 94281 (a suspected launch pair) imply a relatively MgO-rich composition for the nonmare component [17,18]. Along with Apollo 14, Apollo 17, and Luna 20 data, this finding indicates that MgO-rich compositions are common in regions of "highland" megaregolith below and adjacent to the large basins where the mare lavas erupted. The distinctive composition probably stems from a high proportion of deep-provenance, mostly impact-melted, basin ejecta.

(2) Unfortunately, the lunaites have furnished few nonmare clasts that are unambiguously pristine (in the conventional, composition-only sense). The most distinctive suspected pristine clasts are the "hyperferroan" anorthosites in ALH 81005 [19].

References: [1] Warren P. H. and Kallemeyn G. W. (1995) *LPS XXVI.* [2] Warren P. H. (1998) *LPS XXIX.* [3] Thalmann C. et al. (1996) *Meteoritics & Planet. Sci.* [4] Nishiizumi K. et al. (1996) *Meteoritics & Planet. Sci.* [5] Melosh H. J. (1984) *Icarus.* [6] Warren P. H. (1994) *Icarus.* [7] Arnold J. (1965) *Astrophys. J.* [8] Glandman B. et al. (1996) *Science.* [9] Warren P. H. and Kallemeyn G. W. (1991) *GCA.* [10] Metzger A. E. et al. (1977) *Proc. LSC 8th.* [11] Warren P. H. et al. (1989) *EPSL.* [12] Ringwood A. E. et al. (1987) *EPSL.* [13] Korotev R. L. (1987) *Proc. LPSC 17th,* in *JGR.* [14] Lindstrom M. M. et al. (1986) *Proc. NIPR Symp. Antarct. Met.* [15] Blewett D. T. et al. (1997) *LPS XXVIII.* [16] Misawa K. et al. (1993) *GCA.* [17] Arai T. and Warren P. H. (1998) *Meteoritics & Planet. Sci.,* submitted. [18] Jolliff B. et al. (1998) *Meteoritics & Planet. Sci.* [19] Goodrich C. A. et al. (1984) *Proc LPSC 15th,* in *JGR.*

෴, ෴ -ᎾᎾ

PRISTINE ROCKS, REMOTE SENSING, AND THE LUNAR MAGMASPHERE HYPOTHESIS.

P. H. Warren and G. W. Kallemeyn, Institute of Geophysics, University of California, Los Angeles CA 90095-1567, USA (pwarren@ucla.edu).

The strongest evidence for the lunar magmasphere hypothesis is still the pronounced geochemical bimodality among pristine nonmare rocks. Magnesium-suite (MgS) rocks have a distinctly higher *mg* ratio than ferroan anorthositic suite (FAS) cumulates of otherwise similar geochemistry (e.g., Na/Ca, REE, and especially Eu/Al). Well-sampled FAS rocks are uniformly anorthositic, and must have been buoyant over their FeO-rich parent melts. Well-sampled MgS rocks have consistently moderate plag contents, and must have been negatively buoyant in relation to their parent melts. Ferroan chemistry is an expected outcome of magmasphere fractionation. MgS chemistry is consistent with origin by localized "serial magmatism," where the primary magmas were prone to assimilate magma ocean residuum (urKREEP) on the way from mantle to crust.

Arguably, the recent finding of a "young" (4.29 Ga) Nd age and positive (+3) εNd for FAS noritic anorthosite breccia 62236 [1] has weakened the case for magmasphere genesis of even the FAS. However, these data may merely indicate that absolutely pristine rocks (with compositions totally unmolested by impact effects) are slightly less common than previously supposed; or that pieces of the 4.4–4.5-Ga lunar crust were prone to compositional modification processes, such as metasomatism, not directly related to meteoritic impacts.

The compositional bimodality is strengthened by our new studies of known and suspected pristine nonmare rocks. For example, several clasts dubbed Fe norites by Lindstrom et al. [2] seemingly closed much of the compositional gap between the Mg suite and the FAS. Our study of 15459,343, one of the two most "Fe" of the Fe-norites, indicates that it is polymict, as it contains metal (6.17 wt% Ni, 0.77 wt% Co) of apparent meteoritic derivation. In the case of clast 15405,170, we find much more "normal" high-*mg*, high-Na mineral compositions.

The new Lunar Prospector data [3] have confirmed previous indications [4,5] that Th and other incompatible elements are remarkably concentrated in the eastern Procellarum region. This otherwise mysterious heterogeneity appears easily explained as an indirect consequence of magmasphere evolution. Procellarum is the most ancient of known lunar basins (so ancient that the role of impact in its formation is poorly constrained; it might be a basically endogenous structure [6], although impacts probably at least influenced its detailed shape and final position). If Procellarum formed before the magma ocean had entirely dissipated, the buoyant residual melt (KREEPy red in Fig. 1) would have tended to accumulate within the basin. Later, when the South Pole Aitken basin plumbed deep into the southern farside crust, little KREEP was left to be ejected. Consequently, despite being very similar to Procellarum in size and depth [7], the younger South Pole Aitken is vastly poorer in Th and other incompatible elements.
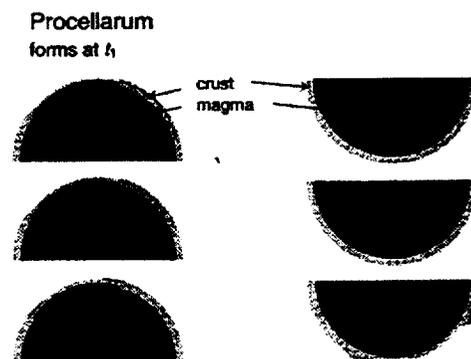
Procellarum
forms at *t₁*

crust
magma

Fig. 1. South Pole Aitken forms at t3; its later origin leads to very different composition.

References: [1] Norman M. D. et al. (1998) *LPS XXIX.* [2] Lindstrom M. M. et al. (1989) *Proc. LPSC 19th.* [3] Feldman W. C. et al. (1998) *LPS XIX.* [4] Warren P. H. and Kallemeyn G. W. (1991) *GCA.* [5] Warren P. H. (1998) *LPS XXIX.* [6] Lucey P. G. et al. (1994) *Science.* [7] Smith D. E. and Zuber M. T. (1997) *LPS XXVIII.*

EFFECTS OF SPACE WEATHERING ON LUNAR ROCKS: SCANNING ELECTRON MICROSCOPE PETROGRAPHY.

S. J. Wentworth[1], L. P. Keller[2], and D. S. McKay[3], [1]Mail Code C23, Lockheed Martin, 2400 NASA Road 1, Houston TX 77058, USA (susan.j.wentworth1@jsc.nasa.gov), [2]MVA Inc., 5500 Oakbrook Parkway, Suite 200, Norcross GA 30093, [3]Mail Code SN2, NASA Johnson Space Center, Houston TX 77058, USA

Lunar rocks that have undergone direct exposure to the space weathering environment at the surface of the Moon commonly have patinas on their surfaces. Patinas are characterized by visible darkening and other changes in spectral properties of rocks. They form as a result of bombardment by micrometeorites, solar wind, and solar flares. Processes of space weathering and patina production have clearly been significant in the formation and history of the lunar regolith. It is very likely that other planetary bodies without atmospheres have undergone similar alteration processes; therefore, it is critical to determine the relationship between patinas and their host rocks in view of future robotic and remote-sensing missions to the Moon and other planetary bodies.

We have been doing detailed SEM (scanning electron microscope), TEM (transmission electron microscope), and microspectrophotometry studies of the effects of space weathering on rocks from the Apollo collection (Apollo 16 dilithologic breccia 62255 and Apollo 17 crystalline matrix breccia 76015), along with similar studies of lunar soils [1–8]. Recently developed field emission electron microscope (FE-SEM) technology enables us to analyze samples at a much higher resolutions than was previously possible (e.g., the SEM studies of 76015 performed by [9,10]). The SEM work described here was done with both a standard SEM (a JEOL 35CF) and a Philips XL-40 FE-SEM.

Typical features of patina at the SEM scale include microcraters, splash glass, vapor deposits, solar wind etching, radiation damage, and accumulation of soil particles. The presence of hypervelocity microcraters and glass "pancakes" (small circular impact glass splashes) was defined by earlier workers [e.g., 9, 10] as diagnostic evidence that a surface has undergone space weathering at the surface of the Moon. That evidence is still considered diagnostic. Figure 1a (backscattered electron image) shows patina surface of the anorthositic portion of 62255. The larger microcrater crater has typical features, which include a glass pit liner and a large spall zone. The rock was highly fractured prior to the formation of the microcrater. Figure 1b shows the contrast between fresh and patina-covered surfaces of plagioclase in 76015. The rock surface at the top of Fig. 1b is a fresh, recently exposed area with no identifiable space weathering effects. By contrast, Fig. 1c (also 76015 plagioclase) and the weathered portion of the surface in Fig. 1b show typical patina as described by earlier workers [9,10]. These images illustrate a wide size of range glass pancakes along with submicrometer-sized craters too small to have spall zones. The glass spherules in Figs. 1b and 1c are not diagnostic of space weathering; they are common on natural surfaces
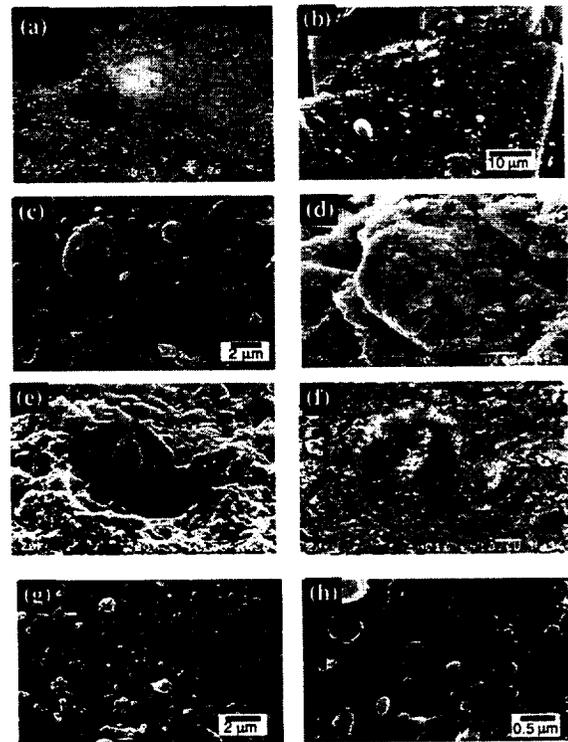

Fig. 1.

of most lunar rocks. The patinas in Figs. 2 and 3 are relatively thin, so the rock substrates (plagioclase) are discernible in SEM and easily identified by energy-dispersive X-ray analysis (EDS). In some areas of 76015 (e.g., Fig. 1d), accretionary material is thick enough (up to 10 μm) to obscure the substrate. In Fig. 1d, impact-glass pancakes and spherules form a thick coating on an ilmenite grain; the ilmenite substrate can be identified by backscatter electron imaging and EDS (not shown). Patina compositions in general are not homogeneous, as dramatically illustrated in Figs. 1e and 1f. Figure 6 is an SEM image of a microcrater that formed on a heterogeneous (plagioclase, pyroxene, possibly other phases) portion of 76015. The backscatter image (Fig. 1f) shows that the impact glass is extremely heterogeneous, which will cause changes in spectral properties (as discussed in [1]), especially because some of the original FeO was reduced to Fe metal (the small round bright spots). Other features recently identified on patinas include vapor deposits [e.g., 8] and evidence of etching of (76015) rock surfaces by solar wind (Figs. 1g,h). Erosion in this area has clearly been significant enough to erode away most of the two microcraters in the center of Fig. 1g (closeup in Fig. 1h) and to have an effect on the shapes of the glass spherules. In summary, patina is the end product of the combined action of a large number of processes operating at the lunar surface. There is a wide range of features present on patina surfaces over the distance of a few micrometers.

References: [1] Keller et al., this volume. [2] Wentworth et al. (1998) *LPS XXIX,* Abstract #1793. [3] Keller et al. (1998) *LPS XXIX,* Abstract #1762. [4] Wentworth et al. (1996) *LPS XXVII,* 1423–1424. [5] Keller et al. (1996) *LPS XXVII,* 661–662. [6] Wentworth et al. (1997) *LPS XVIII,* 1541–1542. [7] Keller et al. (1997) *LPS XXVIII,* 709–710. [8] Keller and McKay (1997) *GCA, 61,* 2331–2341.

[9] Blanford et al. (1974) *Proc. LSC 5th*, 2501–2526. [10] Morrison and Clanton (1979) *Proc. LPSC 10th*, 1649–1663.

350-11

INTEGRATING GEOPHYSICS WITH REMOTELY SENSED DATA AND THE APOLLO SAMPLES.

M. A. Wieczorek and R. J. Phillips, Department of Earth and Planetary Sciences, Washington University, One Brookings Drive, Campus Box 1169, St. Louis MO 63130, USA (markw@wurtzite.wustl.edu).

Introduction: Our understanding of the gravity and topography field of the Moon has improved dramatically with data collected from the recent Clementine mission. Near-global spectroscopic observations of the surface from this mission have also given us a vast dataset that is only beginning to be fully explored. Additionally, even though the expansive Apollo sample collection has been analyzed for more than 20 yr, there are many questions that have not been resolved regarding their origin and original provenance. We ask, from a geophysical perspective, what is the best way to integrate these three seemingly disparate disciplines to address lunar problems?

This is a timely question, for as this is being written, Lunar Prospector is orbiting the Moon collecting global γ-ray data, as well as improved gravity tracking. Within a year or two, we will have an order of magnitude better understanding of both the gravity field, as well as the near-surface composition. Elemental concentration maps should be made available for most major rock-forming elements (e.g., Fe, Mg, Ca, Si, and Ti), as well as some trace elements (e.g., K, Th, U, and H). When these compositional maps are finally released, how will they be used to improve our understanding of the geology of the Moon?

Although there are many ways in which geophysical studies could be integrated with either the sample data or remote-sensing data, we suggest that the most fruitful synthesis will come from investigating both the lateral and vertical variability in the structure and composition of the lunar crust. By investigating the nature of material ejected from large impact basins, the stratigraphy of the preimpact crust can be inferred. Specifically, using a model of the crustal thickness from geophysical studies, it should be possible to predict the radial variation of ejecta mineralogy using impact-cratering scaling relations. Furthermore, elemental concentration maps should be able to independently assess the radial variation in ejecta mineralogy. Since the geophysical models of crustal structure are not unique, the remote-sensing observations will enable us to determine which models of crustal structure are plausible. Additionally, since we have samples that are believed to have come from large impact basins, these samples will provide ground truth for both the remote-sensing data and impact-cratering models.

The Geophysical Dataset: The prime geophysical datasets to be offered in addressing this problem are crustal thickness maps derived from an analysis of lunar gravity and topography. As is widely known, though, modeling the structure of the crust based on gravity and topography alone is not unique. Many subsurface models of crustal structure can explain the observed gravity and topography. In practice, however, one assumes a specific model of the lunar crust, and then uses the seismic profiles beneath the Apollo 12 and 14 sites as a constraint at this one locale.

There are three main models of crustal structure that have been used in computing global crustal thicknesses. The traditional model is to assume that the crust is uniform in composition (i.e., density),

and that the observed gravity field is due to surface topography, as well as relief along the Moho (which is seismically constrained at one locale) [e.g., 1]. As a simple variation of this model, it has been suggested that the crust may be grossly stratified into two crustal layers (a feldspathic upper crust and noritic lower crust) [2]. It has also been suggested that a large portion of the gravity field may be due to lateral variations in crustal density (Pratt compensation) [3], or that heterogeneities in the mantle are responsible for long wavelength features such as the nearside-farside dichotomy [4]. Each of these models may have some validity on a local or global scale, but without additional seismic data (or supporting remote-sensing or sample data), caution should be exercised when using global crustal thickness maps derived from these models.

Typical assumptions that go into these models are (1) whether the crust is grossly stratified, and if so, in how many layers, (2) whether the crustal layers vary in composition laterally or vertically, (3) whether the composition of the upper mantle is heterogeneous or uniform in density, and (4) the density of the mantle and crustal layers. The range of possible parameters in these models could be constrained through a combined analysis of impact processes, remote sensing of basin ejecta, and the Apollo samples.

Predictions of Basin Ejecta Composition Based on Crustal Thickness Determinations: Recent ejecta modeling [5,6] based on modern ejecta scaling relations [7] makes it possible to predict the composition of basin ejecta as a function of distance from the excavation cavity rim. These models take into account the mixing of primary ejecta with the target substrate as a function of radial range. Though the initial modeling that has been done using this new technique has assumed that the preimpact crust is uniform in composition, it would not be difficult to include the effects of crustal stratification or lateral compositional variations within the impact crater's excavation cavity.

Integrating Remote-Sensing and Sample Data: Comparing the observed variation in ejecta composition from remote-sensing studies with that predicted from the geophysical models should tell us which types of crustal thickness models are applicable to the Moon. For instance, this type of synthesis should be able to address the following questions: (1) Is the crust better described by being stratified in multiple layers, zoned, or uniform in composition? (2) Is the nearside-farside dichotomy a result of large crustal thickness variations (Airy compensation), or is it due to a hemispheric disparity in density of the crust (Pratt compensation) and/or mantle? (3) Did any of the basins excavate material from the mantle? (4) Does ejecta mineralogy vary as a function of azimuth, in addition to radial distance (suggesting that the target was heterogeneous on the scale of the excavation cavity)?

Although this type of analysis could be applied to most of the large nearside basins (those basins that are adequately resolved in the gravity field), the Imbrium basin would perhaps be the most fruitful. Due to the proximity of the Apollo landing sites to this basin, it is likely that Imbrium ejecta has been sampled at most of these sites. The relative abundance of primary ejecta, as well as its composition, could both be used as ground truth for both the geophysical ejecta modeling and remote-sensing studies.

References: [1] Neumann G. A. et al. (1996) *JGR, 101*, 16841–16843. [2] Wieczorek M. A. and Phillips R. J. (1998) *JGR, 103*, 1715–1724. [3] Solomon S. C. (1978) *Proc. LPSC 9th*, 3499–3511. [4] Wasson J. T. and Warren P. H. (1980) *Icarus, 44*, 752–771. [5] Moss et al. (1998) *Meteoritics & Planet. Sci.*, submitted. [6] Haskin

L. A. (1998) *JGR, 103*, 1679–1689. [7] Housen et al. (1983) *JGR, 88*, 2485–2499.

55/-9/   , _ _ _

THE IMBRIUM AND SERENITATIS BASINS: IMPACTS IN AN ANOMALOUS LUNAR PROVINCE. M. A. Wieczorek, L. A. Haskin, R. L. Korotev, B. L. Jolliff, and R. J. Phillips, Department of Earth and Planetary Sciences, Washington University, Campus Box 1169, One Brookings Drive, St. Louis MO 63130, USA (markw@wurtzite.wustl.edu).

Introduction: Recent geophysical analyses of the Imbrium and Serenitatis Basins suggest that the crustal structure beneath these basins is highly anomalous [1]. Specifically, Imbrium and Serenitatis appear to have only excavated material from shallow crustal depths, whereas proportional scaling laws (valid for basins at least as large as Crisium) predict that the entire crustal column, as well as a small fraction of mantle material, should have been excavated during these events.

Gamma-ray data from the Apollo [2] and Lunar Prospector missions [3] suggest that the Imbrium and Serenitatis Basins lie within (or on the boundary of) an anomalous nearside high-Th geochemical province [4]. We believe that the anomalous crustal structure associated with the Imbrium and Serenitatis Basins is directly related to these impacts occurring within this anomalous region of the lunar crust. We postulate that the high-Th geochemical province is a manifestation of the final stages of cooling of a global "magma ocean" and that a residual KREEP-rich magma body was located beneath the crust in this region ~3.9 Ga. An impact into this province at this time would have led to voluminous KREEP-basalt volcanism (filling in the excavation cavity of these basins), and the dispersal of KREEP-rich ejecta (the Th-rich mafic impact melt breccias [5]).

The next two sections discuss our motivation for postulating such a scenario from both the geophysical and geochemical perspective. Following this discussion we expand the hypothesis presented above and end with a list of testable predictions.

Imbrium and Serenitatis Have Anomalous Crustal Structures: Geophysical studies have concluded that the Moho is substantially uplifted beneath many lunar basins. Using a new dual-layered crustal thickness model for the Moon [6], the excavation cavities of some young, large, nearside basins were reconstructed by restoring this uplifted Moho to its preimpact position. The resulting depression was assumed to be a first-order representation of the excavation cavity from which the depth and diameter of excavation could be determined [1]. These geophysical results, in combination with photogeological and experimental hypervelocity impact studies, all suggest that the excavation cavity of impact craters (that portion of the preimpact crust that is ballistically ejected) is scale invariant over several decades in size (i.e., they obey proportional scaling laws). Specifically, the depth/diameter ratio of the excavation cavity has been found to be ≈0.1 for craters centimeters in size up to basins the size of Crisium [1,7]. The geophysical reconstructions of the excavation cavity for the two largest nearside basins (Serenitatis and Imbrium), however, do not follow this trend. These two basins appear to have excavated significantly shallower than would have been expected if proportional scaling were also valid for these basins. This observation from the gravity modeling is not an artifact of the adopted dual-layered crustal model (the same qualitative result applies to single-layered crustal models), nor is it strongly dependent on the assumed mare thickness model that was used for these basins (providing the mare density is ≈>3.3 gm/cm³).

The non-proportional scaling theory of Schultz [8] is not capable of explaining the magnitude of shallowing for these basins. Additionally, invoking special impact conditions (e.g., highly oblique impacts) to explain the structure of only the two largest nearside basins would be hard to justify. The apparent shallow excavation cavities for these two young basins could possibly be the result of significant viscous relaxation occurring after the impact event [9], however, basins as old as Smythii (the oldest basin considered in the study of [1]) do not appear to have been substantially modified by this process. If the temperature gradients beneath the Imbrium and Serenitatis Basins were typical of the Moon when they formed, this process should not have played a significant role in modifying the structure of these basins. If, however, this region was hotter than typical of the lunar crust, viscous relaxation could have been accelerated in this region.

One plausible explanation for the apparent "shallowing" of the excavation cavities for Imbrium and Serenitatis is that subsequent to impact, these basins were filled in by volcanic flows. If tens of kilometers of these *ad hoc* volcanic flows were removed from the crustal thickness maps, the depth of the reconstructed excavation cavities for these basins could be shown to be consistent with proportional scaling. However, in order for this interpretation to work, these postulated volcanic flows would need to have a density similar to what was used for the lower crust in the adopted crustal thickness model ($r_1 = 3.1$ g/cm³). Since gravity modeling is only concerned with the density of crustal materials (as opposed to composition), these flows would "look" like lower crust in the crustal thickness model. It would appear as if the lower crust was thicker than it really was, and the reconstructed excavation cavity would be artificially shallowed.

The most common lunar volcanic rocks (the mare basalts), however, are extremely iron rich and dense ($r ≈ 3.3$–3.6 gm/cm³). The only lunar volcanic rock that has a density similar to that of the lower crust is KREEP-basalt ($r ≈ 3.0$–3.2 gm/cm³). Since KREEP-basalt fragments have been found at the Apollo 15 and 17 sites, it is plausible that KREEP-basalt volcanism could have filled in an appreciable portion of the Imbrium and Serenitatis excavation cavities, giving rise to an apparent shallow depth of excavation.

Imbrium and Serenitatis Basins Impacted and Anomalous Geochemical Province: If voluminous KREEP-basalt volcanism occurred within the Imbrium and Serenitatis Basins, why didn't this form of volcanism also modify the other lunar basins, such as Crisium? Our resolution to this question relies on the fact that the Imbrium impact occurred within an anomalous high-Th geochemical province, and that the Serenitatis impact occurred on the boundary of this province [4]. We suggest that KREEP-basalt volcanism occurred primarily within this province, and was rare or absent outside this province.

The concentration of incompatible elements is a natural consequence of crystallizing a lunar magma ocean [10]. Thermal models suggest that the bulk of this magma ocean should crystallize within about 500 m.y. The last remaining dregs of the magma ocean (urKREEP [11]), however, would remain molten much longer (perhaps as long as about 1 b.y. [12]). Though these thermal models assumed that the "urKREEP" formed a global layer a few kilometers in thickness, the existence of the high-Th province suggests that the last remaining dregs of the magma ocean may have been concen-

trated beneath this province as a magma chamber, or partial melt zone.

The preimpact stratigraphy of the Imbrium basin is difficult to infer. At present, a 20-km-thick feldspathic upper crust and a 40-km-thick lower crust is present exterior to this basin. One endmember model for the preimpact stratigraphy of this region is that the present average structure is appropriate, and that the putative KREEP-rich magma body was thin and sandwiched between the crust and mantle. The Imbrium impact would have penetrated into this KREEP-rich layer leading to the extrusion of KREEP basalts. This model predicts that an insignificant amount of "KREEP basalt" was ejected from the excavation cavity of this basin.

The other endmember model is that the preimpact crustal structure of the Imbrium Basin consisted of a 20-km-thick feldspathic upper crust, and a 40-km-thick magma chamber or partial melt zone. Mixing calculations suggest that the high-Th mafic impact melt breccias that are believed to be basin ejecta (a.k.a. LKFM) can be modeled as a three-component mixture of KREEP-basalt, feldspathic crust, and forsteritic olivine [13, 14]. Since the high-Th mafic impact melts have been interpreted as Imbrium ejecta [5], this suggests that the more extensive magma chamber is a more appropriate model for the original crustal structure of this province.

Scenario: Our preliminary scenario for the origin of the anomalous Imbrium and Serenitatis crustal structure is as follows:

1. Crystallization of a lunar magma ocean resulted in an extensive KREEP-rich magma body (or partial melt zone) having the composition of KREEP-basalt beneath what is now the nearside Th-rich geochemical province.

2. The Imbrium impact penetrated this magma body, excavating feldspathic upper crust, KREEP-rich magma, and mantle material. The primary ejecta of Imbrium would be a mixture of these components.

3. KREEP-rich magma from this province flowed laterally into the Imbrium excavation cavity, forming KREEP basalt and giving rise to an apparent shallow structure in the crustal thickness models.

4. The Serenitatis impact occurred on the boundary of the Th-rich geochemical province and likely did not penetrate this magma body. However, the proximity of the Serenitatis Basin to this province resulted in the lateral transport of magma, filling in the excavation cavity of this basin.

Predictions: The following is a list of testable predictions of this theory:

1. KREEP basalts should all have crystallization ages corresponding to the age of the Imbrium and Serenitatis impacts.

2. Since the Serenitatis impact occurred on the boundary of the high-Th geochemical province, the ejecta of Serenitatis should not be rich in Th. KREEP basalts, however, should be present beneath the mare fill of this basin.

3. Thorium-rich ejecta from the Imbrium Basin should be present in the sample collection. The composition of this ejecta should be a mixture of KREEP basalt, feldspathic crust, and mantle materials. The portion of this ejecta that was melted, furthermore, should have crystallization ages corresponding to the Imbrium impact event.

4. KREEP basalts should have a relatively limited range of compositions reflecting the uniformity of the proposed "magma chamber."

5. KREEP basalts are the physical manifestation of "urKREEP."

References: [1] Wieczorek M. A. and Phillips R. J. (1998) *LPS XXIX*, Abstract #1229. [2] Metzger A. E. et al. (1977) *Proc. LSC 8th*, 949–999. [3] Feldman W. C. et al. (1998) *LPS XXIX*, Abstract #1936. [4] Haskin L. A. (1998) *JGR*, *103*, 1679–1689. [5] Haskin L. A. et al. (1998) *Meteoritics & Planet. Sci.*, in press. [6] Wieczorek M. A. and Phillips R. J. (1998) *JGR*, *103*, 1715–1784. [7] Croft S. K. (1980) *Proc. LPSC 11th*, 2347–2378. [8] Schultz P. H. (1988) in *Mercury*, 275–335. [9] Bratt S. R. et al. (1985) *JGR*, *90*, 3049–3064. [10] Warren P. H. (1985) *Annu. Rev. Earth Planet. Sci.*, *13*, 201–240. [11] Warren P. H. and Wasson J. T. (1979) *Rev. Geophys.*, 73–88. [12] Solomon S. C. and Longhi J. (1977) *Proc. LSC 8th*, 583–599. [13] Korotev R. L. (1997) *LPS XXVIII*, Abstract #1087. [14] Korotev R. L., this volume.

List of Workshop Participants

Carlton C. Allen
Mail Code C23
Lockheed Martin Engineering
2400 NASA Road 1
Houston TX 77058
Phone: 281-483-2630
Fax: 281-483-5347
E-mail: carlton.c.allen1@jsc.nasa.gov

Abhijit Basu
Department of Geological Science
Indiana University
1005 East 10th Street
Bloomington IN 47405
Phone: 812-855-6654/5581
Fax: 812-855-7899
E-mail: basu@indiana.edu

Alan Binder
Lunar Research Institute
1180 Sun Rise Drive
Gilroy CA 95020
Phone: 408-847-0969
Fax: 408-846-9770
E-mail: abinder@mail.arc.nasa.gov

Ben Bussey
Code 50
European Space Agency/ESTEC
P.O. Box 299
2200 Ag Noordwijk
The Netherlands
Phone: 31-71-565-4726
Fax: 31-71-565-4697
E-mail: bbussey@estec.esa.nl

Stephen Clifford
Lunar and Planetary Institute
3600 Bay Area Boulevard
Houston TX 77058
Phone: 281-486-2146
Fax: 281-486-2160

Cassandra Coombs
Geology Department
College of Charleston
66 George Street
Charleston SC 29424
Phone: 803-953-8279
Fax: 803-953-5446
E-mail: coombsc@cofc.edu

Dennis Cowles
Audubon Institute
P.O. Box 870610
New Orleans LA 70187-0610
Phone: 504-243-3385
Fax: 504-242-1889
E-mail: d-cowles@msn.net

Rene DeHon
Department of Geosciences
Northeast Louisiana University
Monroe LA 71209
Phone: 318-342-1894
Fax: 318-342-1755
E-mail: gedehon@alpha.nlu.edu

Deborah Domingue
Applied Physics Laboratory
Johns Hopkins University
11100 Johns Hopkins Road
Laurel MD 20723
Phone: 240-228-7945
Fax: 240-228-6670
E-mail: deborah.domingue@jhuapl.edu

Michael B. Duke
Lunar and Planetary Institute
3600 Bay Area Boulevard
Houston TX 77058
Phone: 281-244-2036
Fax: 281-244-2006
E-mail: duke@lpi.jsc.nasa.gov

Eric M. Eliason
U. S. Geological Survey
2255 North Gemini Drive
Flagstaff AZ 86001
Phone: 520-557-7113
Fax: 520-556-7100
E-mail: eeliason@usgs.gov

Rick Elphic
Mail Stop D466
NIS-1 Space and Atmospheric Sciences
Los Alamos National Laboratory
Los Alamos NM 87545
Phone: 505-665-3693
Fax: 505-665-7395
E-mail: relphic@lanl.gov

William C. Feldman
Mail Stop D466
Los Alamos National Laboratory
1516 45th Street
Los Alamos NM 87545
Phone: 505-667-7372
Fax: 505-665-7395
E-mail: wfeldman@lanl.gov

Cliff Fenton
1031 West Tunnel Boulevard
Houma LA 70360
Phone: 504-879-3829
E-mail: clifff@cajun.net

Lisa R. Gaddis
Astrogeology Branch Laboratory
U.S. Geological Survey
2255 North Gemini Drive
Flagstaff AZ 86001
Phone: 520-556-7053
Fax: 520-556-7014
E-mail: lgaddis@flagmail.wr.usgs.gov

Jeffrey J. Gillis
Department of Earth and Planetary Sciences
Campus Box 1169
Washington University
One Brookings Drive
St. Louis MO 63130-4899
Phone: 314-935-8611
Fax: 314-935-7361
E-mail: gillis@levee.wustl.edu

Jennifer A. Grier
Lunar and Planetary Laboratory
University of Arizona
Space Sciences Building
Tucson AZ 85721
Phone: 520-621-1507
Fax: 520-621-4933
E-mail: jgrier@lpl.arizona.edu

John E. Gruener
Hernandez Engineering
Suite 200
17625 El Camino Real
Houston TX 77058
Phone: 281-483-1842
E-mail: john.e.gruener1@jsc.nasa.gov

Edward Guinness
Washington University
Campus Box 1169
One Brookings Drive
St. Louis MO 63130
Phone: 314-889-5493
Fax: 314-935-4998
E-mail: guinness@wunder.wustl.edu

Bruce W. Hapke
Department of Geology and Planetary Science
University of Pittsburgh
321 Old Engineering Hall
Pittsburgh PA 15260
Phone: 412-624-8876
Fax: 412-624-3914
E-mail: hapke@vms.cis.pitt.edu

Larry A. Haskin
Department of Earth and Planetary Sciences
Campus Box 1169
Washington University
One Brookings Drive
St. Louis MO 63130
Phone: 314-935-5613
Fax: 314-935-7361
E-mail: lah@levee.wustl.edu

B. R. Hawke
Hawai'i Institute for Geophysics and Planetology
University of Hawai'i
2525 Correa Road
Honolulu HI 96822
Phone: 808-956-3133
Fax: 808-956-6322

Jim Head
Department of Geological Sciences
Box 1846
Brown University
Providence RI 02912
Phone: 401-863-2526
Fax: 401-863-3978
E-mail: james_head_iii@brown.edu

David J. Heather
Department of Physics and Astronomy
University College London
Gower Street
London WC1E 6BT
United Kingdom
Phone: 44-171380714452
Fax: 44-171-380-7145
E-mail: djh@star.ucl.ac.uk

Christopher E. Heil
Planetary Sciences Department
University of New Mexico
P.O. Box 29173
Santa Fe NM 87592
Phone: 505-424-7464
E-mail: cheil@unm.edu

Robert R. Herrick
Lunar and Planetary Institute
3600 Bay Area Boulevard
Houston TX 77058
Phone: 281-486-2116
Fax: 281-486-2162
E-mail: herrick@lpiip2.jsc.nasa.gov

Paul C. Hess
Department of Geological Sciences
Box 1846
Brown University
Providence RI 02912
Phone: 401-863-1929
Fax: 401-863-2058
E-mail: paul_hess@brown.edu

Harald Hiesinger
Department of Geological Sciences
Box 1846
Brown University
Providence RI 02912
Phone: 401-863-1437
Fax: 401-863-3978
E-mail: harald.hiesinger@dlr.de

Friedrich Horz
Mail Code SN2
Solar System Exploration
NASA Johnson Space Center
Houston TX 77058
Phone: 281-483-5042
Fax: 281-483-5276
E-mail: friedrich.p.horz1@jsc.nasa.gov

Odette B. James
U.S. Geological Survey
955 National Center
Reston VA 20191
Phone: 703-648-6753
Fax: 703-648-6032
E-mail: ojames@usgs.gov

Kandy S. Jarvis
Mail Code C23
Lockheed Martin Engineering
2400 NASA Road 1
Houston TX 77058
Phone: 281-483-5165
Fax: 281-483-5276
E-mail: kandy.s.jarvis1@jsc.nasa.gov

Ralf Jaumann
Institute for Planetary Exploration
DLR German Aerospace Center
Rudower Chaussee 5
12489 Berlin
Germany
Phone: 49-30-67055-400
Fax: 49-30-67055-402
E-mail: ralf.jaumann@dlr.de

Brad Jolliff
Department of Earth and Planetary Sciences
Campus Box 1169
Washington University
One Brookings Drive
St Louis MO 63130
Phone: 314-935-5622
Fax: 314-935-7361
E-mail: blj@levee.wustl.edu

John Jones
Mail Code SN2
NASA Johnson Space Center
Houston TX 77058
Phone: 281-483-5319
Fax: 281-483-1573
E-mail: john.h.jones1@jsc.nasa.gov

Lindsay P. Keller
MVA, Inc.
5500 Oakbrook Parkway #200
Norcross GA 30093
Phone: 770-662-8509
Fax: 770-662-8532
E-mail: LKeller@mvainc.com

Randy Korotev
Department of Earth and Planetary Sciences
Campus Box 1169
Washington University
One Brookings Drive
St. Louis MO 63130-4899
Phone: 314-935-5637
Fax: 314-935-7361
E-mail: rlk@levee.wustl.edu

David J. Lawrence
Mail Stop D466
Los Alamos National Laboratory
Los Alamos NM 87545
Phone: 505-667-0945
Fax: 505-665-7395
E-mail: djlawrence@lanl.gov

Stefanie Lawson
Campus Box 392
University of Colorado
Boulder CO 80309-0392
Phone: 303-492-6527
Fax: 303-492-6946
E-mail: lawson@argyle.colorado.edu

David J. Lindstrom
Mail Code SN2
Planetary Science Branch
NASA Johnson Space Center
Houston TX 77058
Phone: 281-483-5012
Fax: 281-483-1573
E-mail: david.j.lindstrom1@jsc.nasa.gov

Marilyn M. Lindstrom
Mail Code SN2
NASA Johnson Space Center
Houston TX 77058
Phone: 281-483-5135
Fax: 281-483-5347
E-mail: marilyn.m.lindstrom1@jsc.nasa.gov

Gary Lofgren
Mail Code SN4
NASA Johnson Space Center
Houston TX 77058
Phone: 281-483-6187
Fax: 281-483-5276
E-mail: gary.e.lofgren1@jsc.nasa.gov

Paul G. Lucey
Hawai'i Institute for Geophysics and Planetology
University of Hawai'i
2525 Correa Road
Honolulu HI 96822
Phone: 808-956-3137
Fax: 808-956-6322
E-mail: lucey@pgd.hawaii.edu

Sylvestre Maurice
Observatorie Midi-Pyrenes
14 Avenue Edouard Belin
31400 Toulouse
France
Phone: 33-5-6133-2947
Fax: 33-5-6133-2840
E-mail: maurice@obs-mip.fr

Stewart McCallum
Department of Geological Sciences
Box 351310
University of Washington
Seattle WA 98195
Phone: 206-543-9494
Fax: 206-543-3836
E-mail: mccallum@u.washington.edu

Alfred S. McEwen
University of Arizona
1629 East University Boulevard
Tucson AZ 85721-0092
Phone: 520-621-4824
Fax: 520-621-9628
E-mail: mcewen@pirl.lpl.arizona.edu

David S. McKay
Mail Code SN1
NASA Johnson Space Center
Houston TX 77058
Phone: 281-483-5048
Fax: 281-244-8892
E-mail: david.s.mckay1@jsc.nasa.gov

Gordon A. McKay
Mail Code SN2
Planetary Science Branch
NASA Johnson Space Center
Houston TX 77058
Phone: 281-483-5041
Fax: 281-483-1573
E-mail: gordon.a.mckay1@jsc.nasa.gov

Wendell Mendell
Mail Code SN2
NASA Johnson Space Center
Houston TX 77058
Phone: 281-483-5064
Fax: 281-483-5347
E-mail: wendell.mendell@ems.jsc.nasa.gov

Charles Meyer
Mail Code SN2
NASA Johnson Space Center
Houston TX 77058
Phone: 281-483-5133
Fax: 281-483-5347
E-mail: charles.meyer1@jsc.nasa.gov

Donald Morrison
Mail Code SN2
NASA Johnson Space Center
Houston TX 77058
Phone: 281-483-5039
Fax: 281-483-1573
E-mail: donald.a.morrison1@jsc.nasa.gov

Noriyuki Namiki
Deparment of Earth and Sciences
Kyushu University
6-10-1 Hakozaki
Higashi-ku, Fukuoka 812
Japan
Phone: 81-92-642-2313
Fax: 81-92-642-2684
E-mail: nori@geo.kyushu-u.ac.jp

Clive Neal
Department of Civil Engineering
University of Notre Dame
Notre Dame IN 46556
Phone: 319-631-8328
Fax: 219-631-9236
E-mail: neal1@nd.eduu

Gregory Neumann
Mail Code 926
Space Geodesy
NASA Goddard Space Flight Center
Greenbelt MD 20771
Phone: 301-286-9291
Fax: 301-286-1757
E-mail: neumann@tharsis.gsfc.nasa.gov

Stewart D. Nozette
141 Gradton Street
Chevy Chase MD 20815
Phone: 301-913-2007
Fax: 301-913-2008
E-mail: nozette@atech.pzinet.com

Laurence E. Nyquist
Mail Code SN2
NASA Johnson Space Center
Houston TX 77058
Phone: 281-483-5038
Fax: 281-483-1573
E-mail: laurence.e.nyquist1@jsc.nasa.gov

James J. Papike
Institute of Meteoritics
Northrop Hall 313
University of New Mexico
Albuquerque NM 87131-1126
Phone: 505-277-1644
Fax: 505-277-3577
E-mail: jpapike@unm.edu

Chris A. Peterson
Hawai'i Institute for Geophysics and Planetology
University of Hawai'i
2525 Correa Road
Honolulu HI 96822
Phone: 808-956-3131
Fax: 808-956-6322
E-mail: chrisp@pgd.hawaii.edu

Carle Pieters
Department of Geological Sciences
Box 1846
Brown University
Providence RI 02912
Phone: 401-863-2417
Fax: 401-863-3978
E-mail: pieters@pds.geo.brown.edu

Andrew E. Potter Jr.
Lunar and Planetary Institute
3600 Bay Area Boulevard
Houston TX 77058
Phone: 281-486-2115
Fax: 281-486-2162
E-mail: potter@lpi.jsc.nasa.gov

David Rajmon
Department of Geosciences
University of Houston
Houston TX 77204-5503
Phone: 713-743-3417
Fax: 713-748-7906
E-mail: rajmon@bayou.uh.edu

Robert C. Reedy
Mail Stop D436
Group NIS-2
Los Alamos National Laboratory
Los Alamos NM 87545
Phone: 505-667-5446
Fax: 505-665-4414
E-mail: rreedy@lanl.gov

Arch Reid
Department of Geosciences
University of Houston
Houston TX 77204-5503
Phone: 713-743-3404
Fax: 713-748-7906
E-mail: areid@uh.edu

Sue E. Riegsecker
Indiana University
1005 East 10th Street
Bloomington IN 47401
Phone: 812-855-2154
E-mail: riegseck@indiana.edu

Sanders D. Rosenberg
In-Space Propulsion, Limited
628 Commons Drive
Sacramento CA 95825-6642
Phone: 916-927-6629
Fax: 916-927-6629
E-mail: inspacepro@aol.com

Malcolm J. Rutherford
Geology Department
Brown University
324 Brook Street
Providence RI 02912
Phone: 401-863-1927
Fax: 401-863-2058
E-mail: macr@brown.edu

Graham Ryder
Lunar and Planetary Institute
3600 Bay Area Boulevard
Houston TX 77058
Phone: 281-486-2141
Fax: 281-486-2162
E-mail: zryder@lpi.jsc.nasa.gov

R. S. Saunders
  Mail Stop 183-335
  Jet Propulsion Laboratory
  4800 Oak Grove Drive
  Pasadena CA 91109
  Phone: 818-354-2867
  Fax: 818-393-6546
  E-mail: saunders@scn1.jpl.nasa.gov

Paul Schenk
  Lunar and Planetary Institute
  3600 Bay Area Boulevard
  Houston TX 77058
  Phone: 281-486-2157
  Fax: 281-486-2162
  E-mail: schenk@lpi3.jsc.nasa.gov

Charles K. Shearer
  Department of Earth and Planetary Science
  Institute of Meteoritics
  University of New Mexico
  Albuquerque NM 87131
  Phone: 505-277-9159
  Fax: 505-277-3577
  E-mail: cshearer@unm.edu

Atsushi Shiraishi
  NASDA-Tsukuba Space Center
  AMRC/NASDA Tsukuba Space Center
  2-1-1, Sengen
  Tsukuba-shi, Ibaraki-ken 305-0047
  Japan
  Phone: 81-298-52-2131
  Fax: 81-298-52-2247
  E-mail: shiraishi.atsushi@nasda.go.jp

Richard A. Simpson
  Center for Radar Astronomy
  Durand Building, Room 232
  Stanford University
  Stanford CA 94305-9515
  Phone: 415-723-3525
  Fax: 415-723-9251
  E-mail: rsimpson@magellan.stanford.edu

Gregory Snyder
  Department of Geological Sciences
  Planetary Geosciences Institute
  University of Tennessee
  Knoxville TN 37996-1410
  Phone: 423-974-6023
  Fax: 423-974-6022
  E-mail: gasnyder@utk.edu

Paul Spudis
  Lunar and Planetary Institute
  3600 Bay Area Boulevard
  Houston TX 77058
  Phone: 281-486-2193
  Fax: 281-486-2162
  E-mail: spudis@lpi.jsc.nasa.gov

David Stewart
  U.S. Geological Survey
  National Center 926A
  Reston VA 20192
  Phone: 703-648-6945
  Fax: 703-648-6953
  E-mail: dbstewart@usgs.gov

Steve Symes
  Mail Code SN4
  NASA Johnson Space Center
  Houston TX 77058
  Phone: 281-483-5436
  Fax: 281-483-1573
  E-mail: steven.j.symes1@jsc.nasa.gov

Allen Taylor
  Pacific University
  16101 South Hilltop Road
  Oregon City OR 97045
  Phone: 503-656-0845
  E-mail: taylor@pacificu.edu

Lawrence A. Taylor
  Department of Geological Sciences
  Planetary Geoscience Institute
  University of Tennessee
  Knoxville TN 37996
  Phone: 423-974-6013
  Fax: 423-974-6022
  E-mail: lataylor@utk.edu

Stefanie Tompkins
  Science Applications International Corp.
  4501 Daly Drive Suite 400
  Chantilly VA 20151
  Phone: 703-814-7713
  Fax: 703-817-9601
  E-mail: thompkinss@saic.com

Allan Treiman
  Lunar and Planetary Institute
  3600 Bay Area Boulevard
  Houston TX 77058
  Phone: 281-486-2117
  Fax: 281-486-2162
  E-mail: treiman@lpi.jsc.nasa.gov

Mark A. Trotter
Audubon Institute
P.O. Box 870610
New Orleans LA 70187-0610
Phone: 504-243-3385
Fax: 504-242-1889
E-mail: strotter@communique.net

Faith Vilas
Mail Code SN3
NASA Johnson Space Center
Houston TX 77058
Phone: 281-483-5056
Fax: 281-483-5276
E-mail: Faith.Vilas1@jsc.nasa.gov

Richard Vondrak
Mail Code 690
Laboratory for Extraterrestrial Physics
NASA Goddard Space Flight Center
Greenbelt MD 20771
Phone: 301-286-8112
Fax: 301-286-1683
E-mail: vondrak@gsfc.nasa.gov

Paul H. Warren
Institute of Geophysics
University of California
Los Angeles CA 90095-1567
Phone: 310-825-3202
Fax: 310-206-3051
E-mail: pwarren@ucla.edu

Catherine Weitz
Mail Stop 183-335
Jet Propulsion Laboratory
4800 Oak Grove Drive
Pasadena CA 91109
Phone: 818-354-1568
Fax: 818-393-6546
E-mail: cweitz@jpl.nasa.gov

Susan J. Wentworth
Mail Code C23
Lockheed Martin Engineering
2400 NASA Rd 1
Houston TX 77058
Phone: 281-483-5047
Fax: 281-483-5347
E-mail: susan.j.wentworth@jsc.nasa.gov

Mark Wieczorek
Department of Earth and Planetary Sciences
Campus Box 1169
Washington University
One Brookings Drive
St. Louis MO 63130
Phone: 314-935-4192
Fax: 314-935-7361
E-mail: markw@wurtzite.wustl.edu

Herbert A. Zook
Mail Code SN2
NASA Johnson Space Center
Houston TX 77058
Phone: 281-483-5058
Fax: 281-483-5276
E-mail: herbert.a.zook1@jsc.nasa.gov